Erosion Dynamics of a Sediment Depleted Coastal Embayment and Dunefield

By

Samuel G Davidson
BSc (Hons)

Thesis
Submitted to Flinders University
for the degree of

Doctor of Philosophy

College of Science and Engineering

June 10, 2022

TABLE OF CONTENTS

TABLE OF CONTENTS ..... **I**
DECLARATION ..... **V**
COAUTHORSHIP ..... **VI**
ACKNOWLEDGEMENTS ..... **VII**
SUMMARY ..... **IX**
LIST OF FIGURES ..... **XI**
LIST OF TABLES ..... **XVI**
CHAPTER 1 ..... **1**
Introduction 1
1.1 Research Question 1
1.2 Research Aims 2
1.3 Contribution of this PhD 6
CHAPTER 2 ..... **7**
CONTROLS ON DUNE SCARPING **7**
2.1 Abstract 7
2.2 Introduction 8
2.3 Foredune Scarping 10
2.4 Controls on the Degree of Scarping 14
2.4.1 Water Levels 14
2.4.2 Height, Volume and Original Morphology of the Foredune 18
2.4.3 Levels of vegetation cover, density and rootmass 23
2.4.4 Large Woody Debris and Beach Wrack 29
2.4.5 Compaction 31
2.4.6 Beach Type 32
2.5 Effects of Scarping 34
2.5.1 Foredune translation 34
2.5.2 Development of Blowouts, Parabolics and Transgressive Dune fields 36
2.6 The Future 39
2.6.1 Sea Level Rise 40
2.6.2 Changes in Wave Climate 41
2.7 A Model of Scarp Controls 42
2.8 Conclusion 44
CHAPTER 3 ..... **47**

RAPID SHORELINE AND DUNEFIELD CHANGE, SALMON HOLE, SOUTH AUSTRALIA 47
3.1 Abstract 47
3.2 Introduction 48
3.2.1 Study Site 52
3.3 Methodology 54
3.3.1 Aerial Imagery 54
3.3.2 Shoreline Analysis 57
3.3.3 Potential Errors 59
3.3.4 Time Series 60
3.3.5 Wave Data 60
3.3.6 Digital Surface Models 61
3.3.7 Topographic Profiles and Erosion Volumes 62
3.4 Results 63
3.4.1 Shoreline variability 63
3.4.2 Key Periods of Change 67
3.4.2.1 Pre-Tombolo Breakthrough 67
3.4.2.2 Tombolo Erosion 69
3.4.3 Storm Record 73
3.4.3.1 Pre-Tombolo Breakthrough 73
3.4.3.2 Tombolo and Post-Tombolo Breakthrough 73
3.4.4 Volumetric Analysis of Topographic Profiles 74
3.4.5 Change Within the Last 3 Years 77
3.5 DISCUSSION 80
3.5.1 Response 80
3.5.2 Resistance 82
3.5.3 Resilience 82
3.5.4 Recursion 82
3.5.5 Dunefield Changes 86
3.5.5.1 Scarping 86
3.5.5.2 Moderate-scale Transgressive Dunefield Changes 86
3.5.5.3 Change Within the Last 3 Years 87
3.5.6 Volumetric Analysis 89
3.5.7 Conceptual Change Model 89
3.6 Conclusion 91
CHAPTER 4 93
FLOW DYNAMICS OVER A HIGH, STEEP, EROSIONAL COASTAL DUNE SLOPE 93
4.1 Abstract 93

4.2 Introduction 94
4.2.1 Study Site 101
4.3 Methodology 105
4.3.1 Analysis Methods 108
4.4 Results 109
4.4.1 Incident Wind Conditions 109
4.4.2 Flow Dynamics 110
4.4.2.1 Flow Direction 110
4.4.2.2 Wind Speed 113
4.4.2.3 Perpendicular vs Oblique Wind Approach Wind Effects 114
4.4.2.4 2D Wind Velocity Profiles 118
4.4.2.5 Turbulence 119
4.4.3 Smoke Cake Visualization 121
4.4.4 Blowout 124
4.5 Discussion 125
4.5.1 Wind Flow Dynamics 125
4.5.1.1 Speed Up and Turbulence 125
4.5.1.2 Topographic Steering 128
4.5.2 Effect of Wind Flow Processes on Scarp/Blowout 129
4.6 Conclusion 131
CHAPTER 5 133
5. DYNAMICS OF SUBAQUEOUS DUNES IN A REEF-FRINGED HEADLAND BAY BEACH 133
5.1 Introduction 133
5.1.1 Subaqueous Transverse dunes 135
5.2 Method 141
5.2.1 Bathymetric Surveys 141
5.2.2 Current measurements 141
5.2.3 Additional hydrodynamic measurements (water levels and local currents) 143
5.2.3.1 Water levels 143
5.2.3.2 Local currents over a dune 144
5.2.4 Aerial surveys 145
5.3 Impacts of waves, winds and tides in the lagoon's hydrodynamics 146
5.3.1 Flow over dunes 154
5.3.2 Variation in wave height around bay 157
5.4 Spatial and Morphological Changes in Transverse Dunes 160
5.5 Conclusion 174
CHAPTER 6 175

CONCLUSION **175**
6.1 Summary of findings 175
6.2 Future Work 178
6.2.1 Chapter 2 – Controls on Dune Scarping 178
6.2.2 Chapters 3, 4 and 5 - Salmon Hole Beach Dynamics 179
APPENDICES **1**
Appendix 1 1
Appendix 2 2
REFERENCES **1**

DECLARATION

I certify that this thesis does not incorporate without acknowledgment any material previously submitted for a degree or diploma in any university; and that to the best of my knowledge and belief it does not contain any material previously published or written by another person except where due reference is made in the text.

Signed.....

Date 20/06/22

COAUTHORSHIP

This PhD thesis is a compilation of a series of journal publications in leading international scientific journals. Chapters 2 - 4 have been written as individual journal papers. At the time of submission two papers were published (Chapter's 2 and 3), one was accepted and in the final stages of copy editing (Chapter 4), and another was undergoing revision and is anticipated to be published presently (Chapter 5).

I am the first author on each journal publication and led and conducted the majority of the research within them, including the final write up and publication of the research.

My supervisors/co-authors have provided ongoing advice, editing, and input which has highly benefited the work found within each paper of this thesis. The papers have also been improved through the peer review process.

ACKNOWLEDGEMENTS

I cannot begin to express how thankful I am to those who have made this thesis a reality. Each step of the way I have had the help of so many wonderful people who I am privileged to have in my life.

I would like to thank my wife Cassie who has worked lovingly and tirelessly to provide for us through my studies and who without none of this would be possible. Thanks Cass; I love you.

To my parents, thank you for your constant love in addition to your support of me and my education. To Grandma, thank you for looking after me once a week for the majority of my studies it was a joy to spend that time with you. To my family, thank you for always being there, your love and support knows no bounds.

To my supervisors, Patrick and Graziela I could not have done it without you. If it wasn't for your examples through my undergrad and honours, I would never have undertaken this PhD. You have both gone above and beyond what I could ever have expected from you. I have enjoyed every moment of transitioning from your student to colleague and friend. I cannot thank you enough for the time you have given me, the kindness you have shown and the fun we have had together.

To Rob, I have lost count of the number of times I have visited your office to ask for advice. You have had so much patience and have been so critical to the success of all my fieldwork and software endeavours. I cannot thank you enough.

Thank you, Martim for your guidance at the beginning of this journey and Marcio for the help you have provided me; your talents will serve you well as you pursue your PhD. Thank you, Thomas, for your assistance with sonic anemometry. To the rest of the BEADS lab, it’s been a blast! I cannot think of a better environment than the coast to study together! Thanks for all the good times.

Thank you to my internal assessors Cathy, Adrian, Eddie, and Howard for keeping me on track.

I would also like to thank Lauren and the Wattle Range Council for all their support over the last few years. The assistance and accommodation that you have provided have been very much appreciated.

And of course, thank you to the organisations that have funded me throughout my candidacy. This work was supported by: 1) Flinders University and the Australian Government Research Training Program Scholarship, 2) The Wettenhall Environment Trust, and 3) The Royal Society of South Australia (RSSA).

Finally, I would like to thank the one who makes all things possible.

SUMMARY

Climate change induced sea level rise and increased storm magnitude and frequency will result in more frequent coastal erosion through scarping (Psuty and Silveira, 2010; Maximiliano-Cordova et al., 2019). Scarping occurs when foredunes and other dunes situated foremost at the coast are partially eroded by waves, generally during periods of high-water level (Carter et al., 1990; Sallenger, 2000; Hesp, 2002; Pye and Blott, 2008; Splinter and Palmsten, 2012; Houser et al., 2018). This thesis specifically investigates the effect an increase in scarping will have on complex coastal embayment's with limited to no sediment supply. The study uses Salmon Hole, located near Beachport, South Australia, a rapidly eroding headland bay beach system, backed by a heavily eroded dunefield and partially protected by an aeolianite reef as a proxy for how similar systems will be affected into the future. This PhD addresses four key components of scarping and the erosion at Salmon Hole to gain insight into this question.

Firstly, the controls that dictate the degree of spatio-temporal change to foredunes following scarping are reviewed. A new conceptual model summarising the key controls and their relationship/significance to the magnitude and extent of scarping is presented. Water level height and duration is found to be the most significant control. The effects scarping has after the initial erosion event are discussed and include moderate changes such as the foredune translating landwards to large change such as the transition of an entire dune system into a new transgressive dunefield phase.

Secondly, the progress, dynamics and cause of the erosion at Salmon Hole were analysed in detail by examining historical shoreline change and the processes driving it. This was primarily achieved using historical aerial imagery and shoreline change statistics. Findings show that a combination of the formation of the 'lagoon' between the mainland/dune system and the offshore reef and the resultant breakthrough of the tombolo that have led to the acceleration of the erosion processes

seen at Salmon Hole. The formation of the lagoon initiated a divergent evolution that continues in the form of a significant geologically controlled longshore current and terminal rip that enhances removal of sediment during and following erosion of the beach and dunes.

Thirdly, flow dynamics over the steep scarp at Salmon Hole with a larger, higher and longer stoss slope than previously studied were observed through a wind flow experiment. The scarp slope is comprised of segments of varying slope angles that have a significant impact on flow dynamics over the dune. Wind flow dynamics observed include percentage speed up, fluctuations in turbulence, topographic steering, flow expansion and a leeward reversing vortex.

Finally, unique subaqueous transverse dunes found lined perpendicular to the shore in the Salmon Hole lagoon were studied for the first time using bathymetric surveys, orthomoasics, oblique aerial imagery and current meter data. The morphology of the dunes changes seasonally with fluctuations in wave energy and current speed transitioning the dunes between being narrow, asymmetric, and transverse to wide and symmetric.

The four components of this study demonstrate that a lack of sediment delivery back to the beach and thence to the dune between storm events results in the inability for dune recovery or much translation (small blowouts do occasionally form in the dune crest) and that this will result in similar sandy coastlines and dunefields being removed with increased erosion due to climate change.

LIST OF FIGURES

Figure 1: Sequence of scarping by high energy storm waves and swash at Post Office Rock, South Australia. Photographs A to C taken 1 second apart. Note the subsequent slope failure and collapse in D. 13

Figure 2: Examples of foredune scarps from (A) small (1m high, with some post-scarp fill and echo dune), (B) moderate (8m high), to (C) large (20m high) (top to bottom). The ability of the foredune to recover and the subsequent stability is generally lower as the scarp height increases. 17

Figure 3: Degree of scarping determined by the height of water level reached during an erosion event. Generally, all other factors being equal, the greater the water level height at the backshore, the more significant the erosion. 18

Figure 4: Level of scarping determined by original height and volume of the foredune impacted by increasing water level heights. Smaller foredunes may eventually be overwashed or removed as water level increases as indicated in the bottom right box. 20

Figure 5: Ecomorphological types of foredunes (modified from Hesp, 2000). Types 1 and 2 are potentially less susceptible to scarping due to ample vegetation cover and greater stability. Types 3, 4 and 5 become morphologically complex as vegetation cover decreases and hence more susceptible to erosion/inundation by scarping and overwash, and subsequent greater instability. 22

Figure 6: Two foredunes with significantly different morphologies and vegetation cover. In (A) vegetation cover is sparse resulting in minimal resistance to scarping compared to the dense vegetation cover in (B). Prince Edward Island, Canada (A), and Northern NSW, Australia (B). 25

Figure 7: Degree of scarping determined by the degree of vegetation cover on the foredune. The greater the vegetation cover the less erosion via scarping will occur. Root density and rooting depth are also important. 26

Figure 8: Image of (A) a foredune scarp in Tasmania showing the high density and considerable depth of *Ammophila arenaria* (marram grass) root mass vertically through the dune, compared to (B) the quite limited root mass and rooting depth in a dune covered in *Lepidosperma viscidum* at Wyomi Beach, SE Australia. A is roughly 1 meter high whilst B is ~2 meters. 28

Figure 9: A reduction in root mass, rooting depth and density will lead to an increase in scarping extent due to a loss of structural stability and the reduction of cohesion in the sediment. These attributes will vary depending on species type as shown. 28

Figure 10: (a) large and small woody debris on the backshore and inlaid in the foredune at Otaki, New Zealand. (b) Extensive seagrass wrack on the beach at Cape Jaffa, South Australia. 31

Figure 11: Significant alongshore foredune morphological variability produced by large rips creating an alongshore variation in the degree of dune scarping, French Atlantic coast (Photograph courtesy B. Castelle). 33

Figure 12: Example of dune migration and the formation of blowouts at Post Office Rock located near Beachport, South Australia. The scarp is 15 m high at the point where the person (in red jacket) is standing in (A). 36

Figure 13: Blowouts and parabolic dunes forming within and cannabalising relict parabolic dunes at the top of a destabilising scarp at Great Beach, Point Reyes, S. California. 38

Figure 14: A conceptual model of scarping controls demonstrating the effect a high and low level of each control has on producing a larger or smaller degree of foredune scarping. The solid arrows indicate a larger degree of scarping and dashed arrows smaller. 44

Figure 15: Salmon Hole study site situated near Beachport SE South Australia (image from 2013). The reef which extends across the bay is semi-exposed at low tide as shown in this image. A prominent scarp may be observed along the dune edge. An artificial rock 'tombolo' is present at the northern margin of the bay. The beach originally reached the seawards edge of the exposed reef in 1946. 50

Figure 16: Aerial image of Salmon Hole taken in 1946 (left panel) and in 2016 (right panel). Severe erosion and development of a lagoon has occurred at Salmon Hole. 54

Figure 17: Grid point (in red circle) used for significant wave height data due to its proximity to Salmon Hole at 37.4881° S, 140.0133° E (star). 60

Figure 18: Topographic survey lines set up by the State Department of Environment and Water and utilised to conduct repeat surveys of the dunes and bay. 61

Figure 19: Shoreline change at Salmon Hole from 1946 to 2019 overlaid on a 2013 orthorectified aerial image. The shoreline was located on the edge of the reef in 1946. 63

Figure 20: Shoreline variability in decadal intervals from 1946 to 2019 at Salmon Hole overlaid on a 2013 orthorectified aerial image. 64

Figure 21: (Top) Transect positions, shoreline intersection points and given numbers overlayed on image of Salmon Hole and Pleasant Cove. This figure also shows the Linear Regression Rate (LRR) for all shorelines. The LRR provides a rate of erosion statistic that includes all the shorelines by fitting each intersection point of the transect with a least-squares regression line. The linear regression rate is the slope of that line. (Bottom) Linear regression rate (LRR) measured in meters per year for each transect from north to south. Transects 1-9 are from Pleasant Cove and 10-31 are from Salmon Hole. A clear pattern of overall accretion at Pleasant Cove versus overall erosion at Salmon Hole can be identified between 1946 and 2019. 65

Figure 22: Sequence of shoreline erosion and lagoon development behind the reef of Salmon Hole between 1946 and 1999. Note that in 1946 the beach was attached to the landward margin of the aeolianite reef, whereas by 1999 a significant lagoon had been formed behind the reef. The yellow arrow in the 1946 image shows waves are opening up the lagoon on the southern end of the reef. The erosion can be seen to begin from this end and then extend into and along the modern-day lagoon over time. The yellow arrows in the 2016 image show the propagation of wave energy into the lagoon. This helps to drive a current around the bay even under small wave conditions and has resulted in the development of subaqueous transverse dunes. 67

Figure 23: Time series showing erosion and accretion in meters between 1999 and 2009. Including transects 9 and 10 (either side of the tombolo) and transect tombolo which is a transect drawn at the tombolo on the Salmon Hole side as shown in Figure 10. A correlation between erosion at Salmon Hole and accretion at Pleasant Cove can be seen during the breakthrough of the tombolo. 70

Figure 24: Natural tombolo break through and artificial tombolo implementation sequence between 1999 and 2016. The location of the tombolo transect is indicated in the 1999 image. 71

Figure 25: Average Hs for each month for the years between 1979 and 2019 that have at least one monthly average Hs in the top 3%. A (top panel) shows years between 1979 and 2003; B (bottom panel) shows years from 2004 to 2019. Raw data source: European Centre for Medium-Range Forecasts. 73

Figure 26: Profile 710027 located in the middle of the embayment. Significant levels of erosion can be seen particularly between 2002 (grey) and 2017 (orange). Sea is to the left. The dune is rapidly becoming smaller as erosion continues and no sediment is supplied between storm and erosion events. 75

Figure 27: Comparison of profiles taken from DSM's created from drone surveys undertaken on the 28-8-17 and 15-2-19. 6 profiles have been drawn along the scarped dune including areas of interest such as differing stages of blowout formation. 77

Figure 28: Oblique angle of DSM's of Salmon Hole created though drone surveys and Pix4D photogrammetry software. Surveys from 28-8-2017, 15-2-2019, and 16-5-2020 are shown. Both the survey from 2017 and 2020 show recent scarping at the base of the dune in contrast to the summer survey in 2019 where lack of storm activity has led to a completely avalanched profile. Blowout depositional lobes on the dune scarp crest have increased in size from 2017 to 2020. 78

Figure 29: Key periods of change and their corresponding erosion rate in m/yr. Increase erosion can be seen as the lagoon expanded and once the tombolo was breached. 80

Figure 30: Swash entering a blowout during a storm at Salmon Hole 17/7/18. 88

Figure 31: Model demonstrating the development of the coastal system at Salmon Hole. Wave energy propagating over the reef on the right-hand side of the bay has led to this side of the bay eroding first as seen in the 1975 depiction. The angle of the reef causes wave energy to produce a south to north current flowing around the bay producing further erosion and revealing more of the reef on the left-hand side of the bay. A rock-controlled rip running parallel to the left headland transports sediment seawards out of the bay. Eventually the dunefield may be completely eroded and the sea will break though into the Pool of Siloam and create a new embayment (2050 future). 90

Figure 32: 2013 aerial photograph of the Salmon Hole study site situated near Beachport, SE South Australia. The scarp has been formed on the seaward face of a relict transgressive dunefield. Yellow arrow indicates experiment location. 103

Figure 33: Aerial image taken in 1946 (on the left) in comparison with an image taken in 2016 (on the right). Salmon Hole has undergone severe erosion whilst the bay to the north has accreted. The transgressive dunefield was more active in the 1940's with significant areas of active, mobile dunes at that time. 104

Figure 34: Digital Surface Model (DSM) of the scarped dune at Salmon Hole created via a drone survey undertaken on the day of the experiment. Anemometer positions are indicated by markers with 3D only positions represented by blue circular markers, 2D and 3D positions designated with red diamond markers and the green triangle on the beach showing the position of the reference anemometer. The toe of the backshore is located at the first blue marker. 105

Figure 35 DSM of the scarped dune at Salmon Hole created using a drone survey undertaken on the day of the experiment. The blowout depositional lobe can be seen on the lee slope of the dune. Anemometer positions are indicated by markers with 3D only positions represented by blue circular makers, 2D and 3D positions designated with red circular markers, and the green marker on the beach showing the position of the reference anemometer. 105

Figure 36: Experimental set up looking downslope from the 18 m mark. 108

Figure 37: A) 1-minute averages of total wind speed in m s^{-1} (solid line) and wind direction in degrees (True North, dotted line) from the reference 3D ultrasonic anemometer 3D1 positioned on the beach at 2.2m high. Measurements were taken between 9:02am and 12:34pm as indicated on the x axis. B) 1-minute averages of total wind speed in m s^{-1} (solid line) and wind direction in

degrees (dotted line) for the experimental period from the Robe Airport weather station. 111

Figure 38: A) One-minute averages of wind direction from 3D anemometers at positions 2, 6 and 9 situated at a height of 40 cm above the bed. 3D2 is located at the toe of the dune, 3D6 is approximately at the mid-way point, and 3D9 near the crest. Topographic steering caused flow to turn more crest normal toward the crest whilst streamline compression has resulted in less variation in direction up the slope. B) One-minute averages of wind direction from 3D anemometers at positions 2, 9 and 10 situated at a height of 40 cm above the bed. 3D2 is located at the toe of the dune, 3D9 near the crest and 3D10 at the crest. Topographic steering caused flow to turn more crest normal toward the crest whilst streamline compression has resulted in less variation in direction up the slope from 3D2 to 3D9. However, there is a distinct increase in variation in wind direction at the crest. 113

Figure 39: One-minute averages of wind velocity from 3D anemometers at 40 cm above the bed at 3m up-slope intervals over the dune. 114

Figure 40: Percentage mean velocity ($u/u^{2.2}$) from 9:02am to 12:34pm for each anemometer relative to a reference anemometer at 2.2 m on the backshore during predominantly oblique incident winds. The orange line indicates the foredune topography. Percentage velocity initially decreases at the base of the dune and then rapidly increases as topographic forcing creates speed up the dune. Once the crest of the dune is reached the percentage velocity drops significantly. 115

Figure 41: Flow speed and direction for more oblique, average, and more perpendicular incident winds. Positions of 3D anemometers are indicated by triangles. Arrows indicate average direction and arrow size indicates percentage speed. 118

Figure 42: A) Average percentage velocity ($u^{2D}/u^{2.2}$) recorded at position 8 and position 9 from 9:02am until 12:34pm relative to a reference 3D anemometer at 2.2 m height in the backshore during mostly oblique incident winds. B) Average percentage velocity ($u^{2D}/u^{2.2}$) recorded at position 8 and position 9 from 9:02am until 12:34pm relative to a reference 3D anemometer at 2.2 m height in the backshore during mostly oblique incident winds. 120

Figure 43: Averages of standard deviation of wind direction for all data from 9:02am until 12:34pm. The orange line indicates the foredune topography. The standard deviation remains relatively consistent dropping gradually as height increases and then significantly increases at the crest. 121

Figure 44: Total average coefficient of variation of wind speed from 9:02am until 12:34pm. The orange line indicates the foredune topography. The coefficient of variation in wind speed steadily drops as speed up occurs over the dune. There is a sudden increase at the crest indicating strong turbulence. 122

Figure 45: One-minute averages of the standard deviation of wind speed from 3D anemometers at 40 cm above the bed at 3D2 and 3D9. 123

Figure 46: A) One minute average coefficient of variation in wind speed from 3D anemometers at 0.4 m above the bed at 3m intervals over the dune. B) One minute average coefficient of variation in wind speed from 3D anemometers at 0.4 m above the bed at 3m intervals over the dune. 124

Figure 47: A) The smoke hugs the surface on the steep portion of the slope where negative W is higher and speedup at a maximum. Flow expansion due to the change in slope at postion 8 is portrayed in the vertical expansion of the band of blue smoke. B) View of the upper slope

comprising anemometers atpositions 8 and 9. The smoke spreads vertically with a change in slope indicating flow expansion. 125

Figure 48: Reversing vortice on the lee side of the dune crest observed using smoke cakes. Flow in A indicates that at times strong downward and oblique gusts interact with the lee slope and the reverse flow is fluctuating and moving across-slope. In B through to D the surface flow is separated and flowing upslope against the incident flow indicated by the pink smoke. 127

Figure 49: Flow separation vortice made visible by the yellow smoke. 127

Figure 50: Georectified historical aerial imagery of the growth of the blowout. The blowout has expanded between 2010 and 2019. 129

Figure 51: A) The flow dynamics revealed by the smoke 1 – Surface flow compression 2- Flow expansion and 3- Flow separation. B) flow dynamics over the scarp responsible for changes in wind speed, direction and turbulence over the scarp. Inset: Figure 40 showing percentage speed up the scarp is for comparison. 133

LIST OF TABLES

Table 1: Acquisition date of imagery used in analysis along with associated data including source, type, pixel size, original image scale, total RMS and RMS error in meters. 55

Table 2: DSAS statistics descriptions.....58

Table 3: Volume analysis for profiles (column A) undertaken in 2001, 2009 and 2017. The base datum for volume calculations was 2 m AHD. Columns B, C and D show the profile volumes for each year. The volumes loss at each profile between these years is presented in columns E, F and G. 76

Table 4: Height above mean sea level, distance from the toe of the dune up the profile and the slope angle for each anemometer position. 106

Table 5: Average wind speed, percentage speed-up, and average direction for winds during the entire recording period, when the reference wind direction was more oblique and when it was more perpendicular. 116

Table 6: Positions of the loggers along with the time in which they were positioned, reset, and then taken out, the sensor and water depth at these times and the overall logging time at each position. 144

Table 7: Comparison measurements for the longest and shortest dunes found in Salmon Hole in the 2013 orthrectified image, the orthomosaic/georeferenced image from 25/07/20 and the orthomosaic image from the 28/10/20. 165

Table 8: Measurements of dunes in similar locations within the bay. Comparisons between the orthomosaic/georeferenced image from 25/07/20 and the orthomosaic image from the 28/10/20. 168

CHAPTER 1

Introduction

1.1 Research Question

Climate change induced sea level rise and both an increase in storm magnitude and frequency are set to amplify coastal erosion (Morton and Sallenger Jr, 2003; Zhang et al., 2004; Castelle et al., 2015; Vousdoukas et al., 2018). Due to their dynamic nature, sandy coastlines will be first to react to this change (Phillips, 2009). To best manage this erosion into the future it is critical to understand the processes involved. Erosion along coastlines backed by dune systems predominantly occurs through the process of foredune scarping, or scarping of the foremost dune where foredunes are absent (Parker, 1975; Bird, 1976; Carter, 1988; Carter et al., 1990; Hanley et al., 2014). Scarping is the partial erosion of the first dune at the back of the beach, typically during highwater levels created by storm surge and/or large waves (Carter et al., 1990; Bird, 2000; Sallenger, 2000; Hesp, 2002; Davis Jr and FitzGerald, 2004; Pye and Blott, 2008; van Rijn, 2009; Splinter and Palmsten, 2012; Suanez et al., 2015; Phillips et al., 2017; Houser et al., 2018; Splinter et al., 2018). Following scarping a dune will generally recover as sediment is brought back to the base of the scarp through hydrodynamic and aeolian processes (Carter et al., 1990; Ruz and Anthony, 2008; Hesp et al., 2013; Ollerhead et al., 2013; Jackson and Nordstrom, 2018). It is this scarping followed by recovery that is thought to be a critical component of the upwards and landwards translation of dunes during sea level rise, as put forward by Davidson-Arnott (2005). As sediment fills in the scarp, it reaches a point where wind flow can then carry it up and over the crest, this in affect heightens the dune and moves it landwards (Hesp, 1988; Bauer and Sherman, 1999; Christiansen and Davidson-Arnott, 2004; Davidson-Arnott et al., 2018). Dunes already act as an important natural defence against seawater inundation of

economically and environmentally significant land (Hanley et al., 2014; Maximiliano-Cordova et al., 2019; Fernández-Montblanc et al., 2020). Sea level rise is going to put increasing pressure on these systems and the upwards and landwards translation of dunes through scarping and recovery is the main mechanism through which coastal dune systems and the protection they provide will be maintained (Davidson-Arnott, 2005; Ollerhead et al., 2013).

This thesis specifically investigates the effect increased scarping will have on sandy coastlines with limited to no sediment supply under climate change conditions. In particular, how will complex sandy embayment's typical of those found along the South Australian coastline react? This study uses Salmon Hole, a rapidly eroding headland-bay beach backed by a heavily scarped transgressive dunefield located in the southeast of South Australia, as a proxy for future shoreline change. Although the erosion here is not primarily driven by sea level rise (as far as we know, as it may be influenced by the past ~150 years of sea level rise), the processes involved in scarping and the effects it is having on the bay and dune system are the same and therefore applicable.

1.2 Research Aims

This thesis will address four key components of scarping and the erosion at Salmon Hole to gain insight into this question. The analysis undertaken varied both spatially and temporally in scale to fully capture the effect that frequent scarping is having on Salmon Hole as an entire system. The flow on effects of scarping are not isolated to the base of the first dune at the back of the beach but rather impact the system as a whole. Therefore, while each component studied can stand alone as a paper, their purpose when combined is to provide a detailed overview of how increased scarping will affect embayment's like Salmon Hole in

their entirety. This is achieved by firstly determining what controls dictate the magnitude of a scarping event. Secondly, by analysing scarping's effect on shoreline position at Salmon Hole both in the past and present as a proxy for the future. Thirdly, by studying wind flow over Salmon Hole's negative sediment budget beach-dune system post-scarping to determine what role scarping plays in dune dynamics and possible dune translation. Then finally, by briefly examining the nature of subaqueous transverse dunes, and where sediment is being transported post scarping within the lagoon which exists between the aeolianite reef enclosing the bay and the beach. These aims are the focus of four chapters (including three published papers) presented in Chapters 2 through to 5.

The first three manuscripts have been published in leading international scientific journals, whilst the fourth is undergoing revision and expected to be published in due course. The specifics of each of these chapters and how they approach meeting these aims is detailed below:

I. Before the mechanisms responsible for the scarping and its effects on the dune system at Salmon Hole could be analysed it was important to have a complete understanding of what controls the magnitude of scarping events. This is achieved in Chapter 2 through the compilation of a systematic review culminating in a new conceptual model. This model illustrates how each of the identified controls effect the scale and degree of scarping magnitude be it positive or negative. These controls include: high water level, beach width, beach gradient/grain size, vegetation cover/rootmass, foredune size/volume, compaction, and large woody debris/beach wrack (Short and Hesp, 1982; Hesp, 1988; Nishi and Kraus, 1997; Pye and Blott, 2008; Coco et al., 2014; Feagin et al., 2015). A better understanding of how each of

these factors effects levels of erosion through scarping is useful for a better understanding of scarp dynamics and will be necessary for managing our coasts into the future. The review also details the secondary effects of scarping such as foredune translation and its impact on the development of blowouts, parabolic and transgressive dune fields. The future consequences of sea level rise and changes to wave climate on scarping are also discussed.

II. Using this knowledge as a basis, Chapter 3 is a study of the ongoing extreme erosion at Salmon Hole. The progress, dynamics and cause of the erosion are analysed in detail by examining historical shoreline change and the processes that have and continue to drive it. This was done using historical aerial imagery, shoreline change statistics, hindcast wave data, drone surveys, photogrammetric software digital surface model (DEM's) comparison and volumetric analysis of topographic profiles. The complexity of the coastal processes at Salmon Hole led to a fascinating study that highlights the multifaceted nature of coastal embayment's with complex geologically inherited features. Salmon Hole is similar to a myriad of rocky headland embayment's backed by dunes systems and fronted by reef found along the South Australian (and many parts of the SW Western Australian) coastline (Short and Hesp, 1982; Short and Hesp, 1984; Short, 2006; 2010). It therefore provides insight into how these systems will react to increased erosion.

III. Once the reasons for the significant and sustained erosion at Salmon Hole had been determined, windflow patterns over the scarp itself are then examined in Chapter 4 through a wind flow experiment. Given the significant role that aeolian processes play in the recovery of a scarped dune it was important to analyse their effect on a scarp in a sediment starved system (Carter et al., 1990; Christiansen and Davidson-

Arnott, 2004; Hesp et al., 2013; Ollerhead et al., 2013; Davidson-Arnott et al., 2018; Jackson and Nordstrom, 2018). The dune at Salmon Hole also provided the opportunity to study flow dynamics over a high scarp with a steep stoss slope that is larger, higher, and longer than previously researched in the literature. The stoss slope was also made up of segments of varying slope angle that can have a significant impact on flow dynamics over the dune. The secondary effects that scarping can have on a dune system were also able to be analysed through the assessment of a blowout that has developed at the dune crest through aeolian processes.

IV. The transverse dunes which occur in the lagoon are then examined in Chapter 5. These dunes are aligned perpendicular to the shore in the bay, and generally have slipfaces or steep lee slopes facing NE. This is the first time that subaqueous transverse dunes have been studied in a small headland embayment. A current meter was positioned in the bay to record speed and direction data in order to help explain current processes in the bay. Bathymetric surveys, drone imagery orthomosaics, and oblique aerial imagery were used to monitor changes in the dunes position and morphology. Given that this study is about what effect coastal erosion will have on sediment depleted/starved coastal embayment's it was important to examine the reason for Salmon Holes lack of sediment supply back to the beach, and where the sediment was being lost from the system. In addition, the subaqueous transverse dunes in the bay were also worthy of study purely because of their relatively unique formation.

1.3 Contribution of this PhD

In researching the erosion at Salmon Hole and using it as a proxy to better understand how increased scarping will affect complex coastal embayment's with limited to no sediment supply, this PhD has made multiple contributions to current knowledge in this area. This research has contributed the following.

I. Chapter 2 is the first review on scarping controls and includes a new conceptual model demonstrating their effects on the magnitude of scarping events.
II. Chapter 3 provides an in-depth understanding of the shoreline change and coastal processes at Salmon Hole. It also clearly demonstrates that sandy coastlines with a deficit in sediment supply or negative sediment supply will be removed through increased coastal erosion in the future.
III. Chapter 4 indicates that the net erosion of the dune system will occur as of a result of wind flow being unable to translate the dune upwards and landwards with sea level rise due to insufficient, or no sediment being returned to the beach between storm and erosion events. It is also the first study of wind flow dynamics over a large, scarped dune slope.
IV. Chapter 5 is the first study of the morphology and dynamics of unique subaqueous transverse dunes in a small coastal embayment.

CHAPTER 2
CONTROLS ON DUNE SCARPING

Published in *Progress in Physical Geography - Earth and Environment:* Davidson, S.G. (80%), Hesp, P.A. (10%) and Silva, G.M.D. (10%) Controls on dune scarping.

https://doi.org/10.1177%2F0309133320932880

2.1 Abstract

As sea levels rises and climate changes, dune scarping will become more common. Thus, it is critical to understand what factors contribute to the magnitude of scarping, and what effect this has on dune systems in order to better manage coastal erosion into the future. Scarping occurs when foredunes are partially eroded by waves, generally during periods of high-water level. The controls on the degree and magnitude of scarping examined include water level, foredune vegetation cover and species present, plant root mass, height and volume of the foredune, the original foredune morphology, surfzone-beach type, and compaction of sediment. Water level is the most significant control, in particular, the height it reaches and the duration for which it stays elevated, as this determines the elevation at which wave action can erode the dune and therefore the extent of scarping and dune volumetric loss. Higher plant density, greater rooting depth, high root mass, and greater compaction aid in reducing the degree of scaping. The presence of large woody debris and wrack may also influence the degree of scarping. The effects scarping has on the morphology of a foredune after the initial erosion event can range from small changes (e.g. minor, small scarps and slight slumping), to moderate changes such as the foredune translating landwards, to large change such as the transition of an entire dune system into a new transgressive dunefield

phase. A new model summarising the key controls and their relationship/significance to the magnitude and extent of scarping is presented.

2.2 Introduction

The purpose of this paper is to review the controls that affect the degree of spatio-temporal change to foredunes following scarping, with a focus on the morphological behaviour of foredunes during and after scarping. Key factors that determine the extent and magnitude of scarping are examined in detail and summarised in a new model. The hydrodynamic processes involved in producing dune erosion and scarping are specifically not examined, see e.g. (Edelman, 1969; Van Thiel de Vries et al., 2007; Davidson-Arnott, 2010; Sancho et al., 2011), and, apart from brief comments, nor is overwash. In addition, this review does not cover the general geomorphology of foredunes (see Hesp (2002) for a review).

The significance and importance of coastal dune systems is well known (Arens, 2001; Ruz et al., 2009; Hanley et al., 2014). Coastal sand dunes, and particularly foredunes, act as a protective barrier on many of the world's coastlines (Carter, 1991; Simm et al., 1996; Doody, 2012; Maximiliano-Cordova et al., 2019) and hence are an important natural defence against inundation by seawater of economically and environmentally significant land, infrastructure, and activities (Hanley et al., 2014; Maximiliano-Cordova et al., 2019; Fernández-Montblanc et al., 2020). They are also intrinsically areas of high ecological significance themselves, as well as sources of raw materials, grazing land and recreation (Martínez et al., 2007; Everard et al., 2010; Doody, 2012; Hanley et al., 2014). In order to function as a successful defence, coastal dunes must endure storm damage and erosion (Roelvink et al., 2009; Hanley et al., 2014). Therefore, there is a large amount of interest in the drivers that control dune erosion and accretion as they can dictate the response to, and

interactions of coastal sand dunes with the beach and nearshore (Davidson-Arnott, 2005; Saye and Pye, 2007; Pye and Blott, 2008; Castelle et al., 2015; Masselink et al., 2016; Castelle et al., 2017; Maximiliano-Cordova et al., 2019), and dictate the degree of resilience of coastal dune systems (Houser et al., 2015).

One of the principal ways in which foredunes change and evolve is via wave-driven scarping. Foredune scarping is often an important part of the surfzone-beach-dune interaction process for supplying sediment to the surfzone and nearshore during storms, and also as a mechanism that allows the foredune to grow in height and translate landwards as scarps recover (Carter et al., 1990; Hesp, 2002; Davidson-Arnott et al., 2018).

As we move forward under a scenario of climate change and sea level rise, it is critical to have an understanding of the processes involved in scarping and the effect it has on coastal dunes systems, as sea-level rise and increased storm activity leads to more wave-driven dune erosion (De Winter and Ruessink, 2017; Maximiliano-Cordova et al., 2019). It is paramount that we understand the mechanisms and processes involved in how dunes respond to scarping if we are to successfully manage our coasts into the future. Foredunes (and other dune types that exist behind the backshore) offer a natural buffer for mitigating sea level rise to various extents, but we do not yet fully understand or appreciate the degree of control that various factors including water level height (Guisado-Pintado and Jackson, 2018), tidal state (Guisado-Pintado and Jackson, 2019), height and volume of the foredune (Splinter et al., 2018), vegetation density and distribution (Silva et al., 2016), root mass (Bryant et al., 2019), compaction of sediment (van de Graaff, 1994; Hanley et al., 2014), the original foredune morphology (Christiansen and Davidson-Arnott, 2004; Hanley et al., 2014) and surfzone-beach type (Hesp, 1988; Masselink and Short, 1993) play in increasing,

decreasing or mitigating dune erosion. This review attempts to provide a first pass at assessing these various controlling factors and their importance.

The following review comprises six sections: (1) a summary of foredune scarping (2) a review of the controls on the degree of scarping (3) the effects of scarping; (4) future impacts of climate change and sea level rise on scarping processes; (5) a new model based on a synthesis of the current literature depicting the effect key controls have on the extent of scarping; (6) conclusion and suggested areas for further research.

2.3 Foredune Scarping

Dunes, beaches and surfzones are in a continuous state of dynamic equilibrium continually being changed by tides, waves, currents and climatic factors. This results in the reworking and exchange of sediment between the offshore, nearshore and foredune, with scarping playing a major role in this process (Parker, 1975; Bird, 1976; Carter, 1988; Carter et al., 1990; Hanley et al., 2014). Scarping of dunes (i.e. excluding beach scarping) occurs when foredunes (or any dune at the back of the beach) are partially eroded by waves, generally during high water levels, storm surge and/or large wave events (Carter et al., 1990; Bird, 2000; Sallenger, 2000; Hesp, 2002; Davis Jr and FitzGerald, 2004; Pye and Blott, 2008; van Rijn, 2009; Splinter and Palmsten, 2012; Suanez et al., 2015; Phillips et al., 2017; Houser et al., 2018; Splinter et al., 2018). High magnitude, low frequency storm events are able to displace large volumes of sediment through scarping, impacting the morphology of the foredune, and altering the coastline (Guisado-Pintado and Jackson, 2018). Scarping can also occur due to high spring tides (Shepard, 1950; Ruz and Meur-Ferec, 2004; Ruz et al., 2009), elevated water levels, as, for example, on lakes due to meteorological effects, and by creeks and washouts on occasion (Fuller, 2002; da Silva et al., 2003; Figueiredo and Calliari, 2006).

Here we focus on coastal foredune scarping as it occurs during high water level conditions (including high tides and storm surges). In the following, when scarping is mentioned, the scarping process will apply to any dune at the back of the beach unless otherwise stipulated.

Foredunes can be severely eroded within a few minutes to hours of storm surge or large waves due to their loose sedimentary structure (Reade, 1881; Nichols and Marston, 1939; Parker, 1975; Carter, 1988; Carter and Wilson, 1990). During storm surges, sea level may be raised from a few cm to up to several meters. For example, a global review of tropical storm surge data sources by Needham et al. (2015) found that in the western North Atlantic low-magnitude surges occur regularly with the coast of China averaging 54 surges >1 m per decade. On the other end of the height spectrum, Needham et al. (2015) found that in the northern Indian Ocean and in the Bay of Bengal five storm surges >5 m are recorded per decade and this included a credible observation of a storm tide level reaching 13.7 m. This can result in high waves reaching the base of the foredune, and often further up the stoss slope (Figure 1). Considerable wave reflection, turbulence, and erosion of the beach, backshore, and base of the foredune, then results in sediment transport (Vellinga, 1982; Aagaard et al., 2004; Zhang et al., 2004). Sallenger (2000) described this level of impact as 'collision' in his storm impact scale. The cliffing/scarping and undercutting is enhanced when the storms occur during high tides (Leatherman, 1979; Hesp, 1988; Thornton et al., 2007), and locally exacerbated for example due to the presence of rip currents (Short, 1979; Wright et al., 1980; Hesp, 1988; Castelle et al., 2017).

Scarping is not the only process that can occur under high water level conditions. After 'collision' on Sallenger (2000) impact scale is 'overwash', and this occurs if the foredune is relatively low, and/or the water level is relatively high, or if the beach slope and the dune

stoss slope have a similar gradient (Leatherman and Zaremba, 1987; Wang and Horwitz, 2007; Figlus et al., 2010; Hacker et al., 2012). Overwash refers to the flow of swash and suspended sediment during high water levels from the beach face to the back barrier or over the top of a foredune into the swale or hinterland/landward of the dunes behind (Fisher et al., 1975; Leatherman and Zaremba, 1987; Donnelly et al., 2006). As the overwash passes over the foredune (or other dune or coastal landform), the foredune itself and potentially additional beach sediment are eroded, transported and deposited as a washover fan or terrace on the lee side of the dune (Leatherman and Zaremba, 1987; Sallenger, 2000; Morton and Sallenger Jr, 2003; Donnelly et al., 2006; Matias et al., 2008; Houser et al., 2018). Dune height and/or volume is critical in determining whether overwash occurs (Leatherman, 1979). For example, pre- and post- storm surveys by Quilty and Wearne (1975) in Australia showed that overwash and backwash generally occur when foredunes were low (3-5m above MSL), whilst higher dunes were more commonly scarped.

Scarping can significantly change the morphology of the foredune both during and after the erosion event (Hesp, 2002; Christiansen and Davidson-Arnott, 2004; McLean and Shen, 2006; Pries et al., 2008). As an example, Figure 1 shows storm swash first running up the scarp (A), then it recedes as backwash (B/C), followed by slope failure and slumping (D). Scarping can occur from direct undercutting of the dune from plunging waves, or as seen in Figure 1 (A to D) when swash uprush and backwash occurs on the face of the dune.

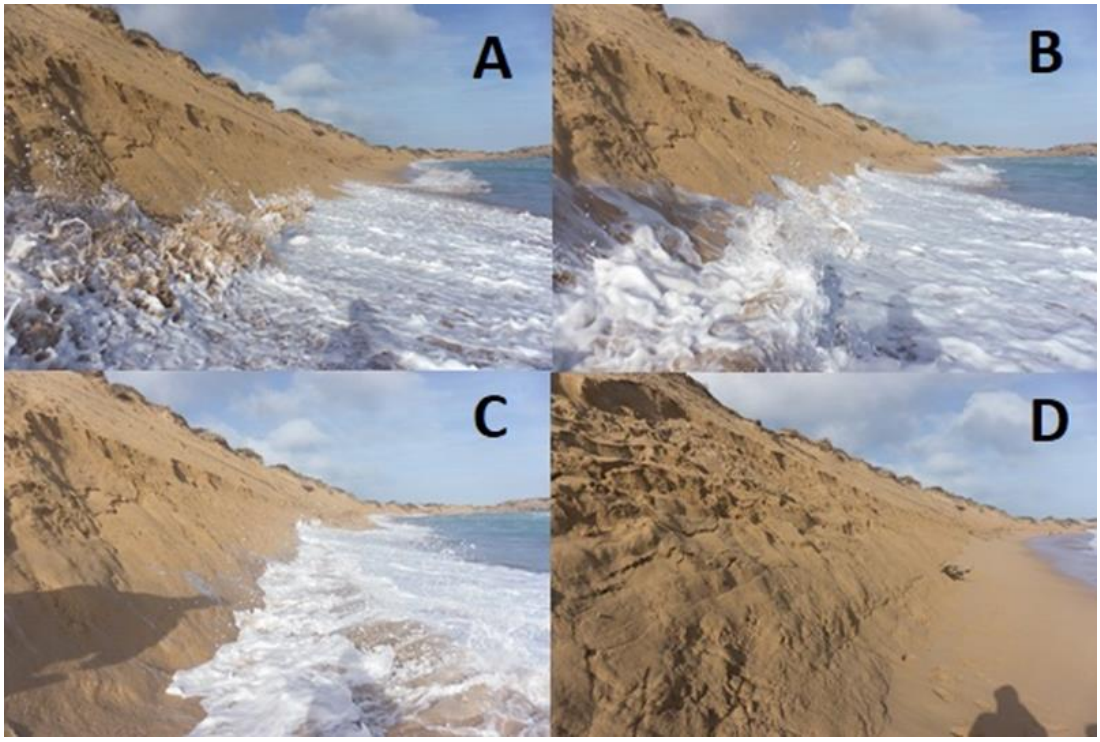

Figure 1: Sequence of scarping by high energy storm waves and swash at Post Office Rock, South Australia. Photographs A to C taken 1 second apart. Note the subsequent slope failure and collapse in D.

Following a storm event, a foredune will occasionally have a homogenous level of erosion across the entire length. However, very commonly this is not so; the response is often more complex as each individual section of foredune differs in both alongshore and cross-shore morphology and is influenced by offshore conditions (Brodie and McNinch, 2011; Guisado-Pintado and Jackson, 2018; Houser et al., 2018), and the presence or absence of rips, bars, subtidal rocky outcrops, and reefs. This alongshore variation can enhance or hinder storm response of certain sections of the beach, allowing greater wave runup in particular sections of beach compared to other sections thus changing the balance between occurrence and degree of scarping, and overwash along a foredune (Pries et al., 2008; Brodie and McNinch, 2011; Houser, 2013; Guisado-Pintado and Jackson, 2018; Splinter et al., 2018). The foredune morphology can also vary in height, volume, and shoreline extent along the beach/coastline

(Thieler and Young, 1991; Hesp, 2002; Houser et al., 2008; Houser and Mathew, 2011; Houser et al., 2018; Splinter et al., 2018). Sections of a continuous but non-uniform foredune can therefore have differing levels of erosion and subsequent post storm recovery, and erosion hotspots are determined by variations in alongshore high water level, wave energy, existing foredune gaps and low-lying areas (Dolan and Hayden, 1981; Suter et al., 1982; Orford and Carter, 1984; Houser, 2013). Scarping alone can lead to a narrowed foredune, potentially leading to overwash during the next high water level event (Hanley et al., 2014). The variability in foredune morphology is often reinforced each storm as overwash goes through the same gaps repeatedly (Buynevich and Donnelly, 2006; Houser, 2013; Weymer et al., 2013; Houser et al., 2018). Hence individual storm events cannot be examined in isolation but rather in a longer temporal context that includes previous wave and water level conditions (Masselink and van Heteren, 2014).

2.4 Controls on the Degree of Scarping

In this review the *degree* a foredune is scarped principally refers to the volume of dune sediment loss. The degree of scarping and associated spatial and temporal changes to foredunes is a function of, or is to various levels controlled by storm attributes, beach/nearshore characteristics, and dune size/volume, morphology, degree of compaction, vegetation cover, root density and presence of large woody debris or beach wrack, acting individually or in various combinations. These controls are discussed individually below.

2.4.1 Water Levels

The degree of scarping and the magnitude of volumetric loss of a foredune can vary enormously as noted above. Scarp heights generally range from <0.1 to 10 meters but can even reach up to 20 meters high (Nishi et al., 1995; Castelle et al., 2015). Figure 2 indicates a

range of examples of scarp heights and volumetric loss. Note that scarp height is not an ideal measure of storm erosion or degree of scarping since a low dune must of necessity have a low scarp, and a large high dune may have a short scarp if three quarters of the dune is removed.

One of the most significant factors effecting the magnitude of spatial and temporal change to a foredune during an erosion event is the height of the mean water level during the storm (Edelman, 1969; Vellinga, 1982; Ruggiero et al., 1997; Coco et al., 2014). This is shown in Figure 3, where three differing water levels 'low', 'medium' and 'high' result in corresponding magnitudes of scarping. The mean water level is driven by storm surge amplitude and duration, seasonal changes in geostrophic currents, wave height, and tide height on top of sea level at any point in time (van de Graaff, 1994; Sallenger, 2000; Weaver and Slinn, 2005; Weisse and Plüβ, 2006; Pries et al., 2008; Pye and Blott, 2008; van Rijn, 2009; Mathew et al., 2010; Suanez et al., 2015; Phillips et al., 2017; Houser et al., 2018; Segura et al., 2018). The duration of a high water level event is also important (Guisado-Pintado and Jackson, 2018). These factors combine to exacerbate wave runup (maximum elevation water reaches for each wave) on the face of the foredune by increasing its vertical reach (Sallenger, 2000). It should be noted that although the height of the water level is paramount it is the relative height to the toe of the foredune that is the critical factor (Suanez et al., 2015). Assuming a dune of homogeneous height, and other factors (discussed below) are comparable, the water level determines the height of the scarp produced and volume of sediment eroded (assuming dune size is significant enough to avoid overwashing) (van de Graaff, 1986; Carter et al., 1990; Castelle et al., 2015; Suanez et al., 2015). If these factors above (e.g. tide state, water level) oppose each other, then the degree to which the

foredune is scarped can be drastically different. For example, if the peak period of storm surge or wave height coincides with low tide then the level of scarping will be significantly less, particularly in an area that has a large tidal range as the water level will no longer be high enough to reach the toe of the foredune (Guisado-Pintado and Jackson, 2018).

Guisado-Pintado and Jackson (2019) demonstrated this when examining two storm events, Ophelia in 2017 and Storm Hector in 2018 off the coast of NW Ireland. During storm Ophelia, 2 m wave heights coincided with a low tide resulting in minimal erosional impact and the dune toe only being slightly scarped as shown under the 'low' water level scenario in Figure 3. Storm Hector was a comparatively lower energy event, yet the resultant scarping was significantly greater due to the synchronisation of both a spring high tide, high waves and onshore wind as show in the 'high' water level scenario in Figure 3.

Castelle et al. (2015) examined extreme scarping along the Gironde coast in SW France. The main cause of this large-scale erosion was a 2-month stormy period during the 2013/2014 winter where the average wave height exceeded 3.6m, reaching up to 9.6m at its peak. This type of erosion corresponds to the 'high' water level section of Figure 3 and resulted in scarps over 10m high and across-shore erosion of 20-30m in some areas. Only the last in the sequence of 4 storms occurred during a spring high tide of 5m, whereas the other storms all occurred for tidal ranges less than 3m. Castelle et al. (2015) state that if the other 3 storms had been contemporaneous with spring tides as well, then both the scarp height and dune retreat would have increased significantly. There were, however, locations along the Gironde coast where the size of scarps was smaller due to protection from highwater levels by 3-5 m-high paleo-soil outcrops in the upper part of the beach. This protection results in a smaller scarp due to a 'low' water level reaching the base of the dune as shown in Figure 3.

Suanez et al. (2015) monitored both erosion and accretion at Vougot beach, France between 2004 and 2014. They analysed how the foredune changed both in position and morphology after each erosional extreme water level event. They found a good correlation (R^2 0.85) between scarping and high-water level events. However, this was only if the water level height exceeded the toe of the foredune.

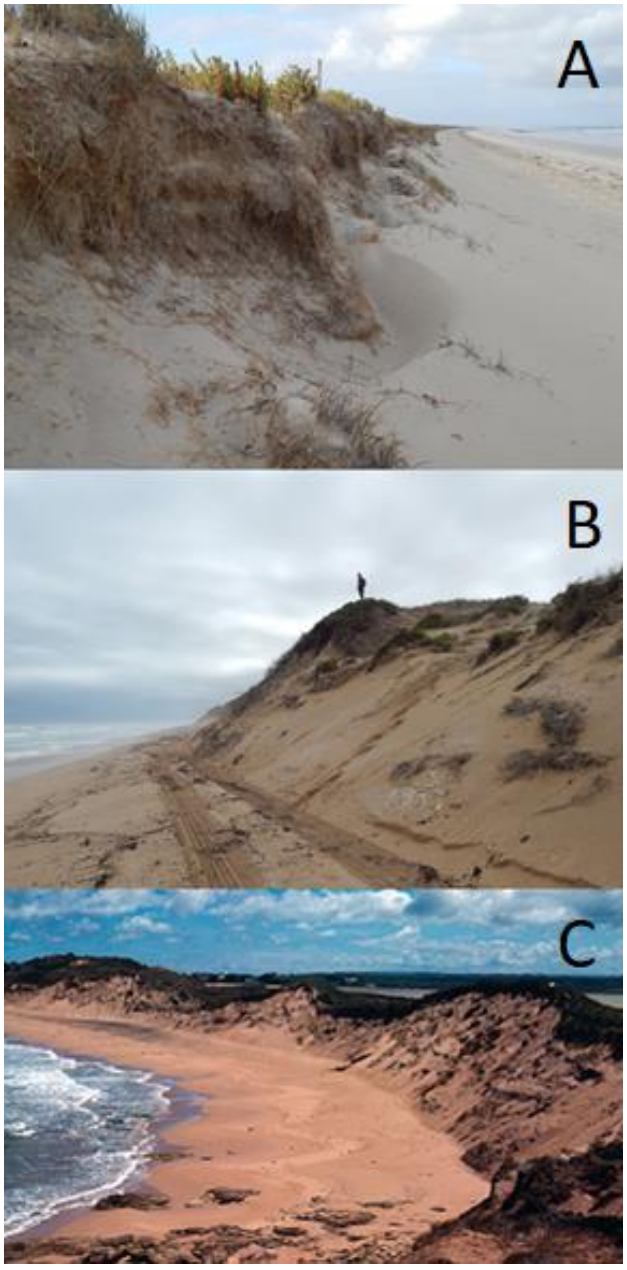

Figure 2: Examples of foredune scarps from (A) small (1m high, with some post-scarp fill and echo dune), (B) moderate (8m high), to (C) large (20m high) (top to bottom). The ability of the foredune to recover and the subsequent stability is generally lower as the scarp height increases.

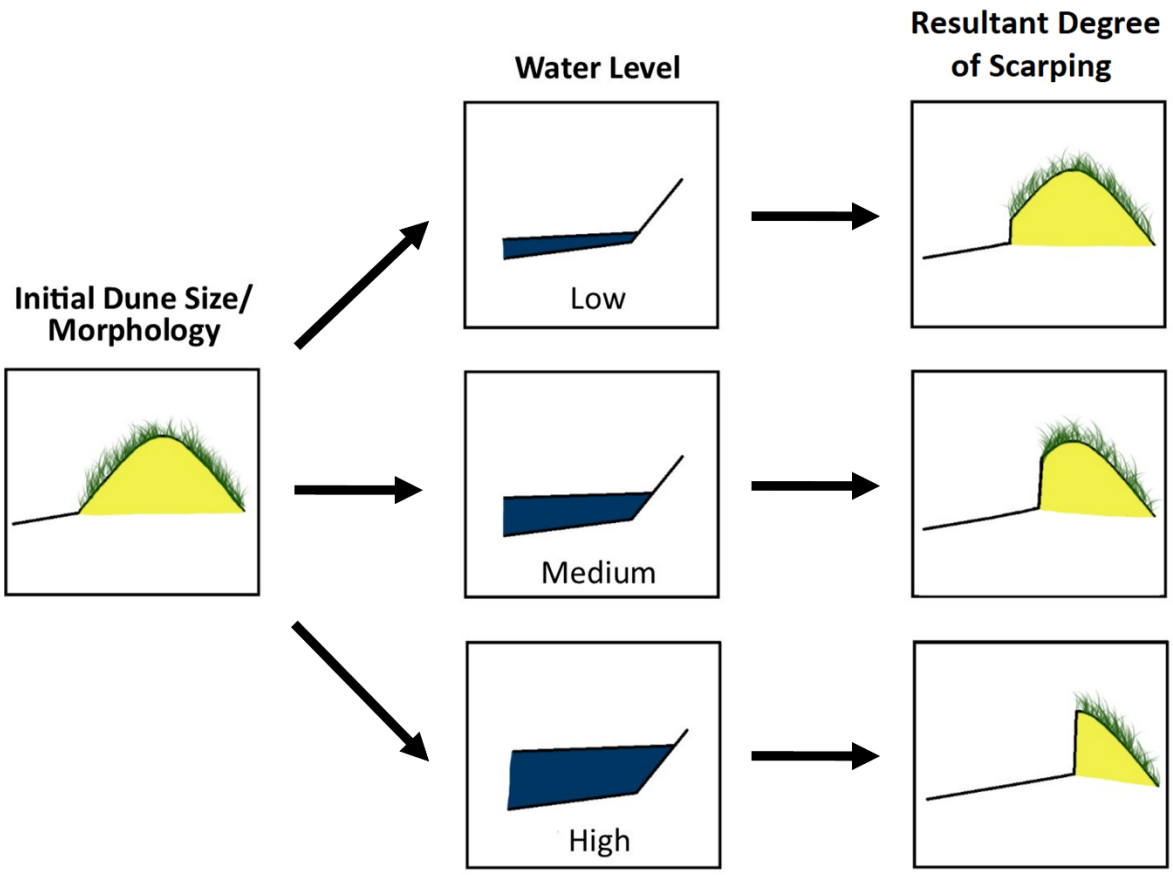

Figure 3: Degree of scarping determined by the height of water level reached during an erosion event. Generally, all other factors being equal, the greater the water level height at the backshore, the more significant the erosion.

2.4.2 Height, Volume and Original Morphology of the Foredune

The scale to which varying water levels during storms impact a foredune changes depending on the original height and volume of the foredune (Hesp, 1988; Sallenger, 2000; Pries et al., 2008; Hanley et al., 2014; Feagin et al., 2015; Houser et al., 2018; Splinter et al., 2018), as well as on other factors discussed below (Figure 4). The larger and higher the foredune, the greater the potential for a large scarp. However, a large foredune does not always equate to a considerable scarp as this is dependent on the water level as noted above, and the volume of sand required by waves to establish an equilibrium condition. For a given water level height, the volumetric loss should be similar whether the foredune is large, medium or small. However, the effect of extremely highwater levels can be very significant, as a large

dune will still be severely scarped but a small dune may be overwashed or even eroded completely ((Edelman, 1969; Morton, 2002; Morton and Sallenger Jr, 2003; Houser, 2013; Masselink et al., 2016; Bateman et al., 2018); Figure 4)).

Pries et al. (2008) studied the effect that foredune height and width played on barrier island resilience due to hurricane storm surge and wave attack. They compared foredunes along Santa Rosa Island, in the Gulf of Mexico both before and after hurricanes Ivan (2004) and Dennis (2005). Before hurricane Ivan, small foredunes (<0.25 ha) comprised 86.1% of the foredunes analysed. After Ivan 62.3% of the original foredunes were completely destroyed with 71.9% of total foredune area removed. Those foredunes left behind were the widest and tallest. This is demonstrated in the 'high' water level component of Figure 4 where smaller dunes are overwashed or eroded completely whilst larger dunes are severely scarped. Due to the extreme nature of the erosion, Pries et al. (2008) also analysed the erosion that occurred to the secondary (or more landward) dunes behind the foredunes. Smaller secondary dunes lost on average 42.1% of their total area whilst larger dunes lost on average of 14.8% of their total area. This is demonstrated in the 'low' to 'medium' water level section of Figure 4 where the volume loss is similar for each dune size, but the impact and significance of the erosion is very different.

Note that for a given dune, scarp height will vary considerably depending on the degree of volumetric loss. For example, a 10m high symmetrical foredune could have a 10m high scarp if erosion occurred to the point where exactly half the dune was removed. However, if more of the dune was removed, then the scarp becomes progressively lower as the scarp is then forming in the landward lower lee slope.

The potential for morphological change and instability of the foredune increases with an increase in dune height or scarp extent (Hesp, 1988a; Figure 2). The larger the scarp created, the more likely the occurrence of dune crest failure and blowouts forming due to greater instability and a longer recovery time. In addition, there is significantly greater wind velocity speedup over a higher stoss slope compared to a smaller one (Arens et al., 1995; Hesp et al., 2009; Hesp and Smyth, 2016). This can then potentially lead to the breakdown of the foredune and the formation of parabolic and transgressive dune fields (Hesp, 2013).

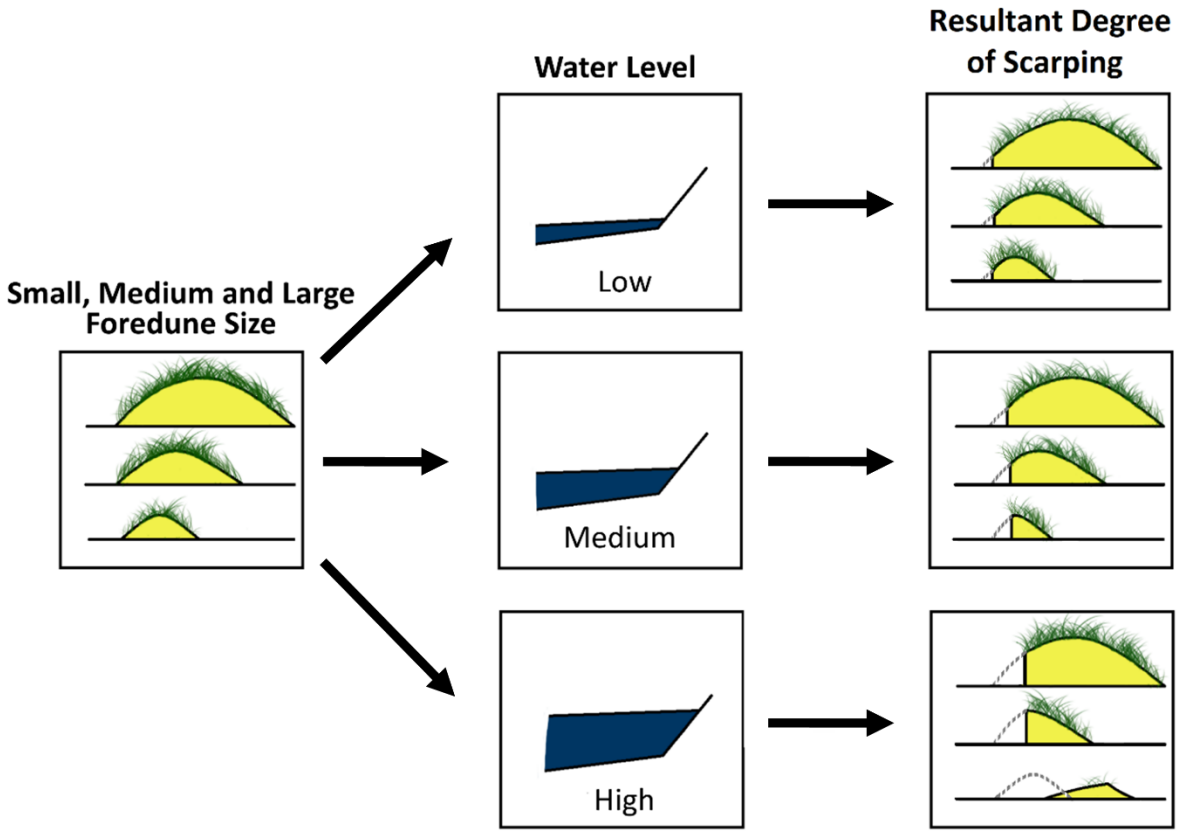

Figure 4: Level of scarping determined by original height and volume of the foredune impacted by increasing water level heights. Smaller foredunes may eventually be overwashed or removed as water level increases as indicated in the bottom right box.

The initial profile and morphology of the foredune plays a role in determining the magnitude of scarping (van de Graaff, 1986; Pye and Blott, 2008). Foredunes are commonly

not uniform across- or alongshore, and exhibit variability in height, volume and landward extent (Houser, 2013). Foredunes can be classified into 5 morpho-ecological types as defined by Hesp (1988), each potentially responding differently to erosion (Figure 5). From type 1 to 5, vegetation cover decreases and the morphology of the foredune becomes more complex (Hesp, 1988). Therefore, under the same water level conditions, and similar beach and nearshore morphology, type 1 and 2 foredunes, described by Hesp (1988) as having simple undulating topography, being laterally continuous and very well to well vegetated, will be scarped to a less degree compared to a type 3 foredune. Following wave scarping, stage 1 and 2 foredunes are likely to have a mostly uniform scarp. Hesp (1988) states that type 3 foredunes are characterised by a hummocky topography. They display a 45-75% vegetation cover, and contain small to moderate size blowouts, concave vegetated stoss faces, irregular crests and semi – distinct ridges and knolls. Their limited level of vegetation compared to type 1 and 2 foredunes potentially leads to less resistance to scarping and a higher degree of erosion than types 1 and 2 under the same high-water level conditions. However, it is also likely that the variability in along shore morphology will lead to overwash occurring through the low-lying areas of the dune whilst the higher vegetated areas are scarped. This was shown to be the case by Houser (2013) through use of computer modelling. By adding small variations in height along the length of an otherwise uniform foredune, overwash channels were created. This increased the along shore variability in dune height and post storm morphology as well as made the dune more susceptible to further change under the next high-water level conditions. Type 4 foredunes contain moderate to large scale blowouts, pronounced topographic variability, partial vegetation cover and sand sheets. Type 5 foredunes are remnant (erosional) knobs. They contain large deflation basins, blowouts, sand sheets and have minimum vegetation cover (Hesp, 1988;

2002). Type 4 and 5 foredunes are less vegetated than the first three types and therefore potentially more susceptible to inundation and erosion often through overwash, particularly in blowouts and across sand sheets.

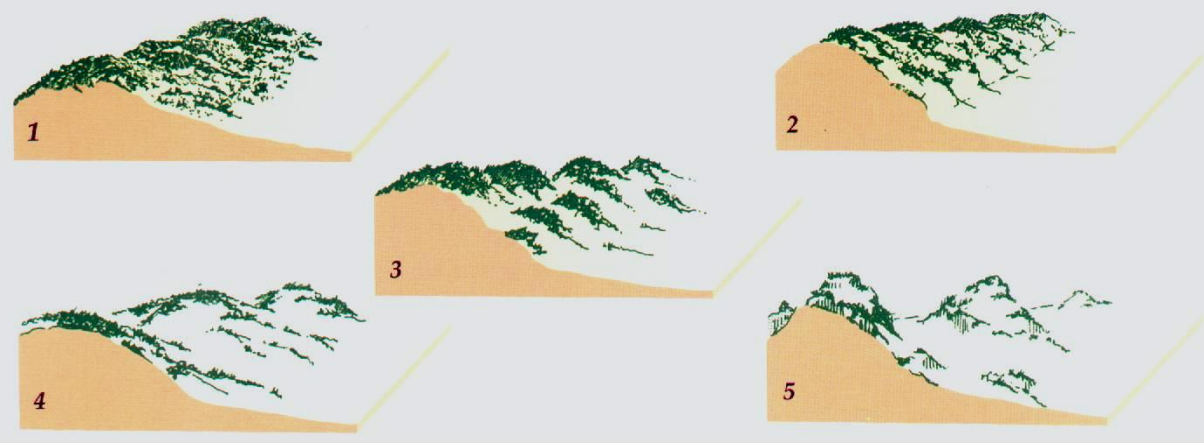

Figure 5: Ecomorphological types of foredunes (modified from Hesp, 2000). Types 1 and 2 are potentially less susceptible to scarping due to ample vegetation cover and greater stability. Types 3, 4 and 5 become morphologically complex as vegetation cover decreases and hence more susceptible to erosion/inundation by scarping and overwash, and subsequent greater instability.

The original steepness of the stoss slope may also be important according to De Winter et al. (2015) as it partially dictates the amount of slumping that will occur during a high-water level event. Slope failure and slumping increases with an increase in the steepness of the dune, and the size or height of the final scarp/failed slope may therefore be greater as the angle of the foredune stoss slope increases.

2.4.3 Levels of vegetation cover, density and rootmass

The degree to which the beach and dune sediments are consolidated by vegetation and their roots also determines scarping magnitude (Hesp, 1988; Doody, 2012; Hanley et al., 2014; Lapetina and Sheng, 2014; Maximiliano-Cordova et al., 2019). Foredune vegetation cover changes significantly depending on the species present as shown in Figure 6. For the same incident water level conditions and foredune morphology, as the vegetation cover on the foredune increases, there is a reduction in erosion levels as demonstrated by various studies (Kobayashi et al., 2013; Silva et al., 2016; Maximiliano-Cordova et al., 2019), and as shown in Figure 7. This is because the presence of the vegetation roots, stems and rhizomes increases structural stability of the dune by binding the sand. In addition, the particle cohesion between the sediment grains is increased due to the presence of organic matter and mycorrhiza (Carter, 1980). It is thought that organic matter potentially also alters the composition of the sediment by increasing the sediment size which results in more friction and, hence, less erosion (Wischmeier and Smith, 1978). During a storm event, the above-ground vegetation stems and leaves modify the flow within the aquatic boundary layer as the mean current is reduced by profile drag and skin friction, resulting in turbulence within the vegetation canopy, thus reducing the swash energy and velocity resulting in less erosion (Bouma et al., 2009) in similarity to aeolian flows in vegetation (Hesp et al., 2019). Friction and turbulence are dependent on the plant height, morphology, strength and density, and degree and depth of root mass of each species (Maximiliano-Cordova et al., 2019). The greater each of these variables is, the less the potential extent of the scarping for dunes of the same volume.

This was shown by Maximiliano-Cordova et al. (2019) in their wave tank study comparing the effectiveness of various dune plant species for reducing scarping. They examined a 1:1

scale artificial dune and covered it with differing combinations of plant species, and they found in each case (bar one) that dune erosion from their simulated “storm waves” was reduced with the addition of vegetation. However, the level of protection against erosion was species -specific and varied over time. They found *Ipomea* species to be the most effective species they tested and noted that this was due to its large carpet like density and deep roots. This is demonstrated in Figure 7 where a relatively high amount of plant cover results in less scarping, and in Figure 9 where an increase in rootmass and density reduce scarping levels. Charbonneau et al. (2017) demonstrated in the field the same principles when examining differences in erosion between two sections of a foredune that were morphologically near identical but differed in percentage of vegetation cover. The section of foredune that was covered in the native *Ammophila breviligulata* was more heavily scarped after Hurricane Sandy than the section comprising the invasive species *Carex kobomugi. Carex Kobomugi* had a much higher density and a more extensive root system.

It must be noted, however, that the effectiveness of vegetation in limiting erosion and scarping is dependent on the size of the dune, and species present. For example, root penetration will generally be confined to the upper layers on a larger dune limiting its ability to reduce scarping where the plants are grasses or shrubs. Trees, however, may have very deep roots. Despite the importance to the stability of a foredune under scarping conditions, very little research has been conducted on the effect species diversity and functional characteristics have on erosion levels (Hanley et al., 2014; Maximiliano-Cordova et al., 2019). In fact, many wave tank studies on dune erosion have utterly ignored the effects of sand compaction, particle size and roundness, vegetation cover and root mass. How the

vegetation then responds to seawater inundation and frequency, and timing of saline inundation events is also poorly understood (Hanley et al., 2014).

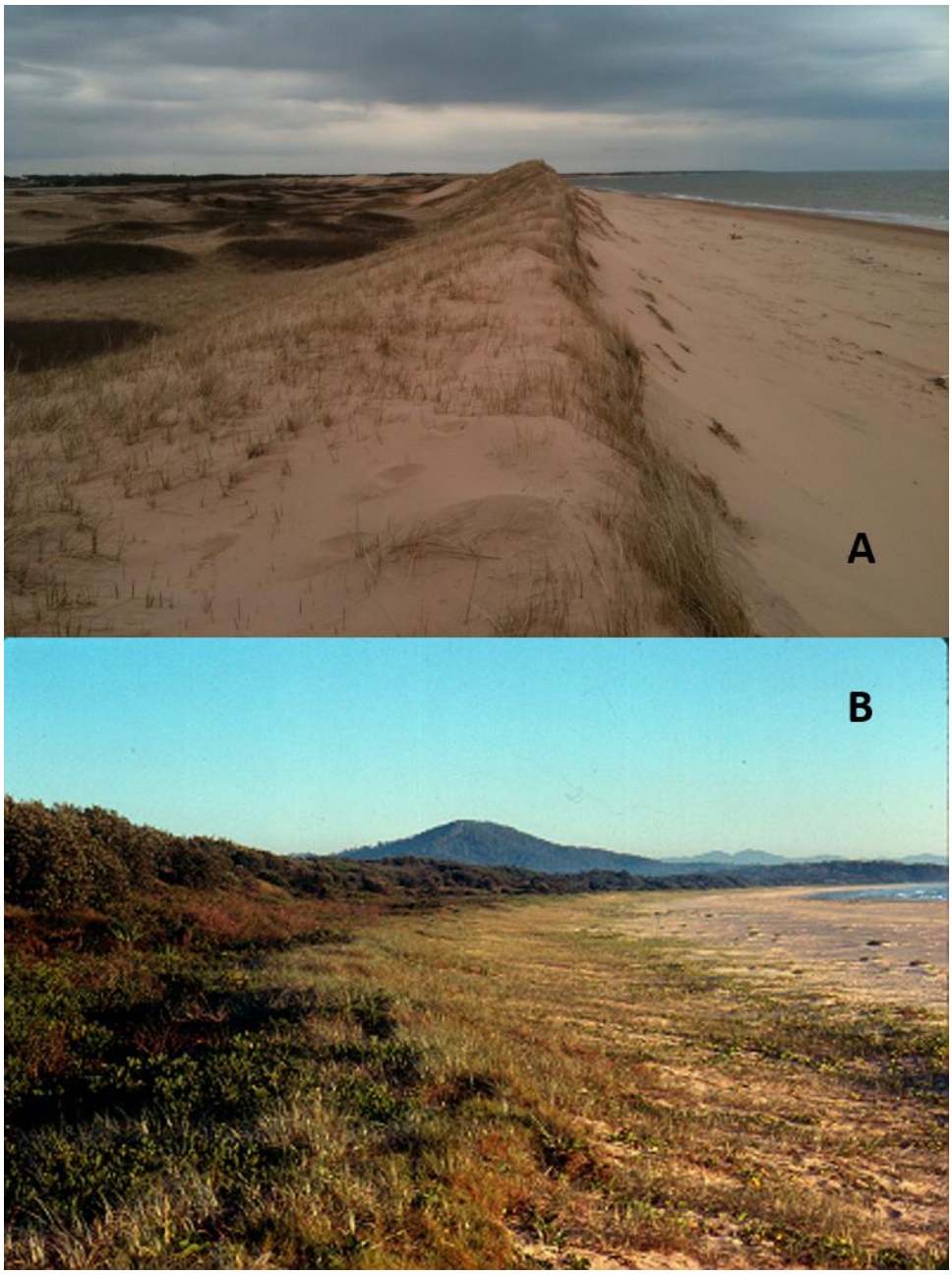

Figure 6: Two foredunes with significantly different morphologies and vegetation cover. In (A) vegetation cover is sparse resulting in minimal resistance to scarping compared to the dense vegetation cover in (B). Prince Edward Island, Canada (A), and Northern NSW, Australia (B).

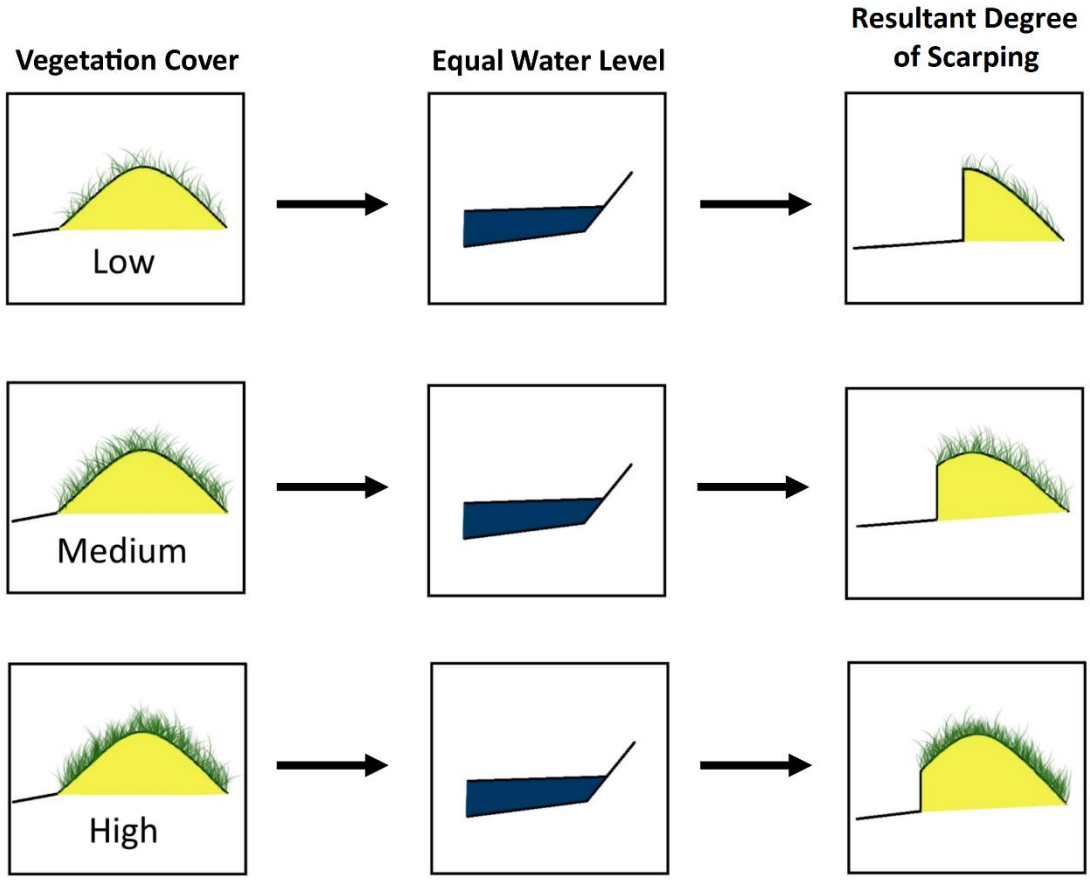

Figure 7: Degree of scarping determined by the degree of vegetation cover on the foredune. The greater the vegetation cover the less erosion via scarping will occur. Root density and rooting depth are also important.

Figure 8 illustrates a comparison between the significant level of *Ammophila arenaria* (marram grass) rootmass in a scarped dune in Tasmania and the substantially less root mass in a dune covered in *Lepidosperma viscidum* at Wyomi Beach, SE Australia. The amount of structural integrity provided to the foredune by the rootmass of the *Ammophila* in Figure 8A indicates that rootmass is likely an important factor in determining the structural integrity of a foredune undergoing scarping. To date there is little research on this factor or control as noted by Feagin et al. (2015) in their review on the role of vegetation in coastal dune erosion protection. Bryant et al. (2019) conducted experiments to investigate the effect of above and below ground biomass (using wooden dowels and coir fibres as proxies for

vegetation) in a model dune under wave attack. Erosion was reduced under both collision and overwash conditions, with the greatest reduction occurring where both above and below ground biomass were present. De Battisti and Griffin (2020) conducted a similar experiment. However, they used actual cores taken from real foredunes and subjected them to simulated swash in a flume. When comparing *Ammophila arenaria, Cakile maritima* and *Salsola kali* their findings showed that the most important characteristic for reducing scarping was the total below ground biomass. The greater the ratio of roots, rhizomes and buried shoots to sediment below the surface the greater the reduction in erosion.

The importance of root mass for structural integrity has been widely demonstrated in research on landslides (Schmidt et al., 2001). Although triggered differently, landslides and dune scarping involve similar processes such as rotational slumping. In landslides and scarp failure, cohesion of sediment, structural integrity of the slope and resistance to erosion are assisted by rootmass (Schwarz et al., 2010). The effectiveness of this structural integrity is highly dependent on species type because differing species characteristics dictate the density and morphology (diameter, strength and length) of the roots as shown in Figure 9 (Schmidt et al., 2001). These same characteristics in the roots of riparian vegetation have been shown to reinforce river and stream bank soils, increasing their stability and reducing the risk of failure (Abernethy and Rutherfurd, 2001; Micheli and Kirchner, 2002).

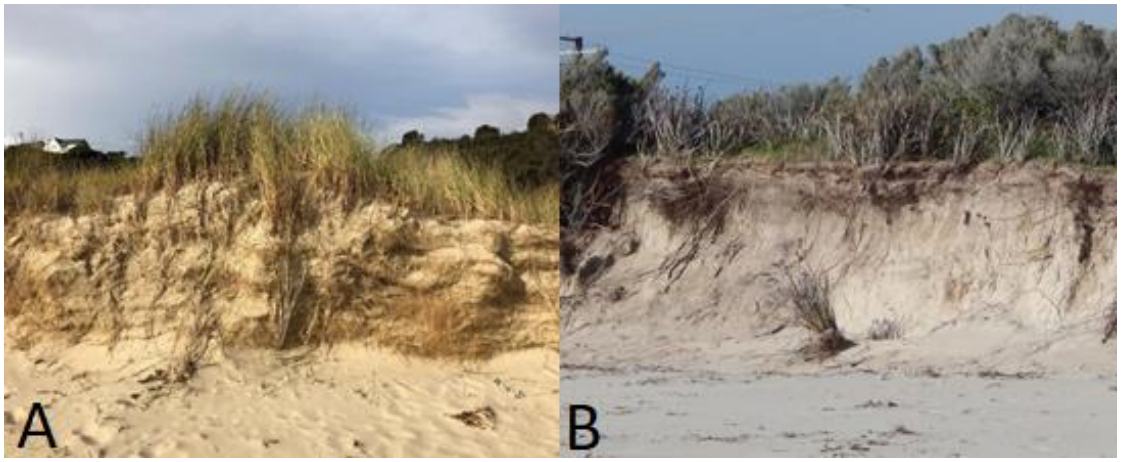

Figure 8: Image of (A) a foredune scarp in Tasmania showing the high density and considerable depth of *Ammophila arenaria* (marram grass) root mass vertically through the dune, compared to (B) the quite limited root mass and rooting depth in a dune covered in *Lepidosperma viscidum* at Wyomi Beach, SE Australia. A is roughly 1 meter high whilst B is ~2 meters.

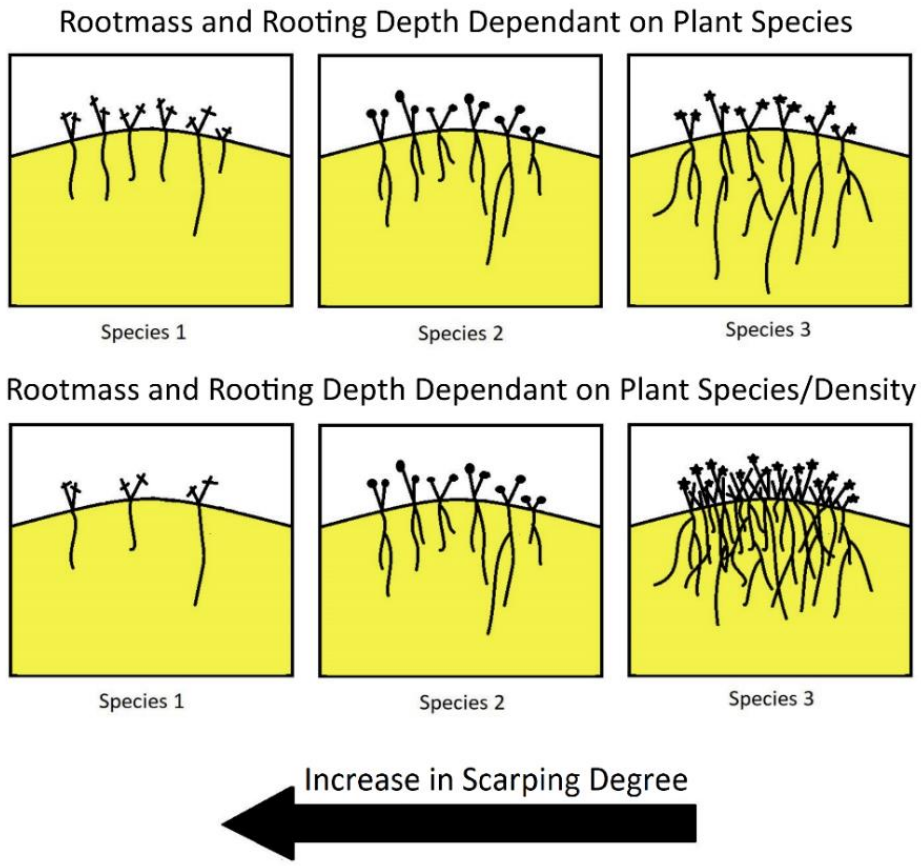

Figure 9: A reduction in root mass, rooting depth and density will lead to an increase in scarping extent due to a loss of structural stability and the reduction of cohesion in the sediment. These attributes will vary depending on species type as shown.

2.4.4 Large Woody Debris and Beach Wrack

Coasts can often be littered with large woody debris (LWD) especially where they have forested hinterlands that are being logged or are associated with high energy streams and rivers, active tectonic regions, landslides and high rainfall events, and/or significant bank erosion (e.g. NZ west coast; Canadian west coast). The debris may be spread across a beach but is often wave transported to the backshore, and can line the foot of the foredune, or eventually be buried underneath it as seen in Figure 10 (Eamer and Walker, 2010; Grilliot et al., 2018). The LWD can play an active role in trapping aeolian sediment and therefore becomes embedded in the foredune as either part of the stoss slope or by aiding the formation of an incipient foredune (Kennedy and Woods, 2012; Grilliot et al., 2019). Grilliot et al. (2019) conducted an analysis of the role of LWD in beach dune interactions. They observed that when highwater level reaches the base of a dune covering LWD, that foredune scarping will occur exposing the LWD, and this then once again aids subsequent aeolian sediment trapping. They found that the magnitude and frequency of high water level events determined the extent to which the LWD matrix was reorganized, its effectiveness to modulate aeolian sediment transport and the ability for an additional sediment store to build and act as an effective buffer against further erosive events (Anderson, 2009; Heathfield and Walker, 2011). Although this additional sediment store buffer has been linked to a reduction in erosion, the effect that LWD within the dune has on reducing foredune scarping has not been fully examined. There are currently no studies that have compared levels of erosion in foredunes with a large percentage of LWD compared to those with a low percentage, or none. One might assume that if the debris is large, heavy and tightly packed, then it would act to reduce the rate of scarping, and potentially the total volume loss.

Beach wrack and/or seagrass litter is commonly found on beaches, particularly low energy beaches and regions with major seagrass meadows in the nearshore. Wrack is increasingly washing up on shorelines around the globe often forming significant deposits and terraces on beaches and in front of foredunes (Smetacek and Zingone, 2013). Beach wrack is generally considered to stabilize shorelines and reduce erosion during high water level events (Ochieng and Erftemeijer, 1999; Cardona and García, 2008), and massive thick banks of seagrass wrack have been observed to act in similarity to vertical seawalls. However, it was only recently that experiments in a wave flume were conducted (Innocenti et al. (2018). Innocenti et al. (2018) examined an incipient foredune either covered or not in wrack and subjected it to swash. They found dune erosion decreased with increasing volumes of wrack. Further field studies are required in order to fully analyse the protective effect the level of wrack seen in Figure 10 has on a foredune. More importantly, since wrack can also be covered by the development of a new foredune, and also incorporated by wind action within a foredune as it forms, one also assumes that the material wrack may have a stabilising or protective effect. The degree of the effectiveness of wrack within the dune reducing scarping is largely, as yet, unknown.

Figure 10: (a) large and small woody debris on the backshore and inlaid in the foredune at Otaki, New Zealand. (b) Extensive seagrass wrack on the beach at Cape Jaffa, South Australia.

2.4.5 Compaction

As a foredune forms on the backshore the sediments slowly become compacted over time (Nishi and Kraus, 1997; Prasetya, 2006). Vertical shear stress is introduced between the grains as new sediment is transported up onto the foredune burying the older sediment and increasing the weight of overburden (Worden and Burley, 2003). Overburden creates a stress that equates to the difference between lithostatic pressure and fluid pressure (Gretener, 1979). In dune systems the fluid pressure corresponds to hydrostatic pressure and therefore increases with depth (Worden and Burley, 2003). Compaction is also reliant on the ratio of brittle to ductile sand grains (Worden et al., 2000). The level of compaction at any given point in the dune then is a combination of the depth of burial, the lithology of the

sediment and the fluid pressure (Worden and Burley, 2003). Compaction can be measured as a percentage of the porosity of the sediment before burial or by specific values based on the compressibility strength of the sediment (Worden and Burley, 2003). After the initial mechanical compaction has taken place chemical processes such as solution and cementation in calcareous dunes, and chemical compaction further reduces porosity and leads to the eventual diagenesis and lithification of the dune (Ireland, 1959; Yaalon, 1967; James et al., 2018). All other factors being equal, the level of compaction of the foredune determines the degree to which it will be eroded under high water levels (Pye and Blott, 2008; Hanley et al., 2014). Nishi and Kraus (1997) compared both non-compacted and compacted dunes in a wave tank and showed that there was not only less erosion from the highly compacted foredune, but it also eroded differently. Compaction led to a stronger dune with thicker layers separating off the scarp face as it was eroded and resulted in a steeper scarp angle. The uncompacted dune face had an angle of 68° after storm conditions were simulated, and this was notably less than the artificially compacted dune which had a scarp slope angle of 87°. Note, however, drying of the scarp face or slope will eventually result in slope failure to the angle of response, if vegetated blocks are absent.

2.4.6 Beach Type

Beach type affects the level to which a foredune will be scarped as the beach profile and dynamics determines the ease at which high water level reaches the base of the dune (van de Graaff, 1986; Pye and Blott, 2008; Suanez et al., 2015). The greatest level of erosion under the same high-water level conditions is likely to occur on moderate to high energy intermediate beaches (T. Aagaard & M. Hughes, pers. comm. 2019). Intermediate beaches are often rhythmic in nature, have crescentic-shaped surf zone transverse bars, cusps and associated rip channels (Short and Wright, 1983; Wright et al., 1985; Aagaard et al., 2013;

Castelle et al., 2015). It is a combination of this alongshore variability in width of the beach, created by the rip channels, cusp embayments and horns, and the alignment of the rip channels with the narrow section of these embayment's that enhance the erosion in these zones (Figure 11) (Thornton et al., 2007; Castelle et al., 2015). Therefore, one would expect to see the greatest maximum scarping on average to occur on intermediate beaches, although locally as opposed to continuously alongshore. However, to the authors' knowledge, no studies have been conducted that compare dune scarping processes concurrently on reflective, intermediate and dissipative beaches under the same high-water level conditions, so there is little information currently available on this topic.

Figure 11: Significant alongshore foredune morphological variability produced by large rips creating an alongshore variation in the degree of dune scarping, French Atlantic coast (Photograph courtesy B. Castelle).

There is no decisive answer in the literature on whether greater erosion occurs on dissipative or reflective beaches under the same water level conditions. It is thought that dissipative beaches will dissipate wave energy over their broad flat profile, leading to decreased foredune erosion (Short and Hesp, 1982; Hesp, 1988; Houser et al., 2008; van

Bemmelen, 2018). However, attributes that may allow high-water level conditions to more easily reach the dune toe include their low gradient beach profile and reduced degree of percolation due to their fine grain size, the fact that they are generally saturated, and that they often occur on high energy, open coastlines (Wright et al., 1979; McArdle and McLachlan, 1991). Reflective beaches are significantly narrower than dissipative beaches which could indicate that high water level conditions would more easily reach the foredune (Short and Hesp, 1982). However, the steepness of the beach profile and the loss of swash due to greater percolation as a result of their typically coarse grain size may counter this to some degree (Wright et al., 1979; Masselink and Puleo, 2006).

2.5 Effects of Scarping

Scarping often acts as a catalyst for further change to the morphology of a foredune following the initial erosion event (Bird, 1976; Short and Hesp, 1982; Carter, 1991; Pye and Tsoar, 2008). Both short term and long term changes in dune morphology can be triggered by a scarping event depending on the extent of the scarping, sediment supply, rate of return of sediment to the beach and dune, frequency of incidence of high water levels, and storm frequency (Hesp, 2002; Christiansen and Davidson-Arnott, 2004). In the following section key morphological changes that can be triggered post-scarping are discussed.

2.5.1 Foredune translation

One direct result of scarp recovery is the net movement of the foredune upwards and landwards, given that some sediment is returned and supplied to the backshore and base of the dune following scarping. First, block falls, rotational slumping, and avalanching occurs as the dune fails and/or dries. Aeolian transport then supplies sand from the beach commonly forming echo dunes (but not always) and then producing a scarp fill deposit or sand ramp

(Carter et al., 1990; Ruz and Anthony, 2008; Hesp et al., 2013; Ollerhead et al., 2013; Jackson and Nordstrom, 2018). Once this ramp has reached near the top of the scarp, sand may then be transported up the sand ramp and across the scarp crest by aeolian transport. This produces crest and lee slope accretion causing the dune to increase in height and translate landwards (Hesp, 1988; Bauer and Sherman, 1999; Christiansen and Davidson-Arnott, 2004; Davidson-Arnott et al., 2018). This process may occur repeatedly on some dunes if the beach is in long term recession/retrogradation.

Davidson-Arnott (2005) included foredune translation when redeveloping the Bruun rule (Bruun, 1988). This rule commonly used to determine sandy shoreline retreat in response to changes in sea level neglects any beach dune interaction such as aeolian sediment transport from the beach and/foredune translation. Davidson-Arnott (2005) improved model includes foredune scarping and recovery and therefore predicts nearshore erosion, landward translation and preservation of the foredune. Ollerhead et al. (2013) confirmed this conceptual model for a beach-foredune system in P.E.I., Canada (see foredune in Figure 6A). They observed that the foredune migrated landwards whilst roughly keeping its form and noted that overall, the decadal foredune evolution was consistent with Davidson-Arnott (2005) model despite varying rates of foredune recovery after scarping over time due to morphological feedbacks. Dune translation/migration can involve possible changes in the alongshore morphology of the foredune including the formation of blowouts and parabolics (Figure 12).

Figure 12: Example of dune migration and the formation of blowouts at Post Office Rock located near Beachport, South Australia. The scarp is 15 m high at the point where the person (in red jacket) is standing in (A).

The potential for scarp filling, revegetation and recovery tends to increase as the height of the dune decreases and/or as the extent of the scarping decreases because plant recolonization can occur more quickly (less area to cover), and/or scarp fill processes can occur more rapidly as less volume is required (Hesp, 1988; Hesp, 2000; Castelle et al., 2017). Foredune recovery will be hindered on eroding coasts where there is a long-term negative sediment budget and frequent major storms. There is also the possibility that a foredune may never fully recover, and net recession may occur, as, in fact, is currently occurring at Post Office Rock in South Australia (Figure 12). Eventually, the foredune may even become completely eroded away (Pye and Blott, 2008).

2.5.2 Development of Blowouts, Parabolics and Transgressive Dune fields

Beaches that are severely scarped can take years to decades to recover (Thom and Hall, 1991; Morton et al., 1994; Douglas and Crowell, 2000; Zhang et al., 2004; Castelle et al., 2017). This length of time is not limited to large dunes, as Mathew et al. (2010) states that

even small dunes that are only from 2-6 metres high can take up to a decade to recover. The reasons for this can include limited sediment supply, repeated erosion events, the timing and extent of revegetation, narrow beach widths, wind direction and velocity, and fetch length (Hesp, 2002; Bauer et al., 2009; Houser et al., 2015; Castelle et al., 2017). During this time, wind erosion may create a blowout, or series of blowouts in the foredune or scarped dune (Gares and Nordstrom, 1995; Fraser et al., 1998). Blowouts may occur in at least two locations, within the middle region of an arcuate rip-formed scarp (Short and Hesp, 1982), and in the crest region where wind velocities are highest (Hesp et al., 2009; Hesp and Smyth, 2016; Preoteasa and Vespremeanu-Stroe, 2017).The zero to low vegetation cover on the stoss slope of the scarped foredune, dune crest failure, and high local wind velocities over the crest aids in providing conditions for the formation of blowouts (Bate and Ferguson, 1996; Hesp, 2002; Pye and Tsoar, 2008).

The destabilisation of a foredune and subsequent blowout formation can potentially lead to the creation of parabolic dunes, particularly on long term eroding coasts (Arteaga et al., 2008; Psuty, 2008; Girardi and Davis, 2010). Parabolic dunes formed at or near the coast typically occur due to landwards translation of a blowout, through the downwind migration of the depositional lobe (Hesp and Hyde, 1996; Pye and Tsoar, 2008; Hansen et al., 2009; Konlechner et al., 2016); Figure 13).

Figure 13: Blowouts and parabolic dunes forming within and cannabalising relict parabolic dunes at the top of a destabilising scarp at Great Beach, Point Reyes, N. California.

A significantly large scarping event or series of events can potentially lead to the formation of a completely new dune field phase (Short and Hesp, 1982) and the development of a transgressive dune sheet or dune field may also take place. This will only occur in the event of significant scarping both in terms of the degree of the scarping as well as the spatial extent of the scarp alongshore. Localised scarping will generally not be sufficient, and scarping likely needs to occur along a significant stretch of a dune system in order to trigger a new dune sheet or dunefield phase (Short and Hesp, 1982). The transgressive sheets and dune fields are made up of large, active to partially to fully vegetated dune systems (depending on their evolutionary state) (Hesp and Thom, 1990; Hesp, 2013). Transgressive dune fields typically occur in the lee of high energy intermediate and dissipative beaches with high sediment supply, but may also result due to foredune destabilisation following storm impacts (Hesp and Thom, 1990; Thom et al., 1992; Barboza et al., 2011; Hesp, 2013).

Jackson et al. (2019) investigated which processes lead to transgressive dune fields developing in the 'Little Ice Age' that effected Europe from about 1400 to 1900. They developed a conceptual model indicating that destabilisation and loss of vegetation occurred due to storm erosion and scarping of the foredune, followed by blowout formation, transition from blowouts to parabolics, and then development of transgressive dune fields. Jackson et al. (2019) state that increased storminess and a decrease in atmospheric air temperatures during The Little Ice Age provided the perfect conditions for these developments. Increased storm frequency and intensity led to an increase in high water level conditions and thus foredune vegetation loss through scarping. Strong winds also associated with the storms increased vegetation burial. This plus the decrease in temperature prevented vegetation regrowth from keeping pace with loss caused by scarping. Blowouts, parabolics and finally transgressive dune field formation then followed.

2.6 The Future

Climate change is highly likely to have major implications for coastal dune erosion globally, posing a pronounced threat to our coasts (Hanley et al., 2014). Sandy beaches make up 31% of the world's ice free coasts worldwide according to a study by Luijendijk et al. (2018). They found that between 1984 to 2016, 24% of these were eroding at rates exceeding 0.5 m/yr and that most marine protected areas were undergoing shoreline retreat. Sea level rise and increased storm frequency and intensity induced by climate change will have significant impacts on the level of scarping effecting these coastlines (Saye and Pye, 2007; Pye and Blott, 2008; Coco et al., 2014; Pachauri et al., 2014; Masselink et al., 2016; De Winter and Ruessink, 2017).

2.6.1 Sea Level Rise

Relatively rapid sea level rise and fall has had major impacts on dune erosion and migration (Carter, 1991). Sea level is currently rising on a global scale (Rahmstorf, 2007; Allison et al., 2009; Nicholls and Cazenave, 2010). The International Panel of Climate Change in their AR5 report projected a range of sea level rise between 0.52 to 0.98m by 2100 (Church et al., 2013; IPCC, 2014). There is a significant relationship between sea level rise and the erosion of beaches (Le Cozannet et al., 2016). As noted earlier, high water level is one of the most critical factors in determining the degree to which a foredune is scarped during a storm. A rise in sea level allows wave energy to reach higher up the face of the foredune more often causing increased scarping under storm conditions. (Carter, 1991; Saye and Pye, 2007; Splinter et al., 2018). This effect will likely be further amplified since according to modelling conducted by Wang and Yang (2018), storm surge will react in an highly nonlinear manner to an increase in sea level rise creating higher extreme sea levels (ESLs). They determined that the magnification of maximum storm surge height may be up to two times that of increases in sea level rise in locations at risk to severe storm surge. Vousdoukas et al. (2018) showed that 1 in 100-year ESLs will likely increase by 34-76cm between the year 2000 and 2100 under a moderate emission scenario and by 58-172cm if climate change action is ignored.

Foredunes are able to respond quickly to change due to being made up of low strength materials (Hanley et al., 2014). Their ability to translate landwards as sea level rises through scarping and recovery allows them to potentially adjust to changing sea level. This natural process of adjusting as sea level rises, given there is some sediment supply or some sediment is returned to a beach following a storm, allows coastal dune systems to potentially survive a rising sea level without being completely eroded away (Carter et al.,

1990; Carter, 1991; Bauer and Sherman, 1999; Christiansen and Davidson-Arnott, 2004; Davidson-Arnott et al., 2018). However, it is when fixed anthropogenic infrastructure is placed behind or within a dune system that erosion becomes an issue.

Sea level rise will not impact all coastal dunes to the exact same degree as its effect will likely vary spatially and temporally. This will be dependent on such factors as the rate of sea level rise, sediment supply, geological inheritance (low countries will be highly affected), the wind regime, and subsidence (Saye and Pye, 2007; Hanley et al., 2014). In some cases, where sea level rise is accompanied by a given sediment supply, beach barrier progradation might even result as occurred during the last Post-glacial sea level transgression (Cowell et al., 1992; Dillenburg and Hesp, 2009).

2.6.2 Changes in Wave Climate

Along certain coastlines it has been demonstrated that changes to the wave climate, a key driver of sediment budgets, will have more of an effect on coastal erosion than sea level rise. (Cowell et al., 1995; Coelho et al., 2009; Hemer et al., 2013). Masselink et al. (2016) concluded from their study on the 2013/14 Atlantic winter storms that the changes to the extreme wave climate will cause the equilibrium state of beaches to change. According to them beach gradient, coastal alignment and nearshore bar positions will all change, resulting in beaches that are sediment depleted and more susceptible to scarping.

Young and Ribal (2019) conducted a global study of trends in wind speed and wave height using satellite data ranging from 1985 to 2018. Their results indicate a minor increase in mean winds and significant wave height. However, the increase in extreme wind speeds and wave conditions was much more significant. Young and Ribal (2019) determined that this increase was most pronounced in the Southern Ocean where some of the world's largest

waves are already found. Here the top 10% of significant wave heights recorded increased in size on average by 1 cm per year, adding up to a total of 33cm since 1985. This significant increase will have a direct impact on scarping extent if the trend continues as climate changes. As stated, wave height, in particular, extreme wave height associated with storm conditions, is a key component of high-water level and therefore its landward reach and scarping potential.

2.7 A Model of Scarp Controls

While there exist a few models on scarp behaviour (Christiansen and Davidson-Arnott, 2004) and scarp recovery (Carter et al., 1990), a model demonstrating the effect key factors that affect or control scarping does not exist. Figure 14 illustrates the individual factors that control or affect the spatial and temporal change to a foredune (or dune fronting the backshore) due to scarping and combines them into one tentative model. The controls are separated into two categories: primary and secondary. Primary controls determine whether scarping will occur or not by either allowing or restricting high water level from reaching the toe of the foredune. Secondary controls, along with the primary controls, then dictate the morphological response and degree of scarping that occurs after a given high water level has impacted the dune.

A high and low level of each factor and the effect it has on producing a greater or lower degree of scarping is presented. This is indicated by arrows with solid arrows indicating greater scarping and dashed arrows less. Figure 14 demonstrates that a higher level of vegetation cover, greater beach width, beach gradient/grain size, compaction, and greater amount of large woody debris or wrack results in less foredune scarping magnitude (Hesp, 1988; Nishi and Kraus, 1997; Pye and Blott, 2008; Feagin et al., 2015). This indicates that

when each of these controls is amplified, foredune scarping will occur to a lesser extent. When they are combined, the level of spatial and temporal change post-scarping is further reduced. Figure 14 also indicates that a higher high water level and larger foredune size and volume results in an increase in scarp magnitude (Short and Hesp, 1982; Pye and Blott, 2008; Coco et al., 2014). Thus, the degree of scarping that occurs during an erosional event will be increased by how high the water level reaches (including duration). Overall, the model shows that the greatest foredune scarping will occur when an extreme high water level passes easily over a flat and narrow beach and then impacts a large dune with a low level of vegetation cover/rootmass and compaction.

Ideally Figure 14 would also indicate the relative significance of each of the controls on the degree of scarping. However, it is currently difficult to determine which factor or control is the most significant after high water level as comparative studies have not been conducted, and this is obviously an area for future research.

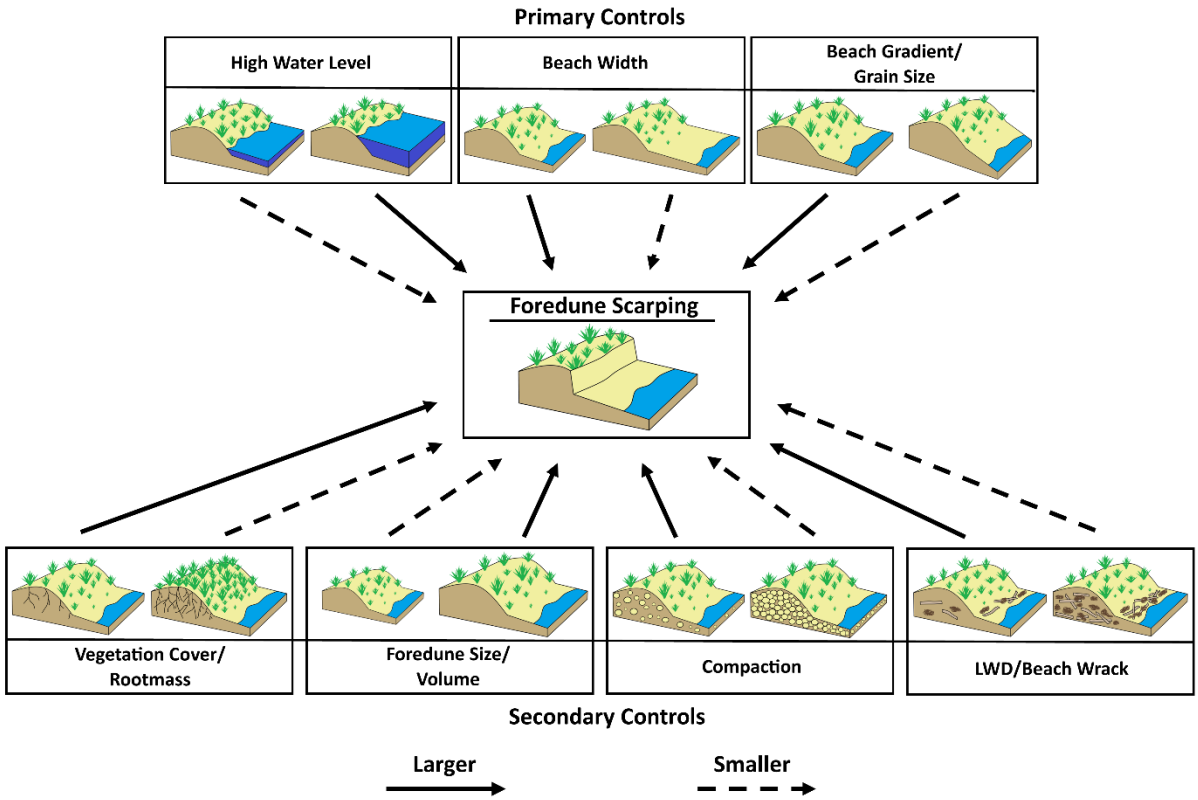

Figure 14: A conceptual model of scarping controls demonstrating the effect a high and low degree of each control has on producing a larger or smaller degree of foredune scarping. The solid arrows indicate a larger degree of scarping and dashed arrows smaller.

2.8 Conclusion

This review indicates that to better understand dune erosion and scarping processes, and subsequent dune evolution, further research is required on the following:

1. The effects of plants on levels of erosion and scarping. In particular, how do different pioneer and shrub plant species affect dune stability and scarping? What does the variation in plant root and stem density, depth, strength, and mass have on dune stability? Observations and analysis of data obtained in the field are critical as it is difficult to nigh impossible to replicate field characteristics in wave tank studies.

2. Surfzone–beach type controls on beach erosion and the degree of scarping. Observations and tests that record the difference in the magnitude or degree of scarping occurring on reflective versus intermediate versus dissipative beaches under the same storm and offshore swell conditions would be very useful.

3. The effect of compaction, particle size, and particle roundness on scarping. These have been largely ignored in experiments.

4. The influence of LWD and wrack on the degree of scarping.

5. How Robin's Rule (Davidson-Arnott, 2005) operates post-scarping and how dune translation occurs as sea level rises. Such studies should include the role of sediment supply to the beach following an erosion event.

6. The extent to which scarping and its controls will be affected by climate change. For example, how will dune vegetation respond to warmer temperatures, and will species change occur as the climate changes thereby potentially increasing or decreasing dune resilience? How will this affect scarping and the likelihood of scarping triggering blowout/parabolic formation or entire dune system change?

7. The factors that determine the degree to which a foredune will be scarped have been shown to include water-level height, height and volume of the foredune, vegetation density and distribution, plant root mass and rooting depth, compaction of sediment, presence or not of wrack and LWD, the original foredune morphology (antecedent conditions), and surfzone–beach type. A tentative new model summarising many of these factors has been presented. Apart from the significance of water level, the significance of each of the factors controlling the degree of scarping is not yet fully certain. Scarping can lead to subsequent

changes to the morphology of the foredune, and on occasion the entire dune system. These changes include potential dune translation, blowout and parabolic dune formation, the transition to a transgressive dune sheet or dunefield, and potentially complete removal of a dune system.

8. Sea-level rise and climate change are certain to bring about an increase in the frequency and magnitude of scarping. It is, therefore, critical to better understand the factors that control the magnitude of scarping and what effect this may have on dune systems. Further research is required to determine the relative importance of some of the controls on the degree of scarping detailed here, and future investigations on what constitutes the most vulnerable beaches and dune systems, and why, is required.

CHAPTER 3

RAPID SHORELINE AND DUNEFIELD CHANGE, SALMON HOLE, SOUTH AUSTRALIA

Published in *Science of the Total Environment:* Davidson, S.G. (80%), Hesp, P.A. (10%) and Silva, G.M.D. (10%) Rapid shoreline and dunefield change, Salmon Hole, South Australia.

3.1 Abstract

Since the 1940's, rapid shoreline and dunefield changes have been ongoing at Salmon Hole, an embayment situated near Beachport in the SE of South Australia. Storm induced erosion has nearly removed the entire dunefield and created a lagoon confined by a calcarenite reef. This study examines the progress, dynamics and causes of the erosion to determine why it has been so severe, using historical aerial imagery, wave reanalyses data, Digital Surface Models (DSM's) from drone surveys and through the volumetric analysis of topographic profiles. The results gained through analysing shoreline change at Salmon Hole are then discussed based on Phillips (2009) change assessment system. This study found that a combination of the formation of the 'lagoon' between the mainland/dune system and the offshore reef and the resultant breakthrough of the tombolo that have led to the acceleration of the erosion processes seen at Salmon Hole. The formation of the lagoon initiated a divergent evolution that continues in the form of a significant geologically controlled longshore current and terminal rip that enhances removal of sediment during and following erosion of the dunes. It appears that each time the lagoon widened post storm erosion it resulted in an increase in the efficiency of the current, resulting in a

positively reinforcing feedback loop furthering the erosion level during each successive storm. The profiles taken from the drone survey DSM's reveal the processes involved in scarping and demonstrate how dune systems with zero sediment supply will respond to future climate and wave conditions. Coastal systems experiencing a deficit in sediment supply will not be able to translate landwards/upwards resulting in their removal. If the current rate of erosion at Salmon Hole is maintained into the future, the entire system is likely to be fully eroded within the next 30 years.

3.2 Introduction

Erosion of the world's coastlines is becoming ever more prevalent as anthropogenic pressures continue to rise and the consequences of climate change begin to be observed (Vitousek et al., 2017). Shoreline erosion is set to increase both in magnitude and frequency due to sea level rise and increase in storminess (Morton and Sallenger Jr, 2003; Zhang et al., 2004; Castelle et al., 2015; Vousdoukas et al., 2018). While changes in wave energy, increase in storm frequency and magnitude, and changes in sediment supply will undoubtedly affect coastal evolution in the future, geological inheritance will also play a large role in determining how coastal sections will respond (Short, 2010).

Geological inheritance plays a significant role in influencing the coastal processes that contribute to shoreline change (Short, 2010; Gallop et al., 2020). This is often the case on Australian beaches which are commonly surrounded by the presence of bedrock, calcarenite or laterite, and coral reefs positioned both on and offshore (Short, 2010). By manipulating wave energy these features can affect flow circulation and therefore sediment transport

within a system (McCarroll et al., 2014; Gallop et al., 2020). This in turn controls beach location, shape and type plus impacts to any connected dunefield (Short, 2010).

Sediment transport within, and between geologically controlled embayment's has been observed to be initiated by bypassing and embayment scale circulation (Castelle et al., 2016; Valiente et al., 2020). Normal beach circulation and rip formation is modified in embayment's by headlands and their associated end effects. As wave energy increases and bay width decreases more of the bay's circulation is affected (Short, 1999). Cellular rips form at either the centre of the embayment or at one or both headlands depending on a combination of shadowing, deflection and channelization mechanisms (Castelle et al., 2016). When these rips form under high wave energy conditions their size and strength means they are often referred to as 'mega -rips' (Wright et al., 1978; Short, 2007). Mega rips have been observed to flow at high velocity and further seawards than regular rips resulting in rapid and severe erosion (Short, 1999). This results in periodic flushing of sediment out of the embayment allowing it to be transported alongshore from bay to bay via wind and wave generated currents (Castelle and Coco, 2013). Similar rips on a lesser scale can be formed by low to moderate wave energy conditions for narrower embayment's (Castelle et al., 2016).

At any given moment a coastal geomorphological system is in constant and highly variable flux as sediment is shifted by hydrodynamic and aeolian forces (Phillips, 2009). A system may be divergent and tending towards increasing variability or convergent and evolving towards stability (Phillips, 2014). A system can also be said to be at equilibrium when it has adjusted to all its environmental constraints and context. However, this equilibrium can collapse when significant change to the variables or dynamics of a coastal system occur. Depending on the extent of the change the system will often revert to its steady state.

(Bracken and Wainwright, 2006; Phillips, 2009; 2011). Phillips (2009) developed a framework for change assessment based on four categories: Response, Resistance, Resilience and Recursion: Response is the rate of geomorphic reaction to change, resistance is the ability of the system to impede the change, resilience is the ability of the system to return to the pre disturbance state and recursion is the potential for either positive or negative feedbacks to the change (i.e. the rate of the change increasing or decreasing overtime due to an aspect of the change itself) (Phillips, 2009). In the following we utilise this change assessment system to examine major shoreline and dunefield changes at Salmon Hole an embayment situated near Beachport in the SE of South Australia (Figure 15). The shoreline changes at Salmon Hole have been significantly dictated and enhanced by geological inheritance, alongshore current and rip formation.

Figure 15: Salmon Hole study site situated near Beachport SE South Australia (image from 2013). The reef which extends across the bay is semi-exposed at low tide as shown in this image. A prominent scarp may be observed along the dune edge. An artificial rock 'tombolo' is present at the northern margin of the bay. The beach originally reached the seawards edge of the exposed reef in 1946.

Coastal erosion and shoreline change due to storm conditions has been extensively documented (Carter et al., 1990; Hesp, 2002; Pye and Blott, 2008; van Rijn, 2009; Castelle et al., 2015; Splinter et al., 2018; Sytnik et al., 2018; Davidson et al., 2020). Recently, shoreline change ranging over days to years has been increasingly a focus of research as historical aerial imagery datasets have been built over time (Masselink and Pattiaratchi, 2001; Boak and Turner, 2005; Castelle et al., 2018). For example Pye and Blott (2008) have analysed historical shoreline change along the Sefton Coast in the UK finding a section of coastline that had eroded at a relatively high long-term average of 3m/yr between 1958 and 2008. Fearnley et al. (2009) observed an extreme average erosion rate of 27m/yr between 1855 and 2005 along the Chandeleur Islands, situated of the coast of Louisiana. This extreme example is due to erosion from repeated hurricane events including the recent Camille, Ivan and Katrina events. This study aims to use aerial imagery along with wave data reanalysis to examine rapid coastal erosion and the role of geological inheritance has had in the historical past and continues to play at Salmon Hole (Figure 15). This erosion has been ongoing since the 1940's and has nearly removed an entire transgressive dunefield. The changes to the dunefield will also be examined using Digital Surface Models (DSM's) from drone surveys and through the volumetric analysis of topographic profiles. The results gained through analysing shoreline change at Salmon Hole will be discussed based on Phillips (2009) change assessment system. This change assessment system has been chosen as it considers the magnitude of the event, its temporal facets, and spatial aspects (Phillips 2009). This study aims to examine the causes, dynamics and progress of the erosion and therefore determine why it has been and continues to be so severe.

3.2.1 Study Site

Salmon Hole is a small headland-bay beach situated in Beachport, SE South Australia (Figure 1). It is characterised by a reflective beach/surfzone fronted by a Pleistocene aeolianite calcarenite reef located approximately 100 m offshore (Short and Hesp, 1982; Short and Hesp, 1984; Short, 2019). The SE of South Australia is known for the preserved carbonate dominated Pliocene - Pleistocene barriers and inter barrier depressions that lithified as the coast slowly uplifted during sea level oscillations, providing a 7 million year record of barrier and sea level history (Short and Hesp, 1982; Short and Hesp, 1984; Short, 2019). Some of the barriers that were formed at lower sea levels than present were eroded and submerged during the last marine transgression creating reefs and islands. Located between the reef and beach at Salmon Hole is a permanent shallow 'lagoon' similar to the Yanchep Lagoon in Western Australia (Gallop et al., 2020). Geological controlled lagoons of this nature are also found in coral reef systems (Kennedy and Woodroffe, 2002; Kennedy, 2003).

A natural tombolo existed at the northern end of the bay (**Figure 16**). The tombolo was eventually breached by storm waves in 2000 and then replaced by an artificial rock tombolo in 2003 (**Figure 16**).

The dunefield backing Salmon Hole was originally a transgressive dunefield which was significantly active in the post-1946 period (when the earliest photography is available), and over time it has become increasingly vegetated. The remaining dunes reach up to 20 m and have been severely scarped which has led to the formation of a major blowout and several small ones in the scarped dune crest. The dune vegetation comprises shrub and tree species rather than grasses due to the extent of the erosion into the dune system. The scarped dune is not a foredune despite being the foremost dune adjacent to the beach (Hesp, 2002); it is,

in fact a transgressive dunefield remnant (compare the photographs in Figure 2). Behind the dunefield at the northern end of the bay is a saline lake called the Pool of Siloam (Figure 16). To the north of Salmon Hole, a bay called Pleasant Cove is characterised by a reflective beach backed by a low stage 1 foredune that has been recently scarped (Figure 16).

The coastline faces south to south west and experiences persistent high energy south westerly swell provided via midlatitude cyclones enhanced by south west storms and south easterly sea breezes (Short and Hesp, 1982; Short and Hesp, 1984; Short, 2019). The wave climate is described by Short and Hesp (1984) as being 'persistent year-round moderate to high southwest swell, peaking during April to September, while periods of low swell are infrequent and calms rare'. This region is microtidal with the mean spring tide ranging from 1.1 m at Port MacDonnell (82 km to the southeast of the study site) to 1.3 m at Cape Jervis (271 km to the northwest of the study site). The coastline surrounding Salmon Hole is made up of both long sections of uninterrupted beach such as the 180km long Younghusband Peninsula barrier system and similar sandy embayment's to Salmon Hole that are separated intermittently by sections of calcarenite rocky features, headlands and reefs (Short and Hesp, 1982; Short and Hesp, 1984; Short, 2019). Beach and dune erosion, possibly due to a lack of modern sediment supply, and to anthropogenic activities is common to this area but not to the extent observed at Salmon Hole.

In Salmon Hole, under conditions of storm surge and particularly when storm surge and high tide occur simultaneously, the raised water level allows higher wave energy to pass over the reef and erode the dune system (Fotheringham, 2009). Storm surge in South Australia develops due to intense low-pressure systems and generally ranges between 1.5 and 2 m

for the southern coast of South Australia (Short and Hesp, 1982; Short and Hesp, 1984; Short, 2019).

Figure 16: Aerial image of Salmon Hole taken in 1946 (left panel) and in 2016 (right panel). Severe erosion and development of a lagoon has occurred at Salmon Hole.

3.3 Methodology

3.3.1 Aerial Imagery

Aerial imagery was obtained from aerial photography and georectified imagery from the Department of Environment and Water (DEW), Google Earth historical satellite imagery, and UAV/drone orthomosaics (see Table 1).

After imagery georectification were conducted in ArcMap. Ground Control Points (GCP's) of key features on the study site and visible from the air where obtained using a Trimble Real Time Kinematic (RTK) Global Navigation Satellite System (GNSS).

The GCP's were aligned with their corresponding feature in the imagery using Arcmap. Given some of the images have already been orthorectified by DEW these were used to assess the accuracy of the georeferencing of the photographs, google earth images and

drone orthomosaics. In order to further align the imagery, key points visible in DEW's georectified imagery were identified and new tie points created to obtain the best fit (Hanson and Seeger, 2015).

Table 1: Acquisition date of imagery used in analysis along with associated data including source, type, pixel size, original image scale, total RMS and RMS error in meters.

Date	Source	Type	Pixel Size (m)	Scale	Total RMS	RMS Error (m)
14/02/1946		Light Aircraft Survey Frame	2.22	-	2.85	6.327
13/12/1950	DEW	Light Aircraft Survey Frame	0.39	1:32,000	3.47	1.3533
27/01/1951	DEW	Light Aircraft Survey Frame	0.37	1:32,000	2.85	1.0545
25/02/1975	DEW	Light Aircraft Survey Frame	0.28	1:10,100	1.28	0.3584
18/02/1978	DEW	Light Aircraft Survey Frame	0.81	1:40,000	0.99	0.8019
19/2/1978	DEW	Orthorectified	-	1:40,000	-	within 2
3/03/1982	DEW	Light Aircraft Survey Frame	0.49	1:40,000	2.68	1.3132

7/09/1989	DEW	Light Aircraft Survey Frame	0.52	1:16,000	2.91	1.5132
30/1/1992	DEW	Light Aircraft Survey Frame	0.8	1:40,000	2.339	1.8712
4/2/1997	DEW	Light Aircraft Survey Frame	0.81	1:40,000	2.47	2.0007
29/11/1999	DEW	Light Aircraft Survey Frame	0.83	1:40,000	3.88	3.2204
17/1/2002	DEW	Light Aircraft Survey Frame	0.98	1:40,000	2.94	2.8812
23/1/2003	DEW	Light Aircraft Survey Frame	1	1:40,000	-	within 2.5
1/01/2007	DEW	Orthorectified	0.4	Not relevant	-	within 2
18/2/2008	DEW	Orthorectified	0.9	Not relevant	-	within 4
3/03/2013	DEW	Orthorectified	0.5	Not relevant	-	within 1

20/10/2014	Google Earth	Google Earth Image	1.02	-	2.22	2.2644
28/12/2015	Google Earth	Google Earth Image	1.02	-	2.22	2.2644
15/3/2016	Google Earth	Google Earth Image	1.03	-	2.22	2.2866
15/2/2019	Drone Orthomosaic	Orthomosaic	0.012	-	-	0.14

3.3.2 Shoreline Analysis

To accurately represent historical coastal erosion or accretion a consistent definition of what constitutes the 'shoreline' is required. The most commonly used proxy to define shoreline position for microtidal regions is the wet/dry line (Smith and Zarillo, 1990; Anders and Byrnes, 1991; Sekovski et al., 2014; Serafim and Bonetti, 2017; Sytnik et al., 2018). The wet/dry line was identified in the imagery as the change in colour tone between the wet and dry sand (Boak and Turner, 2005). The shorelines were manually digitised using ArcGIS Pro. Salmon Hole as well as Pleasant Cove were both digitised (Figure 19). Tidal correction was not carried out due to the majority of the images not having timestamps.

Shoreline change was examined using Digital Shoreline Analysis (DSAS) version 5.0 (Thieler et al., 2009). This software expansion allows ArcMap to calculate rate of change statistics from the distances between shorelines by the addition of cross shore profiles or transects

placed at the user's discretion. This method has been widely used in shoreline change studies (To and Thao, 2008; Oyedotun, 2014; Bheeroo et al., 2016; Sytnik et al., 2018; Nassar et al., 2019). Statistics produced by DSAS are generated based on the spatial and temporal change between each of the shorelines and are described in Table 2.

Table 2: DSAS statistics descriptions

Shoreline Change Envelope - SCE	Distance in meters from the shoreline closest to the baseline to the one furthest away, calculated for each transect (Himmelstoss et al., 2018).
Net Shoreline Movement - NSM	Distance between the oldest and youngest shorelines for each transect. This number is given a sign either positive or negative depending on whether erosion or accretion has occurred (Himmelstoss et al., 2018; Sytnik et al., 2018).
End Point Rate - EPR	The rate of change measured in m/yr between the youngest and oldest shoreline for each transect using the distance from each NSM value (Himmelstoss et al., 2018).
Linear Regression Rate - LRR	All shoreline points on a transect are fitted with a least-squares regression line. The linear regression rate is the slope of that line (Dolan et al., 1991; Crowell et al., 1997; Genz et al., 2007; Himmelstoss et al., 2018).

Of all the statistics in Table 2 the linear regression rate Linear Regression Rate (LRR) method is the most suitable for shoreline change that involves both erosion and accretion within a certain time period as all of the shorelines are fitted with a least-squares regression line and thus taken into account. This is in contrast to the other statistics in Table 2 which are either based on the oldest and youngest shorelines or the two shorelines furthest apart. However, the LRR often underestimates rate of change when compared to other methods like End Point Rate (EPR) (Dolan et al., 1991; Crowell et al., 1997; Genz et al., 2007; Himmelstoss et al., 2018).

Two baselines were drawn following the entire curvature of Salmon Hole and Pleasant Cove. Transects were placed 25 meters apart resulting in a combined total of 31 transects.

3.3.3 Potential Errors

Shoreline detection and digitising can be hindered by several factors (Sytnik et al., 2018). Identifying the wet/dry line was difficult in certain earlier images, for example, in the black and white imagery, so the instantaneous water line was used instead. The instantaneous water line is defined as the line on a photograph that indicates where the upper swash has stopped. Due to Salmon Hole's steep narrow reflective beach, this line is actually very close to the wet/dry line. Given this, and the extent of the time difference between images this was considered a very minor limiting factor (Sytnik et al., 2018).

Images from peak swell/storm times (specifically winter) and with significantly visible high tides were excluded to give a better representation of the average shoreline at any given time (Sytnik et al., 2018). Shoreline analysis was conducted on all available images, as well as to roughly 10 year intervals (as best as the available imagery would allow) to reduce potential short-term errors and to indicate a more representative long-term shoreline trend

(Eliot and Clarke, 1989; Dolan et al., 1991). These years were 1975, 1989, 1999, 2008 and 2016. The earliest (1946) and most recent (2019) imagery was also included.

3.3.4 Time Series

To better visualize the period of change specifically related to the breakthrough of the tombolo a time series for Transects 9 and 10 (transects closest to the tombolo and on either side of it) was created. A time series was also created using erosion/accretion statistics based on a new transect (transect tombolo, shown in Figure 24) closer to the point of tombolo breakthrough on the Salmon Hole side. These time series were created by determining the Net Shoreline Movement (NSM) distance between each shoreline available between 1999 and 2009. For example, the distance of -10.4m shown in 2000 is the distance eroded between 1999 and 2000. Note that data is not available for every year, so in some cases the calculations relate to more than one year's difference (e.g., the 2002 data point is for 2 years: 2000 to 2002). As stated above, some error might be introduced due to tide state and wave energy on the day the photograph/image was taken. However, where there are significant levels of erosion and accretion such errors are largely negated.

3.3.5 Wave Data

In order to identify storm events that could have a significant impact on shoreline changes, significant wave height (Hs) was obtained from the ERA5 monthly averaged reanalysis product from 1979 to present, developed by the European Centre for Medium-Range Weather Forecasts (ECMWF) and downloaded through the online climate data store. Reanalysis was used as the closest wave observation is ~160 km away to the East in Cape Bridgewater. The significant wave height (Hs) data was taken from the grid point shown in Figure 17 due to its proximity to Salmon Hole at the coordinates 37.4881° S, 140.0133° E.

The top 3% of monthly Hs averages were considered to represent significant storm periods. The top 3% is made up of months where the averaged Hs is above 3.87 as shown further below in Figure 25.

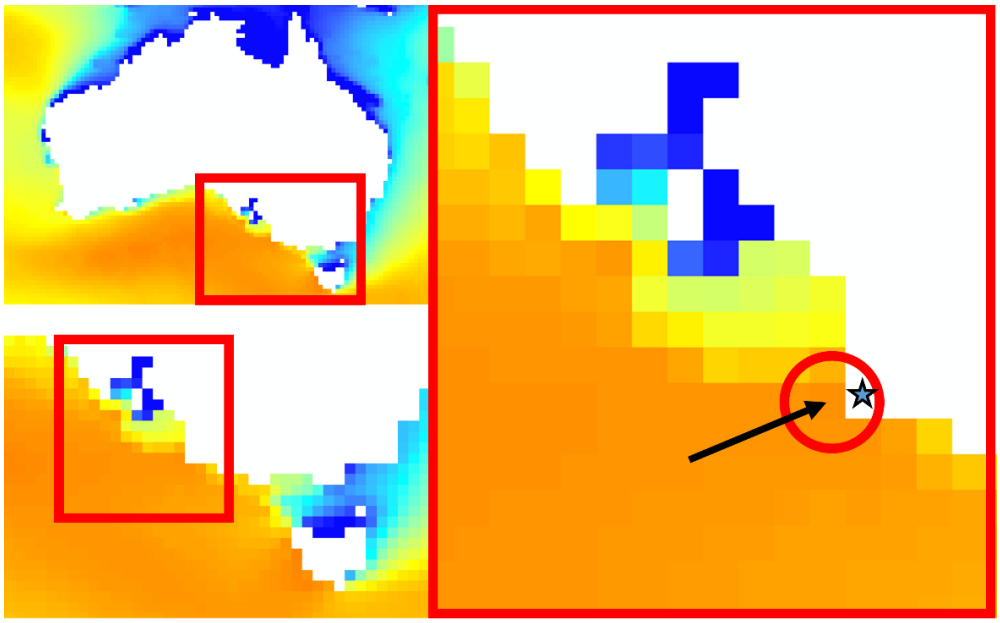

Figure 17: Grid point (in red circle) used for significant wave height data due to its proximity to Salmon Hole at 37.4881° S, 140.0133° E (star).

3.3.6 Digital Surface Models

Three Digital Surface Models (DSM's) were analysed as part of the study on the ongoing erosion at Salmon Hole. This was done to gain further insight into the processes involved in the erosion by providing a three-dimensional comparison of the stoss slope before and after erosion events. These were created through UAV surveys conducted on the 28/8/2017, 15/2/2019 and 16/5/2020. Ground control was achieved using ground control point (GCP) targets placed throughout the flight area. The height relative to GHD and location was obtained using a Trimble RTK – GNSS unit. The vertical view images from these surveys where stitched together in Pix4D photogrammetric software (Suziedelyte Visockiene et al., 2014). Arc GIS was then used to make 2D profiles from the DSM's for comparison.

3.3.7 Topographic Profiles and Erosion Volumes

Fifteen topographic profile lines were emplaced at Salmon Hole by the Department of Environment and Water (DEW) in 2001 (Figure 18). These beach-dune profiles were placed roughly 30 m apart and were surveyed by DEW in 2001, 2009 and 2017 (Fotheringham, 2009; Hesp et al., 2018). Profiles were surveyed using a highly accurate RTK GPS system with vertical and horizontal accuracy within a few cm in reference to the Australian Height Datum (AHD). Volume loss at each profile was calculated using the programmes CalcVol and CalChainage. Total volume loss along the entirety of the bay was then determined by using each profile to represent the distance halfway between it and the next profile on either side. The volume loss from the profiles were then multiplied by these distances and added together (Hesp et al., 2018). Topographic data and volume loss were provided by DEW and Hesp et al. (2018).

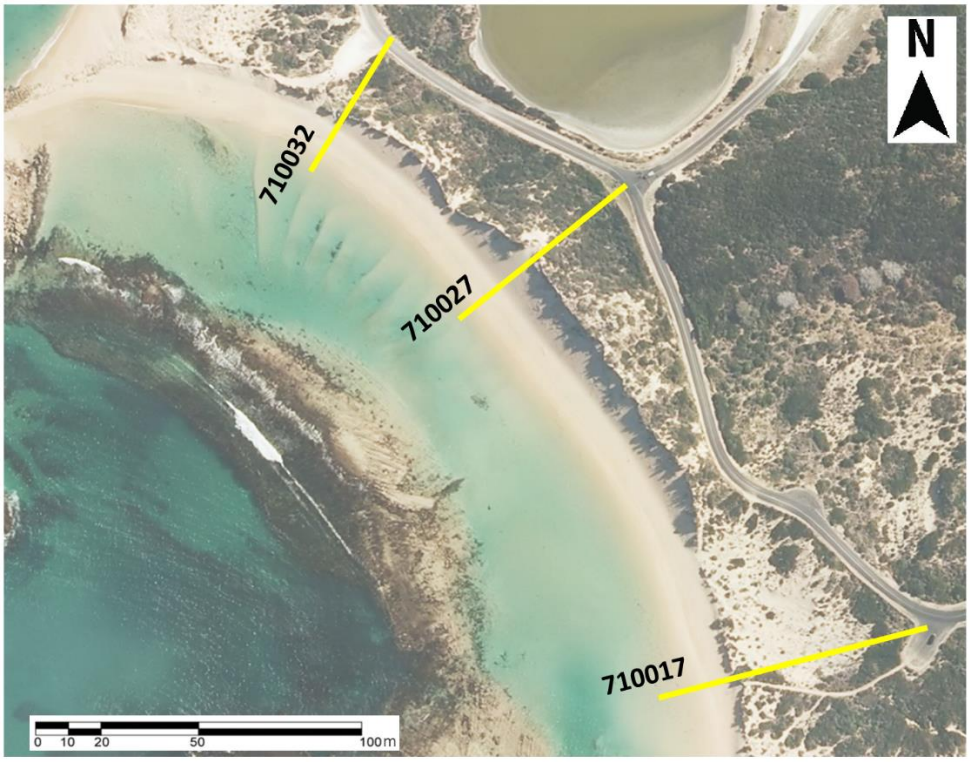

Figure 18: Topographic survey lines set up by the State Department of Environment and Water and utilised to conduct repeat surveys of the dunes and bay.

3.4 Results

3.4.1 Shoreline variability

Figure 19 and Figure 20 show considerable shoreline change between 1946 and 2019 at Salmon Hole and Pleasant Cove. Both embayment's have undergone significant spatial change over a relatively short time. In this section the average distance of erosion or accretion is taken from the Net Shoreline Movement (NSM) statistic and the erosion rate is the Linear Regression Rate (LRR).

The average overall erosion at Salmon Hole using shoreline map spaced roughly a decade apart was -100.17 m over 73 years (1946 to 2019) as shown in Figure 20. The maximum distance eroded was -113.36 m at transect 5 (see Figure 21). The average rate of change was -1.44 m/yr (Figure 21) while the maximum rate of change was -1.7m/yr on transect 14 towards the northern end of the bay (Figure 21).

When analysing the shorelines at a decadal rate of change for Pleasant Cove the overall average amount of accretion was 24.89 m (Figure 20). The maximum was 30.57 m of accretion which occurred on transect 5 (Figure 20). Interestingly, the Shoreline Change Envelope's (SCE) average distance was significantly larger at 46.18 m with a maximum distance of 52.41 m. This is due to the 2008 shoreline being the furthest away from the baseline rather than the most recent shoreline from 2016. This indicates that erosion has occurred post-2008 (Figure 20). However, it must be noted that using the SCE to analyse only two shorelines like this introduces the potential for greater error as seasonal change in shoreline position, for example, can have more of an effect. Overall, the average rate of erosion was 0.52 m/yr. The maximum rate was 0.61m/yr on transect 6 positioned near the middle of the bay (Figure 21).

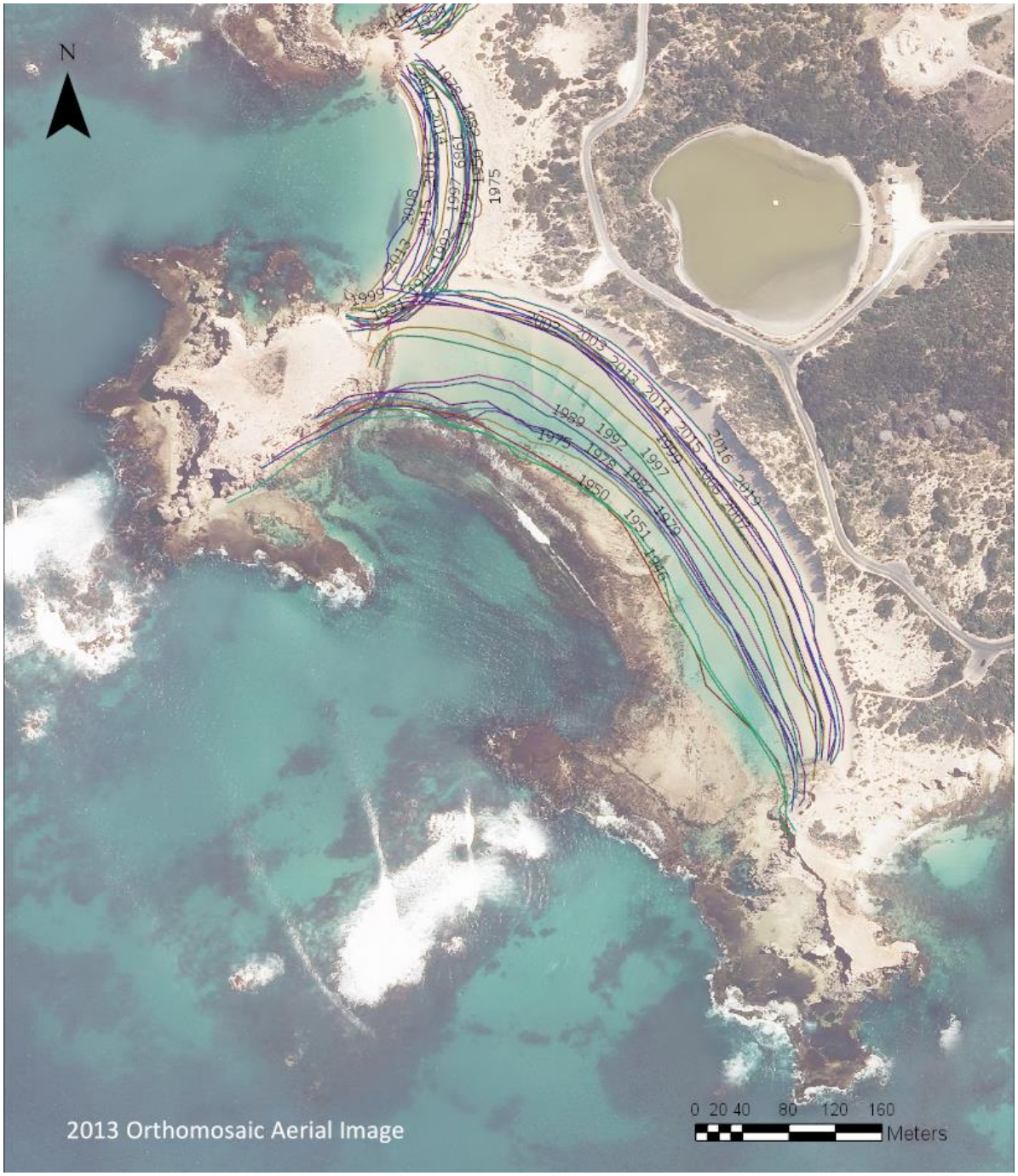

Figure 19: Shoreline change at Salmon Hole from 1946 to 2019 overlaid on a 2013 orthorectified aerial image. The shoreline was located on the edge of the reef in 1946.

Figure 20: Shoreline variability in decadal intervals from 1946 to 2019 at Salmon Hole overlaid on a 2013 orthorectified aerial image.

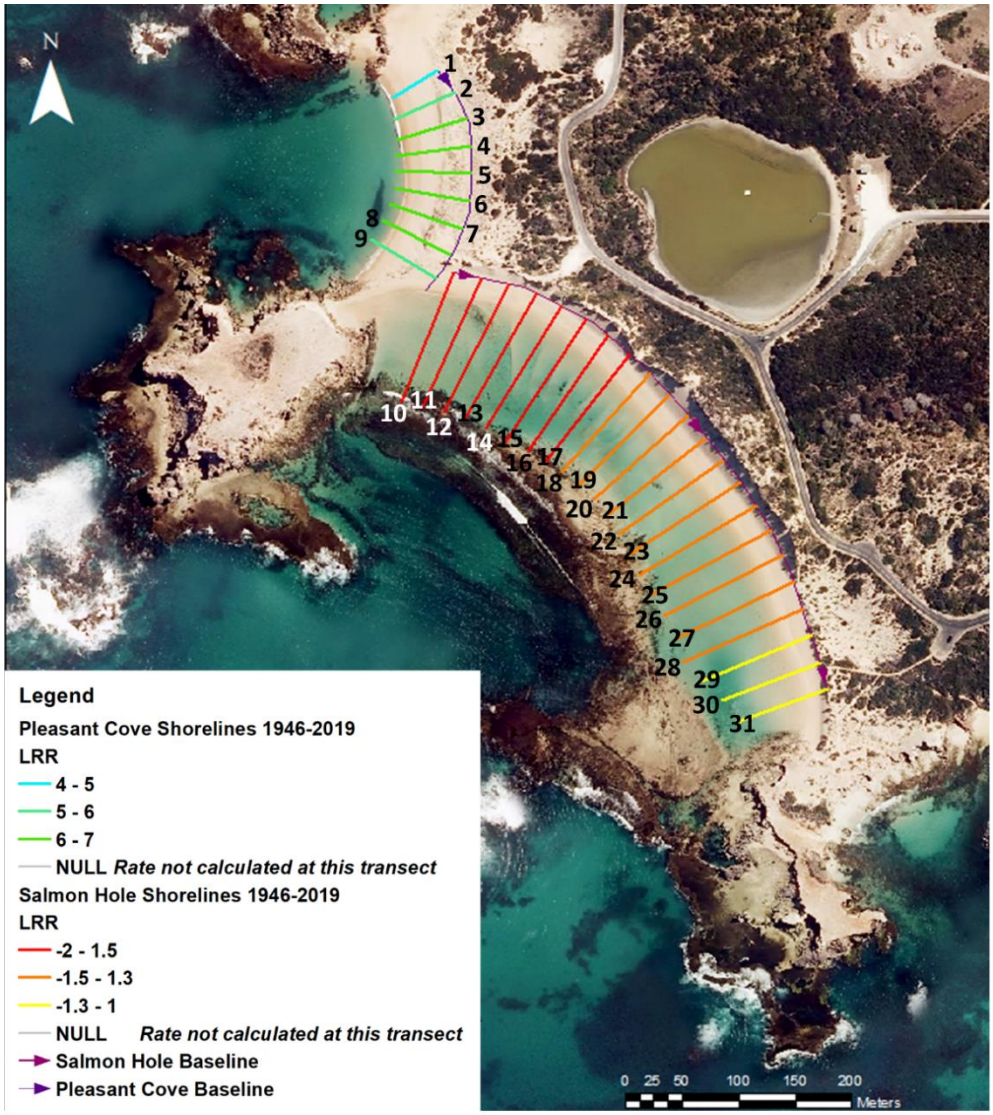

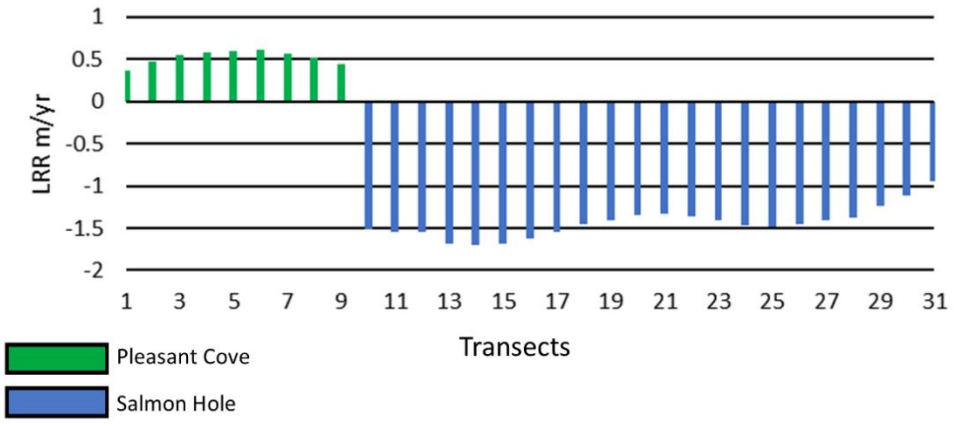

Figure 21: (Top) Transect positions, shoreline intersection points and given numbers overlayed on image of Salmon Hole and Pleasant Cove. This figure also shows the Linear Regression Rate (LRR) for all shorelines. The LRR provides a rate of erosion statistic that includes all the shorelines by fitting each intersection point of the transect with a least-squares regression line. The linear regression rate is the slope of that line. (Bottom) Linear regression rate (LRR) measured in meters per year for each transect from north to south. Transects 1-9 are from Pleasant Cove and 10-31 are from Salmon Hole. A clear pattern of overall accretion at Pleasant Cove versus overall erosion at Salmon Hole can be identified between 1946 and 2019.

3.4.2 Key Periods of Change

Thus far the statistics have been conducted on all the shorelines collectively. Further analysis was conducted on shorelines from periods that showed significant together erosion/accretion or related to apparent significant events (Figure 29). This was done to identify what has driven the shoreline change. For this section, the End Point Rate (EPR) statistic has been used for determining the erosion rate as often the distance between only a few shorelines are discussed. The LRR was not used as it often underestimates rate of change when compared to End Point Rate and relies on multiple shorelines for its least-squares regression line to be effective. The statistics for the shorelines grouped together for closer examination of specific spatial and temporal change can be seen in Appendix 1 and 2.

3.4.2.1 Pre-Tombolo Breakthrough

Figure 22 shows the expansion of the lagoon at Salmon Hole from its initial development from 1946 to 1975 to just before the tombolo was breached in 1999. The 2016 image indicates the direction of the current and the position of the headland-controlled rip at the northern end of the lagoon. From 1946 until 1999 when the tombolo broke through the average erosion rate was 1.25 m/yr, similar to the 1.8 m/yr average erosion rate from 1999 onwards. This indicates that significant erosion was occurring prior to the breakthrough of the tombolo. Within this period, little erosion was seen between 1946 and 1975 as shown by the comparatively low average erosion rate of only -0.63 m/yr (Figure 29). This changed between 1975 and 1999 where large levels of erosion were seen at Salomon Hole (Figure 20 to 9). The average distance eroded was -48.89 m with a maximum of -74.75 m seen at transect 11 near the tombolo (Figure 21). The average rate increased to -1.97 m/yr (Figure 29). Between 1992 and 1997 alone the beach alongside the northern headland displayed -42.98 m of erosion (specific transect drawn along this area). From 1992 to 1999 Salmon

Hole eroded an average of 23.96 m at an average rate of -3.19 m/yr with a maximum rate of -6.14 m/y found at transect 10 (Figure 29). This is very similar to the rate of -3.49 m/yr of erosion seen directly after the tombolo broke through between 1999 and 2003. This indicates that the breakthrough of the tombolo did not have as large an effect on an increase in erosion as would be expected as significant erosion was an ongoing event prior to the breakthrough.

Progradation corelating to the erosion at Salmon Hole between 1975 and 1999 occurred at Pleasant Cove, as can be seen in Appendix 2.

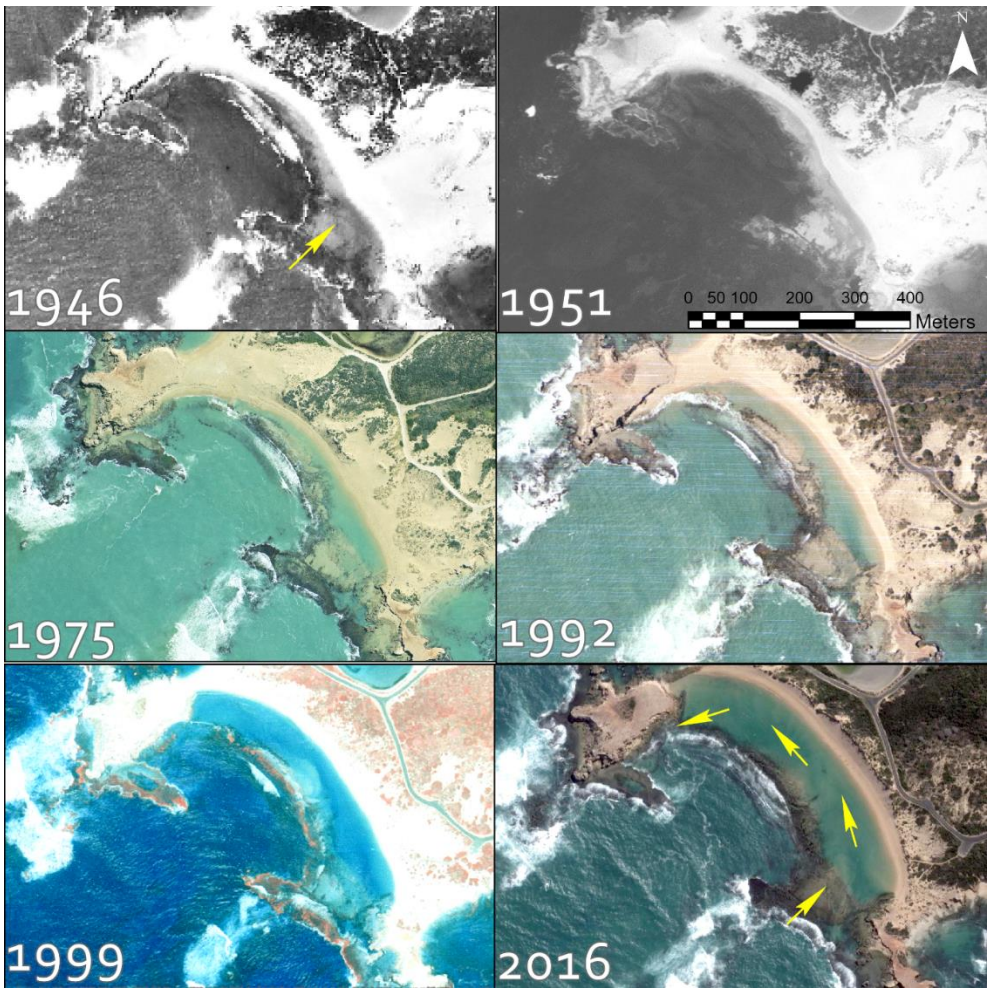

Figure 22: Sequence of shoreline erosion and lagoon development behind the reef of Salmon Hole between 1946 and 1999. Note that in 1946 the beach was attached to the landward margin of the aeolianite reef, whereas by 1999 a significant lagoon had been formed behind the reef. The yellow arrow in the 1946 image shows waves are opening up the lagoon on the southern end of the reef. The erosion can be seen to begin from this end and then extend into and along the modern-day lagoon over time. The yellow arrows in the

2016 image show the propagation of wave energy into the lagoon. This helps to drive a current around the bay even under small wave conditions and has resulted in the development of subaqueous transverse dunes.

3.4.2.2 Tombolo Erosion

Up until this present study the breakthrough of the tombolo had been placed between 1997 and 2001 by (Fotheringham, 2009). However, the aerial imagery shows a gap formed in the tombolo between 29/11/1999 and 14/07/2000 (Figure 24). The storm responsible for the initial gap development was most likely an event recorded at Cape Jaffa, located 65 km NNW of Salmon Hole, in The Bureau of Meteorology's severe storm archive. On the 27th of May 2000, gale force winds blew at Cape Jaffa for 5 hrs, followed by a secondary frontal system that resulted in severe gusts at Cape Willoughby, 246 km NW of Salmon Hole, and continued to generate gale force winds across the southeast on the 28th May. The gap remained open until 2003 (Figure 24).

During the period the tombolo was open between 1999/2000 and 2003, the average erosion rate increased to 3.49 m/yr with rate as high as -6.15 m/y found at transect 13. On average -13.82 m of erosion was seen with a maximum distance of -24.34 m of erosion at transect 13 near the tombolo end. Both transect tombolo and transect 10 time series indicate that the majority of the erosion occurred during and directly after the breakthrough. A loss of up to -16.36 m was recorded in 2000 at the tombolo transect and -13.17 m in 2002 at transect 10 (Figure 23). Minor accretion is shown for both 2003 and 2005 (Figure 23) but note that this period includes the period after the artificial tombolo was put in place. As stated above this is not as significant an increase from before the breakthrough as would be expected given sediment now had a much more efficient means to exit the bay. During the same period, it is very likely that sediment transported through the gap in the tombolo caused Pleasant Cove to accrete on average 23.96 m. The average rate of accretion

was 6.06 m/yr, a significant increase from the overall average of 0.36 m/yr. The transect 9 time series from Pleasant Cove indicates that initial sediment transport was not as immediate as the erosion at Salmon Hole with slight erosion being recorded in 2000 (Figure 23). However, this was followed by 37.25 m of rapid accretion between this time and 2002 (Figure 23).

An artificial rock tombolo was put in place in 2003 to close the gap, and this was initially effective even becoming partly covered by sand (Figure 24). The placement of the tombolo resulted in 6.16 m of accretion between 2003 and 2005 at transect tombolo (Figure 24). However, according to Fotheringham (2009) it was clear that by 2004 issues had developed. The beach to the northern side began to erode undermining and outflanking the artificial tombolo and causing it to be directly impacted by waves. This resulted in smaller rocks being dislodged which weakened the structure leading to a breach during a large swell event in 2006 (Fotheringham, 2009). This led to -2.26 m of erosion at transect tombolo between 2005 and 2007 (Figure 23). However, this was not reflected along the entirety of the bay with 0.42 m of accretion occurring at the nearby transect 10 during this period (Figure 23). In 2007 the artificial tombolo was rebuilt with larger rocks and designed to allow wave overtopping during storm events (Fotheringham 2009). The average distance of erosion between 2003 and 2007 at Salmon Hole reduced to -2.95 m and the mean rate of erosion also dropped to -0.94 m/yr. Pleasant Cove transitioned from accretion to erosion with an average distance of -13.16 m eroded at a mean rate of a high -4.2 m/yr. -13.33 m of erosion was seen at transect 9 between 2003 and 2005 (Figure 23).

After repairs and reinforcement were complete, sediment again initially built up on both sides of the artificial tombolo between 2007 and 2008 (Figure 23 and Figure 24). In 2008

accretion was recorded on both sides of the tombolo with 3.13 m at transect tombolo and 14.44 m at transect 9 (Figure 23). Again, the accretion at the tombolo was not matched at transect 10 with minor erosion occurring there and likely contributing to the progradation at pleasant cove (Figure 23). Overall an average of 10.62 m of accretion occurred at Pleasant Cove during this time. However, after 2008, the Bay began to retreat again and continues to do so until the most recent image of the area taken in 2016 (Figure 24). This can be seen in Figure 24 as sediment is eroded either side of the artificial tombolo. Between 2008 and 2016 an average of -13.55 m was eroded at a mean rate of -1.68 m/yr.

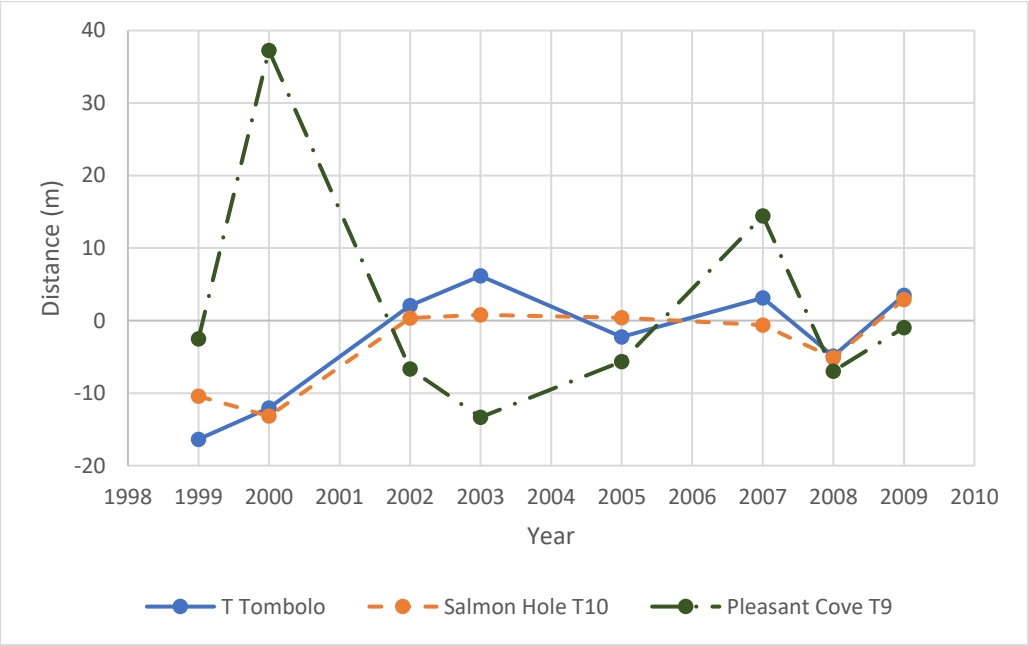

Figure 23: Time series showing erosion and accretion in meters between 1999 and 2009. Including transects 9 and 10 (either side of the tombolo) and transect tombolo which is a transect drawn at the tombolo on the Salmon Hole side as shown in Figure 24. A correlation between erosion at Salmon Hole and accretion at Pleasant Cove can be seen during the breakthrough of the tombolo.

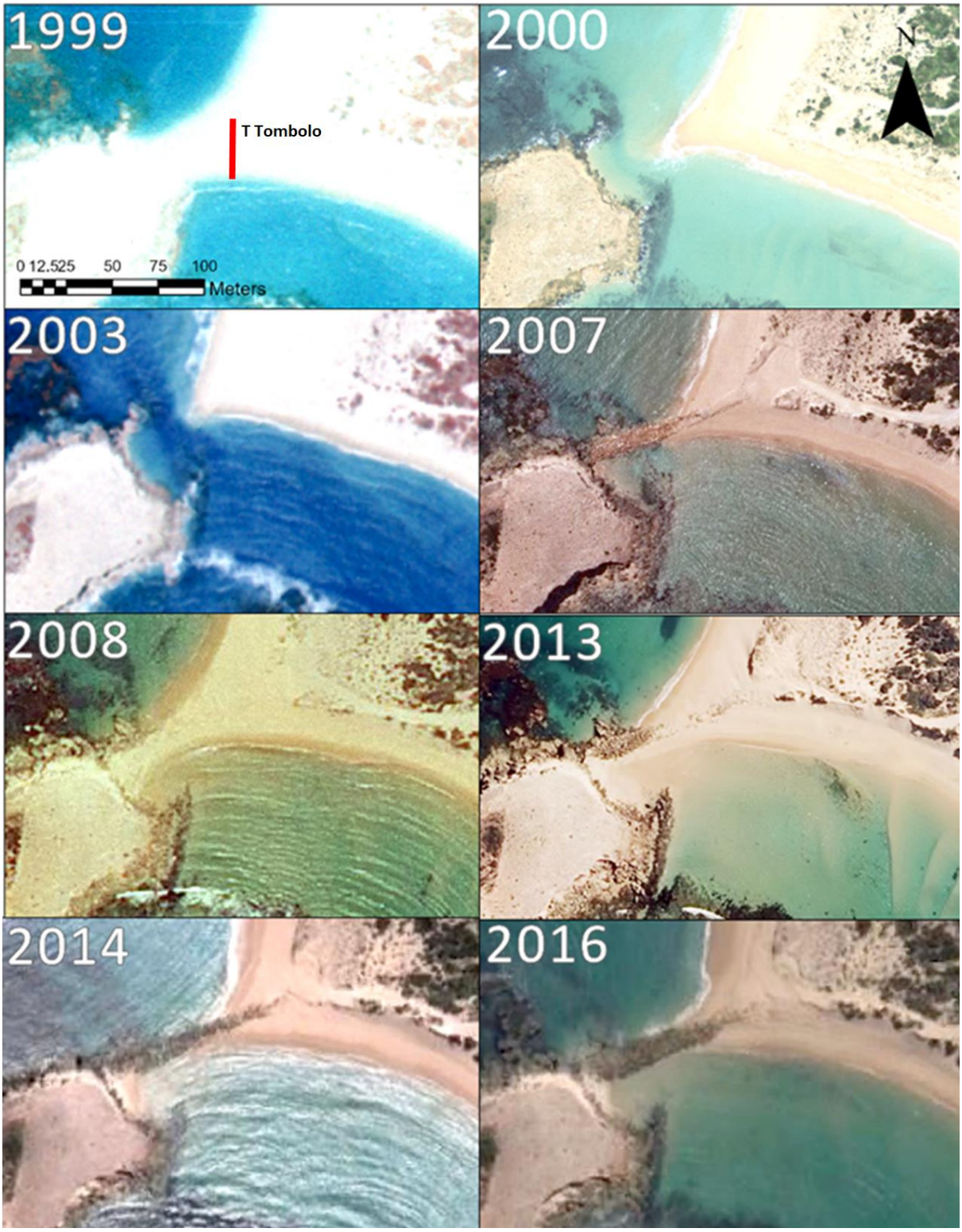

Figure 24: Natural tombolo break through and artificial tombolo implementation sequence between 1999 and 2016. The location of the tombolo transect is indicated in the 1999 image.

3.4.3 Storm Record

3.4.3.1 Pre-Tombolo Breakthrough

Figure 25 shows significant wave height (Hs) for years which had at least one month with Hs in the top 3% (3.87 m or above) within a year between 1979 to present. The hindcast data which dates back to 1979 shows a major storm occurring during both September 1980 and August 1991 (Figure 25). However, there were no notable periods of increased significant wave height between 1992 and 1999, and yet there was a significant increase in erosion particularly at the tombolo end as seen in

Figure 22. This erosion is well correlated with a significant widening of the lagoon and the northern edge of the shore is therefore eroded due to the landward expansion of the lagoon.

3.4.3.2 Tombolo and Post-Tombolo Breakthrough

The gap in the tombolo formed between 1999 and 2000 (Figure 24). Figure 25 shows large values of significant wave height during May of 2000 suggesting that this could be the period in which the gap was created. Several storm periods with significant wave height averaging above 3.87 m were recorded in the years that followed whilst the gap was open. These include September of 2000, August of 2001, and July and September of 2002 which likely acted to drive large volumes of sediment though the gap (Figure 25).

After the artificial tombolo was built, several years with significant storms occurred including in 2003, 2004, 2009, 2013, 2016, 2017, 2018 and 2019 continuing to drive the erosion, although at a slower rate (Figure 25).

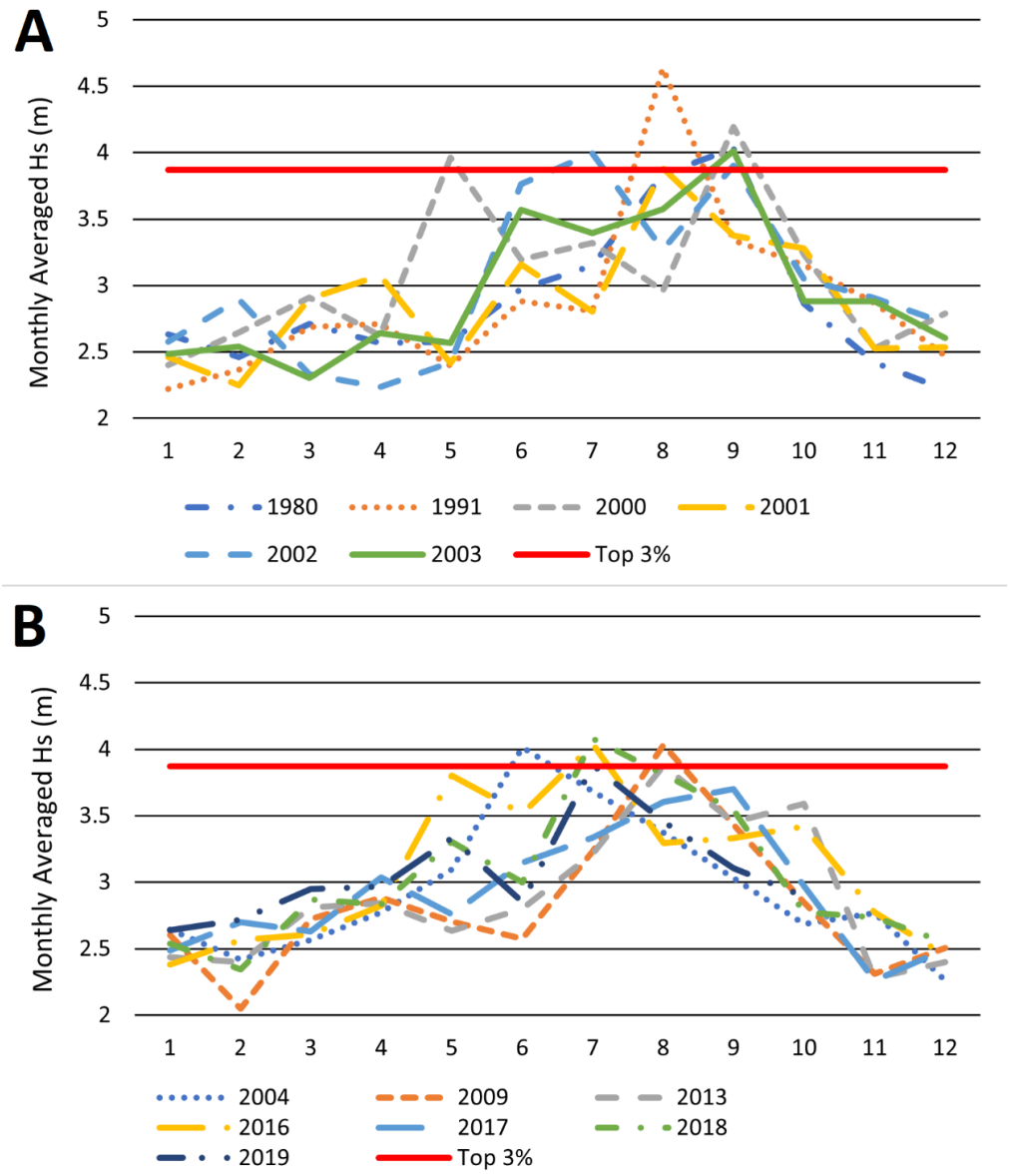

Figure 25: Average Hs for each month for the years between 1979 and 2019 that have at least one monthly average Hs in the top 3%. A (top panel) shows years between 1979 and 2003; B (bottom panel) shows years from 2004 to 2019. Raw data source: European Centre for Medium-Range Forecasts.

3.4.4 Volumetric Analysis of Topographic Profiles

Table 3 shows the volumetric analysis of topographic profiles 710017 (southern end), 710027 (middle) and 710032 (northern end) measured in 2001, 2009 and 2017 by the SA Department of Environment and Water (DEW) (see Figure 18 for locations). Columns B, C

and D show the profile volumes for each year. The volumes loss at each profile between these years is presented in columns E, F and G.

Profile 710017 covers a large section of low lying dunefield at the southern area of the bay (Figure 18). Only 17% of the original volume of sediment was lost from this section between 2001 and 2017 with a reduction of 141 m^3 (

Table 3). At the northern end of the bay at profile 710032 and during this same period a similar level of sediment was lost (164 m^3), however this was 44% of the original volume of sediment (Figure 18,

Table 3). Profile 710027 located in the middle of the bay and lines up with both a high and wide section of the remaining dunefield (Figure 18). This section started with the highest volume at 1028 m^3 and lost 547 m^3 of sediment between 2001 and 2017 leaving it with less volume than is now at profile 710017 (southern end of the bay) and a loss of 53% (

Table 3). A ~3 m decrease in the height of the dune crest at profile 710027 in Figure 26 visually demonstrates how dramatic the erosion has been. The loss between 2001 and 2009 is significantly higher than the loss between 2009 and 2017 for all profiles.

Over the 16-year period (2001 - 2017), the total volume loss along the entire length of the bay, determined by taking into account the distance along shore between the profiles, equated to 175,520 m^3/m. This reflects an annual loss of 10,970 m^3/m. A loss of 15,337

m^3/m/year was observed from 2001 to 2009 significantly higher than the 6,603 m^3/m/year for the period 2009 to 2017. This indicates the rate of erosion has decreased since 2009, corresponding with the removal of the natural tombolo and the instalment of the artificial tombolo (Hesp et al., 2018).

Table 3: Volume analysis for profiles (column A) undertaken in 2001, 2009 and 2017. The base datum for volume calculations was 2 m AHD. Columns B, C and D show the profile volumes for each year. The volumes loss at each profile between these years is presented in columns E, F and G.

A Profile	B 2001 (m^3)	C 2009 (m^3)	D 2017 (m^3)	E 01-17 Loss (m^3)	F 01-09 Loss (m^3)	G 09-17 Loss (m^3)
710017	809	702	668	-141	-107	-34
710027	1028	675	481	-547	-353	-194
710032	375	249	211	-164	-126	-38

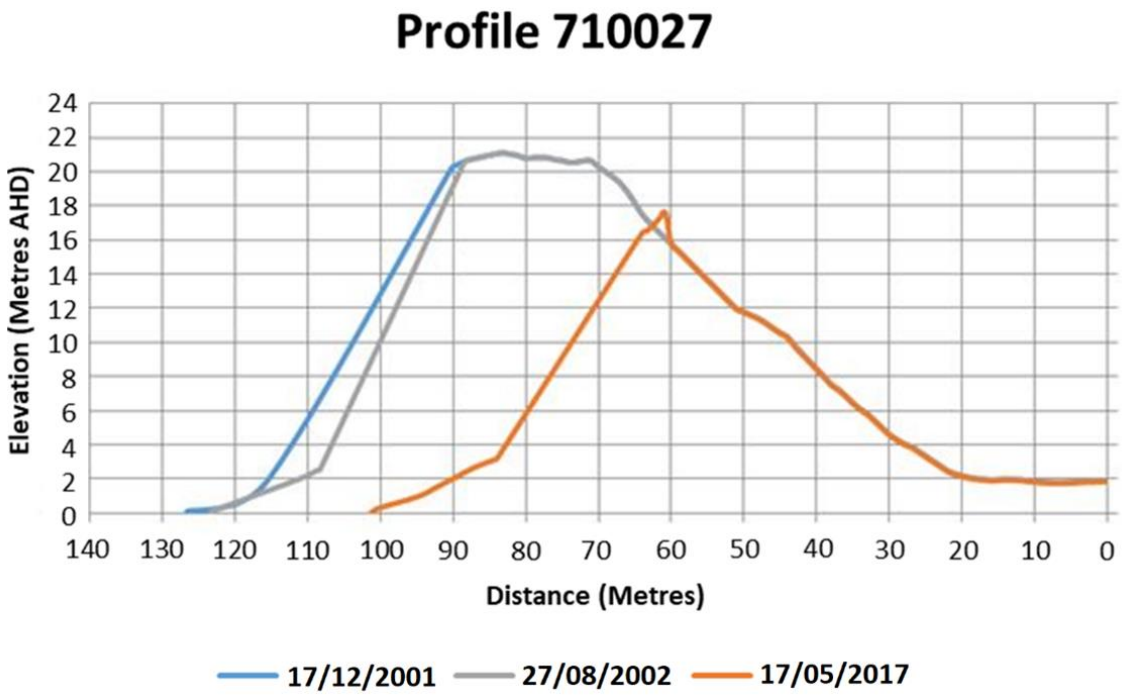

Figure 26: Profile 710027 located in the middle of the embayment. Significant levels of erosion can be seen particularly between 2002 (grey) and 2017 (orange). Sea is to the left. The dune is rapidly becoming smaller as erosion continues and no sediment is supplied between storm and erosion events.

3.4.5 Change Within the Last 3 Years

Figure 27 illustrates topographic profiles taken from the Drone DSM's that demonstrate the effect the erosion is having on the dune system backing the beach. Significant erosion occurred in each of the profiles, and Profile 1 for example shows visible retreat at both the toe and crest of the dune.

Profiles 3, 4 and 5 demonstrate the process of scarping and avalanching that is causing sediment loss from the dune system. In Profile 4 for example, scarping that occurred due to a storm that hit Salmon Hole in August 2017 (Figure 25) actually places the toe of the dune further inland than the 2019 profile due to avalanching post erosion in 2017.

The depositional lobe of the blowout at Profile 1 is translating landwards as expected due to the predominance of onshore winds. A growing depositional lobe also occurs on the lee side of the dune some 40 – 50 m from the waterline in profiles 3 and 4 in (Figure 27). There is

clear visible growth of the same depositional lobe in the DSM's in Figure 28. Further south along the beach at profile 6 in Figure 27 no scarping occurred in 2017; however, obvious retreat is visible in 2019. Further scarping and retreat can be seen in the 2020 profile.

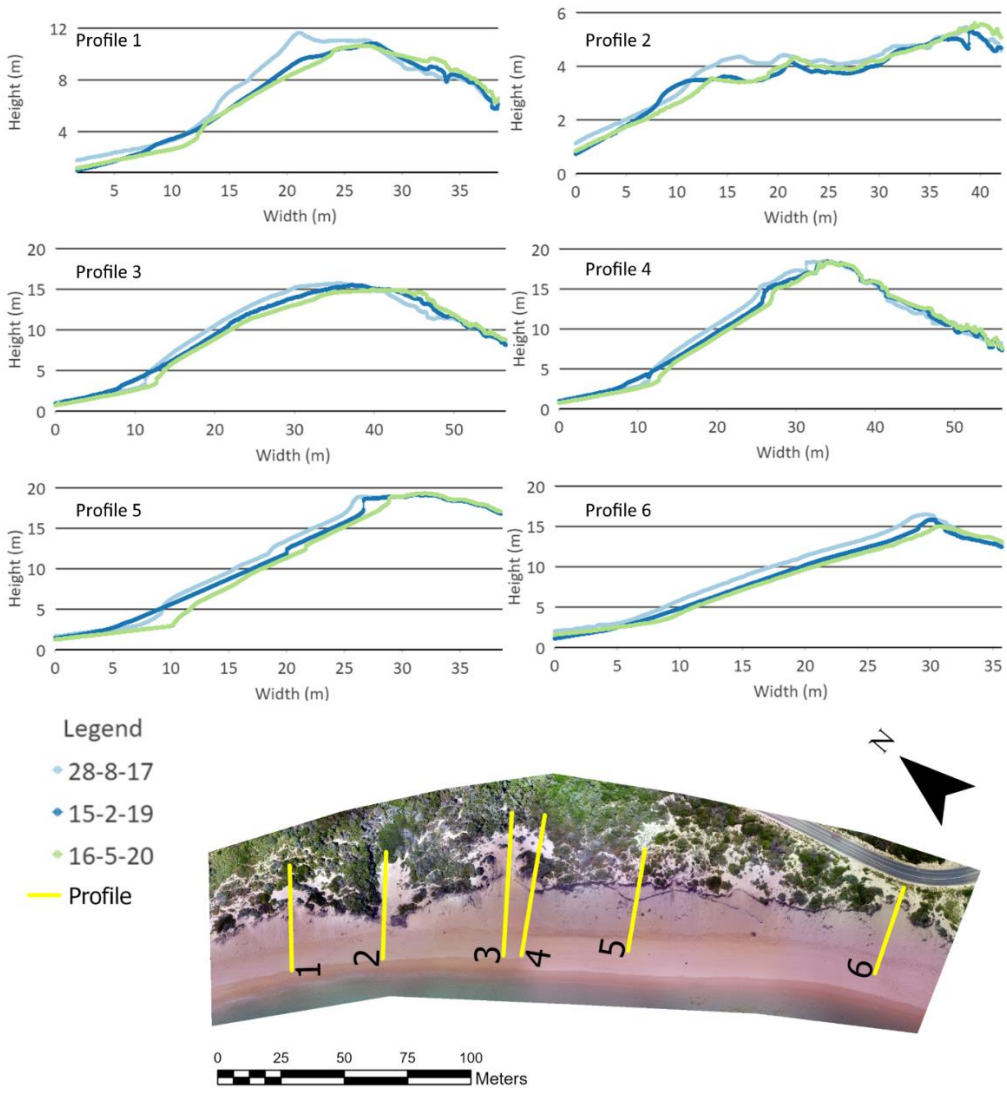

Figure 27: Comparison of profiles taken from DSM's created from drone surveys undertaken on the 28-8-17 and 15-2-19. 6 profiles have been drawn along the scarped dune including areas of interest such as differing stages of blowout formation.

Figure 28: Oblique angle of DSM's of Salmon Hole created though drone surveys and Pix4D photogrammetry software. Surveys from 28-8-2017, 15-2-2019, and 16-5-2020 are shown. Both the survey from 2017 and 2020 show recent scarping at the base of the dune in contrast to the summer survey in 2019 where lack of storm activity has led to a completely avalanched profile. Blowout depositional lobes on the dune scarp crest have increased in size from 2017 to 2020.

3.5 DISCUSSION

Phillips (2009) change assessment system may be used to describe the shoreline changes at Salmon Hole as follows:

3.5.1 Response

Response is made up of two components, the reaction time (time taken for the system to start responding) and relaxation time (time taken for the change to be complete) (Phillips, 2009). Whether Salmon Hole was eroding prior to 1946 is unknown, but little change was observed in 1951 (Figure 9), so it is likely that the erosion trend began sometime after 1951. The reaction time at Salmon Hole has varied as the change has evolved. Initially the reaction time was slow as seen in Figure 29 with an average erosion rate of only 0.63m/yr between 1946 and 1975. A distinct increase in the average rate of the erosion to 1.97m/yr occurred between 1975 and 1999 (Figure 29). During August 1991 Hs averaged above 4.6m, the largest wave heights hindcast from 1979 to present. The extreme storm conditions in 1991 may have led to the subsequent high erosion rate of 3.19 m/yr which occurred between 1992 and 1999 because of recursion in the system (which will be discussed below). It may be that this event tipped the balance in favour of more or increased erosion even though the 1992-1999 period was characterised by a lack of major storm events. However, wave energy was frequent and large enough to drive the alongshore current in the lagoon system furthering erosion even without a major trigger type event.

The tombolo acted as an anchor point for the system that became increasingly unstable as the lagoon widened. Once the tombolo was broken through, the average rate of erosion at Salmon Hole increased to 3.49 m/yr. This is because the creation of the gap clearly resulted

in the alongshore directed lagoon current being able to transport sediment directly out of the bay (rather than out the narrow rock-controlled rip in the bay; Figure 22).

When the artificial tombolo was first put in place in 2003 the reduction in sediment supply from Salmon Hole was so substantial that Pleasant Cove not only stopped accreting but eroded between 2003 and 2007 by around 13.16 m horizontal distance. This drastic change in erosion rate indicates the significance of the tombolo in slowing down the level of sediment loss at Salmon Hole. Post-2008, Pleasant Cove has continued to retreat aided by an increase in years with significant storm periods (Figure 25). Although the rate of erosion at Salmon Hole has decreased since the addition of the artificial tombolo, the system does not appear to be relaxing or reaching a new steady state as erosion continues (Figure 26).

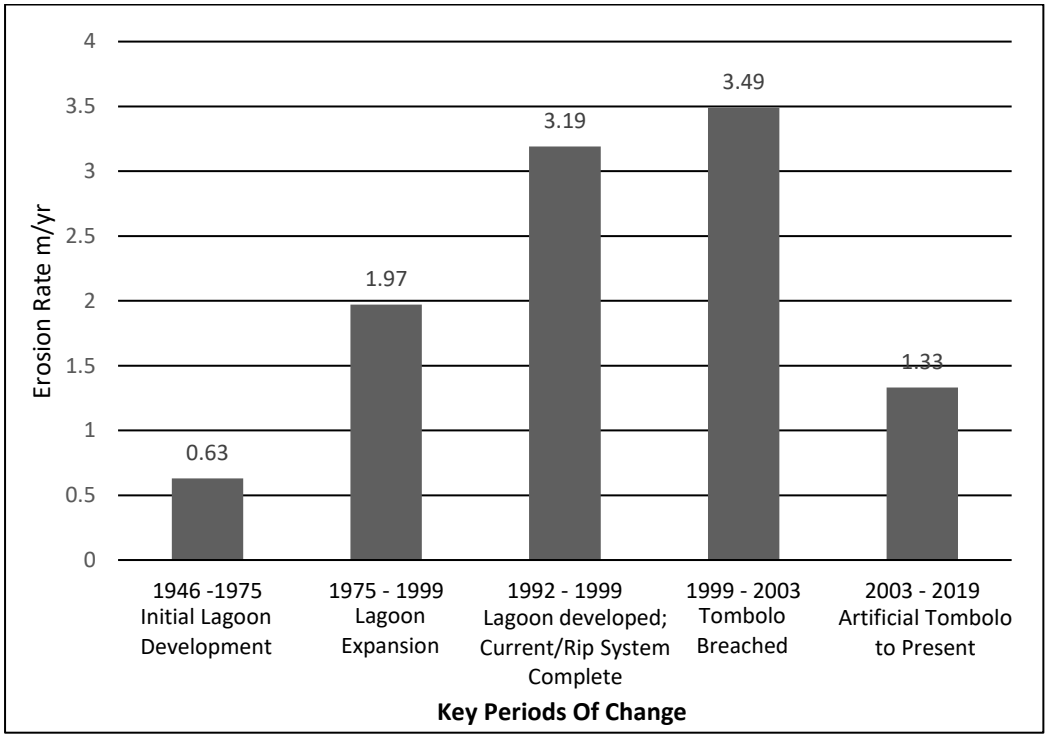

Figure 29: Key periods of change and their corresponding erosion rate in m/yr. Increase erosion can be seen as the lagoon expanded and once the tombolo was breached.

3.5.2 Resistance

Resistance describes how well the system can minimize the impact of a change to the system (Phillips, 2009). It is again made up of two parts. Firstly, the strength of the materials involved in the change, and secondly, the capacity of variables in the system and their ability to absorb any changes. The strength of the dune system to mitigate erosion is low due to the ease at which sediment can be eroded, particularly when little to no vegetation is present on the stoss slope as is the case on the large scarped dune face of Salmon Hole (Kobayashi et al., 2013; Silva et al., 2016). The capacity of the system to reduce the severity of the erosion is also minute due there being zero sediment supply, as no sediment is returned to the beach following storms. The low resistance to the change is partially responsible for the extreme rate and extent of the erosion.

3.5.3 Resilience

Resilience is the capacity of a system to revert to its pre disturbance state (Phillips, 2009). The resilience of Salmon Hole is very low. Due to the extent of the shoreline change, the continued erosion and the lack of sediment supply, it is highly unlikely that Salmon Hole will ever recover towards its pre-disturbance state; in fact, almost an entire Holocene transgressive dunefield has been removed during this post 1950's erosion process.

3.5.4 Recursion

Recursion has been quite pronounced and a key part of the ongoing erosion at Salmon Hole. Recursion results from the response of the change continuing to positively feedback upon itself (Phillips, 2009). To understand how recursion is playing a role at Salmon Hole, it is first necessary to attempt to understand how the extreme erosion is occurring.

Although shoreline change due to erosion is both common place and well documented elsewhere, Salmon Hole is unique due to the means through which this storm induced erosion has occurred (compare Carter et al. 1990; Pye and Blott 2008; van Rijn 2009; Castelle et al. 2015; Sytnik et al. 2018). Salmon Hole's geological inheritance plays a large role in the evolution and present-day processes in the bay which offer insight into what has led to the divergent evolution and severe erosion. During low wave conditions, the bay is protected by the offshore calcarenite reef. However, under storm conditions a geologically controlled longshore current is formed as observed by Fotheringham (2009) as well as latter by the author in chapter 5 of this thesis. As waves break over geological controls on lagoon systems, such as rock and coral reefs, gradients in water level are created due to wave set up, contributing to the "piling" up of water on the lee side of the reef due to impeded return flow (Dean et al., 1997; Lowe et al., 2009; Gallop et al., 2020). This results in the formation of longshore and rip currents that shift dependent on wave direction and tidal stage (Lowe et al., 2009; Gallop et al., 2011; Taebi et al., 2011; Horta et al., 2018), Under storm conditions at Salmon Hole this leads to an increase in erosion as firstly the heightened water level in the bay amplifies scarping and then secondly the current transports the sediment to the structurally-controlled rip adjacent to the northern headland.

Ongoing study of the dynamics of the bay via drone/UAV surveys indicate that waves breaking over the southern end of the reef continue to propagate over the shallow reef and lagoon and then diffract around the bay driving the current even during mid-sized (~1 m high) wave conditions. The angle of the reef allows this as shown by the arrows on the 2016 image shown in

Figure 22 and Figure 31 . It is theorised that this process is amplified under storm conditions. Of note is the fact that the formation of the lagoon between the reef and the dune system began at the southern end of the bay in line with this section of reef as is seen in the 1975 image in

Figure 22. Unlike the processes occurring in a typical embayed beach discussed in the introduction, the reef at Salmon Hole dominates both the in shore and near shore processes. Circulation and cellular rip formation usually seen in such embayment's is predominantly dictated by the headlands, the width of the bay and wave energy (Wright et al., 1978; Short, 1999; Castelle et al., 2016). Here, however, the reef is hindering the formation of both a central rip by creating a barrier against returning wave energy and a rip at the southern headland by focusing wave energy at this point. This encourages circulation in the form of an alongshore current around the bay towards a narrow rock reef-controlled rip channel at the northern end of the bay. Even under large wave conditions a central rip is not formed as shown in Figure 15 and Figure 18 where a crescent of sand can be seen in 2013 positioned up against the centre of the reef. This feature appears to be permanent as it occurs on all aerial imagery and in the recent 3 years of drone survey observations. There has been no evidence of any other forms of circulation within the bay. Salmon Hole is representative of many bays across Southern Australia where normal rip circulation is unable to function due to the presence of an offshore reef.

The erosion of Salmon Hole began post-1950's. The reason for this erosion is currently unknown, but it is possible that over the past ~7000 years of approximate sea level stillstand, the reef was eroded down to a point where recently waves more easily traverse it and higher waves reaching the shoreline initiated the erosion. Subsequently, the reef

created a geologically inherited barrier whose presence created conditions for lagoon formation. Once formed, a longshore current and rip system developed that amplified the erosion. In 1946, Figure 22 shows the beach and dune was still sitting on the reef with waves breaking on the rocks before reaching the sandy shore. By 1975 the lagoon was forming behind the reef, an exit point for waves and sediment was formed at the northern end of the bay allowing sediment to be transported seawards, and the rate of erosion increased (Figure 22 and Figure 29). The large storm in August 1991 may have led to the rapid increase in size of the lagoon and the further development of a rip along the northern headland as shown in the 1992 image in

Figure 22. This led to a significant increase in the amount of erosion between 1992 and 1999 despite minimal storm or significant wave energy during this period (Figure 8). The breakthrough of the tombolo in 2000 then increased the rate of erosion yet again.

Recursion was seen at Salmon Hole, as the rate of erosion was positively reinforced as the lagoon widened. When a storm large enough to erode the base of the dune occurred, the lagoon widened, and this potentially resulted in an increase in the efficiency of the lagoons alongshore current and rip resulting in a positively reinforcing feedback loop furthering the erosion level during each successive storm. Rather than the eroded sand filling the lagoon, the sediment is removed seawards via alongshore current and the rip.

The rate of erosion has reduced since the instalment of the artificial tombolo despite multiple large storms (Figure 25). So, it is possible that the positive reinforcing of the current/rip has reached its peak. The instalment of the artificial tombolo has evidently had an impact by reducing the ease at which sediment can be transported out of the lagoon, however, the rate of erosion was very high before the tombolo broke through when

sediment was also only able to exit via the rip. The reason for the decrease in erosion rate could be due to the way in which the erosion has migrated from south to north, with the current erosion at the northern end of the bay until it cut through the tombolo itself (

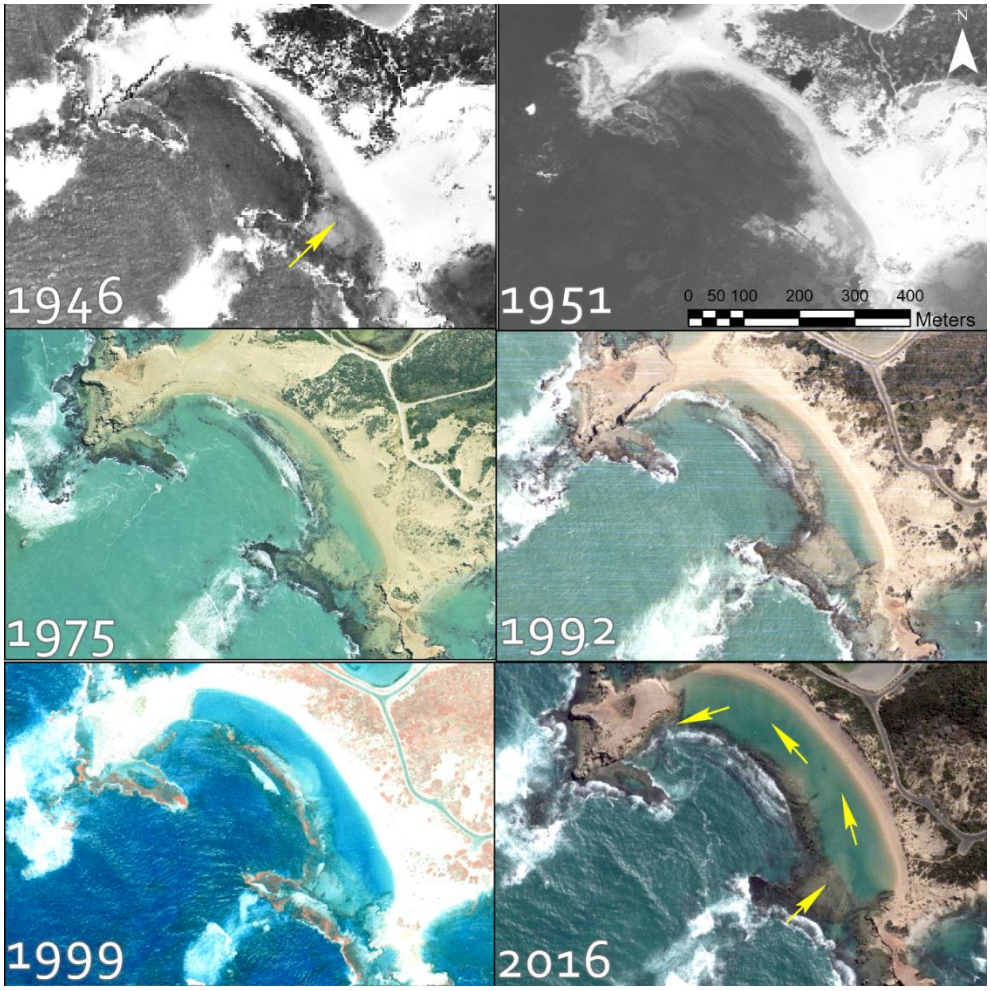

Figure 22). This caused the rate of erosion to steadily increase until the tombolo was broken through (

Figure 22). The lagoon shape has gone from being asymmetric (erosion initiating at southern end) to more symmetric with a similar lagoon width encompassing the bay. This has created a system that is now possibly closer to an equilibrium-like state and this has potentially decreased the rate of erosion.

3.5.5 Dunefield Changes

3.5.5.1 Scarping

The ongoing erosion observed at Salmon Hole is a product of repeated scarping events and a lack of onshore sediment supply to offset the losses. After scarping, eroded sediment is commonly deposited offshore and then often transported back to the beach and dune system through normal wave action and aeolian processes (Carter, 1991; Davidson-Arnott, 2005; Hesp, 2012). However, as has been stated above, this is not the case at Salmon Hole as the eroded sediment is being transported into the lagoon and out of the bay. The dune therefore is not recovering resulting in the further recession of the dunefield after each scarping event.

3.5.5.2 Moderate-scale Transgressive Dunefield Changes

The moderate-scale predominantly active transgressive dunefield backing Salmon Hole in the 1940's has reduced in size by approximately one third whilst the vegetation cover has increased stabilizing it over time (

Figure 22). By 1975 a large parabolic had formed in line with the tombolo whilst at the southern end of the dunefield vegetation cover increased (

Figure 22). By 2016 this parabolic had been severely eroded and the remainder had become vegetated. The southern end of the dunefield was now also mostly vegetated (

Figure 22).

3.5.5.3 Change Within the Last 3 Years

The profiles extracted from the drone survey DSM's support the shoreline change statistics and demonstrate the mechanisms involved in the erosion of the remnant dunefield through scarping (Figure 27). The scaping/avalanching cycle is demonstrated in profile 4 with the

dune toe in 2017 being further back than in 2019. This is because the 2019 profile was undertaken in summer when the dune had time to completely dry out and avalanche causing the overall stoss slope to retreat but the toe to accrete. The deposition at the toe of the dune has then been scarped once more in the winter of 2020 starting the cycle again. Similar scarp retreat processes are described by (Carter et al., 1990). This is also demonstrated by the oblique DSM's shown in Figure 28 where clear recent scarping at the toe of the dune is seen in the 2017 and 2020 surveys whilst the 2019 survey taken during summer has a smooth stoss slope.

There is visible retreat of the stoss face in each profile, however, due to the rate of the erosion, the dune is not translating but rather becoming smaller and disappearing. According to Carter et al. (1990) scarp recovery (scarp fill and ramp development) can lead to the translation of a dune landwards and upwards (Christiansen and Davidson-Arnott, 2004; Hesp et al., 2013; Jackson and Nordstrom, 2018). Although there is clear dune retreat at Salmon Holes the dune is not growing in height, nor translating. The extreme rate of erosion and lack of sediment supply results in dune loss. The height of the dune is declining as the scarp has now passed the original crest/highest point of the dunefield. This means the scarp is now retreating landwards into a lower and lower lee slope and, thus, the dune is gradually reducing in height the further it retreats.

Small blowouts and their associated depositional lobes are also developing in the dune crest as the scarp retreats. Figure 27 also shows depositional lobes at profile's 1, 3, 4 and 6 which are a result of aeolian sediment transport occurring from the exposed upper stoss slope and the development of a blowout at the crest in similarity to studies conducted elsewhere (Hesp, 2002; Christiansen and Davidson-Arnott, 2004). It is unlikely that any of the new

blowouts will ever fully develop. As the dune scarp retreats, the blowouts will be captured by the slope retreat resulting in less sediment available to the depositional lobe. This will not only reduce the blowouts current size but also impact their ability to further develop and grow.

During storm conditions waves can also make their way into the mid bay blowout shown in profile 2 of Figure 27 (Figure 30). With continued erosion a breach through the dunefield to the low-lying lake behind it is imminent. Profile 2 clearly shows a deepening in the blowout's basin as sediment is transported to the downwind depositional lobe.

Figure 30: Swash entering a blowout during a storm at Salmon Hole 17/7/18.

3.5.6 Volumetric Analysis

Table 3 showed a significant drop in the amount of volume lost between 2009 and 2017 compared to between 2001 and 2009. This is not only due to the decrease in erosion rate, although that does play a major role, but it is also due to the decrease in overall dune height

(Figure 26 and Figure 27). As the dunefield height deceases there is less volume of sediment available for erosion above the toe of the dune as it gets scarped. Therefore, the total volume lost is significantly less despite the shoreline still retreating relativity rapidly.

Hesp et al. (2018) estimated the length of time before the dune system is completely eroded by determining the average annual volumetric loss between 2009 and 2017 and dune volume at profile 710027 (Figure 26). If the erosion rate between 2009 and 2017 is maintained the dune will be completely removed by 2048 (30 years from May 2017). At this point in time the 2 m elevation point will be 20 m seaward of the road (Hesp et al., 2018). Storm surge will likely have breached the dune system via the blowout shown in profile 2 (Figure 27). Whether this will aid or hinder the erosion remains to be seen.

3.5.7 Conceptual Change Model

Figure 31 is a conceptual model illustrating the shoreline change from the 1940's to present. The 1940 scenario shows the dunefield initially on the reef as shown in Figure 22. The 1975 scenario shows the lagoon beginning to develop (Figure 31). The development of this lagoon led to an increase in erosion due to the resulting creation of a strong alongshore current and rip system. This resulted in tombolo break through and sediment funnelling out of the gap as shown in the 2000 scenario. The 2020 scenario shows the addition of the artificial tombolo and the current ongoing erosional processes in the lagoon. From the 1940's to present there has also been a substantial loss of the transgressive dunefield that comprised a mix of complex parabolic and transgressive dunes. Finally, the future scenario shows a prediction of what the shoreline will look like in 2050 once the dunefield has been completely eroded away and the artificial tombolo has been outflanked (assuming it is not extended). This new shoreline will be formed around the landward margin of the Pool of

Siloam. This future scenario is subject to change if the erosion uncovers further aeolian calcarenite dune rock units known to variously present in the region.

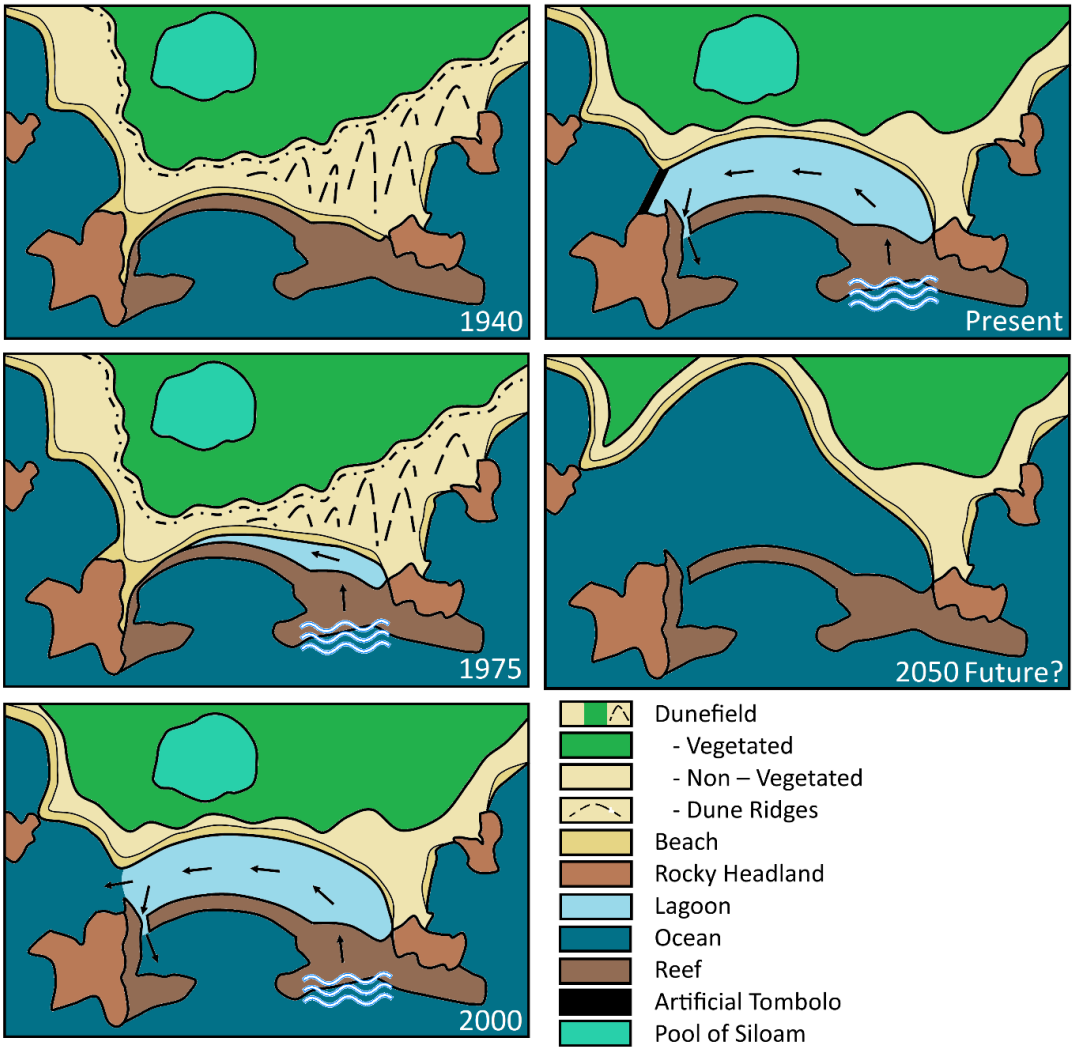

Figure 31: Model demonstrating the development of the coastal system at Salmon Hole. Wave energy propagating over the reef on the right-hand side of the bay has led to this side of the bay eroding first as seen in the 1975 depiction. The angle of the reef causes wave energy to produce a south to north current flowing around the bay producing further erosion and revealing more of the reef on the left-hand side of the bay. A rock-controlled rip running parallel to the left headland transports sediment seawards out of the bay. Eventually the dunefield may be completely eroded and the sea will break though into the Pool of Siloam and create a new embayment (2050 future).

3.6 Conclusion

- The shoreline and dune system at Salmon Hole has eroded an average of 100.17 m in the period 1946 to 2019 at an average rate of 1.44 m/yr. This average rate along the

length of the bay has varied from 0.63 m/yr to 3.49 m/yr depending on storm activity, presence or absence of a tombolo, and lagoon widening and elongation.

- The dynamics observed at Salomon Hole indicate the role geological inheritance can play in bedrock/reef dominated headland-bay systems.
- The cause for the initiation of erosion at Salmon Hole is unknown, however, it may have been that once the reef eroded down to a tipping point where waves could more easily traverse it, higher waves under storm conditions were then able to reach the shoreline and begin to erode it.
- The shoreline change statistics show that it was a combination of the formation of the lagoon between the mainland/dune system and the offshore reef and the resultant breakthrough of the tombolo that have led to the acceleration of the erosion processes observed at Salmon Hole.
- The formation of the lagoon initiated a divergent evolution that continues in the form of a significant longshore current and terminal rip that enhances removal of sediment during and following erosion of the dunes. This does not appear likely to ever return to an equilibrium state closely resembling the initial dune system, since the dune has all but disappeared.
- There are many embayment's similar to Salmon Hole in Australia where reefs dominate the in shore and near shore process environment and normal rip circulation is unable to develop.
- The profiles taken from the drone survey DEM's demonstrate the processes involved in scarping and detail concurrent blowout formation in the scarp crest.
- Salmon Hole strongly indicates how dune systems with little to no sediment supply will respond to future climate and ocean conditions. As sea level rises and storm

magnitude and frequency both increase, shoreline erosion will be the net result. Those shorelines with a lack of sediment supply will not be able to translate landwards/upwards resulting in their removal. If the rate of erosion is maintained into the future, the entire system is likely to be fully eroded within the next 30 years, and the shoreline will then lie along the landward margin of the Pool of Siloam.

- Shoreline change is inevitably going to increase under coming climate change conditions. Anthropogenic pressure on the coast in the form of ever-growing population numbers and infrastructure development mean that analysing and predicating shoreline change is becoming of increasing importance. Despite the close examination of the changes and processes at Salmon Hole the exact nature of the initiation and propagation of the erosion seen here is not yet fully understood. This highlights the difficulty that lies ahead for those managing coastal areas worldwide.

Future work should also consider the impact of wave direction on the historical/current erosion at Salmon Hole Bay as it often plays a key role in the erosion dynamics of embayment's. A look into effect sea level rise has had on the system would also be valuable.

CHAPTER 4
FLOW DYNAMICS OVER A HIGH, STEEP, EROSIONAL COASTAL DUNE SLOPE

Accepted for publication in *Progress in Geomorphology:* Davidson, S.G. (80%), Hesp, P.A. (15%) and Silva, G.M.D. (5%) Flow dynamics over a high, steep, erosional coastal dune slope.

4.1 Abstract

Flow dynamics over a high, unvegetated, and steep scarp slope that fronts a severely eroded relict transgressive dunefield were investigated at Salmon Hole (also known as Post Office Rock), a small headland-bay beach located near Beachport, southeast South Australia. The ~15 m high steep dune at Salmon Hole provided the opportunity to conduct a wind flow experiment on a larger, higher and longer stoss slope than previously studied. The scarp slope is comprised of segments of varying slope that have a significant impact on flow dynamics over the dune. Percentage speed-up and a decrease in turbulence were recorded up the stoss slope due to streamline convergence and flow compression. However, flow expansion at a change in gradient on the upper stoss slope caused a significant drop in wind speed and an increase in turbulence, contrary to what has previously been found in the literature where maximum percentage speed-up is primarily recorded at the crest. Topographic steering typically seen in wind flow over scarps and foredunes was observed at Salmon Hole along with flow separation and the formation of a reversing vortex on the lee slope. This study also demonstrates how a lack of sediment delivery back to the beach and hence to the dune between storm events results in the inability for dune recovery or translation. However, the Salmon Hole study shows that blowouts can still develop and grow through dune cannibalization regardless of the lack of sediment supply from the beach and the recession of the shoreline.

4.2 Introduction

The growth and evolution of foredunes, or other dune types adjacent to the beach are influenced by both aeolian and marine driven processes due to their proximity to the shoreline (Hesp, 2002; Houser and Mathew, 2011; Jackson and Nordstrom, 2018; Cohn et al., 2019). The interplay between wave-driven and aeolian sediment transport is most notable in a post storm erosion period when sediment is, or is not returned to the beach (Carter et al., 1990; Ruz and Anthony, 2008; Hesp et al., 2013).

Scarping is a common occurrence on foredunes and/or the first dune at the back of the beach of sufficient height for overwash not to occur (Carter et al., 1990; Davidson et al., 2020). Storm driven high water level and wave energy often results in undercutting dune stoss slopes leaving a near vertical scarp (Bird, 2000; Sallenger, 2000; Hesp, 2002; Pye and Blott, 2008; van Rijn, 2009; Suanez et al., 2015; Castelle et al., 2017; Houser et al., 2018; Splinter et al., 2018; Davidson et al., 2021). Wind flow then plays a significant role in the recovery of a dune post scarping as a dune ramp (or scarp fill) forms through slumping and avalanching, followed by aeolian sediment transport up the dune ramp, potentially followed by the revegetation of the stoss slope (Carter et al., 1990; Christiansen and Davidson-Arnott, 2004; Hesp et al., 2013; Ollerhead et al., 2013; Davidson-Arnott et al., 2018; Jackson and Nordstrom, 2018). However, if the beach and dune system are in a state of erosional retreat due to repeated scarping and lack of sediment supply, or if sediment is not returned to the beach post-storm, then it can be years to decades for recovery to take place, if it occurs at all (Thom and Hall, 1991; Morton et al., 1994; Zhang et al., 2004; Mathew et al., 2010; Castelle et al., 2017). On coastlines where the foredune is backed by a dunefield, and there is a net sediment deficit, the continual scarping-avalanching sequence can result in the long-term erosion and retreat not only of the foredune but of the dunefield as well (Pye and

Blott, 2008). The higher the dune system behind the beach and the more limited the sediment supply, the lower the potential for recovery after significant scarping, and this can lead to a high scarp with an unvegetated stoss slope (Hesp, 1988; Castelle et al., 2017). The scarp height is directly related to the height of the backing dunes. This lack of vegetation cover, combined with regular wave erosion of the scarp base, can potentially lead to wind erosion, blowout and/or parabolic dune formation (Gares and Nordstrom, 1995; Fraser et al., 1998; Hesp, 2002; Pye and Tsoar, 2008), or even new transgressive sand sheet or dunefield development (Arbogast et al., 2002; Clemmensen et al., 2009; Hesp, 2013; Jackson et al., 2019).

Despite the prevalence of dune scarps, little research has been conducted on wind flow dynamics over them (Hesp et al., 2009; Bauer et al., 2012; Jarmalavicius et al., 2012; Smyth and Hesp, 2015; Hesp and Smyth, 2019; Piscioneri et al., 2019). As scarping events are likely to increase in both frequency and magnitude into the future as sea level rises and storm activity increases under climate change (although it must be noted that not all coastal systems will be affected equally by climate change) (De Winter and Ruessink, 2017; Maximiliano-Cordova et al., 2019; Davidson et al., 2020), it is important to understand the nature of scarp flow dynamics. The key role wind flow plays in the scarp recovery process requires study to improve coastal dune management following erosion events (Piscioneri et al., 2019). Understanding how the presence of a scarp can influence wind flow also provides insight into the significant role scarping plays in shoreline retreat and landwards dune translation as sea level rises (Davidson-Arnott, 2005).

A significant amount of research has been conducted on wind flow over landforms similar to coastal dune scarps such as cliffs, escarpments and forward-facing steps (Tsoar, 1983; Qian

et al., 2011; Pires et al., 2015). In general, as flow approaches a scarp, cliff, or steep slope it is predominantly influenced by the slope gradient (Bowen and Lindley, 1977; Tsoar, 1983; Qian et al., 2011; Pires et al., 2015). On slopes lower than ~55^{o} flow separation at the toe does not occur and speed-up is common upslope (Bowen and Lindley, 1977; Jensen and Peterson, 1978; Emeis et al., 1995). On steeper slope gradients, a reversing vortex often forms within a turbulent flow separation region at the toe of the scarp (Uruba and Knob, 2009; Pires et al., 2011; Qian et al., 2012). The height of this flow separation region is directly proportional to scarp height (Largeau and Moriniere, 2007). There is also the potential for a jet to form at the crest of the scarp (Hsu, 1977; Arens, 1996; Tsoar et al., 1996; Hesp et al., 2009; Jarmalavicius et al., 2012; Yassin and Al Harbi, 2013; Pires et al., 2015; Hesp and Smyth, 2016).

Research that has been conducted on coastal dune scarps includes Hesp et al. (2009) examination of near surface onshore wind flow over an 8 m high foredune with a 0.7 m scarp. They observed helical flow at the base which led to the formation of an echo dune. Smyth and Hesp (2015) analysed wind flow over various steep slopes associated with artificial banks using computational fluid dynamic (CFD) modeling. They found that steeper stoss slopes led to an increased reduction in shear velocity at the toe of these scarp-like structures, and this resulted in greater sediment deposition aiding in foredune recovery. CFD modeling was also used by Hesp and Smyth (2019) to examine wind flow over a 2 m high scarp with varying slope angles (45^{o}, 24^{o}, and 14^{o}), three vertical slopes of differing heights (1 m, 2 m and 4 m) and a 2 m vertical slope subjected to three oblique incident wind approach angles. They found that the extent of wind flow deceleration and separation/reverse vortex development became larger with increased slope angle. Flow

separation at the base was much greater for a vertical scarp than a 45^{o} slope. An increase in scarp height resulted in a greater spatial extent of turbulent wind flow, an enlarged crestal flow separation region, and increased wind speed over the scarp. Hesp and Smyth (2019) also determined that the more oblique the incident wind direction over a vertical scarp the less deceleration occurs and roller vortices are replaced by helicoidal vortices. Piscioneri et al. (2019) examined wind flow patterns over a small scale, vertical foredune scarp. They also observed under incident oblique onshore winds an increase in turbulence and the formation of helicoidal flow vortices within a separation region at the base of the scarp. Flow was then compressed, streamlined, and accelerated at the crest with jet flow occurring under more perpendicular incident flow.

Little work has been done on higher (~+8m), steep (>20—25^{o}), unvegetated slopes particularly in the coastal zone. There has, however, been a significant body of work conducted on flow over the unvegetated stoss slopes of desert transverse or barchan dunes (Bagnold, 1941; Tsoar and Yaalon, 1983; Lancaster, 1985; Lancaster et al., 1996; Wiggs et al., 1996; Neuman et al., 1997; Walker, 1999; Neuman et al., 2000; Walker, 2000; Walker and Nickling, 2002; 2003; Parsons et al., 2004; Schatz and Herrmann, 2006; Araújo et al., 2013; Walker and Shugar, 2013; Smith et al., 2017; Jackson et al., 2020). While the stoss or upwind slopes of transverse dunes typically have gentler gradients than foredunes, these unvegetated dunes share similar morphological features to relatively steep slopes that have partially recovered through avalanching and dune ramp formation (Reffet et al., 2010; Davidson et al., 2020). The main wind flow elements that have been observed over such slopes include: increased turbulence at the dune toe and speed-up upslope towards the crest (Lancaster, 1985; Lancaster et al., 1996; Wiggs et al., 1996; Neuman et al., 1997; 2000;

Walker, 2000; Walker and Nickling, 2003; Parsons et al., 2004; Walker and Shugar, 2013; Smith et al., 2017; Jackson et al., 2020), topographic steering/lee side flow deflection (Tsoar and Yaalon, 1983; Rubin and Rubin, 2013; Walker and Shugar, 2013), and lee flow separation (Walker, 1999; Walker, 2000; Walker and Nickling, 2002; Schatz and Herrmann, 2006; Araújo et al., 2013; Jackson et al., 2020). These processes have also been documented on vegetated foredunes in the coastal zone (Arens et al., 1995; Hesp et al., 2005; Walker et al., 2006; Walker et al., 2009; Hesp et al., 2015; Hilton et al., 2016; Schwarz et al., 2019; de Winter et al., 2020).

Speed-up refers to the topographically forced flow acceleration that occurs over positive (convex) topography (Jackson and Hunt, 1975; Finnigan, 1988; Rasmussen, 1989; Arens, 1997; Hesp et al., 2015). As incident flow approaches a foredune the topography compresses the flow creating a change in the pressure gradient (from high pressure at the toe to low pressure at the crest) leading to an increase in wind speed toward the crest (Arens et al., 1995; Hesp, 2002; Walker et al., 2006; Hesp et al., 2015). Parsons et al.'s (2004) modelling predicted a near surface flow acceleration of 30-50% at the crest, utilizing data of Wiggs et al. (1996) and Neuman et al. (1997). On a bell - shaped or gaussian topography, if all other variables remain constant, near-surface wind speeds will increase with elevation (Jackson and Hunt, 1975; Wiggs et al., 1996). The higher a dune, the greater the convergence of stream lines resulting in increased speed-up (Parsons et al., 2004). The approximate formula for the maximum fractional speed-up ratio as developed by Jackson and Hunt (1975) is as follows:

$$\delta s_{max} = 2H/L \qquad \text{Equation 1}$$

Where δs_{max} is the maximum fractional speed-up, H is the maximum dune height (or hill originally) and L is the dune cross shore half length (Wiggs et al., 1996). This formula indicates the effect an increase in dune or scarp height has on speed-up, since the greater the value of H, the greater the δs_{max}. The steepness of the slope angle also has two key effects on wind speed as flow moves up the stoss slope. The steeper the scarp, the greater the deceleration and stagnation of the flow at the scarp/stoss slope base, whilst the opposite is true at the crest where flow acceleration increases with a steepening of the stoss slope (Wiggs et al., 1996; Parsons et al., 2004; Hesp and Smyth, 2019).

The decrease in flow speed at the base of a scarp, slope or dune occurs due to an increase in the pressure gradient resulting in an increase in turbulence at, or near the toe (Walmsley and Howard, 1985; Neuman et al., 1997; Walker and Nickling, 2002; Walker et al., 2006). This increased turbulence is also due to near surface wind flow reflecting the contours of the windward stoss slope (Zeman and Jensen, 1987; Finnigan et al., 1990; Wiggs et al., 1996; Walker and Nickling, 2002). The flow streamlines become concave at the base which has a destabilizing effect on the flow increasing turbulence and reducing wind speed. The opposite is true as the flow approaches the crest and becomes convex causing it to stabilize, resulting in a reduction of turbulence up slope as flow accelerates (Gong and Ibbetson, 1989; Wiggs et al., 1996; Walker and Nickling, 2003; Weaver and Wiggs, 2011). Once flow passes the crest, flow expansion and deceleration occurs, reversing flow can also form within the separation region or cell potentially assisting in returning sediment to the lee slope (Walker and Nickling, 2003; Parsons et al., 2004; Bauer et al., 2012; Hesp and Smyth, 2019).

Topographic steering refers to the near surface flow deflection that causes the incident wind approach angle to turn to more crest normal as flow proceeds across the stoss slope (Walker et al., 2006; Hesp et al., 2015). This deflection is created by pressure changes upwind of the base of the dune and along the stoss slope that create variation in streamline orientation from the initial flow direction due to mass and momentum conservation (Svasek and Terwindt, 1974; Bradley, 1983). Flow deflection has been frequently observed over dunes whenever incident winds are relatively oblique to the local topography (e.g., Svasek and Terwindt, 1974; Rasmussen, 1989; Arens et al., 1995; Walker et al., 2009; Jackson et al., 2011; Bauer et al., 2012; Lynch et al., 2013; Hilton et al., 2016; Grilliot et al., 2018; de Winter et al., 2020). According to Arens et al. (1995), given the same incident wind direction, the larger a foredune, the greater the degree of topographic steering. They recorded deflections of up to 30^0 on high foredunes (12-15m) (cf. Hesp et al., 2015). Few observations of topographic steering on the windward stoss slope of transverse or similar dunes are recorded in the literature, however, deflection on the lee slope has been commonly observed (Sweet and Kocurek, 1990; Lancaster, 1995; Walker and Nickling, 2002; Baddock et al., 2007; Walker and Shugar, 2013).

Given the dearth of research on steep, high slopes and scarps in the coastal literature, and the few studies in aeolian/desert environments, in this study we examine the following; firstly, flow dynamics (i.e. turbulence, speed-up, topographic steering and flow separation) over a large, unvegetated, steep scarp slope, which backs a narrow reflective beach; secondly, we will further examine why dune recovery has not occurred, including the limited dune translation, the development of scarp slope crest erosion, blowout development and their relationships to shoreline retreat.

4.2.1 Study Site

The experiment was conducted at Salmon Hole (also known as Post Office Rock) a small headland-bay beach located near Beachport, Southeast South Australia (Figure 32). Salmon Hole is characterized by a narrow (~12 m) and steep reflective beach backed by a severely eroded relict transgressive dunefield system that reaches up to 20 m high (Davidson et al., 2021). The south to south west orientation of the coastline in this area results in it facing the full force of prominently south westerly swell and westerly winds off the Southern Ocean (Short, 2019). Wave energy is also persistently high due to mid latitude cyclones that are augmented by west through south storms and south east sea breezes (Short, 2019). For 90% of the year mean significant wave height in the shallow coastal waters of South Australia is approximately 1-2 m high whilst further south offshore waves are 2-3 m high (Young and Holland, 1996).

Since the 1940s the bay has eroded over 100 m at an average rate of 1.52 m/yr, resulting in significant erosion of the dunefield creating a very high scarped unvegetated stoss slope (Davidson et al., 2021). In 1946, the beach was situated on top of the reef consisting of aeolianite calcarenite formed in the Pleistocene positioned approximately 100 m offshore in front of the bay as seen in Figure 33. Over time, the shoreline and dunefield was eroded until a lagoon developed between the reef and the beach. As the lagoon widened, a longshore current/rip system developed which under storm conditions leads to enhanced erosion and sediment transport out of the bay (Davidson et al., 2021). As storm surges and large waves cross the reef, it appears that the water level in the bay is raised as flow out of the bay is restricted by the reef. This not only aids in the scarping of the dune but also creates strong embayment circulation, including the formation of a strong current from south to north and the development of a rip located adjacent to the northern headland

(Fotheringham, 2009; Davidson et al., 2021). Additionally, the orientation of the section of reef at the Salmon Hole southern headland directs wave energy around the bay. This results in the south to north current being present even during moderate wave conditions (Davidson et al., 2021).

Additionally, the tombolo between Post Office Rock and the mainland (see Figure 32) was breached between 1999 and 2000 and remained opened until 2003. During this period, the average rate of erosion at Salmon Hole Bay increased to 3.49 m/yr with a local erosion rate of 6.15 m/yr observed at the northern end of the bay. An artificial tombolo was built in 2004 which has slowed the erosion. Between 2003 and 2019 the bay has continued to erode at an average rate of 1.33 m/yr (Davidson et al., 2021). This erosion, and an apparent lack of sediment supply to the bay has resulted in Salmon Hole's negative sediment budget. While the scarp is formed on the first dune at the back of the beach, we do not consider this dune a foredune as it was not formed by aeolian deposition in pioneer plants on the backshore as per the definition by Hesp (2002); this dune is actually part of the relict (vegetated) transgressive dune system.

Between 1985 and 2018 oceanic wind speed increased by 1.5 m s^{-1}/year and significant wave height by 0.3 cm/year in the Southern Ocean, with larger increases in extreme conditions (Young and Ribal, 2019). This is set to continue with the magnitude of a 1 in 100 year significant wave height event likely to increase by 5 to 15% in the Southern Ocean by the end of the 21st century (Meucci et al., 2020). Using the SSP3-7.0 scenario from the AR6 IPCC report NASA's sea level projection tool, sea level is expected to rise by 0.68 m near Beachport by 2100 (NASA, 2021).

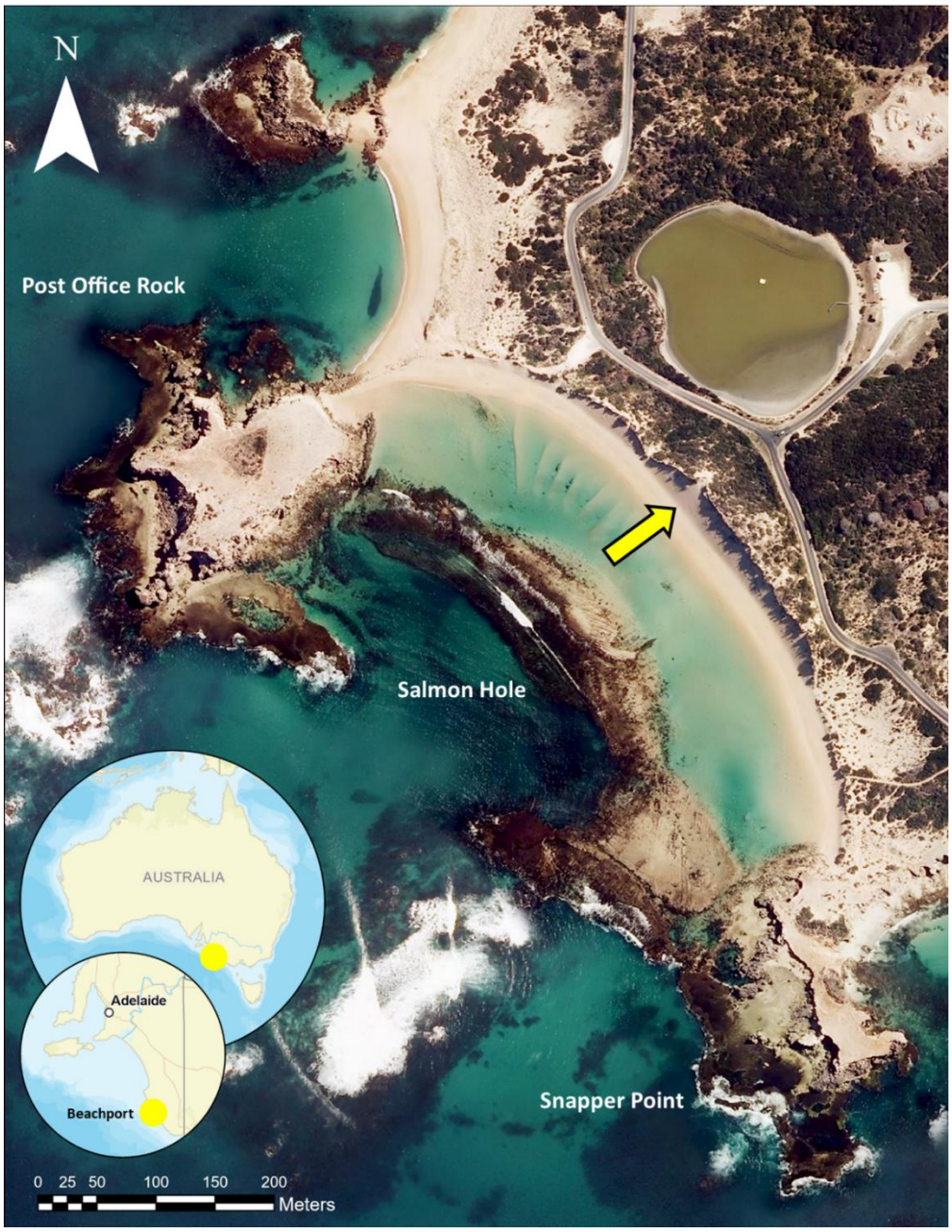

Figure 32: 2013 aerial photograph of the Salmon Hole study site situated near Beachport, southeast South Australia, 37.4878° S, 139.9991° E. The scarp has been formed on the seaward face of a relict transgressive dunefield. Yellow arrow indicates experiment location.

Figure 33: Aerial image taken in 1946 (on the left) in comparison with an image taken in 2016 (on the right). Salmon Hole has undergone severe erosion whilst the bay to the north has accreted. The transgressive dunefield was more active in the 1940's with significant areas of active, mobile dunes at that time.

The section of scarped dunefield where the experiment was undertaken is positioned in the middle of the Salmon Hole embayment (see yellow arrow in Figure 32). It is located near the highest point of the dunefield and backed by a blowout with a landward depositional lobe (Figure 34). The dune crest is 14.86 m high above MSL and is located at the centre of the blowout. The distance from the toe of the scarp to the crest measured up the stoss slope is 34.5 m. The stoss slope is unvegetated and maintains a relatively stable and steep angle of ~30^{o} for the majority of the scarp before a change in slope at the 18 m point upslope. From this change in slope the stoss slope gradually becomes more convex before becoming horizontal at the crest. The position of the anemometers is indicated in Figure 34.

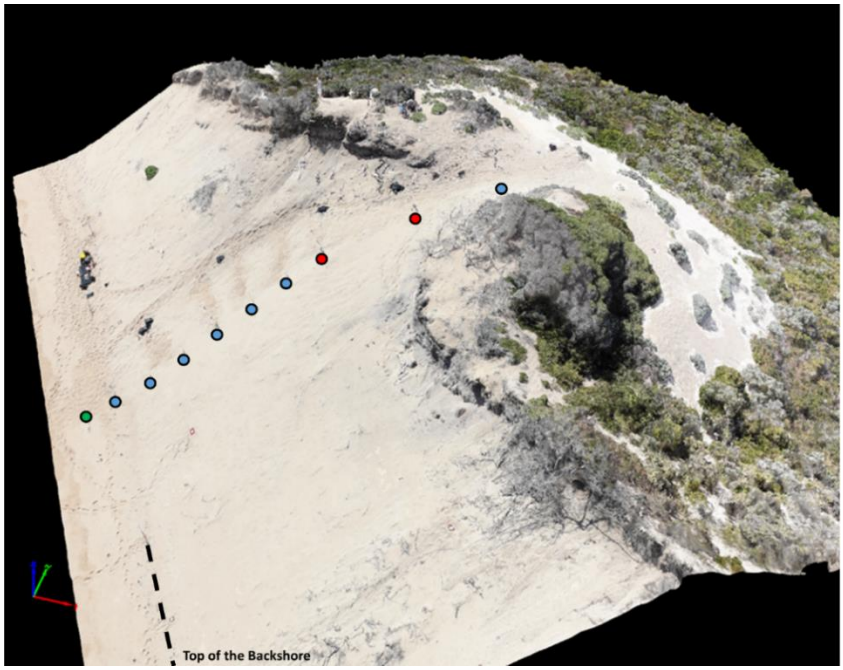

Figure 34: DSM of the scarped dune at Salmon Hole created using a drone survey undertaken on the day of the experiment. The blowout depositional lobe can be seen on the lee slope of the dune. Anemometer positions are indicated by markers with 3D only positions represented by blue circular makers, 2D and 3D positions designated with red circular markers, and the green marker on the beach showing the position of the reference anemometer.

4.3 Methodology

A wind flow experiment was conducted on February 26th, 2020, during a moderate wind speed event. Wind velocity and direction were measured at 1 Hz via RM Young 2D (model 85000) and 3D (model 81000) ultrasonic anemometers. Measurements were taken between 9:02am and 12:34pm. The data measured from each anemometer for the period of the experiment was subsequently averaged as a total and in 1-minute intervals for analysis in the results. The anemometers were set in a line at 49 degrees NE perpendicular to the beach line which was orientated at 321°. Each anemometer was aligned to face North using a compass. The wind direction ranged from a minimum of 258° (WSW) to a maximum of 285° (W). This resulted in a minimum incident wind approach angle of 29° and a maximum of 56°.

Incident wind speed was obtained from a 3D anemometer (3D1) located on the beach 2 m from the base of the scarp at 2.2 m high. Several 3D ultrasonic anemometers were placed up the stoss slope of the dune perpendicular to the beach each at 0.4 m high starting at the base of the dune with 3D2. Sonics 3D3, 3D4, 3D5, 3D6, 3D7 and 3D8 were then placed at 3 m intervals until the change of slope at 18 m (Figure 34 and Figure 35). 3D9 was placed at 25 m and 3D10 was positioned at the crest of the dune 34.5 m upslope from the base (Figure 34; Table 4).

2D sonics were placed at 18 and 25 m up the stoss slope at 3D positions 8 and 9in groups of 3 at various heights, beginning at the base with 2D1 positioned at 0.2 m high, 2D2 at 0.7 m high and 2D3 at 1.44 m high (Figure 34 and Figure 35). The sonics where placed 0.3 m apart and aligned parallel to the slope (Table 4).

Table 4: Height above mean sea level, distance from the toe of the dune up the profile and the slope angle for each anemometer position.

Anemometer	Height Above MSL (m)	Distance Along Profile	Slope Angle
3D1	2.201	2 m from dune toe	16°
3D2	2.668	0	20°
3D3	4.166	3	31°
3D4	5.633	6	31°
3D5	7.218	9	31°
3D6	8.552	12	30°

3D7	9.825	15	30°
3D8	11.277	18	28°
3D9	13.388	25	15°
3D10	14.858	34.5	-1°

Figure 35:Experimental set up looking downslope from the 3D and 2D anemometers positioned at 18 m up the dune slope from the dune toe.

Coloured smoke cakes used for photography special effects were used to visualize 3D flow via video. The footage was then analysed frame by frame at 1 second intervals to determine flow patterns. Multiple mini-wind vanes were also utilized to visually record surface wind directions.

A drone survey of the experiment site was also undertaken during the experimental period. This was conducted using a DJI Mavic 2 Pro drone which took vertical aerial imagery of the experiment site with 80% overlap between images. Ground control was achieved using a Trimble Real Time Kinematic Global Navigation Satellite System (RTK-GNSS) that accurately measured (approx. 2cm error) the positions of 10 targets spaced evenly throughout the survey area. A Digital Surface Model (DSM) was then created using Pix4D photogrammetry software and the images from the drone survey (Figure 34). The position of the instruments was also recorded using a Trimble RTK-GNSS and overlaid on the DSM. A 2D topographic profile was created using the RTK-GNSS.

4.3.1 Analysis Methods

Wind speed was determined using either Equation (2) or Equation (3) subject to the use of either 2D or 3D anemometer data. u – x axis vector of wind speed (west – east), v – y axis vector of wind speed (south – north), w – vertical vector of wind speed.

$\sqrt{((u^2) + (v^2))}$ = Magnitude of the vector (2D anemometers) (2)

$\sqrt{((u^2) + (v^2) + (w^2))}$ = Magnitude of the vector (3D anemometers) (3)

The arctan function was used to calculate wind direction in the opposite (-180°) of the horizontal flow vector so that the direction was relative to the direction it originated from. This was adopted from Jackson et al. (2011) and is shown in Equation (4):

$DEGREES(ATAN2\ u, v)$ = Wind direction in degrees (4)

where DEGREES is Degrees function in excel, ATAN2 – atan2 function in excel (from the 2-argument arctangent), u – x axis vector of wind speed (west – east), and v – y axis vector of wind speed (south – north).

In order to determine the percentage change of wind speed-up the scarp, the ratio u/u2.2 was used. This is the ratio between wind speed measured at each anemometer position up the dune compared to the speed measured at 3D1 positioned at 2.2 m high on the beach following (Taylor et al., 1987; Walker and Nickling, 2002).

To estimate turbulence, the standard deviation was firstly calculated to quantify oscillations in wind direction (Walker et al., 2009; Smyth et al., 2012; 2013). Then secondly, the CV was determined as a gauge of wind speed variation in relationship to the mean wind speed using Equation (5) (Piscioneri et al., 2019).

$$CV = \frac{SD}{mean} \quad (5)$$

4.4 Results

4.4.1 Incident Wind Conditions

1-minute averages of wind velocity and direction for the entirety of the experiment from the reference 3D anemometer on the beach are shown in Figure 36. The average wind speed measured on the beach was 10.64 m s^{-1} at 2.2 m height above mean sea level. Primarily westerly winds (onshore) were recorded with winds progressively becoming more oblique to the scarp throughout the experiment. The average direction at the study site reference was 273^0 (True North). Wind velocity dropped throughout the recording period whilst the winds became, on average, more oblique. In Figure 36, a relationship between wind speed and direction is apparent; although wind speed is increasing overtime, peaks in

wind speed are associated with a direction of approx. 280 ° whilst troughs correspond to the wind direction changing more towards ~ 265 °.

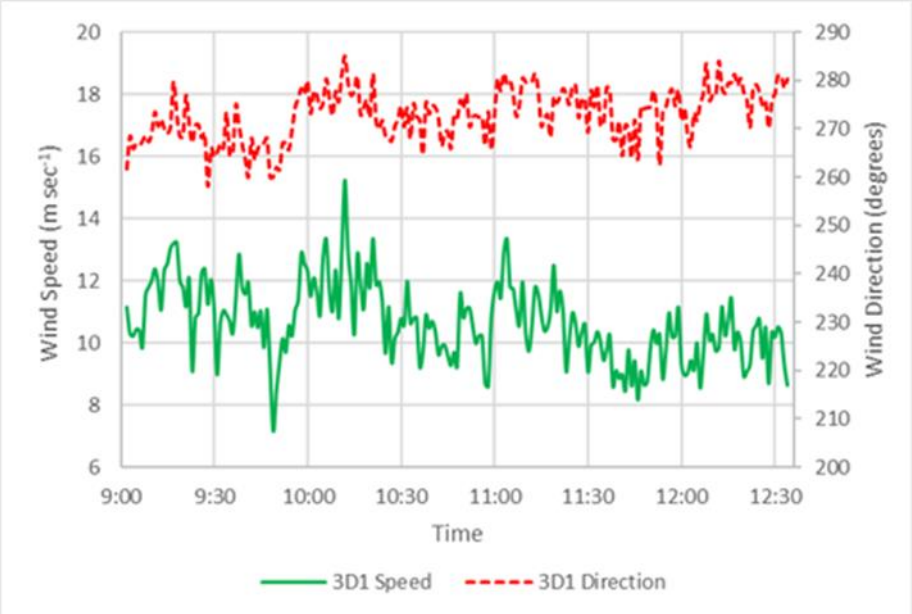

Figure 36: 1-minute averages of total wind speed in m s^{-1} (solid line) and wind direction in degrees (True North, dotted line) from the reference 3D ultrasonic anemometer 3D1 positioned on the beach at 2.2m high. Measurements were taken between 9:02am and 12:34pm as indicated on the x axis.

4.4.2 Flow Dynamics

4.4.2.1 Flow Direction

Wind direction changes towards crest normal as flow progresses over the dune (Table 2, Figure 37). The variation in direction is also reduced up the stoss slope from 3D2 to 3D9. The average direction for the entire experiment period at 3D1 (positioned at 2.2 m high and on the backshore) was 273°, while the average direction at 3D2 was 288° (positioned at the toe of the dune) (Table 2, Figure 40). This difference is potentially due to the difference in height and/or the increased turbulence at 3D2 (CV of 0.18 at 3D2 compared to 0.08 at 3D9). Topographic steering then causes the flow direction to become more perpendicular to the beach as it moves to 3D7 at 258° (Table 2, Figure 40). The flow then swings back marginally

more westerly at 3D8 and 3D9 (Figure 40) to 259^{o} and 262^{o} respectively (Table 2). This appears to be due to the presence of the marginal vertical slope of the blowout that is visible at the top of the scarp and held in place by the vegetation roots on the crest (Figure 34). The blowout wall may be steering the wind slightly back to more perpendicular to the shore at positions 8 and 9. At 3D10 the average wind direction was 255^{o}. However, the direction at 3D10 varied significantly throughout the experiment, similar to that seen at the toe of the dune (Figure 37 (B)). This is unusual with the least amount of variation in wind direction usually seen at the crest (Gong and Ibbetson, 1989; Wiggs et al., 1996; Walker and Nickling, 2003; Hesp and Smyth, 2019). It is therefore likely that the direction of the flow at position 10 is influenced by the marginal erosional walls of the blowout which are responsible for creating further local flow steering. Flow expansion following the change of slope at position 8 may also play a role (Table 2, Figure 40). From the reference anemometer (3D1) to 3D10 at the crest of the scarp there was a deflection of 18^{o} (273^{o} to 255^{o}). However, since 3D10 appears to be influenced by the blowout walls, (Table 2), and if it is ignored, between the beach (3D1) and 3D9 there was an average change of only 11^{o} (273^{o} to 262^{o}). Note, however, a larger deflection of 32^{o} (288^{o} to 256^{o}) occurred between 3D2 and 3D7 which is on the steepest portion of the slope (Table 2). Direction of flow up the dune behaved as expected based on previous observations in the literature (e.g., Rasmussen, 1989; Arens et al., 1995; Wiggs et al., 1996; Parsons et al., 2004; Hesp et al., 2005; Walker et al., 2006; Hesp et al., 2013) until position 8 where the morphological features and change in slope have an impact.

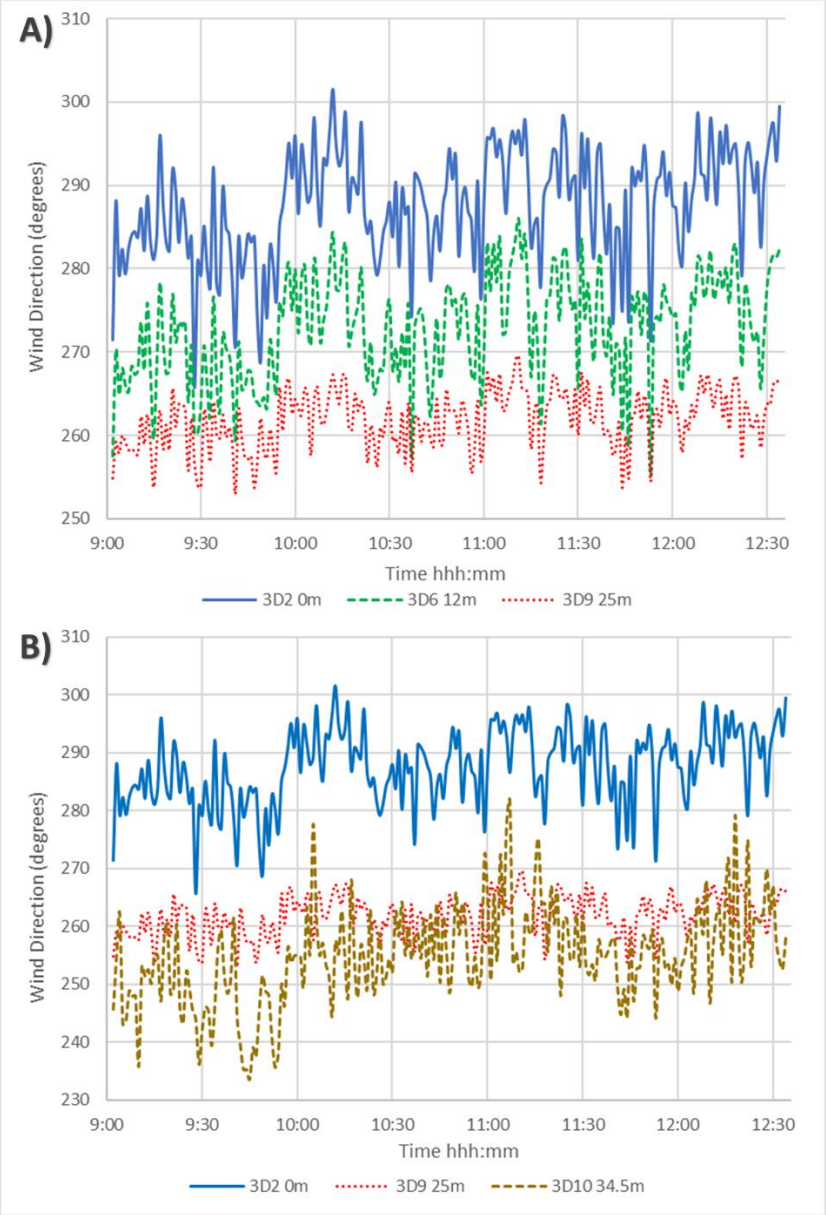

Figure 37: A) One-minute averages of wind direction from 3D anemometers at positions 2, 6 and 9 situated at a height of 40 cm above the bed. 3D2 is located at the toe of the dune, 3D6 is approximately at the mid-way point, and 3D9 near the crest. Topographic steering caused flow to turn more crest normal toward the crest whilst streamline compression has resulted in less variation in direction up the slope. B) One-minute averages of wind direction from 3D anemometers at positions 2, 9 and 10 situated at a height of 40 cm above the bed. 3D2 is located at the toe of the dune, 3D9 near the crest and 3D10 at the crest. Topographic steering caused flow to turn more crest normal toward the crest whilst streamline compression has resulted in less variation in direction up the slope from 3D2 to 3D9. However, there is a distinct increase in variation in wind direction at the crest.

4.4.2.2 Wind Speed

Flow speed-up is clearly apparent from 3D2 to 3D9 and occurred for the entire study period. The same decrease in incident wind speed over time that was recorded at the reference anemometer on the beach is also observed in this data. 3D10 had a more significant drop in both wind speed and extent of variation in speed at 10:00am, and this aligns with the change in wind direction to more oblique winds recorded at this time (Figure 36 and Figure 38).

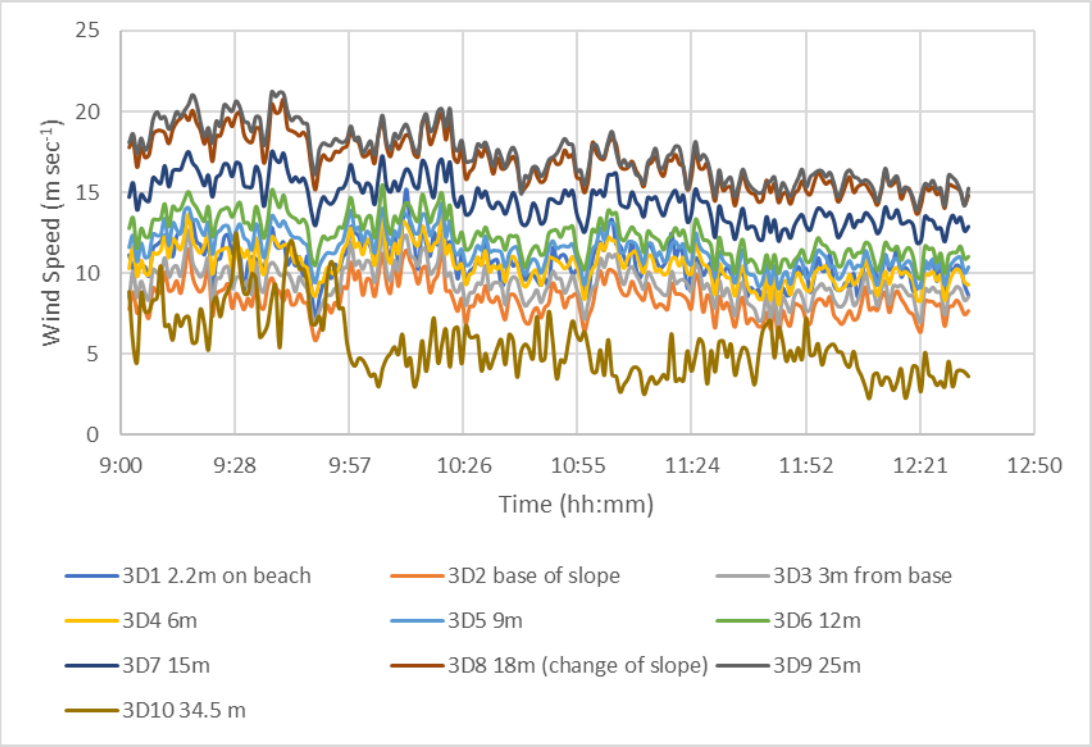

Figure 38: One-minute averages of wind velocity from 3D anemometers at 40 cm above the bed at 3m up-slope intervals over the dune.

In Figure 39 speed is initially reduced at the base of the dune (3D2) with a drop of 20% at the toe of the scarp presumably due to an adverse pressure gradient and an increase in turbulence (cf. Wiggs et al., 1996). Flow speed remains relatively constant until 3D4 where the percentage wind speed on the beach is the same as that at 3D4. From that point there is

a consistent increase of approximately 8% between each anemometer from 3D4 (99.2%) to 3D6 (115.9%) (Table 2). There is then a surge in speed-up with a consistent increase of approximately 22% between 3D6 (115.9%) to 3D8 (159.1%) (Table 2). However, due to the change in slope at 3D8 the increase in speed to 3D9 (163.4%) is only 4.3% (Table 2). A further change in slope results in a significant drop in percentage velocity to 52.6% at the crest (Table 2).

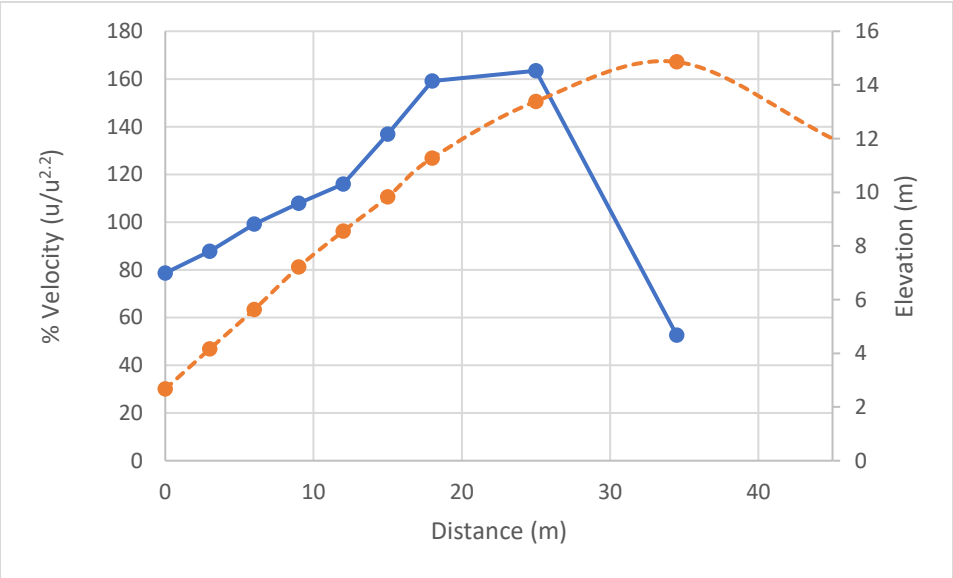

Figure 39: Percentage mean wind speed ($u/u^{2.2}$) from 9:02am to 12:34pm for each anemometer relative to a reference anemometer at 2.2 m on the backshore during predominantly oblique incident winds. The orange(dashed) line shows the foredune topography. Percentage wind speed initially decreases at the base of the dune and then rapidly increases as topographic forcing creates speed-up the dune. Once the crest of the dune is reached the percentage speed drops significantly.

4.4.2.3 Perpendicular vs Oblique Wind Approach Wind Effects

The overall averages of wind speed, percentage speed (relative to the anemometer recording at 2.2m on the beach) and direction for the entire experiment are shown in Table 5 along with the averages from between 9:28 and 9:54am when the incident wind direction was most perpendicular, and between 9:57 and 10:24am when the incident approach angle of the wind was most oblique. The arrows in Figure 40 indicate both wind direction and

change in percentage speed over the dune. The percentage speed has been determined using the average reference speed from each particular time frame. There is a clear increase in percentage speed under more perpendicular winds. At 3D9 the percentage speed was 183% when the wind was perpendicular compared to 154% when the wind was approaching the dune more obliquely (Table 2). This is a result of a reduction in the effective slope angle as flow approach angle becomes more oblique resulting in less speed-up, which has been observed to increase as slope angle increases (Arens et al., 1995; Hesp et al., 2015). At the crest the percentage speed is significantly lower when the winds where more oblique (40% compared to 86%). This, however, is partly due to the shelter created by the erosional walls of the blowout at the crest.

There is also a difference in the degree that wind direction changes up the slope under the two distinct incident wind approach angles. Whilst an increase in speed-up occurred when the wind was more perpendicular to the dune slope, it was the degree of steering that increased under more oblique winds.

A direction change of 34.8 degrees was recorded between 3D2 and 3D7 whilst the winds were oblique (3D1 Ave 277^{o}), compared to 27.8 degrees when the winds were more perpendicular (3D1 Ave 265^{o}) (Table 2). Interestingly, despite the differing incident wind approach angles, the average wind direction during both time periods changed approximately 15 degrees when the incident flow encountered the base of the dune between 3D1 and 3D2 (Table 2).

Table 5: Average wind speed, percentage speed-up, and average direction for winds during the entire recording period, when the reference wind direction was more oblique and when it was more perpendicular.

3D Anemometer	More Oblique	Overall Average	More Perpendicular
3D10	Av 4.79 m s^{-1} 40% 256°	Av 5.54 m s^{-1} 53% 255°	Av 9.02 m s^{-1} 86% 244°
3D9	Av 18.60 m s^{-1} 154% 264°	Av 17.30 m s^{-1} 163% 262°	Av 19.20 m s^{-1} 183% 259°
3D8	Av 18.21 m s^{-1} 151% 262°	Av 16.85 m s^{-1} 159% 259°	Av 18.38 m s^{-1} 175% 254°
3D7	Av 15.82 m s^{-1} 131% 258°	Av 14.50 m s^{-1} 137% 258°	Av 15.59 m s^{-1} 149% 252°
3D6	Av 13.65 m s^{-1} 113% 276°	Av 12.29 m s^{-1} 116% 273°	Av 13.10 m s^{-1} 125% 266°
3D5	Av 12.81 m s^{-1} 106% 275°	Av 11.44 m s^{-1} 108% 275°	Av 11.94 m s^{-1} 114% 268°
3D4	Av 11.91 m s^{-1} 99% 280°	Av 10.52 m s^{-1} 99% 276°	Av 10.72 m s^{-1} 102% 269°
3D3	Av 10.73 m s^{-1} 89% 292.5°	Av 9.33 m s^{-1} 88% 287°	Av 9.23 m s^{-1} 88% 280.3°

3D2	Av 9.76 m s^{-1} 81% 292.8°	Av 8.37 m s^{-1} 79% 288°	Av 8.10 m s^{-1} 77% 279.8°
3D1	Av 12.10 m s^{-1} 100% 277°	Av 10.64 m s^{-1} 100% 272°	Av 10.55 m s^{-1} 100% 265°

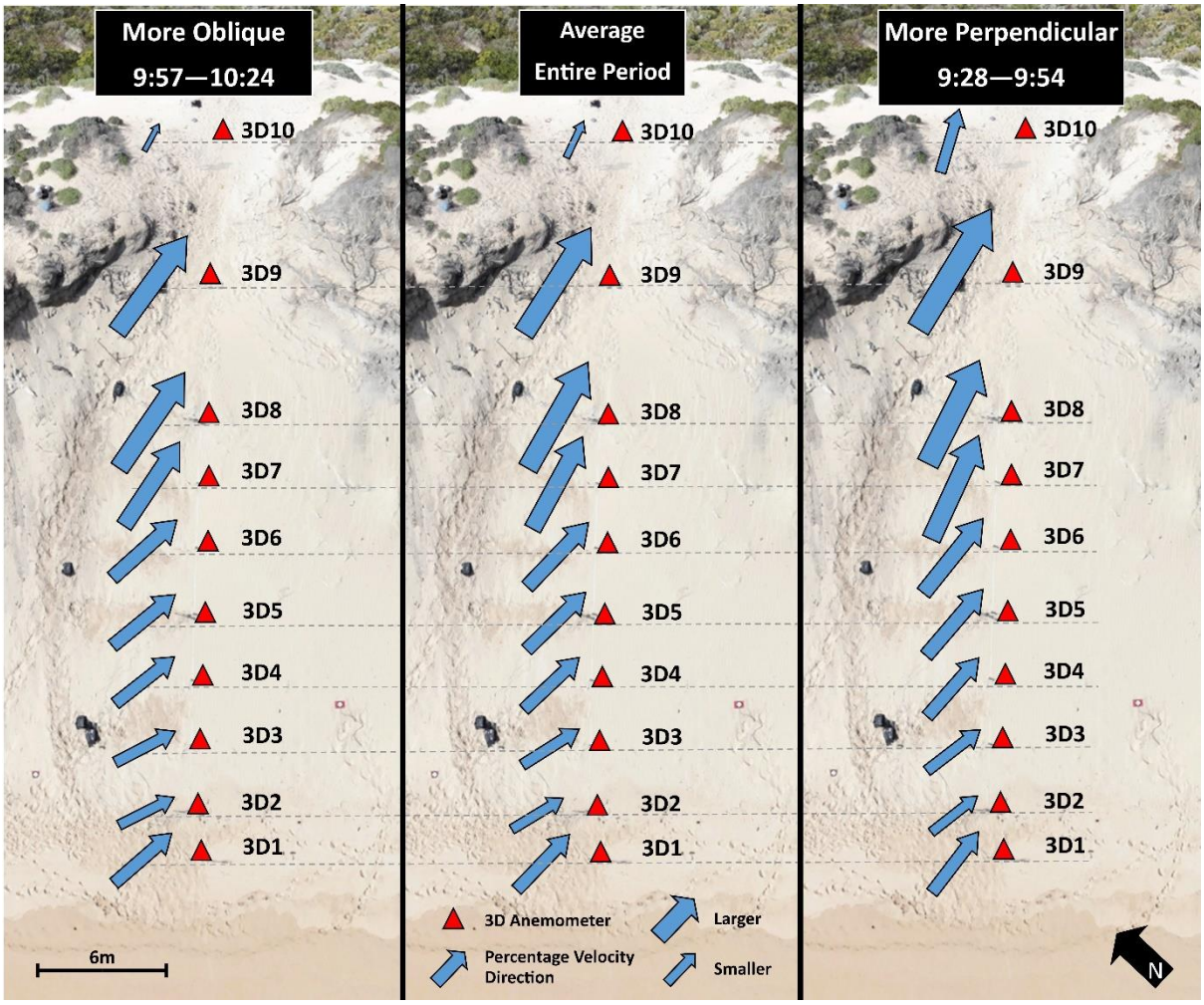

Figure 40: Flow speed and direction for more oblique, average, and more perpendicular incident winds. Positions of 3D anemometers are indicated by triangles. Arrows indicate average direction and arrow size indicates percentage speed.

4.4.2.4 2D Wind Velocity Profiles

The variation in vertical speed is significant with percent velocity at position 8 being 67% near the surface (0.2 m) and rising to 75% higher at 1.44 m above the bed (Figure 41 (A)). A similar increase is seen at position 9; however, the overall speed is slightly higher with 73% at 0.2 m and 82% at 1.44 m (Figure 41 (A)). The vertical speed difference between 0.7 m and 1.44 m is slight at position 8 (73 - 75%) and marginally larger at position 9 (79 - 82%) (Figure 41 (A)). This difference has resulted in the profile at position 8 being non logarithmic whilst at position 9 the three measurement points follow a logarithmic profile (Figure 41 (B)).

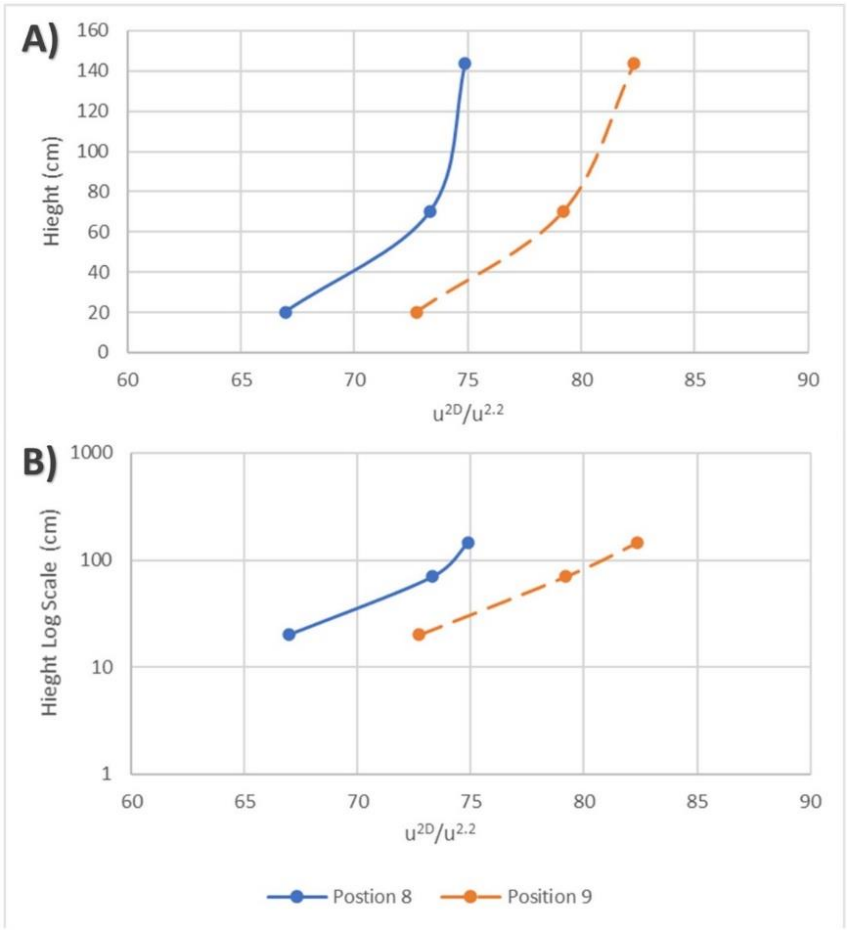

Figure 41: A) Average percentage velocity ($u^{2D}/u^{2.2}$) recorded at position 8 and position 9 from 9:02am until 12:34pm relative to a reference 3D anemometer at 2.2 m height in the backshore during mostly oblique incident winds. B) Average percentage velocity ($u^{2D}/u^{2.2}$) recorded at position 8 and position 9 from 9:02am until 12:34pm relative to a reference 3D anemometer at 2.2 m height in the backshore during mostly oblique incident winds.

4.4.2.5 Turbulence

Between 3D2 and 3D9 the CV in wind speed steadily decreases as flow compresses and speed-up occurs. The CV of wind speed is 0.18 at 3D2 and then drops to 0.08 by 3D9 (Figure 42). As the flow traverses up the dune the decrease in CV slowly plateaus. There was a drop of 0.02 between 3D2 and 3D3 whilst there is only a difference of 0.003 between 3D8 and 3D9 (Figure 42). At the crest there is a large spike in turbulence and fluctuation in wind speed indicated by a significantly increased CV of 0.57 (Figure 42).

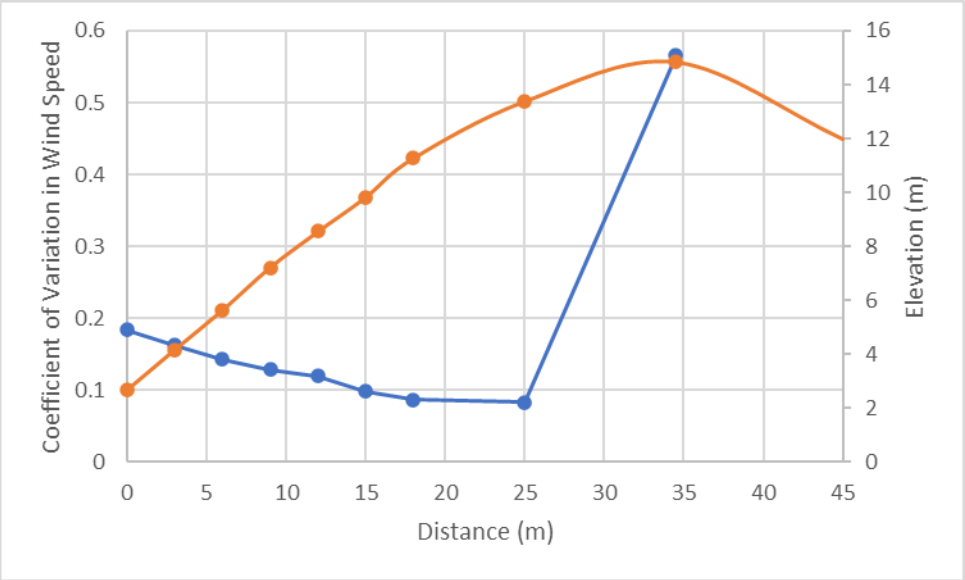

Figure 42: Total average coefficient of variation of wind speed from 9:02am until 12:34pm. The orange line indicates the foredune topography. The coefficient of variation in wind speed steadily drops as speed-up occurs over the dune. There is a sudden increase at the crest indicating strong turbulence.

After analysing the data in one-minute averages the decrease in SD upslope was found to also coincide with a reduction in degree of variation in standard deviation. This is shown by a comparison of 3D2 and 3D9 in Figure 43 where there is clearly less spread in the data recorded at position 9. There is also a decline in standard deviation over time that lines up

with the gradual reduction in wind speed and change in direction that occurred over the duration of the experiment.

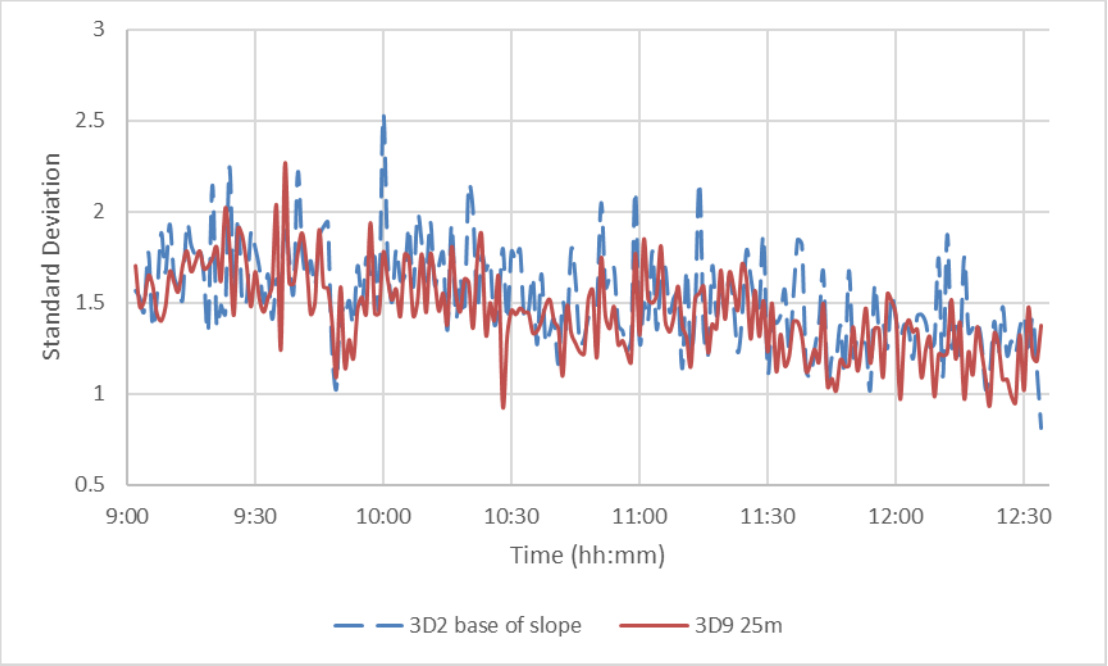

Figure 43: One-minute averages of the standard deviation of wind speed from 3D anemometers at 40 cm above the bed at 3D2 and 3D9.

There was a distinct increase in turbulence at 3D10 at 10:00am (Figure 44 (A)). This correlates with the decrease in wind speed which occurred when the incident wind direction turned more oblique (Figure 36 (A) and Figure 38). This shift in incident wind direction has changed the angle of approach of flow into the blowout potentially increasing the local flow steering driven by the marginal erosional walls of the blowout, thus resulting in increased CV.

In Figure 44 (B) a decrease in flow turbulence occurs as dune height increases. There is also less variation at each anemometer as height increases, indicating there is less deviation in

the CV further up the dune as also seen in Figure 43 for SD.

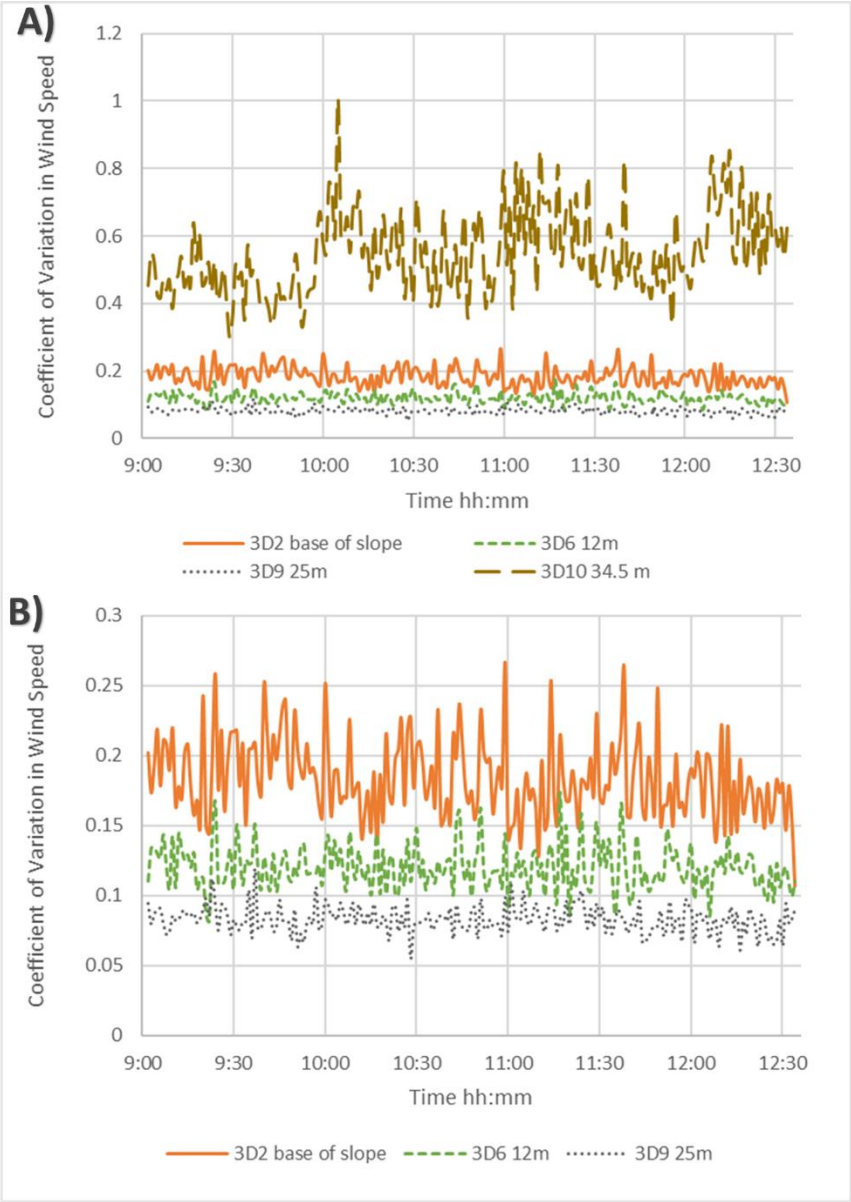

Figure 44: A) One minute average coefficient of variation in wind speed from 3D anemometers at 0.4 m above the bed at 3m intervals over the dune. B) One minute average coefficient of variation in wind speed from 3D anemometers at 0.4 m above the bed at 3m intervals over the dune.

4.4.3 Smoke Cake Visualization

In this study -W averaged -0.51 on the lower slope at position 3 and increased to an average of -1.37 at position 8. After the change in slope however, -W weakened to -0.52 at position 9 before reducing further to -0.21 at the crest as flow expanded. Upwind and downslope of

3D8 the flow closely hugs the surface on the steep portion of the slope where negative vertical velocity (-W) is higher and speed-up is at a maximum (Figure 45 (A)). As flow passes 3D8, the change in slope causes it to decelerate and expand and, thus a wider band of smoke is visible in Figure 45 (A). As the slope gradient continues to lower towards the crest, the flow expansion increases (Figure 45).

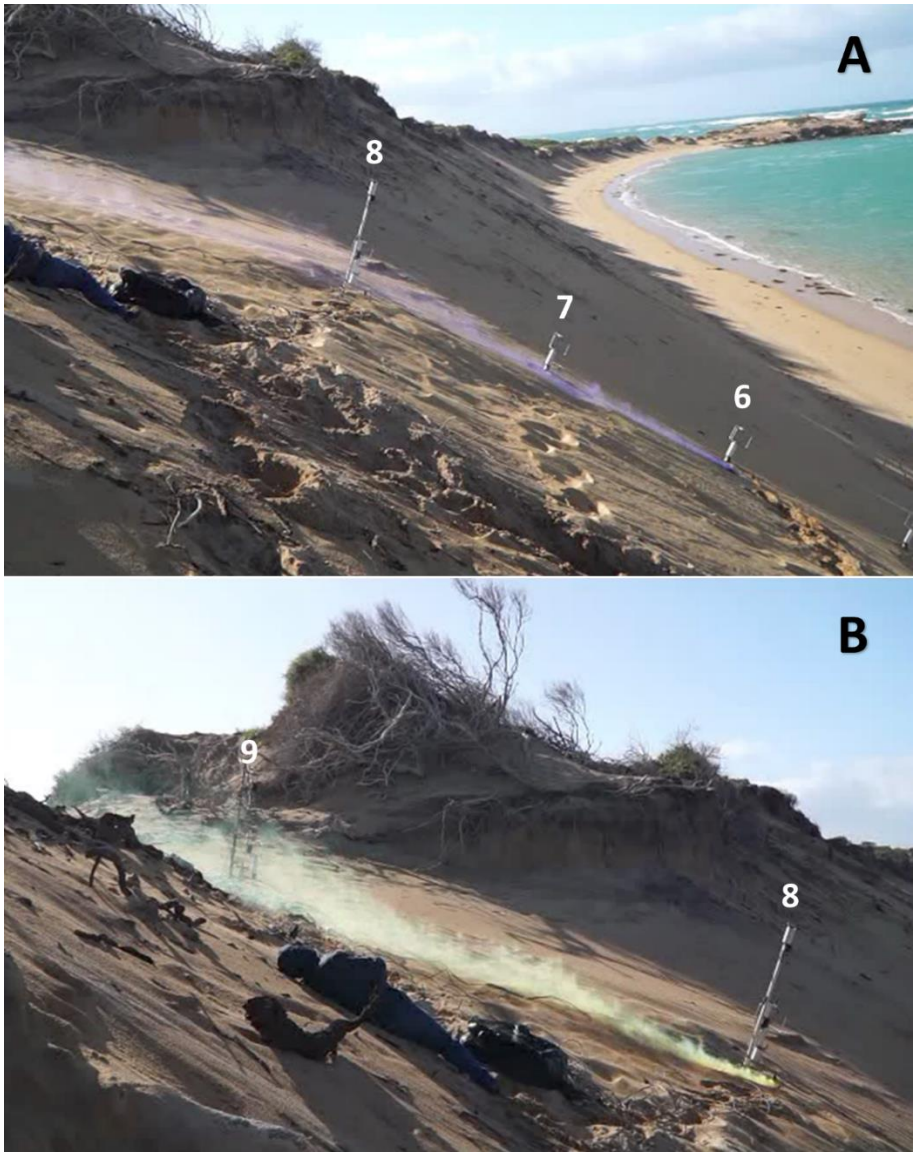

Figure 45: A) The smoke hugs the surface on the steep portion of the slope where negative (downward) vertical velocity is higher and speed-up at a maximum. Flow expansion due to the change in slope at postion 8 is portrayed in the vertical expansion of the band of blue smoke. B) View of the upper slope comprising anemometers at positions 8 and 9. The smoke spreads vertically with a change in slope indicating flow expansion.

One smoke cake was placed on top of the dune crest (red), and another (yellow) positioned on the lee side depositional lobe. A relatively stationary reversing vortex was visible on the lee side of the dune as the flow crossed the crest and separation occurred (Figure 46). Image A of Figure 46 shows that the direction of the flow fluctuated considerably and the turbulence at this site is obvious. However, the reverse flow created by separation past the dune crest is clearly visible in Figure 46 B, C and D. The arrow in Figure 46 D of Figure 46 indicates the flow circulation, and this reverse flow is clearly seen in the yellow smoke in E of Figure 46.

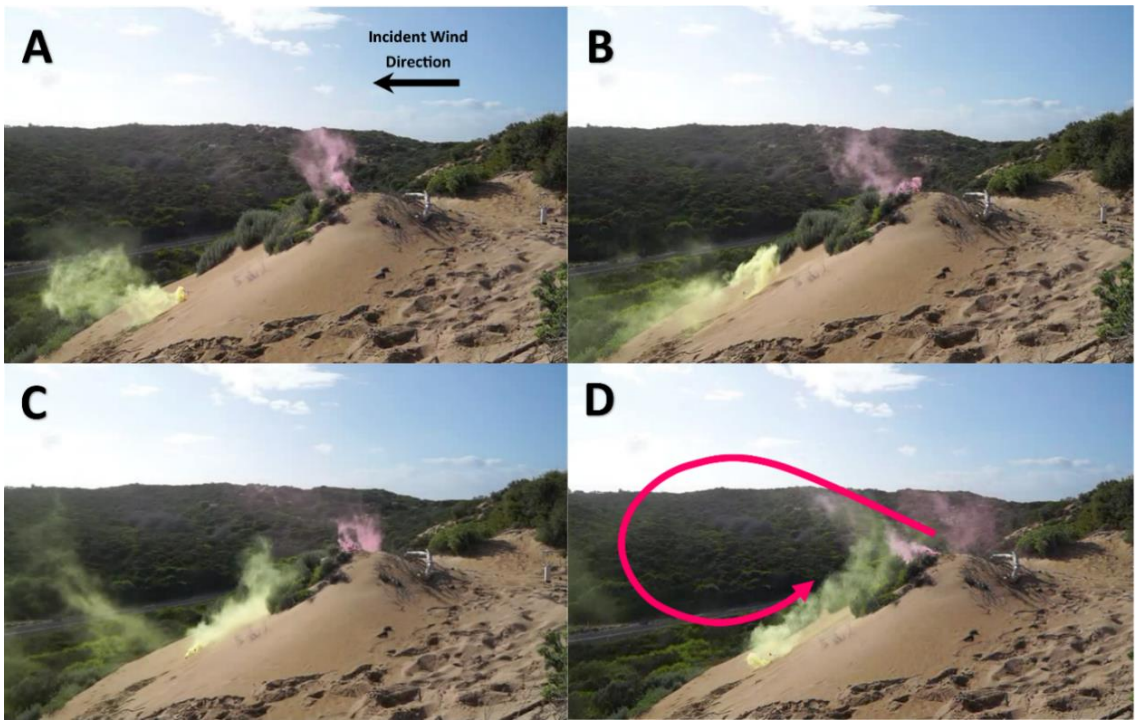

Figure 46: Reversing vortice on the lee side of the dune crest observed using smoke cakes. Flow in A indicates that at times strong downward and oblique gusts interact with the lee slope and the reverse flow is fluctuating and moving across-slope. In B through to D the surface flow is separated and flowing upslope against the incident flow indicated by the pink smoke. Flow separation vortice is made visible in the yellow smoke in E.

4.4.4 Blowout

The blowout located in the dune crest, and which is transected by the experiment line, initially developed prior to 2010 (Figure 47). Since this time, it has progressively increased in both size and complexity despite the ongoing shoreline erosion. This erosion is apparent when comparing the position of the scarp crest in the top left corner of the 2010 image and the image from 2019 in Figure 47. The distance from the top of the image to the crest on the far-left hand side is 10 m whilst in 2019 it is only 3 m. If the blowout had not continued to expand it would have been mostly eroded away by 2019. Instead, the blowout has increased in size from 12.39 m width at its widest point and 14.72 m long in 2010 to 34.86 m wide and 21.86 m long in 2019.

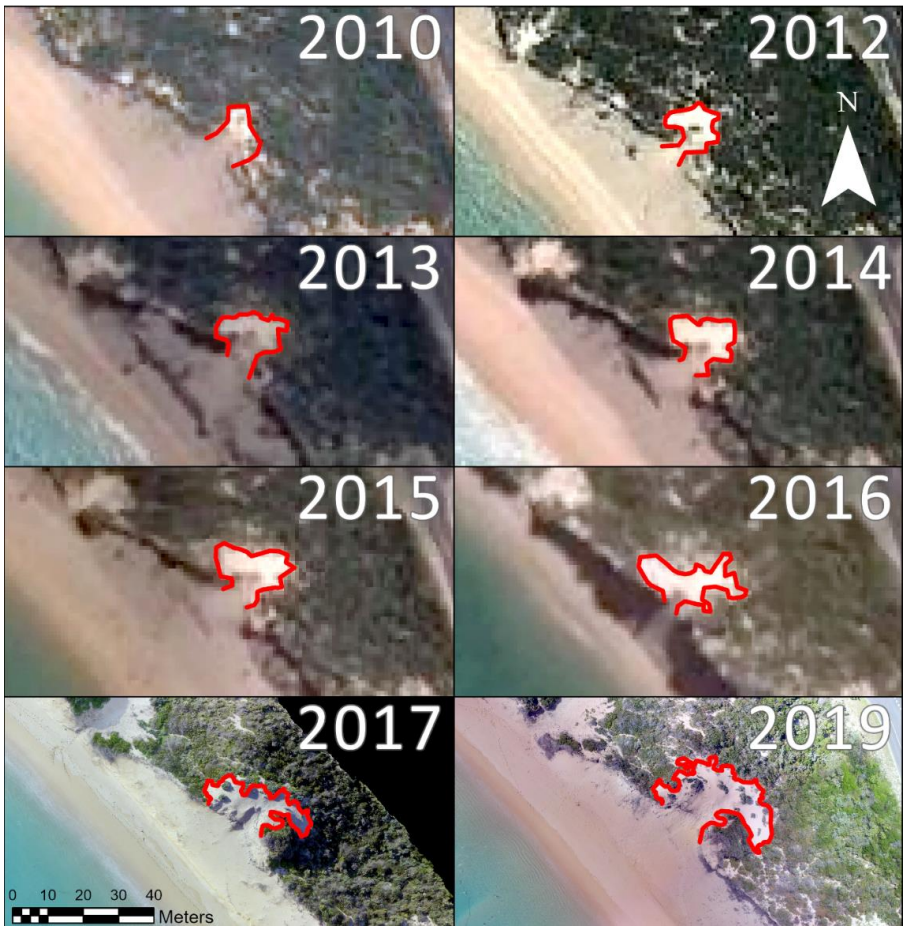

Figure 47: Georectified historical aerial imagery of the growth of the blowout. The blowout has expanded between 2010 and 2019.

4.5 Discussion

Four major wind flow processes were observed in the experiment undertaken over the large scarp slope at Salmon Hole. Firstly, an increase in turbulence at the toe of the dune that gradually reduces up slope until a sharp rise occurs at the crest. Secondly, topographic steering occurs and turns the incident wind approach angle more crest normal across the stoss slope. Thirdly, significant percentage speed-up occurs up the dune until a significant decrease takes place at a change in slope on the upper slope segment. Fourthly, flow separation occurs at, and beyond the dune crest.

4.5.1 Wind Flow Dynamics

4.5.1.1 Speed Up and Turbulence

An increase in turbulence generally results in a decrease in speed whilst streamlined topographically compressed flow is usually associated with an increase in velocity (Jackson and Hunt, 1975; Arens et al., 1995; Neuman et al., 1997; Walker et al., 2006). This was clearly the case with flow recorded at the Salmon Hole scarp.

The main consensus in the literature is that maximum speed occurs at the crest where streamline convergence usually peaks, and convex curvature reduces turbulence (Lancaster, 1985; Arens et al., 1995; Neuman et al., 2000; Hesp, 2002; Walker and Nickling, 2002; Parsons et al., 2004; Hesp et al., 2015). The scarp at Salmon Hole should be conducive to this given its height and steep slope angle (Tsoar, 1985; Wiggs et al., 1996; Parsons et al., 2004). However, the results show wind speed was least and turbulence was greatest at the scarp crest at 3D10. This is contrary to the majority of what has been previously found in the literature and is a result of the morphology of the scarp and blowout presence as will be discussed below.

The flow structure was typical to that observed elsewhere from 3D1 to 3D8 with deceleration at the toe (Figure 48), followed by a steady increase in wind speed and gradual drop in turbulence upslope to position 8 due to streamline convergence up the large and steep stoss slope as often observed in other studies (Figure 48) (Bowen and Lindley, 1977; Weaver and Wiggs, 2011). The effect of flow compression on this part of the stoss slope forces an increase in downward vertical velocity and accordingly the smoke hugs the surface (Figure 48 (A)). Although speed-up continued to 3D9, after 3D8 only a slight increase to 3D9 was observed (Figure 39). For example, between 3D7 and 3D8 there was an increase of 22% from 137% to 159% whilst between 3D8 and 3D9 there is an increase of only 4% to 163% (Figure 39). After this there was a significant drop in speed at the crest to only 53% of that observed on the beach. Figure 48 (A) indicates that this was a result of flow expansion after the change in slope which was clearly visible as the smoke pattern expanded past this point (Figure 45). This resulted in the plateauing of both the increase in speed and decrease in turbulence from position 8 to 9 (Figure 39 and Figure 42). When the flow reached position 10, the flow expansion was such that a dramatic increase in turbulence and a significant drop in wind speed was observed (Figure 48) due to the further change in slope gradient. However, this was also likely influenced by the local flow steering created by the marginal erosional walls of the blowout.

The scarp at Salmon Hole fits within the critical range for Jackson and Hunt (1975) formula analysis as H/L = 0.43 (within their critical range between 0.1 and 0.7). When applying the Jackson and Hunt (1975) formula to the scarp at Salmon Hole in order to determine the maximum speed-up reached at the crest the result is 2H/L = 0.86. This is well above the 0.53

recorded at 3D10 and further demonstrates the effect of the change in slope and possible influence of the erosional walls on the wind speed near, and at the crest.

An increase in speed-up with height above the surface was also observed by the 2D anemometers at positions 8 and 9 (Figure 41). Hesp et al. (2005) noted this as well although it was a result of an increase in drag closer to the surface created by the presence of vegetation. Here surface friction produced by the sandy surface alone has produced a similar response as has also been identified on transverse dunes (Burkinshaw et al., 1993; Parsons et al., 2004).

Once flow passed the crest, flow separation and a reversing vortex were clearly visible in the behaviour of the smoke (Figure 46 and Figure 48). Flow separation has been observed in the lee of foredunes, scarp crests, barchans, and transverse dunes and has been well documented by other studies (Walker and Nickling, 2002; Parsons et al., 2004; Hesp and Smyth, 2019), As high velocity wind overshoots the crest, a region of low pressure forms beneath it in the separation zone. This positive pressure gradient creates circulation within the separation cell in the form of a coherent eddy that causes flow to return back up the lee slope, resulting in a reversing vortice (Kocurek et al., 1992; Walker and Nickling, 2002; Hesp et al., 2005; Lynch et al., 2010; Bauer et al., 2012).

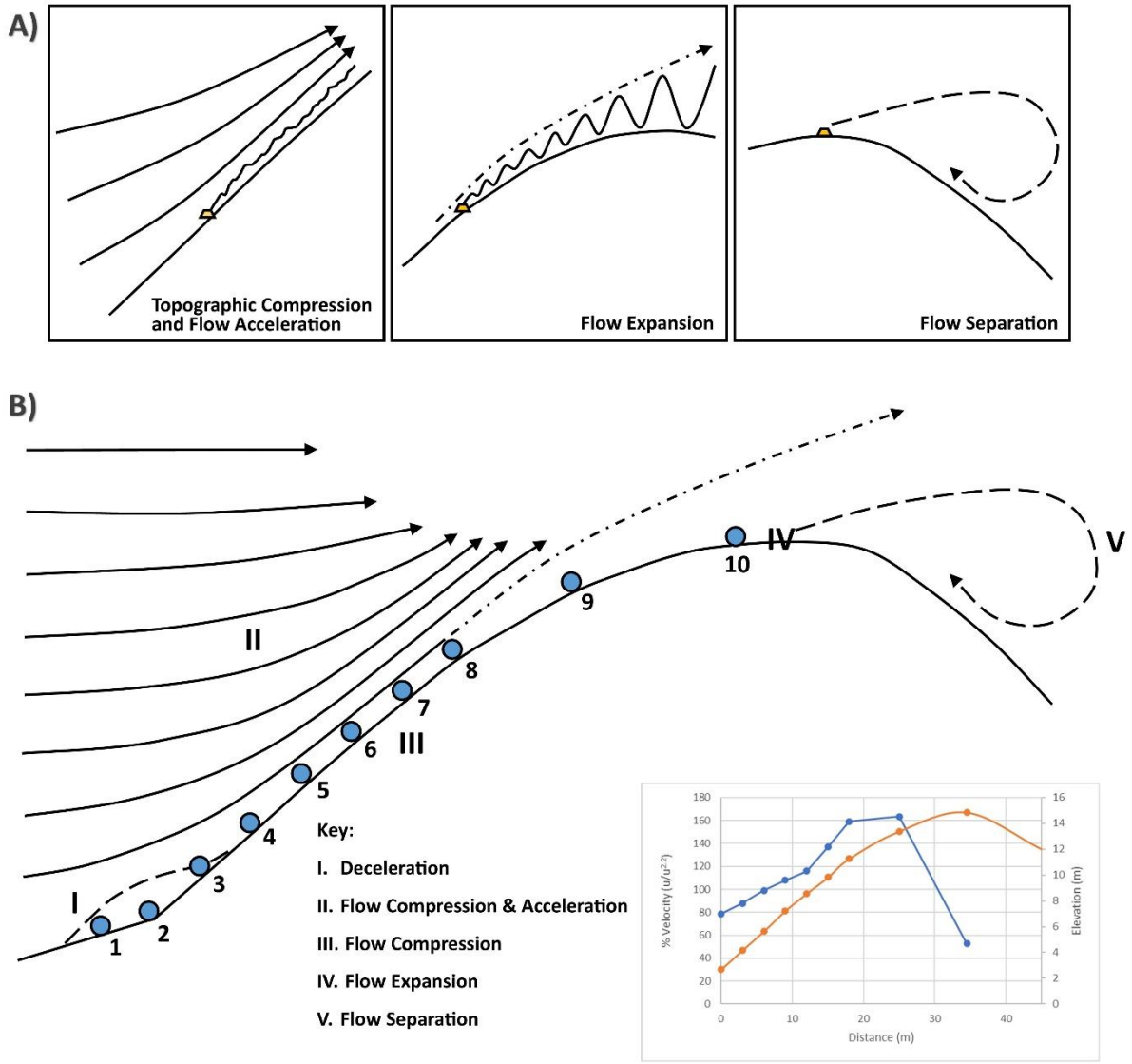

Figure 48: General model of the flow dynamics over the dune slope. (A) Topographic compression and flow expansion, flow expansion, and flow separation. B) flow dynamics over the scarp responsible for changes in wind speed, direction and turbulence over the scarp. Inset: Figure 8 showing percentage speed-up the scarp.

4.5.1.2 Topographic Steering

Arens et al. (1995) recorded flow steering of up to 30^{o} on large foredunes (12-15 m) and stated that the larger a foredune is the greater the effect of topographic steering. Although the average flow deflection from the reference anemometer to 3D9 was only 11^{0} there was a significant change of 32^{o} between 3D2 and 3D7 (Table 2). This is because as the wind

approaches the scarp base it initially turned more parallel to the beach (Figure 40). This was observed by Hesp and Smyth (2019) in their CFD modeling of oblique wind flow patterns over a 2 meter high vertical scarp, as well as by others examining flow over foredunes (Svasek and Terwindt, 1974; Mikelsen, 1989; Rasmussen, 1989; Arens et al., 1995; Walker et al., 2006; Walker et al., 2009; Hesp et al., 2013). As shown in the results, between 3D2 and 3D7, the flow follows convention and is topographically steered towards crest normal as it flows up the scarp (Figure 40; Table 2). This trend is halted, however, as the average wind direction swings slightly more oblique at positions 3D8 and 3D9 further up the dune. Hesp et al. (2015) found that the degree of deflection increases towards the crest and that greatest deflection is seen when the incident approach angle is between 30^{o} – 70^{o}. Given the minimum incident wind approach angle of 29^{o} and a maximum of 56^{o} at Salmon Hole, significant steering toward the crest was expected. However, as noted above, the vertical walls of the blowout present at the top of the scarp (near 3D9) appear to influence the flow steering to more oblique in that region (Figure 34 and Figure 40). Above that area and on the crest at 3D10, the flow steers back towards more perpendicular.

4.5.2 Effect of Wind Flow Processes on Scarp/Blowout

The scarp at Salmon Hole has not recovered since it was first documented as eroding in a 1946 aerial image (Davidson et al., 2021). This is despite the topographic steering, speed-up and increase in turbulence up-slope observed in this experiment, since such near surface flow dynamics are known to assist in foredune scarp recovery by aiding in the development of a dune ramp in front of a scarp (Carter et al., 1990; Ruz and Anthony, 2008; Hesp et al., 2013; Ollerhead et al., 2013; Jackson and Nordstrom, 2018; Piscioneri et al., 2019; Davidson et al., 2020). Topographic steering and speed-up achieve this by increasing sediment transport to the crest, whilst an increase in turbulence at the toe can promote deposition

(Svasek and Terwindt, 1974; Lancaster, 1985; Arens et al., 1995; Lancaster et al., 1996; Wiggs et al., 1996; Neuman et al., 1997; 2000; Walker, 2000; Walker and Nickling, 2002; Walker et al., 2006; Lynch et al., 2008; Hesp et al., 2009; Lynch et al., 2009; Bauer et al., 2012; Hesp et al., 2015; Smith et al., 2017). The formation of a scarp fill - dune ramp then usually allows the dune to both grow in height and translate landwards as flow transports sediment up and over the crest (Hesp, 1988; Bauer and Sherman, 1999; Christiansen and Davidson-Arnott, 2004; Davidson-Arnott, 2005; Davidson-Arnott et al., 2018).

The reason the scarp at Salmon Hole has never recovered despite the wind flow dynamics observed in this experiment is because of the systems negative sediment budget. The ongoing erosion removes sediment and transports it out of the bay leaving minimal sediment for deposition as scarp fill and the formation of a dune ramp (Davidson et al., 2021). Salmon Hole beach therefore demonstrates the net shoreline retreat and dunefield erosion that will occur on similar sandy coasts when there is insufficient time and/or sediment available to recover between erosion events. Due to a lack of sediment delivery back to the beach between storm events, the scarp ramp cannot provide sediment to build the dune crest sufficiently to produce an increase in dune height and dune translation (Hesp, 2000; Pye and Blott, 2008; Castelle et al., 2017; Davidson et al., 2020).

However, despite the lack of sediment supply to the system and the scarp, a blowout and depositional lobe has formed at the crest of the scarp where the experiment was located. The blowout was first observed in a 2010 aerial image and has grown steadily since (Figure 47). This has occurred despite the ongoing erosion cutting into the blowout overtime as seen in Figure 47 (Davidson et al., 2021). The blowout most likely initially formed as speed-up enhanced flow (observed in this experiment) eroded a poorly vegetated or low point

along the scarp crest (cf. Ritchie, 1972; Carter et al., 1990; Saunders and Davidson-Arnott, 1990; Giles and McCann, 1997; Hesp, 2002). This then led to the formation of a deflation zone with erosional walls either side and a depositional lobe downwind (Figure 34). Sediment is added to the depositional lobe via erosion of the scarp slope, and so there is local translation at that point. The continuance of the blowout, however, will be determined by the rate at which the entire seaward slope retreats, and it will likely disappear as the dune becomes smaller due to net slope and dune erosion. At the current rate of erosion, the entire dune system will be removed within the next 30 years (Davidson et al., 2021).

4.6 Conclusion

- Percentage speed-up on the stoss slope is similar to that previously observed over scarp slopes, foredunes and transverse dunes due to streamline convergence and flow compression. However, flow expansion at the change in slope caused a significant drop in wind speed on the upper slope segment. This is contrary to what has previously been found where maximum percentage speed-up is primarily recorded at the crest, and where peak flow streamline convergence is generally found.
- An increase in turbulence was observed at the toe of the Salmon Hole slope. This was followed by a gradual decrease in turbulence up-slope due to streamline convergence. These dynamics are frequently recorded in wind flow studies over dunes. However, the change in slope and subsequent flow expansion that resulted in a decrease in wind speed also created a significant increase in turbulence at the scarp crest. In both foredune and transverse dune studies the least degree of turbulence is typically found at the crest.

- Topographic steering typically seen in wind flow over scarps and foredunes was observed at Salmon Hole. The oblique incident wind direction changed towards more crest normal as it traversed the steep stoss slope. This flow trajectory, however, was altered on the upper slope where flow became more oblique due to local topographic steering created by the vertical wall of the blowout which exists just below, and at the dune crest. Above that, the flow again became more perpendicular.
- Once flow passed the crest at Salmon Hole, flow separation and a reversing vortex were clearly visible. This flow pattern has been observed in previous field, wind tunnel and CFD modelling studies of oblique incident flow over dunes.

The study at Salmon Hole demonstrates how a lack of sediment delivery back to the dune between storm events results in the inability for dune recovery or translation, and therefore net erosion, although local translation via a blowout can occur to a degree, and likely for a finite time. Further sea level rise and increased storm magnitude and frequency due to climate change will result in many similar sandy coastlines with a negative sediment supply also being characterized by dune destruction.

CHAPTER 5
5. DYNAMICS OF SUBAQUEOUS DUNES IN A REEF-FRINGED HEADLAND BAY BEACH

Undergoing revision and is anticipated to be published presently. Davidson, S.G. (80%), Hesp, P.A. (10%) and Silva, G.M.D. (10%). Dynamics of subaqueous dunes in a reef-fringed headland bay beach.

5.1 Introduction

. Within the lagoon at Salmon Hole there are a suite of subaqueous transverse dunes aligned perpendicular to the shore. Typically, the dunes are comprised of a gentle stoss slope followed by a steep slip face on the leeward side (Figure 50). These dunes are between 0.3 to 1 m high and have wavelengths ranging from ~10 to ~40 m. Measured along the dune crest these subaqueous transverse dunes vary in length from ~25 to ~80 m long, whilst the width of the dunes can range from ~8 to ~31 m wide. The dunes are comprised of coarse sand and covered by sand ripples. In the following, some aspects of the flow and currents in the lagoon and the dynamics of the transverse bars are examined.

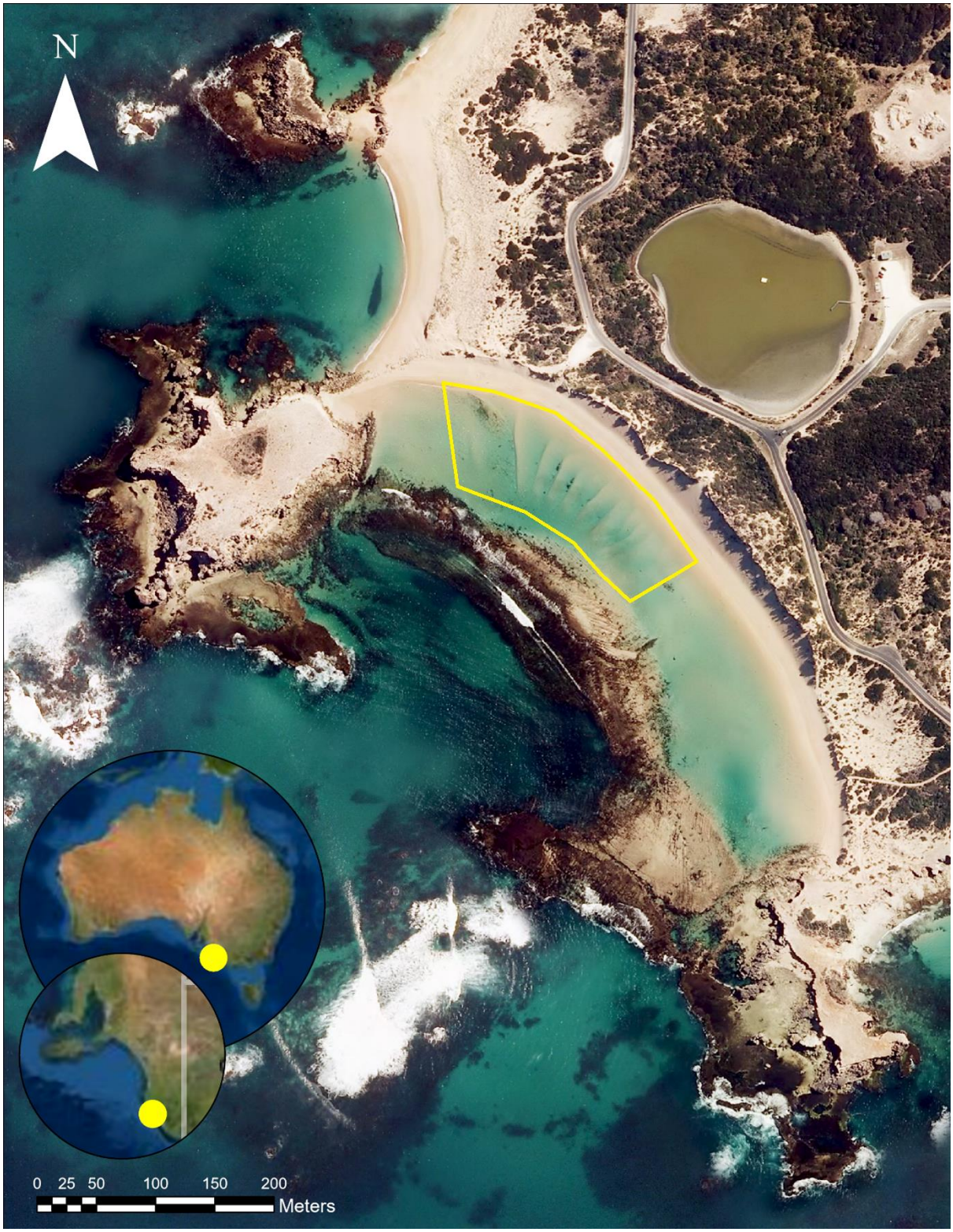

Figure 49: Salmon Hole study site situated near Beachport SE South Australia (image from 2013). The reef which extends across the bay is semi-exposed at low tide as shown in this image. A prominent scarp may be observed along the dune edge. An artificial rock 'tombolo' is present at the northern margin of the bay. The beach originally reached the seawards edge of the exposed reef in 1946. Subaqueous transverse dunes can be seen aligned perpendicular to the shore in the yellow polygon.

Figure 50: 170cm tall person standing next to steep lee slope of a subaqueous transverse dune in the bay on the 23/2/20.

5.1.1 Subaqueous Transverse dunes

Once sandy bed material starts to move in flowing water it generally begins to morph into flow transverse bedforms of varying shapes and sizes (Kostaschuk and Villard, 1996). The larger of these relatively dynamic bedforms are sometimes described as mega ripples (Watson et al., 2020), sand waves (Carey and Keller, 1957; Zhou et al., 2020), sand ridges (Tao et al., 2019), transverse bars (Gustavson, 1978), longitudinal bars (Boothroyd and Ashley, 1975), linguoid bars (Collinson, 1970) or macroforms (Crowley, 1983), however, all fit into the definition of subaqueous dune (Ashley, 1990; Kostaschuk and Villard, 1996; Francken et al., 2004; Mason et al., 2020). Subaqueous dunes are large bedforms often found in subaqueous sedimentary environments where water depths are greater than ~1 m, the sediment size is coarser that 0.15 mm, and mean current velocity is more than 0.4 m s^{-1} (Ashley, 1990). The sediment stored in these various morphological forms moves through time intervals ranging from hours to centuries (Ashley, 1990; Kostaschuk and Villard, 1996;

Francken et al., 2004; Tao et al., 2019). Subaqueous dunes are distinct from smaller current ripples which generally have spacings less than 0.6 m (Yalin, 1964; Allen, 1968; Kennedy, 1969; Harms et al., 1982).

Subaqueous dune size is predominantly determined by flow speed and grain size. Dune growth is proportional to flow speed until the critical suspension threshold for a given grain size is reached (Flemming, 2000; Bartholdy et al., 2005; Coleman and Nikora, 2011; Bradley and Venditti, 2017). The coarser the grain size the greater the critical suspension threshold and thus the larger the maximum subaqueous dune size. Water depth does not play a major role in determining dune growth except where water is shallow and flow velocity is depth limited (Flemming, 2000; Flemming and Bartholomä, 2012; Reesink et al., 2018).

The subaqueous dunes at Salmon Hole are here classified as transverse dunes, given that they fit the definition given by McKee (1979) as sedimentary deposits whose longest axis lies perpendicular to the predominant flow direction. They have low angled stoss slopes and steep slip faces that indicate the direction of flow (Lee et al., 2005). These dunes are quite distinct from transverse bars commonly found in the surf zone and associated with adjacent rip channels (Niedoroda, 1966; Price, 1997; Short, 2006; Marinho et al., 2018). A defining feature that separates subaqueous dunes from transverse bars is that dunes migrate forwards in the predominant direction of the current (Bens et al., 2010). Transverse bars usually form due to oscillatory currents created by waves and tides (Niedoroda, 1966; Marinho et al., 2018). The subaqueous transverse dunes at Salmon Hole are likely to be created because of the presence of a mostly consistent unidirectional current which will also be assessed in this study. However, such dunes may also be due to the presence of oscillatory currents.

Subaqueous dunes have been found in rivers that are unidirectional, channelized and made up of varying grain sizes and hydrological features (Carey and Keller, 1957; Collinson, 1970; Crowley, 1983; Kostaschuk and Villard, 1996; Mason et al., 2020). The sediment transported by fluvial systems is often stored in the form of subaqueous dunes that vary significantly in both size and morphology. (Carey and Keller, 1957; Harms and Fahnestock, 1965; Coleman, 1969; Collinson, 1970; Smith, 1974; Boothroyd and Ashley, 1975; Gustavson, 1978; Crowley, 1983; Kostaschuk and Villard, 1996; Mason et al., 2020). These subaqueous dunes are often found in the channel with their presence and morphological variability primarily dictated by flow strength (Yalin, 1964; Raudkivi, 1966; Southard, 1971). Kostaschuk and Villard (1996) investigated both large symmetric and asymmetric subaqueous dunes in Fraser River, Canada. These dunes ranged in length from 4 m to greater than 100 m and reached from 0.3 m to greater than 4 m, significantly higher than the 1 m high dunes situated in Salmon Hole Bay. They found that high current velocities create symmetrical dunes with rounded crests and slight slope angles ($<8^{o}$). This is as a result of high transport rates over the dune due to high near bed velocity. This increased bed load transport smooths or flattens dune crests and causes suspended sediment deposition in the dune troughs. The asymmetric dunes in the Fraser River on the other hand are formed in low flow velocity and sediment transport conditions and have longer stoss slopes ($<3^{o}$) and straight steep lee side slopes ($>19^{o}$).

Subaqueous dunes have also been found in the marine environment. This includes large coastal embayment's/estuaries with channelized, unsteady and reversing tidal flows as well as relatively deep, continental shelfs where currents are created by geostrophic flows, storms, tides and waves (Jones et al., 1965; Bokuniewicz et al., 1977; Stride, 1982; Francken

et al., 2004; Ryan et al., 2007; Masselink et al., 2009; Dalrymple et al., 2012; Tao et al., 2019; Zhou et al., 2020).

Large coastal embayment's (as opposed to beaches in smaller coastal embayment's such as Salmon Hole) and/or estuaries that are partially enclosed by topography but still have a connection to sea can be dominated by tidal ranges greater than 1 m and/or by low input from fresh water sources in comparison to tidal volume (Ashley, 1990; Wells, 1995; Tessier, 2012). Currents created by these tides reach speeds of up to 2 m s^{-1}, however, this varies significantly through the daily tidal cycle (depending on the phase and amplitude of the tide) and the lunar spring-neap cycle (Francken et al., 2004; Dalrymple et al., 2012). Tidal flow reverses regularly as it floods and ebbs which is unfavourable for the formation of subaqueous dunes, however, if the geometry of a large embayment/estuary allows it then these flows will often not intersect and instead a circular route is followed in and out of the embayment/estuary (Ashley, 1990). This variability within the system along with the frequently changing water levels leads to a wide variety of bedform morphologies including subaqueous dunes (Francken et al., 2004; Ryan et al., 2007; Masselink et al., 2009; Billy et al., 2012; Goodbred and Saito, 2012). Smaller dunes (spacing of a few meters) can change their orientation throughout the tidal cycle whilst the short duration of the tidal cycle does not allow larger dunes (spacing > 10 m) to be completely reworked. The overall morphology of these larger bedforms therefore is in a state of quasi-equilibrium adjustment where the overall shape is determined by the relative strengths of the opposing currents (Ashley, 1990).

Francken et al. (2004) studied the subaqueous dunes found in the Scheldt Estuary located between the Antwerp and Belgium border. Here tidal current velocities are largest during

flood reaching up to 1.6 m s^{-1} during an average tide to 2.0 m s^{-1} during a spring tide. They found that grain size had the most significant effect on dune size in the Scheldt Estuary with dunes of various sizes coexisting in areas of similar current speeds. They also noted that there was a direct correlation between wavelength and dune height, with an increase in dune height linked to longer wavelengths. Ryan et al. (2007) examined Keppel Bay a macrotidal embayment and estuary that links the Fitzroy River with the Great Barrier Reef. In this mixed wave and tide-dominated system, they found large scale subaqueous dunes to the North between Great Keppel Island and the mainland created by a wave-induced longshore current. They also discovered seaward orientated dunes at the southern end of the bay in the outer Fitzroy River channel created by ebbing tide flows. Whilst further offshore large-scale subaqueous dunes orientated landwards were found to be produced by flood tidal currents reaching speeds of 68 cm s^{-1}.

Subaqueous dunes have also been found in shallow marine environments (<200 m) such as sounds and straits (Caston, 1981; Watson et al., 2020). Through the bathymetric mapping of the seafloor Watson et al. (2020) revealed several dune bedforms varying in size and morphology in the Marlborough Sounds, New Zealand, between 50 and 120 m water depth. These dunes ranged from barchans with 25 m wavelengths that were less than 0.5 m high to large scale “sand waves” with 300 m wavelengths reaching 20 m high and ranging between 300 to 600 m long.

Large scale dunes also occur in open shallow marine environments such as on terrigenous or carbonate continental shelves, and epicontinental slopes (less than 20^{o}) (Stride, 1982; Harris et al., 1986; Ashley, 1990). Compared to the smaller dynamic subaqueous dunes formed by tides in coastal embayment’s and estuaries, the large amount of sediment stored in these

shallow marine dunes results in them being much more stable and moving on scales of months to years (Jones et al., 1965; Bokuniewicz et al., 1977; Allen, 1980; Flemming, 1980; Langhorne, 1982; Stride, 1982; Amos and King, 1984; Harris and Collins, 1984).

Tao et al. (2019) modelled the morphodynamics of large-scale radial sand ridges located off the coast of China in the Southern Yellow Sea. These subaqueous dunes stretch out in a fan shape with each ridge up to 100 kms long and 5 to 10 kms wide in a water depth of 30 m. The modelling of these features produced close to reality results and demonstrated the formation is governed by both the tidal regime of the Yellow Sea as well as latitudinal effects such as the Coriolis force. Zhou et al. (2020) analysed the formation of giant sand waves (or dunes) reaching heights of 22.5 m and wavelengths of up to 2.1 kms located on the Taiwan Banks in the southern Taiwan Strait. The size of theses dunes results in their shape remaining stable for up to three years before change. They found that dunes in deeper water were generally more rounded in shape and as has been discussed that larger grain size and increased flow velocity led to an increase in dune height and length.

Subaqueous dunes positioned in a small headland-bay beach system such as those found at Salmon Hole which are the focus of this research have not been previously studied. Salmon Hole is fronted by a calcarenite reef 100 m offshore. Such reefs are known to attenuate wave energy into a lagoon depending on water level over the reef, in this case dictated by tide height (Brander et al., 2004; Davidson et al., 2021). Circulation in geologically controlled reef - lagoon systems however, are not only dependent on both wave energy and tide height but also critically on the morphology of the reef (Brander et al., 2004; Lowe et al., 2010). Currents driving circulation in such systems are usually generated by incident wave forcing as a result of wave setup on the reef. This produces a pressure gradient that drives

flow over the reef and around the bay (Lowe et al., 2009). The transverse subaqueous dunes found at Salmon Hole have likely been formed by geologically controlled embayment circulation. This chapter is an initial investigation into both this, and the role the subaqueous transverse dunes have been playing in the overall sediment transport out of the bay.

5.2 Method

5.2.1 Bathymetric Surveys

Two bathymetric surveys were undertaken in 2018 (9th of April and 13th July). These were conducted using a GPS enabled kayak deployed single beam echosounder which provided position and depth data used to create 3D digital elevation models (DEM's) of the bay's bathymetry. A CEESCOPE sonar system was used to measure depth at a <1cm vertical resolution with a R10 Trimble RTK-GNNS unit to provided 2 - 5 cm accurate positional data. The first survey included 13685 recorded points with survey lines stretching the entire length of the bay, however, the percentage coverage was limited (Figure 67). The second survey was again across the length of the bay, this time in a zig zag pattern that more tightly covered particularly the northern end of the bay where the dunes are situated. The July survey had 14263 recorded points; the overall coverage was again limited.

5.2.2 Current measurements

A current meter (Aanderaa RCM Blue) was positioned in Salmon Hole on the 23/7/20 and recorded until the 2/12/20. The position of the current meter can be seen in Figure 51. The sensor at the time of deployment was at a depth of 2.1 m, and recorded speed (cm/s), direction (degrees), and water depth (m). The current meter logged this data continuously at 4 Hz for one minute every four minutes with the average of each one-minute burst

recorded for the entirety of the 19-week period. These were then converted into hourly averages. Comparisons were then made with hindcast significant wave height (Hs) (m) data for the same period also in hourly intervals. The hindcast Hs grid point is located at longitude 139.9676 and latitude -37.5009 approximately 3.26 kms directly offshore from Salmon Hole (closest available data) and was obtained from the NationalMap data catalogue (nationalmap.gov.au). NationalMap is an online tool that allows access to spatial data from Australian government agencies. The Hs data on the site is sourced CAWCR's (Collaboration for Australian Weather and Climate Research's) Wave Hindcast which was created using the WaveWatch III v4.08 wave model. Tidal data in hourly intervals for Beachport was also obtained using the IHO (International Hydrographic Organization) global tidal model. This was accessed through the Delft Dashboard to assess its impact on the data collected from the current meter. For time periods of specific interest in the current meter data, wind speed and direction data was also obtained from the Bureau of Meteorology from the nearby station at the Robe airport.

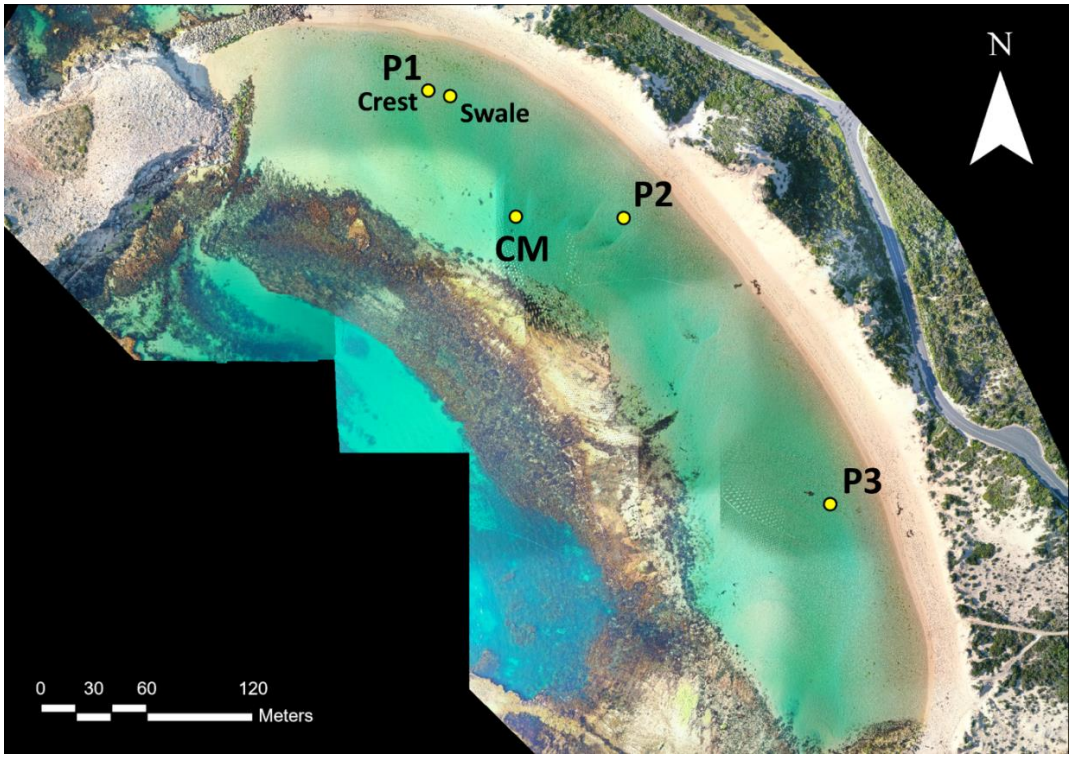

Figure 51: Yellow dots indicate the positions of data loggers in the bay. The dot labelled CM indicates the position of the main current meter positioned in the bay long term. P1, P2 and P3 are the positions of the three water level loggers positioned in the bay during the experiment in October 2020. The fist tilt current meter placed in the bay during the experiment was located on the crest of the dune at P1 and the position of the second in the swale can be seen near P1.

5.2.3 Additional hydrodynamic measurements (water levels and local currents)

On the 26th and 27th of October 2020 an experiment was carried out at Salmon Hole with the aim of recording current speed/direction adjacent to the subaqueous dunes, water level data, together with the autonomous bathymetric survey explained above.

5.2.3.1 Water levels

Three HOBO U20L-04 Water Level Data Loggers capable of measuring water depth up to 4 m were placed around the bay (Table 6). Positions 1, 2 and 3 in Figure 51 show the locations of these loggers in the bay. The data loggers recorded in 1 second intervals and record the height of the water above the position of the sensor. The atmospheric pressure on the day was 101.4 Pa and it varied little over the course of the experiment.

Table 6 contains the positions of the loggers along with the time in which they were positioned, reset, and then taken out, the sensor and water depth at these times and the overall logging time at each position.

Table 6: Positions of the loggers along with the time in which they were positioned, reset, and then taken out, the sensor and water depth at these times and the overall logging time at each position.

Logger	Position	In 27/10/20	Reset 28/10/20	Out 28/10/20	Recording Period 1	Recording Period 2
1	S37 29.023, E139 59.879	3:10pm (reset at 5:00pm)	10:40am	4:30pm	3:10pm – 4:13pm 5:00pm – 2:29am	10:40am - 4:30pm
Sensor Depth		85cm	87cm	65cm		
Water Depth		105cm	145cm	113cm		
2	S37 29.063, E139 59.920	3:25pm	12:30pm	5:30pm	3:25pm – 7:19pm	12:30pm – 5:30pm
Sensor Depth		140cm	125cm	129cm		
Water Depth		180cm	172cm	168cm		
3	S37 29.151, E139 59.998	3:40pm	11:35am	5:15pm	3:40pm – 7:19pm	11:35am - 5:15pm
Sensor Depth		100cm	165cm	90cm		
Water Depth		145cm	205cm	137cm		

5.2.3.2 Local currents over a dune

During the experiment two Lowell Instruments TCM-4 tilt current meters were used to record flow velocity over the subaqueous dunes. These Tilt Current Meters (TCMs) use a drag-tilt principle to record both current speed and direction. Each TCM is made up of a 25.4

cm x 2.54 cm buoyant cylinder that contains a sensor attached to a short length of rope (10 cm) tied to an anchor on the seafloor. The buoyant meter tilts in reaction to the current, this change in position and angle is recorded by a 3-axis accelerometer and 3-axis magnetometer at up to 64Hz. This is sufficiently fast to record oscillations created by currents or waves. The output data from the TCM's is then post processed into speed (cm s^{-1}) and direction (degrees) data using a speed-tilt curve equation developed by Lowell Instruments through tank and field testing whilst comparing results to reference instruments. The TCM's were set to record in 2 second intervals with a burst rate of 4hz, these were later converted to 5 min averages. A TCM was positioned on the crest of a subaqueous dune at position 1 at the northern end of the bay while a second was placed in the swale 12 m away, both positions are shown in Figure 51.

5.2.4 Aerial surveys

Drone surveys over Salmon Hole Bay were conducted on the 25/7/20 and 28/10/20. Ideally more regular surveying would have been undertaken, however, near perfectly calm conditions were necessary to be able to view the subaqueous dunes from the air with sufficient clarity to then be able to create an orthosmosaic from the images. The drone was flown at 120 meters with 50% overlap. The overlapping images were then stitched together using Pix4D photogrammetry software that uses key features visible across multiple images as tie points.

Conducting this process, which is best suited to land-based applications, on subaqueous morphology presented multiple hurdles and has overall reduced the accuracy of the results. Pix4D is designed to create 3D Digital Elevation Models (DEMs) of above surface terrain and therefore could not process the images below water into a DEM. However, the software

could be used to make orthomosaics for comparison. Whilst these orthomosaics provided a good representation of the morphology and general location of the dunes the accuracy of the exact positions of the dunes in the orthomosaics is questionable. There were up to 4 m difference in locations of key permanent features between the two orthomosaics. The main reason for this is inconsistencies between the images resulting in Pix4D being unable to stitch the images together completely accurately. The discrepancy between images is due to multiple factors including: refraction at the air water interface, the general sparsity of key features in images, the movement of seaweed and floating objects between frames and waves, and, ripples and reflections across the water's surface (Casella et al., 2017; van Scheltinga et al., 2020).

Due to the drone flying too low during the first survey in July, Pix4D was unable to identify a sufficient number of key features between images to act as tie points. This resulted in the orthomosaic produced only including the outer edge of the bay where multiple key features between images, i.e., the headlands and parts of the vegetated dune system were present. The remainder of the images were, therefore, georeferenced manually in ArcGIS pro.

From the 15/2/19 to the 28/10/20 oblique images of the dunes were also taken from the air using a DJI drone on occasions when the subaqueous dunes were visible. Oblique Images were taken post drone surveys as well as on occasions where although the dunes were visible the conditions or circumstances were not suitable for a survey.

5.3 Impacts of waves, winds and tides in the lagoon's hydrodynamics

The maximum current speed recorded in Salmon Hole Bay was 84 cm s^{-1} with a maximum hourly average of 67 cm s^{-1} and a mean of 25.85cm s^{-1}. Current speed appears to be highly dependent on wave height with periods of high and low current predominantly associated

with a corresponding magnitude of Hs (Figure 52). The Pearson's correlation between current speed and Hs is 0.77. This relationship clearly shows that the Hs offshore is directly linked to the amount of wave energy transferring over the reef and thus the resultant current speed within the bay itself.

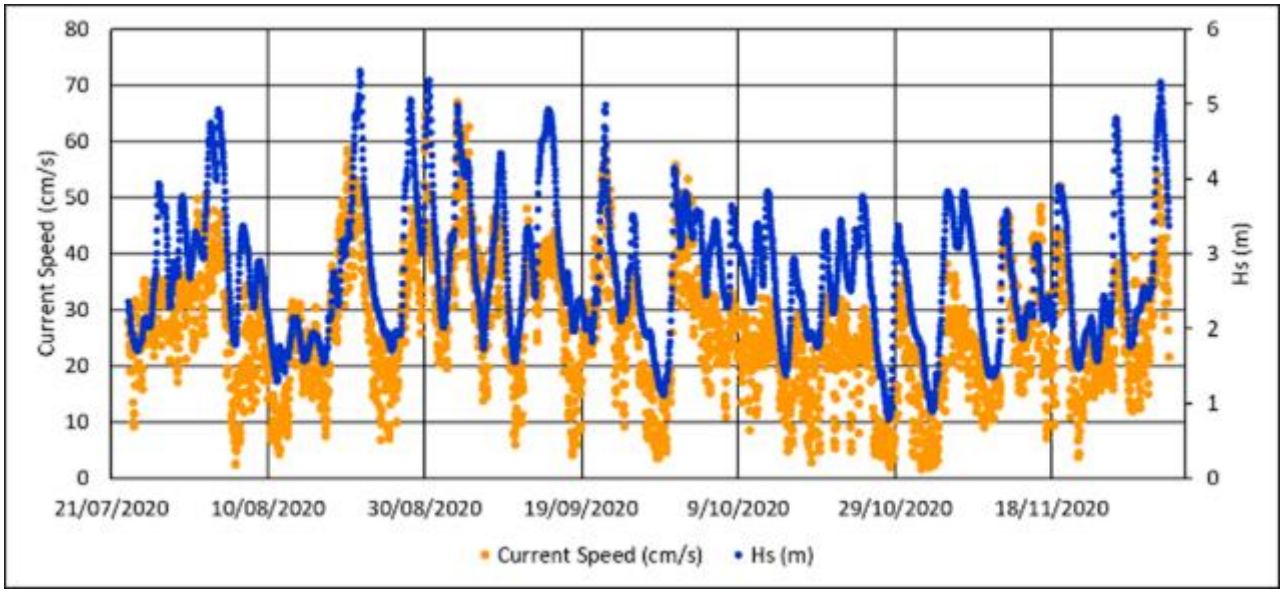

Figure 52: Current velocity (orange) measured in cm s^{-1} between July and November 2020 clearly related to offshore hindcast Hs data (blue).

Tides also influence current speed at Salmon Hole, however, its impact varies significantly under high versus low Hs conditions (Figure 53). Under high wave conditions the tide has little influence on current speed as seen between the 14th and the 16th of September in Figure 53 A). Under low wave conditions, however, the current speed not only drops but also begins to increase and decrease along with the tide as seen on the 18th of September in Figure 53B) (in red box).

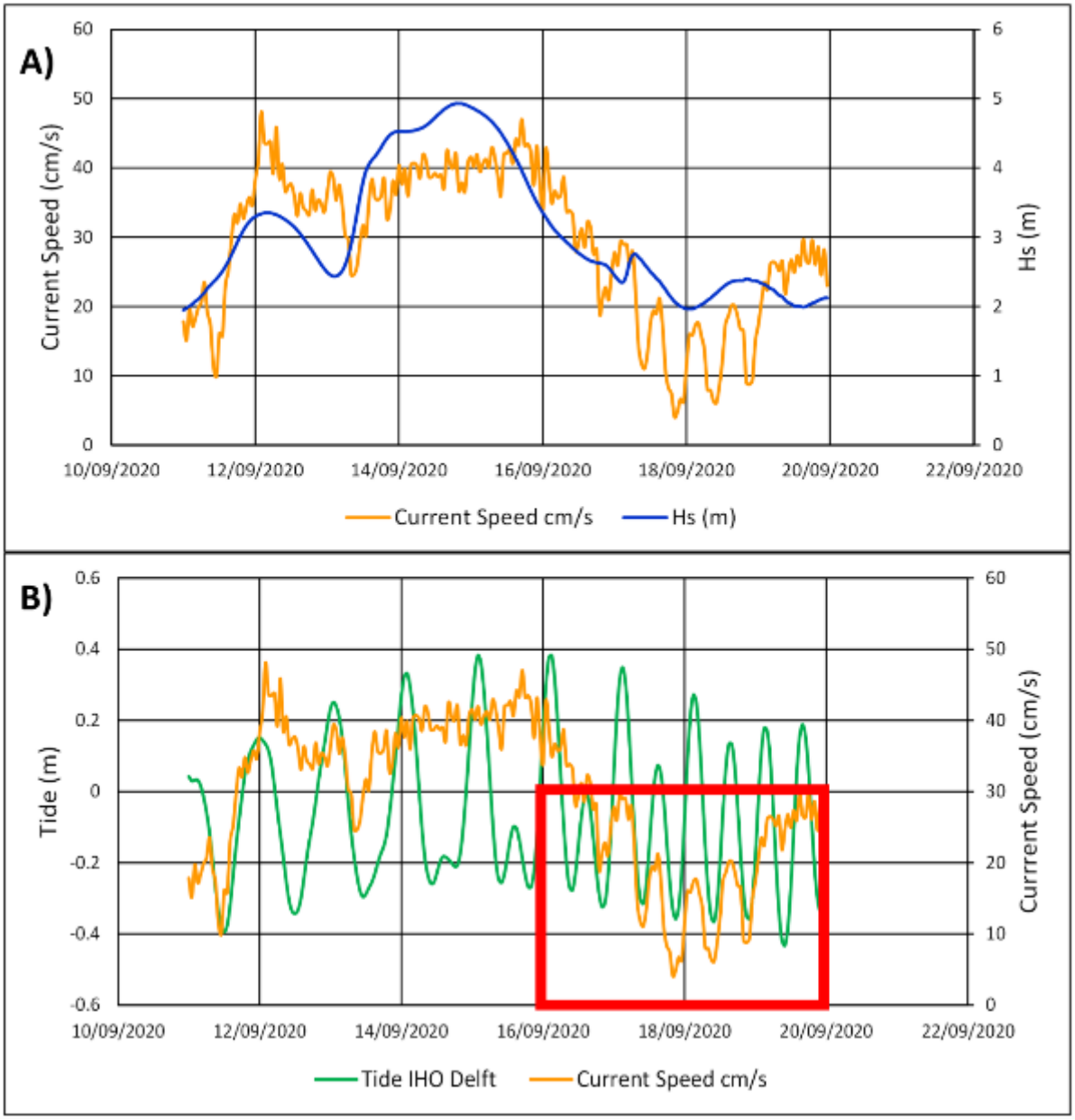

Figure 53: A) Current speed cm/s (orange) compared to Hs in meters (blue). B) Current speed cm/s (orange) compared to tidal variation in meters (green). Tides only significantly affect current speed during periods of low Hs. Red box highlights the current speed rising and falling with the tide under low Hs conditions.

The direction of the current is predominantly toward the NW, with the current running at an average of 294.24 degrees NW between the 23/7/20 to the 26/10/20. This is directly in line with the direction that the subaqueous dunes appear to be migrating around the bay. The current which is shown in hourly averages only swings in the complete opposite direction

three times in the 19-week period (Figure 54). Firstly, on the 28/09/20 between 3:00pm and 9:00pm where the current averaged a direction of 164 degrees SE. Then secondly, shortly after on the 29/09/20 between 7:00am and 10:00am where the direction averaged 159 degrees SE. Then finally, on the 18/10/20 between 8:00am and 9:00am during which the flow direction averaged 152 degrees SE. The first and second changes in direction align with lowest recorded Hs offshore, with an average Hs of 1.26 m between the 28th and 29th of September. All other periods that the current varied significantly from the overall average NW direction were also during low wave energy conditions.

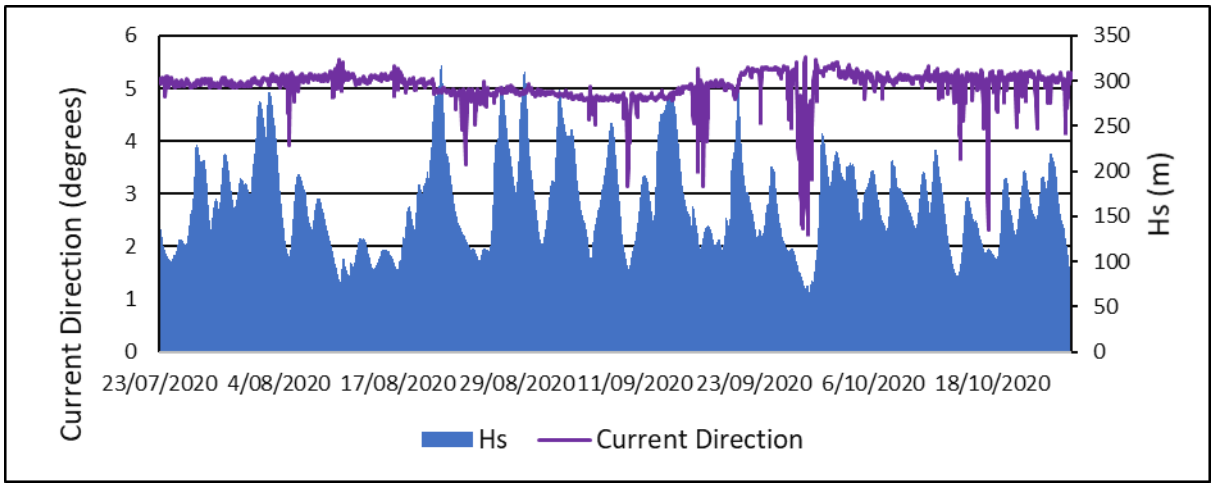

Figure 54: Current direction (purple) measured in degrees between July and November 2020. The direction only deviates from the north westerly direction during periods of low Hs (blue).

Figure 55 shows that although each recorded case of flow reversal occurred during low tide, it alone however, does not equate to a southerly flow direction. Significantly lower tides than those seen during periods of reversed flow occurred whilst the current maintained a NW direction. This suggests that it is a combination of factors that lead to flow reversal in Salmon hole Bay (Figure 55).

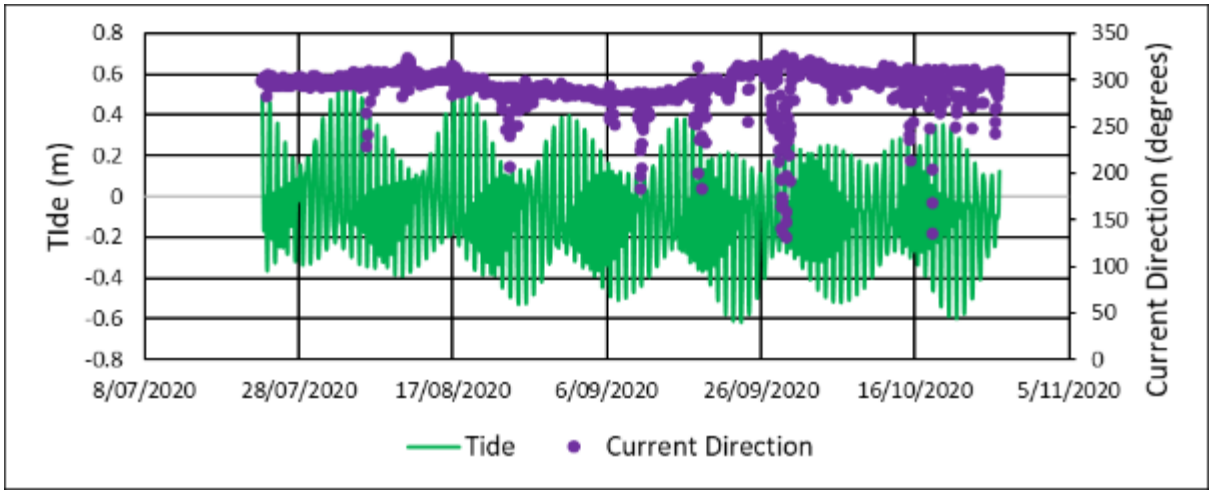

Figure 55: Tidal variation in meters (green) alongside direction in degrees (purple). Although a factor in creating flow reversal from the mean NW direction low tide alone does not equate to southerly flow direction.

Figure 56 and Figure 57 demonstrate this point through a closer look at the prevailing conditions during the first two occasions that the current switched direction. Both figures show that despite the low Hs, low tide on its own was not sufficient to change the current direction a full 180 degrees from the norm. For instance, in Figure 56, the tide was lower at 9:00 am (-0.246) than at 7:00pm (-0.216) and yet the current direction deviated further at 7:00pm. This is because the wind had dropped in speed from 18 to 10km/hr by 7:00pm. The average direction turned back to ~320 degrees with high tide at 3:00am on the 29/09/20 before it again changed to ~130 degrees at 9:00am. This time the swing in direction appears to be due to an increase in wind speed, in an NNE direction, pushing the current back in the other direction as simultaneously Hs continued to drop (Figure 56). After this during the next low tide at 7:00pm the average current direction only deviated to 192 degrees. This was due to a swing in wind direction to 335 degrees and a slight increase in Hs (Figure 60).

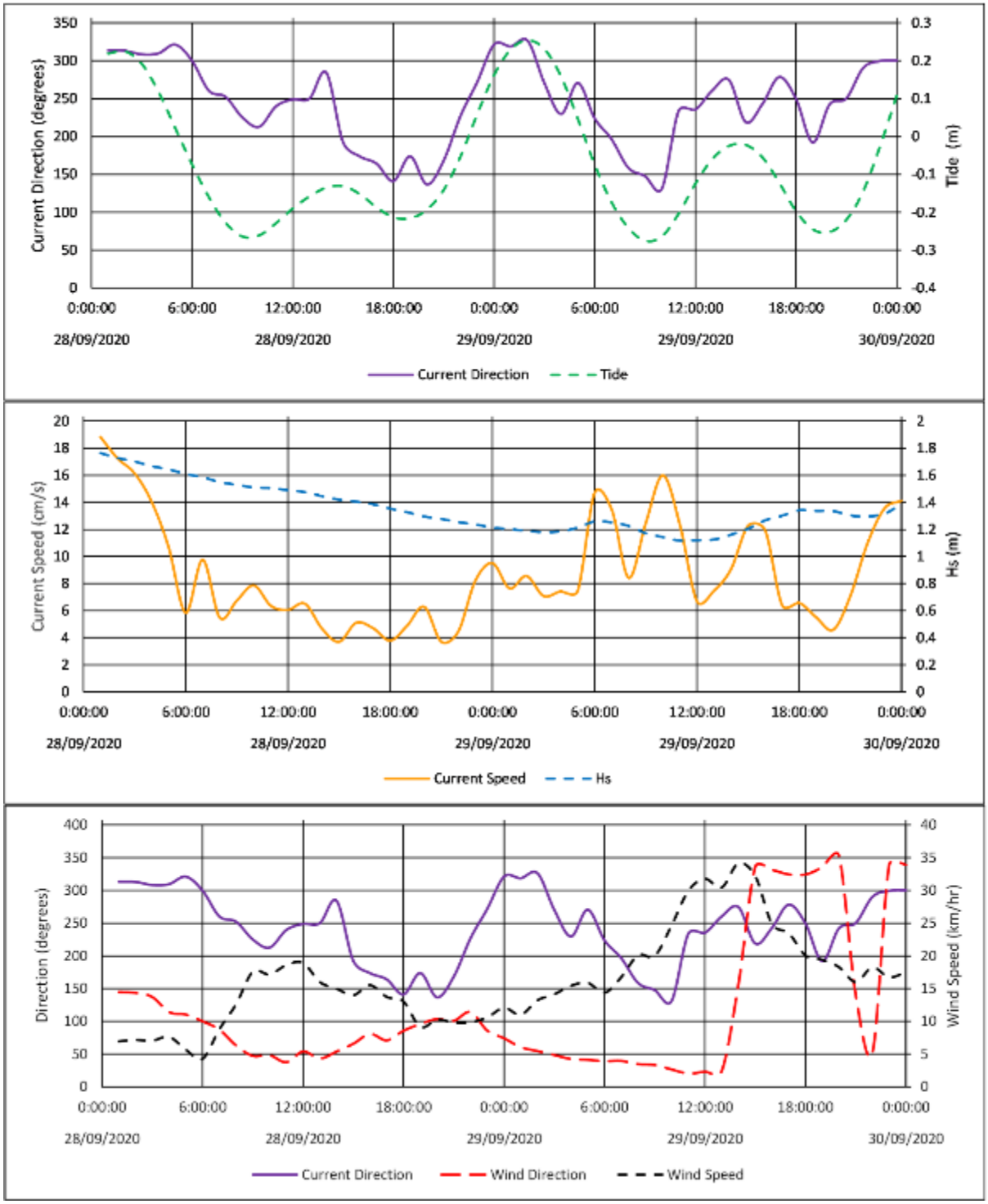

Figure 56: Current speed/direction, tidal deviation, Hs and wind speed/direction for the 28/09/20 to the 29/09/20. Flow reversal from the mean NW direction only occurs under particular rare conditions consisting of extremely low Hs, low tide and low or easterly winds.

The third occasion that the current direction reversed at 9:00am on the 18/10/20 again coincided with low tide and low wave energy (Figure 57). However, as before these two factors were not alone in dictating the change in direction with similar Hs and low tides seen before and after. The drop in wind speed therefore has played a role in causing the average current direction to reverse. The low at 9:00am was also more pronounced than those immediately around it and the Hs was also slowly dropping (Figure 57).

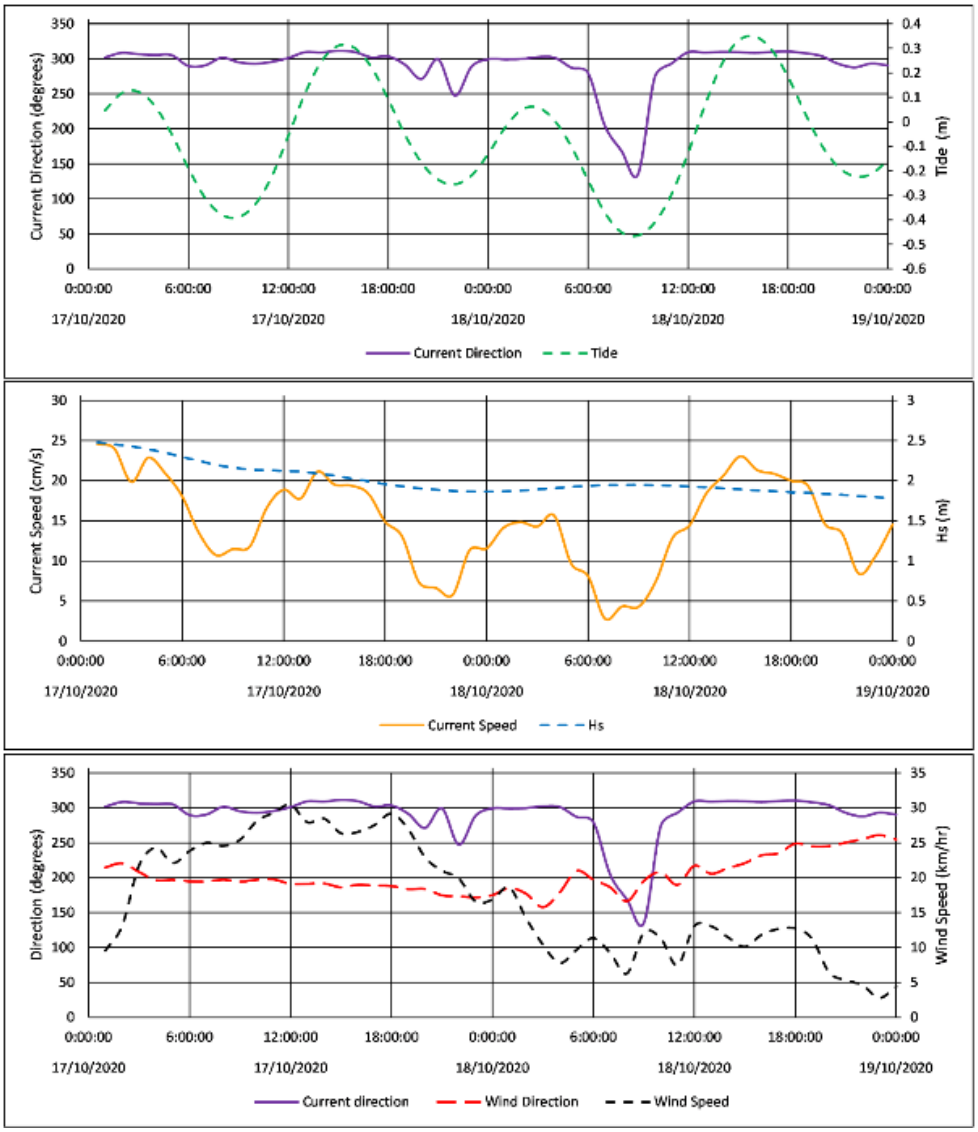

Figure 57: Current speed/direction, tidal deviation, Hs and wind speed/direction for the 17/10/2020 to the 18/10/2020Flow reversal from the mean NW direction only occurs under particular rare conditions consisting of extremely low Hs, low tide and low or eastly winds.

These examples demonstrate that although the current speed varies significantly with Hs the direction remains steadily NW except under particular rare conditions consisting of extremely low Hs, low tide and low or NNE winds. The offshore reef may be responsible for the currents consistency, with waves previously observed propagating over the southern end of the reef and then around the bay (Davidson et al., 2021). However, further study into incident wave direction, the morphology of the reef and wave refraction over it is needed to be conclusive.

Bi/multidirectional flow that regularly oscillates hinders the formation of subaqueous dunes (Ashley, 1990). This means that subaqueous dunes previously studied have generally been found in environments that tend towards near unidirectional flow such as rivers or estuaries with circular flow patterns (Carey and Keller, 1957; Collinson, 1970; Crowley, 1983; Francken et al., 2004; Ryan et al., 2007; Masselink et al., 2009; Billy et al., 2012; Goodbred and Saito, 2012; Mason et al., 2020). Small coastal embayments typically have highly variable currents whose speed and direction depends on wave height, wave direction, tidal cycle, wind speed, storm surge, geological inheritance, and changes in nearshore sedimentary morphology (Ferentinos and Collins, 1980; Holloway, 1996; Stephens et al., 2001; McCarroll et al., 2018). This is likely why subaqueous dunes such as those found at Salmon Hole have not been previously observed/studied in similar small headland embayment's. During the period of data recording the current direction was not only largely consistent at Salmon Hole but on the rare occasions it did reverse direction SE, its speed was minimal (Figure 56Figure 57). Due to the coarse sediment size at Salmon Hole, it is therefore unlikely that this reversed flow would impact the formation of the dunes or mobilise them.

5.3.1 Flow over dunes

The local (over the dunes) currents recorded by the TCM's for the period of the experiment were very slow, averaging at 7 cm s^{-1} on the dune crest and 6.7 cm s^{-1} in the swale (Figure 58). This was to be expected given the minimal amount of wave height recorded by the water level loggers and shown in the hindcast Hs data. The speed of the current also dropped in accordance with the reduction in wave height over the course of the experiment. Figure 58 compares current speed in hourly averages recorded by the TCM's and main current meter positioned closer to the reef. The closer inshore current speed recorded by the TCM's was significantly less effected by tide than that from the main current meter, however, the overall downward trend between the two positions is the same (Figure 58).

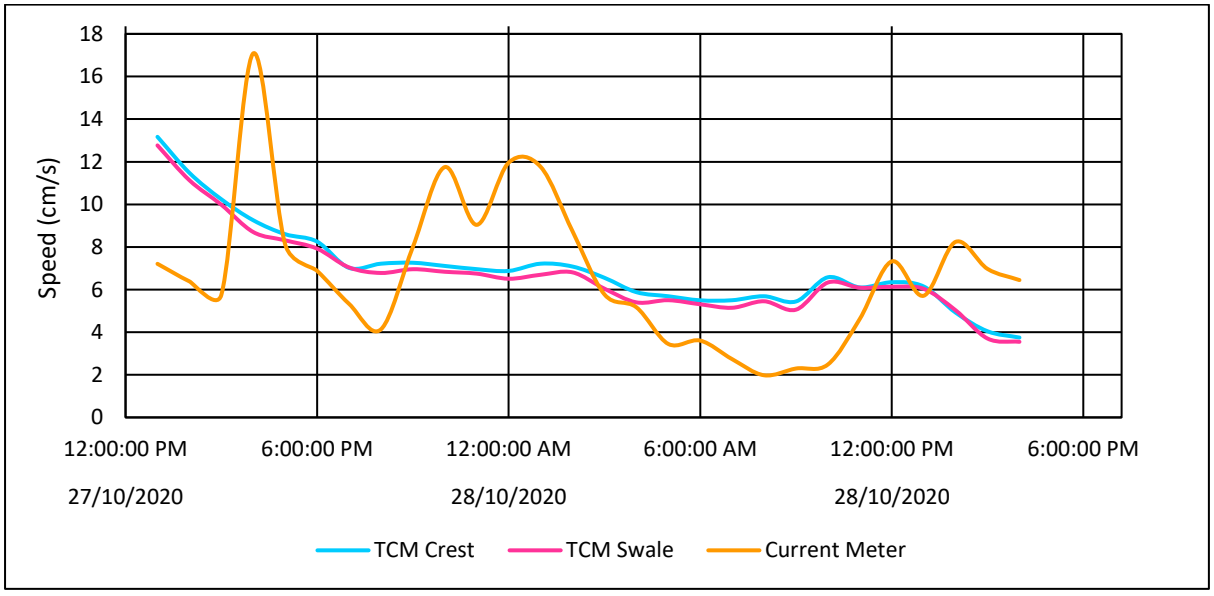

Figure 58: Current speed in hourly averages for the duration of the experiment measured at the main current meter positioned near the reef (orange), the tilt current meter on the crest (blue) and the tilt current meter in the swale (pink). Tide is affecting the speed at the main current meter to a larger degree than the TCM's.

The speed of the flow was slightly higher on the crest than in the swale for the majority of the recording period (Figure 59). This increase in speed is due to what is termed speed-up in aeolian coastal and desert dune literature, which refers to the topographically forced flow acceleration that occurs up the stoss slope of a dune (Jackson and Hunt, 1975; Rasmussen, 1989; Wiggs et al., 1996; Neuman et al., 1997; Hesp et al., 2015). As flow approaches positive topography, such as a dune, it is compressed creating a change in pressure gradient that leads to an increase in speed toward the crest (Arens et al., 1995; Hesp, 2002; Walker et al., 2006).

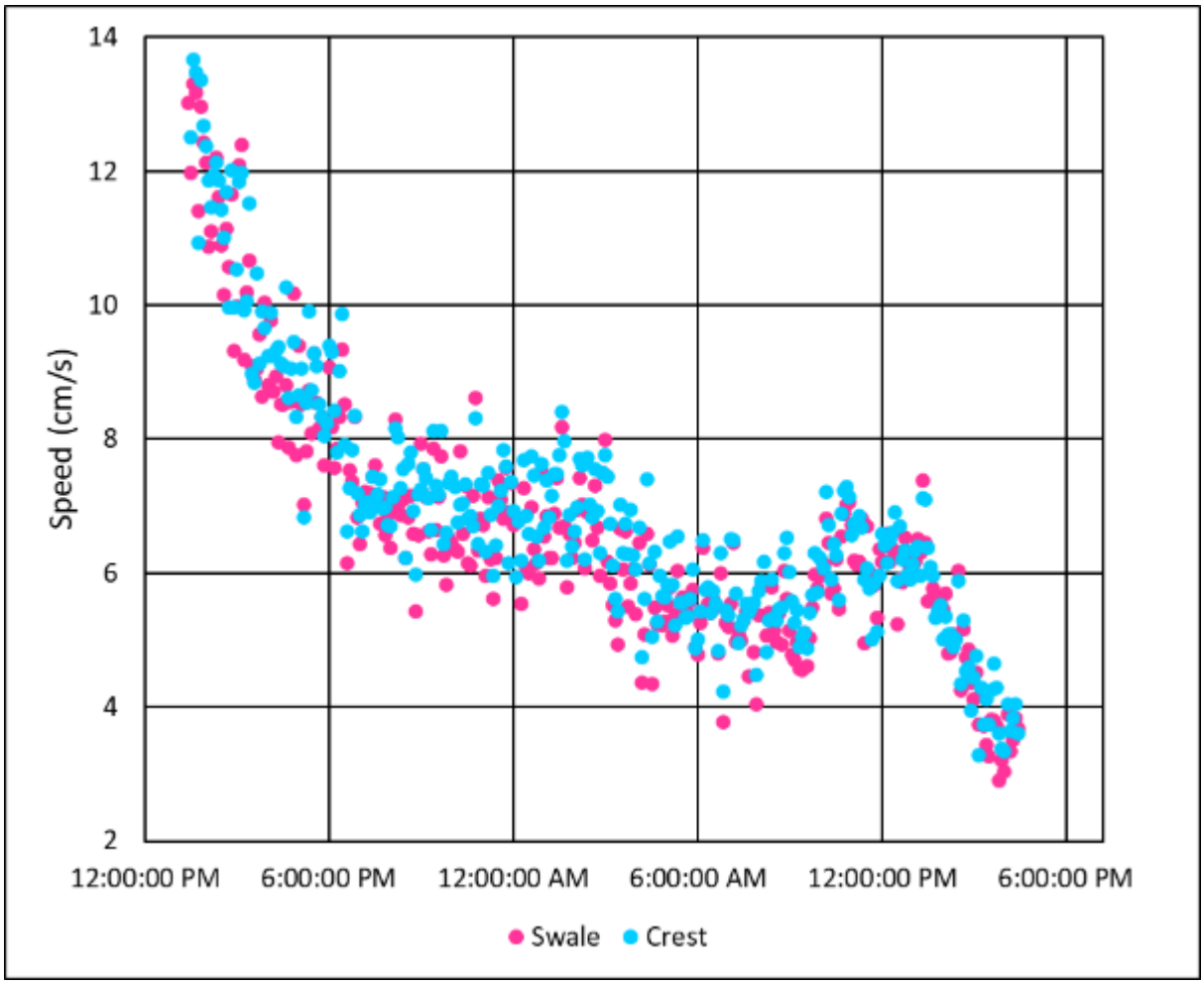

Figure 59: Current speed at the crest (blue) consitantly higher than in the swale (pink) suggesting speed up.

Despite the low current speed, the direction of the current is again predominately WNW in keeping with the data taken off the main current meter (Figure 60). The mean direction at the crest was 302 degrees and, in the swale, it was 294 degrees. As shown above when the current is low the tide plays a role in its direction. The difference here, however, is that the current speed has only fluctuated minimally with the change in tide whilst the change in direction is quite pronounced (Figure 60Figure 61). The change in direction to more northerly occurs predominantly during low tide, with the variation during these periods also increasing as the direction swings back and forth from NW to N (Figure 61). This suggests that the lower water level is allowing wave action to have a greater impact on the direction of the TCM. Further evidence for this being the case is that the effect is greater on the TCM positioned on the crest which lies in shallower water (105 cm deep at time of deployment) than the swale TCM (140 cm deep at time of deployment) (Figure 60Figure 61).

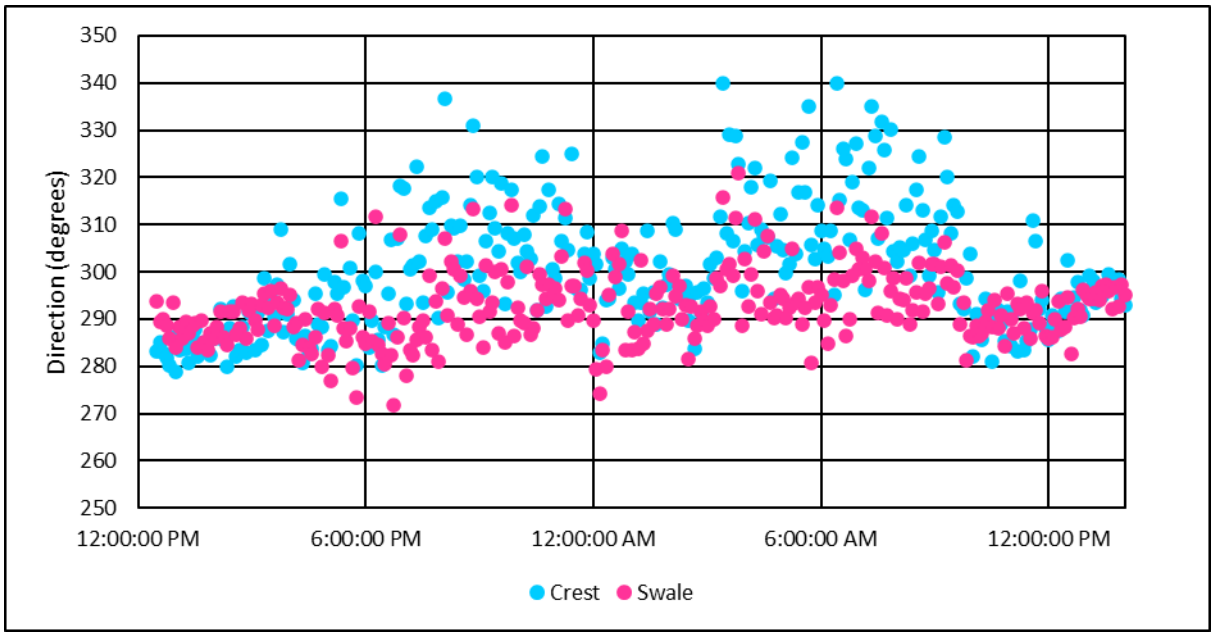

Figure 60: Tilt current meter direction from both the crest (blue) and swale (pink).

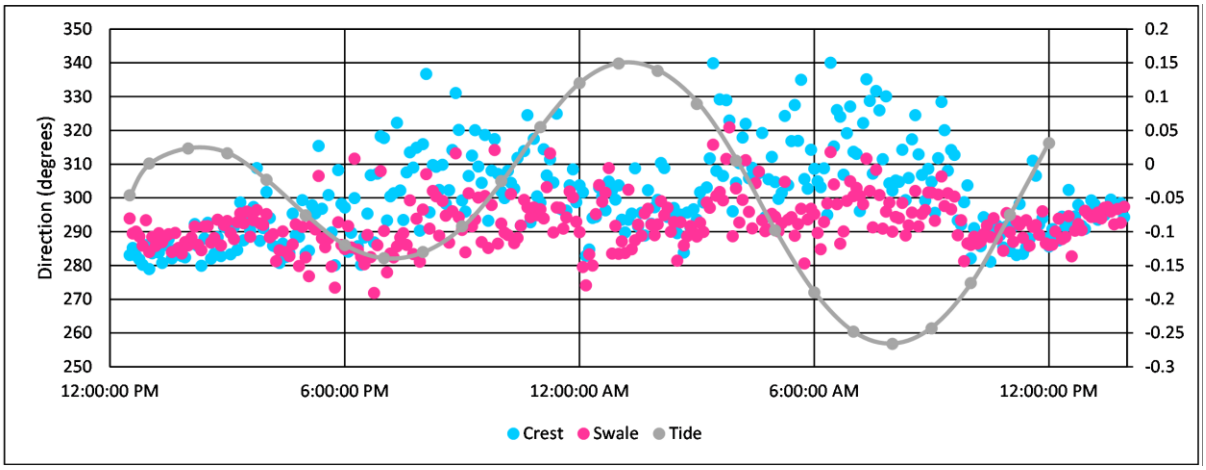

Figure 61: Tilt current meter direction from both the crest (blue) and swale (pink). Changes in direction and an increase in variation are linked to drops in tide height (gray).

5.3.2 Variation in wave height around bay

A comparison of the spread of data points from two ten-minute segments of data from each water level logger position is shown in Figure 66. The first ten-minute segment (A) is taken from 6:00pm to 6:10pm on the 27/10/20 and the second segment (B) is from 4:00pm to 4:10pm on the 28/10/20. The purpose of these figures is not to show the exact water level at each location but rather to use the spread of data points at each position as an indication of wave height. The greater the spread of data points the larger the rise and fall of water level due to wave action. Change in wave height between the water level logger positions around the bay can then be seen. To aid in in this the original data points at positions 1 and 3 each had an amount added to them to bring the data from each position closer together in the graphs for easier comparison. This has not affected the spread of the data points from each position, so comparisons are still valid.

Both A and B of Figure 62 indicate that under low Hs conditions waves are highest at position 1 at the northern end of the bay, followed by position 2 in the middle of the bay and then position 3 at the southern end of the bay (Figure 51). The geological inheritance of Salmon Hole effects the wave exposure of the beach. Headlands can cause wave shadowing

which creates an alongshore gradient in wave energy depending on the direction that waves approach from (Castelle and Coco, 2012; McCarroll et al., 2014; Gallop et al., 2020). However, it appears at Salmon Hole that the reef enclosing the lagoon is having the greatest effect. The reef causes waves to dissipate a percentage of their energy before reaching the lagoon and the shore (Gallop et al., 2020). The greatest dissipation of wave energy is occurring in the southern end of the bay as this is where the reef is significantly wider than the remainder of the bay (Figure 49). The much narrower and potentially deeper (based on observations from field visits) middle and northern sections of the bay allow more wave energy to enter in those portions resulting in higher waves at this end of the bay.

Position 1 and 2 of A have a greater spread than that in B meaning there was a drop in wave height at these locations between the two periods. Figure 63 shows Hs from the CAWCR hindcast data and Tide on both the 27/10/20 and the 28/10/20. The first segment from 6:00pm was during a moderately low tide and low Hs conditions, whereas the 4:00pm segment of data from the next day was during higher tide and slightly higher Hs. At low tide it would be expected that the reef would shelter the bay from wave energy. It seems, contradictory therefore that the spread of data i.e., wave height, in the middle (P2) to northern end (P3) of the bay shown in Figure 51 would be greater in A during lower tide and Hs than B (Figure 61). However, just like with the impact on change in direction of the TCM's, waves are having more of an influence on change in water level at low tide at positions 1 and 3 because the surf zone has moved seawards. Wave height is increased as shoaling is now occurring where the water level logger is located. Position 3 appears to be more representative of the overall conditions of wave height in the bay with a slightly larger

variation in the spread of data points and therefore wave height seen in B when compared to A.

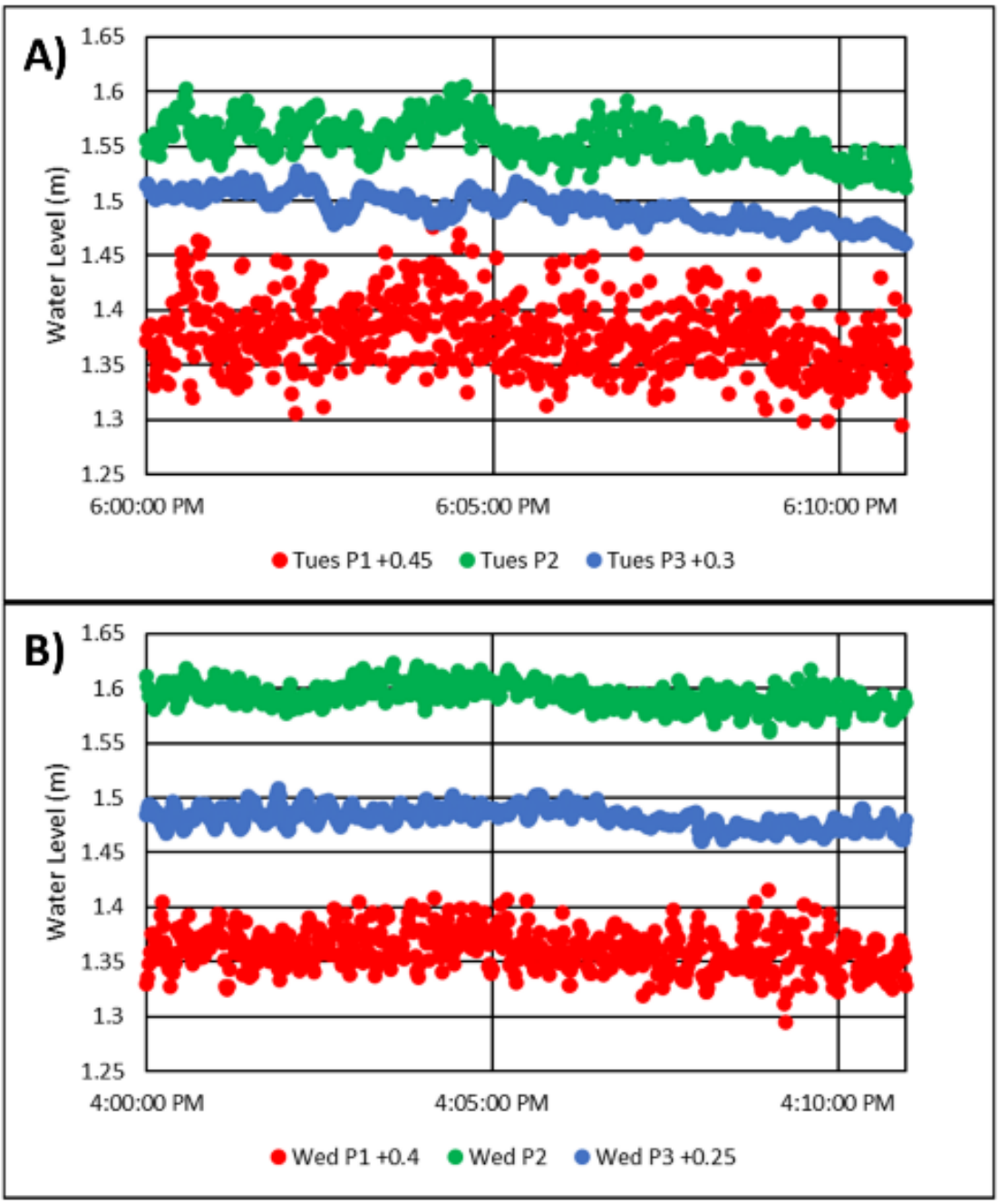

Figure 62: Comparison of the spread of data points from two ten-minute segments of data from each water level logger position. The first ten-minute segment A is taken from 6:00pm to 6:10pm on the 27/10/20 and the second segment B is from 4:00pm to 4:10pm on the 28/10/20. Position 1 (red), Position 2 (green), Wednesday (blue).

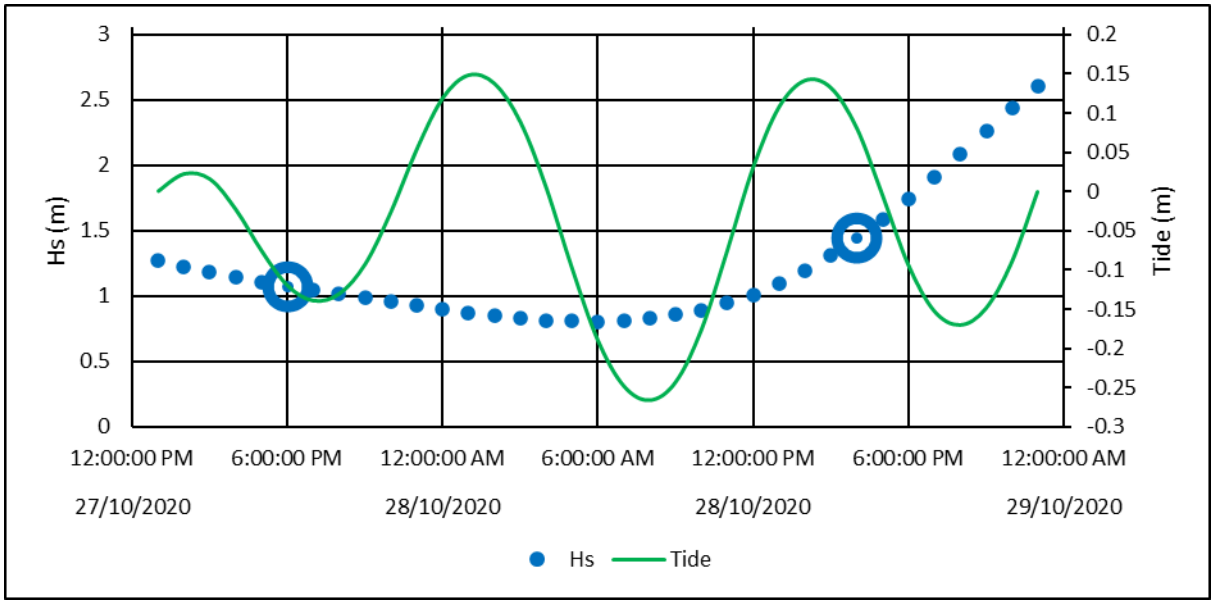

Figure 63: Hs (blue) and Tide (green) on both the 27/10/20 and the 28/10/20. The larger Hs data point on the left indicates the conditions during A and the one on the right B in Figure 66.

5.4 Spatial and Morphological Changes in Transverse Dunes

Oblique aerial images of the middle to northern end of the bay taken between the 15/2/19 and the 28/10/20 on six occasions during periods of calm weather are shown in Figure 64. The orthomosaics created from 26/7/20 and 28/10/20 drone surveys are then show in Figure 65 providing a vertical view of the dunes. Changes to the morphology of the dunes over time are evident in both Figure 64Figure 65 with both the overall shape and position of the dunes differing significantly between images/orthomosaics. This suggests that the dunes may be migrating.

Images were taken in February and May of both 2019 and 2020. The length, width and wavelength of the dunes are similar in each corresponding month (Figure 64). This could suggest that similar seasonal wind and wave conditions produce similar current velocity patterns and therefore similar dunes at the same time of the year however, this would need

to be backed up with observations over a longer period that 2 years. The dunes in May appear to be slightly narrower and steeper than those in February with this being particularly pronounced between the 25/2/20 and the 16/5/20 (Figure 64). By July on the 26/7/20 the average wavelength between dunes has increased while the dunes themselves have begun to widen and become slightly flatter (Figure 64Figure 65). The dunes remain transverse between February and July, however, by October 2020 the majority of the dunes in the bay have significantly flattened and become more symmetrical (Figure 64Figure 65).

Although speculative due to a minimal number of years monitored there does seem to be a pattern. The large swell that peaks between April and September results in strong currents that flatten and round the crests of the dunes. The current remains consistent throughout the summer period but reduces in overall speed due the reduction in wave energy. This allows the dunes to morph into more asymmetric transverse shapes with steeper slopes. Dune height and definition then peaks around May before large winter swells then return and once again rounds the dune crests and flattens them out. In Figure 52there is a clear increase in instances of both high Hs and current speed in August and September of 2020 that likely led to the flattened symmetrical dunes in October.

This morphological cycle is not unique to Salmon Hole. Although the morphological transition being driven by variation in wave energy in a coastal embayment may have not been previously noted in the literature, changes in dune morphology due to seasonal current velocity variation is not new. Generally, when dunes adapt to changes in flow speed it is through the redistribution of sediment between multiple interconnected dunes (Reesink et al., 2018). This occurs through the interchange of sediment between dune crests and swales and the merging or splitting of dunes (Kostaschuk and Villard, 1996; Reesink et al.,

2018). Kostaschuk et al. (1989) found that in the Fraser River, Canada, large symmetric dunes slowly became replaced by smaller asymmetric dunes as flow speed reduced over the discharge season. The lower current velocity was found to create sharper crests whilst less transport in suspension created steeper and straighter lee slopes. Smith and McLean (1977) hypothesized that the opposite is true for an increase in flow speed and sediment suspension as this leads to the infilling of the troughs between dunes. This along with the tendency for the crests of the dune to also round under these conditions was later confirmed by Johns et al. (1990) numerical models. Kostaschuk and Villard (1996) observed crest rounding of dunes to be linked with periods of increased current speed again in the Fraser River, Canada. Here the dunes transition from asymmetric to symmetric forms was associated with both high bed load and suspended load sediment transport. Increased flow led to the rounding of the crest as sediment was transported from the crest into the swale, this both widened and lowered the narrow steep asymmetric dunes. As the period of high velocity continued, increased bed load transport resulted in the formation of long low lee sides as sediment deposition continued to occur in the down-stream swales enlarging the dunes and making them symmetric.

Figure 64: Oblique images of the northend of the bay taken from the air using a DJI drone on occasions when the subaqueous dunes were visible.

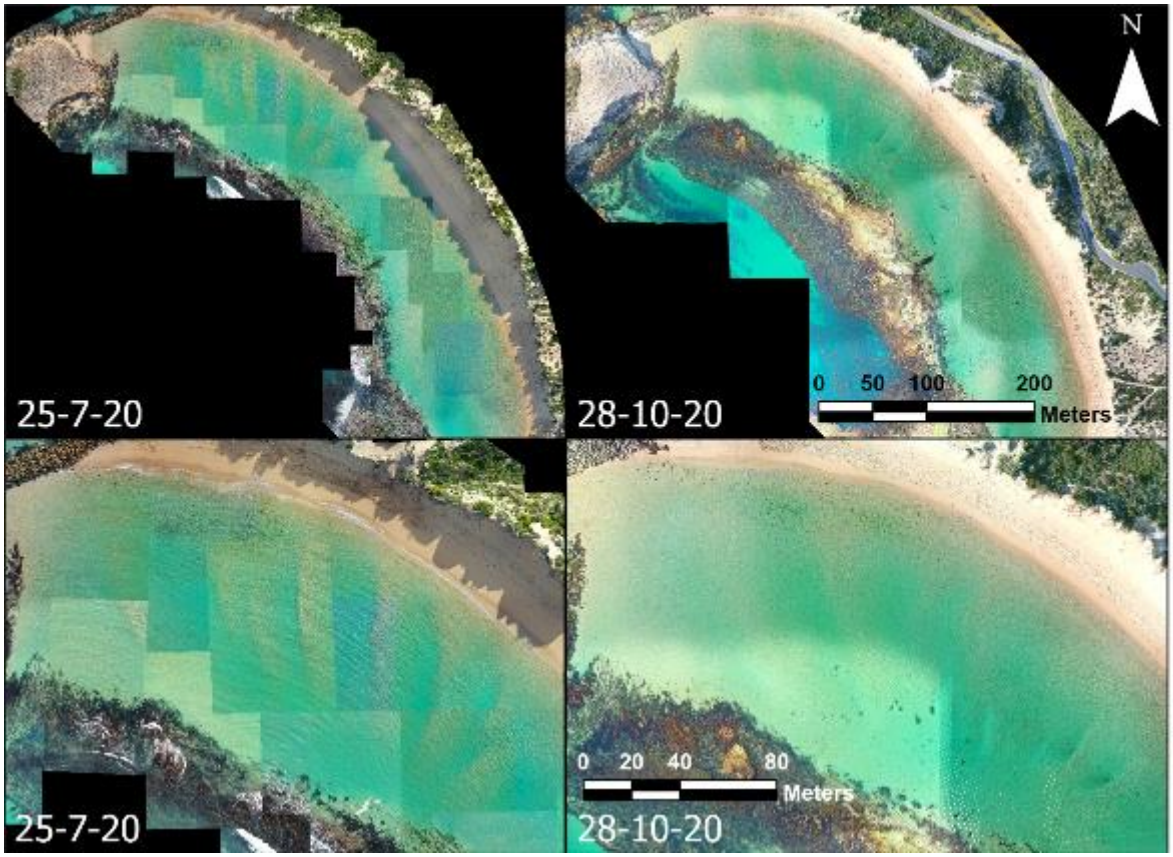

Figure 65: Orthomosaics created from drone surveys over Salmon Hole Bay conducted on the 25/7/20 and 28/10/20. The two upper frames showing the entirety of the bay whereas the lower frames focus in on the location of the dunes. Increases in wavelength and width along with crest rounding can be seen to have occurred between July and October.

The subaqueous transverse dunes visible in the orthorectified aerial images were measured in ArcGis Pro by creating lines along their crests and their widest point (from the toe of the stoss slope to the bottom of the lee slope slip face). This definition of width was used instead of wavelength as a measurement of size as the subaqueous dunes are not spread evenly throughout the bay. This means there is often a significant distance between the dunes making the use of wavelength unfeasible. The measurements for the longest and shortest dunes visible on each occasion are shown in Table 7. The continued erosion of Salmon Holes shoreline has resulted in the widening of the lagoon since 2013 and therefore the longest dune in 2013 is shorter than those from 2020. The longest dune in 2013 was

66.86 m long whilst on the July and October of 2020 the longest dunes were 80.82 and 85.8 m long respectively. The width of the longest dunes in 2020 changed dramatically between July and October with the longest dune more than doubling in width in the three-month period between surveys, from 12.53 to 31.41 m wide. The shortest dunes in the bay on each occasion were of similar length despite the change in lagoon size. Approximately 30 m long dunes were found in both 2013 and July 2020 whilst the shortest dune in October 2020 was 25.72 m (Table 7). The widths were also relatively similar in all instances.

Table 7: Comparison measurements for the longest and shortest dunes found in Salmon Hole in the 2013 orthrectified image, the orthomosaic/georeferenced image from 25/07/20 and the orthomosaic image from the 28/10/20.

Date	Size	Location	Length (m)	Width (m)
Dec 2012 - March 2013	Longest	Nth End	66.86	9.47
	Shortest	Mid Bay	29.78	6.05
25/07/2020	Longest	Nth End	80.82	12.53
	Shortest	Mid Bay	30.1	8.9
28/10/2020	Longest	Nth End	85.8	31.41
	Shortest	Mid Bay	25.72	8.35

Table 8 compares measurements of dunes from the 25/7/20 and 28/10/20 orthomosaics that are in similar locations to observe changes that have occurred over time. It must be noted that although these dunes are in similar locations, they may not be the same dune developing overtime due to potential migration between surveys. The dunes are also compared visually in Figure 66 with the lines used to obtain the measurements indicating which dunes in the orthomosaics are being considered.

Both the longest dunes were found in a similar location at the northern end of the bay and so the measured dunes compared in row A of Table 8 and 70 are also the found in Table 7. As stated above, the biggest difference seen between these dunes is the change in width between them. However, another key difference between July and October is a change in the location of the crest of each dune. This can be clearly seen in Figure 66 and was noted above when comparing the oblique images. The line running the length of the dune that was used to measure it also indicates the position of the crest of the dune. In row A the crest of the measured dune from the 25/7/20 is asymmetric indicating a gradually sloped stoss slope and a sharply angled lee slope (Figure 66). This is in keeping with the morphology of a transverse dune. The crest of the corresponding measured dune in row A from the 28/10/20 on the other hand is symmetric (Figure 66).

The measured dunes compared in row B are positioned slightly more towards the middle of the bay. The measured dune captured in the July drone survey was longer than that recorded in October, at 74 m compared to 65.55 m. (Table 8; Figure 66). The measured dune from the October survey, however, was once again wider at 26.4 m wide compared to 22.64 m in July (Table 8). This is only a difference of 3.76 m compared to the 18.88 m change between the dunes found in row A (Table 8). This could be due to the dune in row B from July being initially wider than the dune July dune from row A (Table 8; Figure 66). Despite this dune being wider, which is assisted by a kink mid-way along its length, its morphology is still transverse in July, while in October the dune has again flattened and became symmetrical in shape.

Row C compares the two smallest dunes from July and October which are located in a very similar area. Here, as mentioned above, the measurements for both were relatively similar.

The smallest dune from the July orthomosaic shown in row C (Figure 66) follows the same pattern as the other dunes from the July survey and has transverse morphology, (ie long stoss slope followed by a steep narrow lee slope). Interestingly, the measured dune from the October orthomosaic, unlike the majority of the dunes from this period, also has an asymmetric crest. Despite this however, the difference between the dunes from July and October in row C is quite stark (Figure 66). The dune in this position has changed in morphology from a regular transverse dune to that reminiscent of a barchan. The crescent shape of both the measured dune and the one next to it in the October orthomosaic is similar to that of barchan dunes found in arid desert environments (Long and Sharp, 1964; Watson, 1986; Durán et al., 2010). Barchans and barchanoid shaped dunes have also been found in marine environments such as those found in the Gra˚dyb tidal inlet channel in the Danish Wadden Sea by Ernstsen et al. (2005). Barchans form in areas with limited sediment supply and similar to transverse dunes in regions of unidirectional flow (Hersen, 2004; Kroy et al., 2005). These barchans may have formed in this area due to a lack of sediment supply to them between July and October due to their location within the bay. The transverse dune in this position in July is the last dune before a relatively flat area that covers the rest of the southern end of the bay. This means there were no dunes upstream of the current to provide sediment to this area under strong current conditions. If dune scarping was minimal then there would be limited additional sediment to aid in maintaining the shape of the transverse dune in this location resulting in the formation of the two barchan-like dunes.

Table 8: Measurements of dunes in similar locations within the bay. Comparisons between the orthomosaic/georeferenced image from 25/07/20 and the orthomosaic image from the 28/10/20.

A) Nth End	**25/07/2020**	**28/10/2020**
Length (m)	80.82	85.8
Width (m)	12.53	31.41
B) Mid Bay Large	**25/07/2020**	**28/10/2020**
Length	74	65.55
Width	22.64	26.4
C) Mid Bay Small	**25/07/2020**	**28/10/2020**
Length	30.1	25.72
Width	8.9	8.35

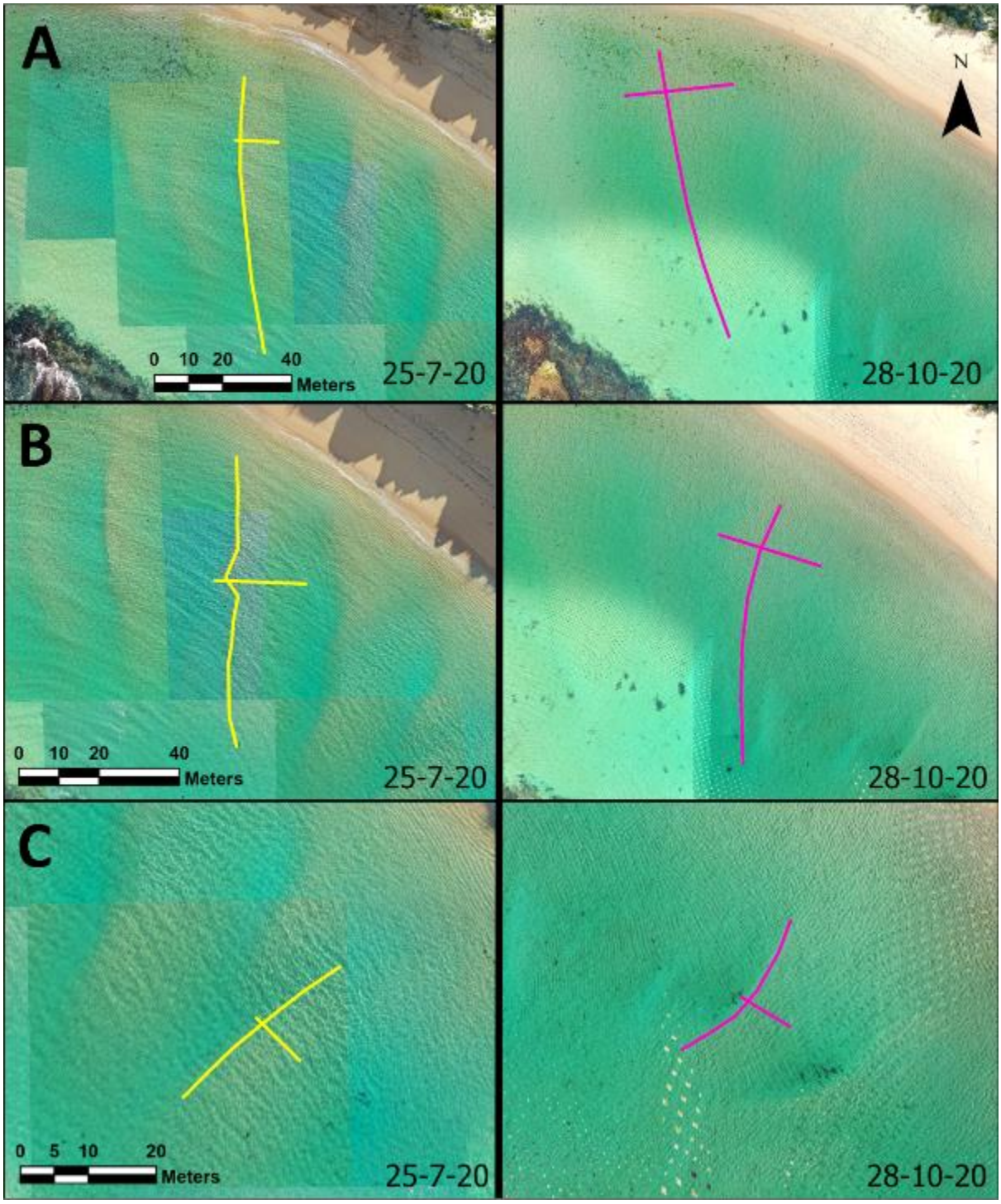

Figure 66: Lines used to measure dunes from the 25/7/20 and 28/10/20 orthomosaics that are in similar locations using ArcGIS Pro. The longer lines drawn perpendicular to the beach measured the dunes crests and the shorter lines measure the width of the dune from the toe of the stoss slope to the end of the lee slope. A) northend end of the bay - large, B) middle of the bay - large and C) middle of the bay - small.

Five profiles were drawn along the kayak derived DEM's in ArcGIS Pro to reveal the 2D outline of several of the dunes found in the bay at the time the surveys were undertaken, firstly on the 9/4/18 and secondly on the 13/7/18 (Figure 67Figure 68). Due to the sparsity of the survey lines, there is insufficient detail for highly accurate DEM's, however, the profiles drawn were either along the survey lines or intersecting multiple measured points (Figure 67). Profiles 1, 4 and 5 were drawn along the April survey lines running parrellel to the beach that intersected dunes running perpendicular to the coast (Figure 67). Profiles 2 and 3 cover the lines from the July survey that were close together (Figure 67). Profile 1 was able to be used as a comparison between the two surveys as it also intersected survey lines from the July survey (Figure 67Figure 68).

From 13 to 34 m along Profile 1 a dune can be seen both in April and July. April's dune is ~70 cm high and has clear transverse morphology, whilst in July the dune appears more symmetrical and is of a similar height but positioned slightly deeper. The increased current speed from winter swells could again be responsible for this rounding of the dune. However, profiles 2 and 3 also show transverse shaped dunes present in the July survey (Figure 68). This is not surprising given the transverse appearance of the dunes also from July albeit in 2020 previously shown in the oblique aerial imagery and orthomosaics (Figure 64Figure 65Figure 66).

The July DEM in Figure 67 indicates that profiles 2 and 3 are cross-sections of the same dune. Profile 2 is closer to shore and roughly crosses the centre of this large transverse dune that is 18 m wide and reaches ~85 cm high, it then goes on to also intersect a smaller more symmetrical dune. Profile 3 crosses the end section of the larger transverse dune, at this point the dune has narrowed to 12 m whilst remaining roughly the same height. Profile 3

still maintains transverse morphology however the crest is further to the centre and the slip face is not as steep as in Profile 2.

Profile 5 crosses five transverse dunes intersected by an April survey line running parallel to shore (Figure 67). The dunes range in size from 10 to 25 m wide and 0.4 to 1 m high (Figure 68). The most northerly dune from Profile 5 is shown in more detail by Profile 4, and clear transverse and asymmetric morphology is visible. The transverse morphology of these dunes indicates that the current was also predominantly NW leading up to April 2018.

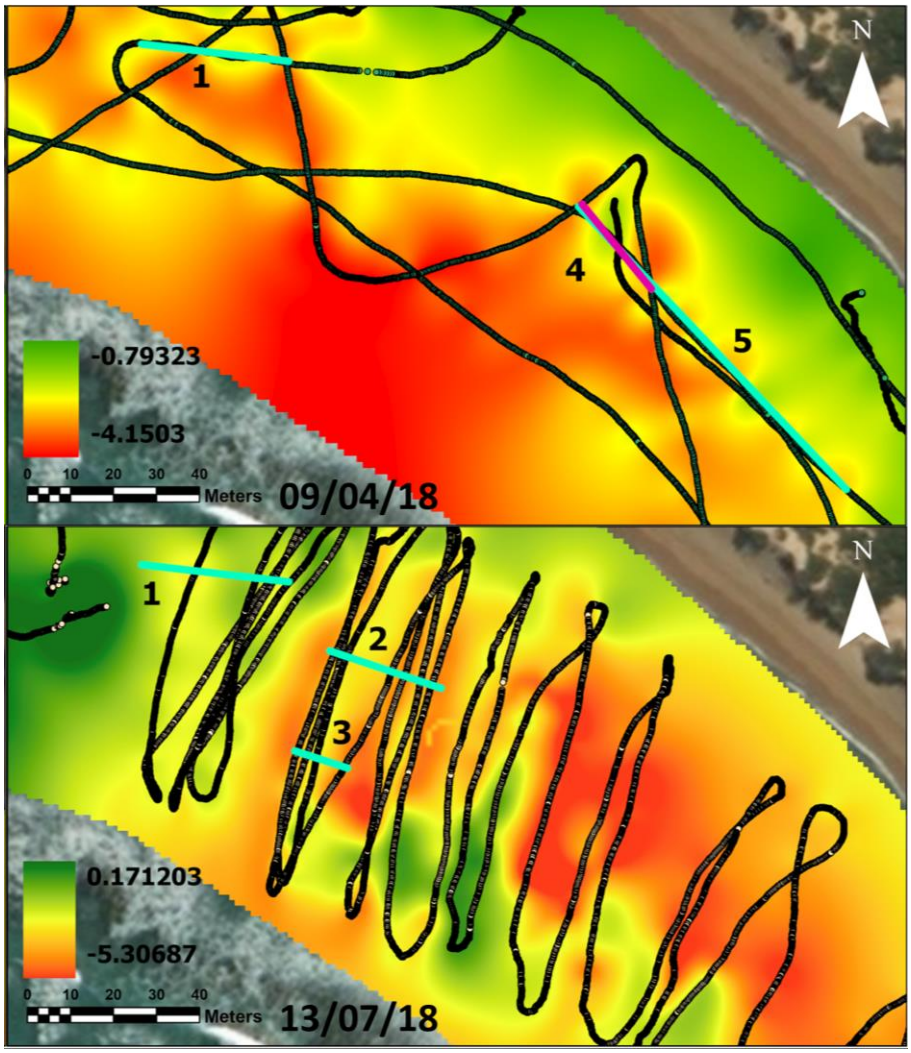

Figure 67: Digtal Elevation Model's (DEM's) created in ArcGis Pro unsing GPS enabled kayak deployed echosounder depth and positional data (9/4/18 above, 13/7/18 below). Positions of profiles are indicated and numbered. The kayak survey lines across the bay are also included.

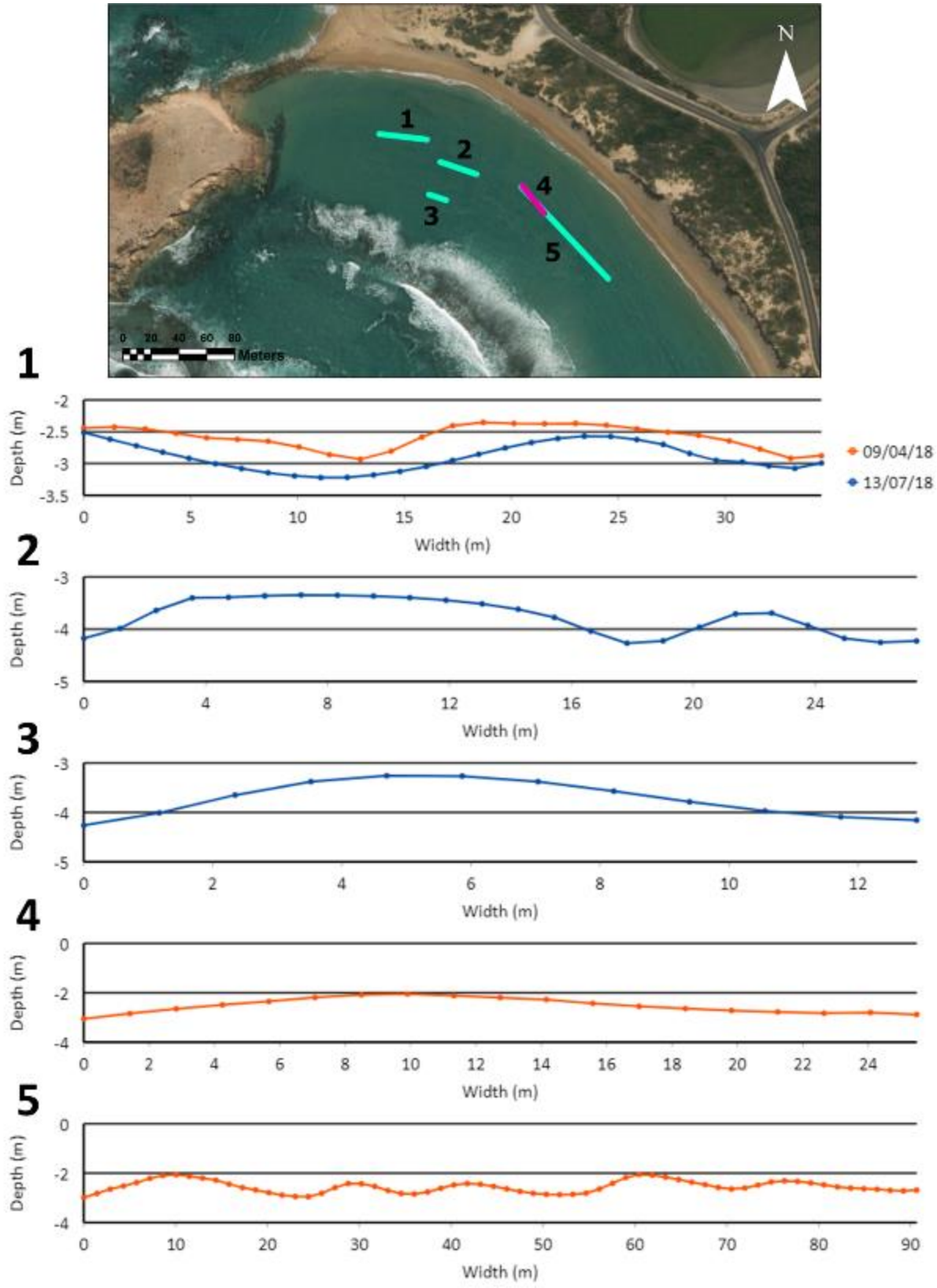

Figure 68: Profiles drawn along the kayak DEM's using ArcGIS Pro profile stack tool to reveal the 2D outline of several of the dunes found in the bay at the time the surveys were undertaken. Firstly, on the 9/4/18 (orange) and secondly on the 13/7/18 (blue).

One of the aims of this study was to better understand the role that the subaqueous transverse dunes are playing in the erosion dynamics of Salmon Hole Bay. Due to the length in time between orthomosaics and DEM's the direct monitoring of the migration of individual transverse dunes has not been possible. However, the study has confirmed that the dunes are in fact generally asymmetric and transverse in morphology for the majority of the year due to the consistency of the current. From what is known of transverse dunes in subaqueous environments, it is common to see migration (Coleman, 1969; Bartholdy et al., 2005; Van Dijk and Kleinhans, 2005; Bradley and Venditti, 2017). The aeolian coastal and desert literature also indicates that it is likely that the Salmon Hole dunes are in fact migrating (Lancaster, 1988; Van Dijk et al., 1999; Momiji and Warren, 2000; Yao et al., 2007; Parteli et al., 2011; Ramos et al., 2011; Walker and Shugar, 2013). Transverse dunes are known to migrate as flow perpendicular to the crest line erodes sediment from the stoss slope and deposits it on the leeward side (Bagnold, 1941). This deposition is caused by a reduction in flow speed after the crest created by flow separation as a result of the steep lee slope of the transverse dune (Tsoar et al., 2004). Another factor that suggests the migration of the dunes at Salmon Hole is that while the exact location of individual dunes was unable to be monitored, it was not only the morphology of the dunes but also the location of the dunes that was observed to change between the different periods compared in the oblique imagery, orthomosacis and DEM's. Thus, the dunes in Salmon Hole are potentially playing a role in sediment transport out of the bay as they migrate, contributing to the ongoing erosion. To be certain however, weekly detailed bathymetric surveying of the bay would be necessary to clearly monitor the dunes movements. Because they consist of coarse

sediment the dunes may only be migrating during high current speed conditions i.e., storms. Meaning despite the extremely consistent unidirectional current they may be stationary features during low energy periods. This again would need to be determined with more consistent detailed bathymetric surveys.

5.5 Conclusion

Three key points can be made from the initial analysis of the subaqueous transverse dunes found in Salmon Hole Bay. These include:

- Effectively unidirectional wave dominated current is responsible for subaqueous transverse dune formation in Salmon Hole Bay.
- A predominantly transverse morphology and change in position between images, orthomosaics and DEM's suggests that the dunes are migrating and therefore aiding the sediment transport out of the bay and continuing erosion of the beach.
- Fluctuation in average current speed throughout the year created by seasonal variation in wave energy causes the dunes morphology to cycle between being narrow, steep, transverse, and asymmetrical to wide, rounded and symmetric.

CHAPTER 6
CONCLUSION

6.1 Summary of findings

The four studies presented in this thesis variously examine the spatio-temporal changes, history, wind flow and subaqueous dune dynamics in a complex, headland-bay-lagoon-beach system at Salmon Hole, South Australia. The components studied include determining what controls dictate the magnitude of a scarping event, analysing an example of scarping's effect both in the past and present as a proxy for the future, a study of wind flow over a sediment starved scarped dune, and monitoring changes in position and morphology of subaqueous transverse dunes within the lagoon. This thesis research has also contributed to a better understanding of the effect increased scarping will have on sandy coastlines with limited to no sediment supply under climate change and sea level rise conditions. In particular, how will complex sandy embayment's typical of those found along the Australian coastline react? The key findings from each of the four specific studies are as follows:

I. Controls that determine scarping magnitude include water level height, height and volume of the foredune, vegetation density and distribution, plant root mass and rooting depth, compaction of sediment, presence or not of wrack and large woody debris, the original foredune morphology (antecedent conditions), and surfzone-beach type (Short and Hesp, 1982; Hesp, 1988; Nishi and Kraus, 1997; Pye and Blott, 2008; Coco et al., 2014; Feagin et al., 2015). A conceptual model summarizing the effect of these factors, be it positive or negative, has been presented. Scarping can lead to changes to the morphology of the foredune, and on occasion the entire dune system. These changes include potential dune translation, blowout and parabolic

dune formation, the transition to a transgressive dune sheet or dunefield, and potentially complete removal of a dune system.

II. The shoreline and dune system at Salmon Hole has eroded an average of ~100 m in the period 1946 to 2019 at an average rate of 1.44 m/yr. This average rate along the length of the bay has varied from 0.63 m/yr to 3.49 m/yr depending on storm activity, presence or absence of a tombolo, both natural and artificial, and lagoon widening and elongation. The dynamics observed at Salmon Hole indicate the role geological inheritance can play in bedrock/reef dominated headland-bay systems with the formation of the lagoon potentially largely responsible for the rapid erosion of Salmon Hole. The development of the lagoon initiated a divergent evolution that continues in the form of a significant longshore current and terminal rip that enhances removal of sediment during and following scarping events.

III. The large, high and long stoss slope of the eroded dune backing Salmon Hole beach was comprised of various slope segments. These had a significant impact on flow dynamics over the dune. Percentage speed up the stoss slope is similar to that previously observed over scarp slopes, foredunes and transverse dunes and due to streamline convergence and flow compression. However, flow expansion at a change in slope caused a significant reduction in wind speed by the time flow reached the upper slope segment. An expected increase in turbulence was observed at the toe scarp followed by a gradual decrease up-slope. However, the change in slope and subsequent flow expansion resulted in a significant increase in turbulence at the crest. Topographic steering of incident flow typically seen in wind flow over scarps and foredunes was observed at Salmon Hole. Once flow passed the dune crest, flow separation and a reversing vortex were produced. A blowout developed and grew

through dune cannibalization despite the lack of sediment supply from the beach and the recession of the shoreline. The study demonstrates that lack of sediment delivery back to the dune between storm events results in the inability for dune recovery or translation, and therefore net erosion.

IV. A near unidirectional wave dominated current and sediment supply from the scarped dune system is likely responsible for subaqueous transverse dune formation in Salmon Hole Bay/lagoon. The dunes are predominantly transverse in morphology and their change in position between images, orthomosaics and DEM's suggests that the dunes are generally migrating towards the NW (i.e. around the lagoon), and therefore aiding sediment transport out of the lagoon/bay and continuing erosion of the beach-nearshore system. Fluctuations in average current speed, created by seasonal variation in wave energy, is causing the transverse dune morphology to cycle between being narrow, steep, transverse, and asymmetrical to wide, rounded and symmetric.

The four studies clearly show that scarping impacts the sediment dynamics of the entire embayment at Salmon Hole. Large decadal shoreline changes, wind flow dynamics, long term dune system morphological changes and sediment transport all revolve around the process of scarping reviewed in Chapter 2. The combined studies in this PhD thesis also demonstrate the effect that increased levels of scarping and a negative sediment budget will have on complex coastal embayment's backed by dunefields. This is highly relevant for understanding a future increased sea level scenario.

Chapter 3 shows that frequent large scarping events can cause major shoreline/dunefield retreat. If, as Chapter 4 highlights, there is a lack of sediment delivery back to the dune

between storm events, dune recovery and/or translation is nigh impossible, and therefore net erosion results. Aeolian processes post-scarping are also shown to initiate morphological changes to dunefields such as blowout formation. Chapter 5 is then an example of how coastal processes in complex embayment's can transport sediment brought offshore post scarping out of the bay.

The significant scarping at Salmon Hole and the processes studied in each of this thesis's chapters therefore indicate that climate change induced sea level rise and increased storm magnitude/frequency will result in the removal of dune systems in similar embayments lacking in sediment supply. These systems are critical for both the rich ecological habitat and protection of infrastructure they provide.

6.2 Future Work

6.2.1 Chapter 2 – Controls on Dune Scarping

The review on scarping controls has highlighted some areas that require attention in the future. These include:

1. Further research conducted on the effects of vegetation on scarping. For example, what does the variation in plant root and stem density, depth, strength and mass have on dune stability?
2. Studies into the control surfzone-beach type has on beach erosion and on the degree of scarping ought to be conducted, including field observations and numerical modelling.
3. The effect of compaction, particle size and particle roundness have on scarping and dune stability needs to be included in future experimentation.

4. Further observation and experimentation of the impact of large woody debris and wrack on the degree of scarping would be very useful in determining the impact of these factors.
5. Determining to what extent scarping and its controls will be affected by climate change conditions. For example, how will dune vegetation respond to warmer temperatures, and will species change occur as the climate changes thereby potentially increasing or decreasing dune resilience? How will this affect scarping and the likelihood of scarping triggering blowout/parabolic formation or entire dune system change?

6.2.2 Chapters 3, 4 and 5 - Salmon Hole Beach Dynamics

There are opportunities to further investigate the erosion at Salmon Hole. The study has also indicated that further work needs to be done on the effect climate change will have on dune systems. The following future research is suggested:

1. To better understand the dynamics of the coastal processes in the bay/lagoon further experiments could be conducted to examine waves, currents and transverse dune migration and sediment transport dynamics. This will allow actual wave height data to be compared to real time current and tide data and dune movement giving a much more complete understanding of the erosional processes in the bay.
2. Further, study into incident wave direction, the morphology of the reef and wave refraction over it is needed to further our understanding of the role the reef on wave processes in the bay, and the origin of the lagoon unidirectional current.
3. The dynamics of the Salmon Hole embayment – lagoon system could be analysed using numerical modelling. This would also aid in better understanding the processes

involved in the erosion as well as potentially answer the question of what initiated the erosion period.

4. To confirm that the subaqueous dunes are migrating and therefore playing a role in the overall erosion of the shoreline, weekly detailed bathymetric surveying of the bay/lagoon would be necessary to clearly monitor the dune movements.
5. Future studies into the effect sea level rise will have on sandy coastlines need to consider the role of sediment supply to the beach following an erosion event. Managing sandy coastlines into the future systems deemed to have a negative sediment budget need to take priority, and we need to better understand what level of sediment supply to a beach post-storm activity is required to allow a dune system to translate as opposed to disappear.

APPENDICES

Appendix 1

Appendix 1: DSAS statistical results for further investigation into significant periods of change for Salmon Hole.

Shoreline Group	NSM Av	NSM Max	EPR Av	EPR Max	EPR Stat Sig %	SCE Av	SCE Max	LRR Av	LRR CI	LRR Max	LRR Stat Sig %
Pre 1999	-67.3	-75.52	-1.25	-1.4	100	70.04	82.56	-1.09	0.31	-1.29	100
Post 1999	-33.87	-33.98	-1.8	-2.08	100	34.21	39.98	-1.3	0.44	-1.69	100
1999 - 2003	-13.82	-24.34	-3.49	-6.15	100	13.95	24.34	-3.41	4.03	-5.99	45.45
Post 2003	-20.05	-28.22	-1.33	-1.85	100	20.42	29.22	-1.03	0.47	-1.39	100
2003 - 2007	-2.95	-8.14, 1.23	-0.94	-2.6, 0.39	40.91e 0a	3.13	8.14	-0.86	21.34	-.2.44e 0.39a	0
1975 - 1999	-48.89	-74.75	-1.97	-3.02	100	49.09	76.43	-1.77	0.56	-3.05	100

Shoreline Group	NSM Av	NSM Max	EPR Av	EPR Max	EPR Stat Sig %	SCE Av	SCE Max	LRR Av	LRR CI	LRR Max	LRR Stat Sig %
1946 - 1975	-18.41	-36.21, 2.08	-0.63	-1.25, 0.07	86.36e 9.09a	21.28	36.21	-0.68	0.64	-1.19	100
1992 - 1999	-25.01	-48.09	-3.19	-6.14	100	25.24	48.09	-3.1	10.45	-6.3	18.18

*e = erosion, a = accretion. Also note where two maximum numbers are given both erosion and accretion occurred along the same shoreline for that period.

Appendix 2

Appendix 2: DSAS statistical results for further investigation into significant periods of change for Pleasant Cove.

Shoreline Group	NSM Av	NSM Max	EPR Av	EPR Max	EPR Stat Sig %	SCE Av	SCE Max	LRR Av	LRR CI	LRR Max	LRR Stat Sig %
N Pre 1999	17.01	22.36	0.32	0.42	100	24.85	31.84	0.2	0.24	0.26	11.11

Shoreline Group	NSM Av	NSM Max	EPR Av	EPR Max	EPR Stat Sig %	SCE Av	SCE Max	LRR Av	LRR CI	LRR Max	LRR Stat Sig %
N Post 1999	7.87	13.57	0.48	0.83	0e 88.89a	30.02	34.99	-0.5	1.08	-1.09, 0.3	88.89e 11.11a
N 1999 - 2003	23.96	29.46	6.06	7.45	100	30.02	34.99	6.79	11.64	7.89	0
N Post 2003	-16.09	-26.19, 1.84	-1.3	-2.12, 0.15	88.89e 0a	18.51	27.45	-0.91	0.87	-1.6, 0.15	55.56e 0a
N 2003 - 2007	-13.16	-18.94	-4.2	-6.04	88.89	13.16	18.94	-4.16	12.41	-5.96,	22.22%
N 1975 - 1999	24.75	31.84	1	1.29	100a	24.85	31.84	0.72	0.52	0.88	100
N 1946 - 1975	-7.74	-13.16	-0.27	-0.45	100	9.28	13.16	-0.27	0.42	-0.39	11.11

Shoreline Group	NSM Av	NSM Max	EPR Av	EPR Max	EPR Stat Sig %	SCE Av	SCE Max	LRR Av	LRR CI	LRR Max	LRR Stat Sig %
N 1999 - 2002	23.92	34.99	11.21	16.39	100	23.92	34.99	-	-	-	-
N 2007 - 2008	10.62	14.43	9.39	12.75	100	10.62	14.43	-	-	-	-
N Pre 2008	24.89	30.57	0.36	0.44	100	51.48	60.51	0.59	0.25	0.66	100
N Post 2008	-13.55	-19.7	-1.68	-2.44	100	14.11	21.87	-1.72	1.22	-2.64	100
N 1997 - 1999	12.64	15.01	4.49	5.33	100	12.64	15.01	-	-	-	-
N 2003 - 2005	-8.35	-13.29	-5.81	-9.25	77.78	8.35	13.29	-	-	-	-

Shoreline Group	NSM Av	NSM Max	EPR Av	EPR Max	EPR Stat Sig %	SCE Av	SCE Max	LRR Av	LRR CI	LRR Max	LRR Stat Sig %
N 2005 - 2008	5.81	9.52	2.05	3.36	100	10.62	14.43	1.67	42.46	2.94	0

*e = erosion, a = accretion. Also note where two maximum numbers are given both erosion and accretion occurred along the same shoreline for that period. Periods with less than three shorelines do not produce LRR statistics.

REFERENCES

Aagaard, T., B. Greenwood and M. Hughes (2013). "Sediment transport on dissipative, intermediate and reflective beaches." Earth-Science Reviews **124**: 32-50.

Aagaard, T., J. Nielsen, S. G. Jensen and J. Friderichsen (2004). "Longshore sediment transport and coastal erosion at Skallingen, Denmark." Geografisk Tidsskrift-Danish Journal of Geography **104**(1): 5-14.

Abernethy, B. and I. D. Rutherfurd (2001). "The distribution and strength of riparian tree roots in relation to riverbank reinforcement." Hydrological processes **15**(1): 63-79.

Allen, J. (1980). "Sand waves: a model of origin and internal structure." Sedimentary Geology **26**(4): 281-328.

Allen, J. L. (1968). Current Ripples. Their relation to patterns of water and sediment motion. . Amsterdam, North Holland Publishing Company.

Allison, I., R. Alley, H. Fricker, R. Thomas and R. Warner (2009). "Ice sheet mass balance and sea level." Antarctic Science **21**(5): 413-426.

Amos, C. and E. King (1984). "Bedforms of the Canadian eastern seaboard: a comparison with global occurrences." Marine geology **57**(1-4): 167-208.

Anders, F. J. and M. R. Byrnes (1991). "Accuracy of shoreline change rates as determined from maps and aerial photographs." Shore and beach **59**(1): 17-26.

Anderson, J. (2009). Morphodynamics of beach-dune systems laden with large woody debris: Haida Gwaii (Queen Charlotte Islands), British Columbia.

Araújo, A. D., E. J. Parteli, T. Pöschel, J. S. Andrade and H. J. Herrmann (2013). "Numerical modeling of the wind flow over a transverse dune." Scientific reports **3**(1): 1-9.

Arbogast, A. F., E. C. Hansen and M. D. Van Oort (2002). "Reconstructing the geomorphic evolution of large coastal dunes along the southeastern shore of Lake Michigan." Geomorphology **46**(3-4): 241-255.

Arens, S. (1996). "Patterns of sand transport on vegetated foredunes." Geomorphology **17**(4): 339-350.

Arens, S. (1997). "Transport rates and volume changes in a coastal foredune on a Dutch Wadden island." Journal of Coastal Conservation **3**(1): 49-56.

Arens, S., H. Van Kaam-Peters and J. Van Boxel (1995). "Air flow over foredunes and implications for sand transport." Earth Surface Processes and Landforms **20**(4): 315-332.

Arens, S., H. Van Kaam-Peters and J. v. Van Boxel (1995). "Air flow over foredunes and implications for sand transport." Earth Surface Processes and Landforms **20**(4): 315-332.

Arens, S. M. J., P.D., and Van der Meulen, F (2001). Coastal dunes. In: Warren, A. and French, J.R. (eds.), Habitat Conservation: Managing the Physical Environment. Chichester, United Kingdom, Wiley.

Arteaga, C., J. Juan de Sanjosé and E. Serrano (2008). "Terrestrial photogrammetric techniques applied to the control of a parabolic dune in the Liencres dune system, Cantabria (Spain)." Earth Surface Processes and Landforms **33**(14): 2201-2210.

Ashley, G. M. (1990). "Classification of large-scale subaqueous bedforms; a new look at an old problem." Journal of Sedimentary Research **60**(1): 160-172.

Baddock, M., I. Livingstone and G. F. Wiggs (2007). "The geomorphological significance of airflow patterns in transverse dune interdunes." Geomorphology **87**(4): 322-336.

Bagnold, R. A. (1941). "The physics of blown sand and desert dunes." London, Chapman and Hall 265 p.

Barboza, E., M. Rosa, P. Hesp, S. Dillenburg, L. Tomazelli and R. Ayup-Zouain (2011). "Evolution of the Holocene Coastal Barrier of Pelotas Basin (Southern Brazil)-a new approach with GPR data." Journal of coastal research **64**: 646-650.

Bartholdy, J., B. Flemming, A. Bartholomä and V. Ernstsen (2005). "Flow and grain size control of depth-independent simple subaqueous dunes." Journal of Geophysical Research: Earth Surface **110**(F4).

Bate, G. and M. Ferguson (1996). "Blowouts in coastal foredunes." Landscape and Urban Planning **34**(3-4): 215-224.

Bateman, M. D., G. Rushby, S. Stein, R. A. Ashurst, D. Stevenson, J. M. Jones and W. R. Gehrels (2018). "Can sand dunes be used to study historic storm events?" Earth Surface Processes and Landforms **43**(4): 779-790.

Bauer, B., R. Davidson-Arnott, P. Hesp, S. Namikas, J. Ollerhead and I. Walker (2009). "Aeolian sediment transport on a beach: Surface moisture, wind fetch, and mean transport." Geomorphology **105**(1-2): 106-116.

Bauer, B. O., R. G. Davidson-Arnott, I. J. Walker, P. A. Hesp and J. Ollerhead (2012). "Wind direction and complex sediment transport response across a beach–dune system." Earth Surface Processes and Landforms **37**(15): 1661-1677.

Bauer, B. O. and D. J. Sherman (1999). "Coastal dune dynamics: problems and prospects." Aeolian environments, sediments and landforms, Chichester: Wiley: 71-104.

Bens, A., C. Olariu and R. Steel (2010). Architecture of Deposits Formed in a Tectonically Generated Tidal Strait, Eocene Ager Basin, South Central Pyrenees, Spain. AGU Fall Meeting Abstracts.

Bheeroo, R. A., N. Chandrasekar, S. Kaliraj and N. Magesh (2016). "Shoreline change rate and erosion risk assessment along the Trou Aux Biches–Mont Choisy beach on the northwest coast of Mauritius using GIS-DSAS technique." Environmental Earth Sciences **75**(5): 444.

Billy, J., E. Chaumillon, H. Féniès and C. Poirier (2012). "Tidal and fluvial controls on the morphological evolution of a lobate estuarine tidal bar: The Plassac Tidal Bar in the Gironde Estuary (France)." Geomorphology **169**: 86-97.

Bird, E. C. (1976). Coasts: and Introduction to Coastal Geomorphology Canberra : Australian, National University Press.

Bird, E. C. (2000). Coastal geomorphology: an introduction, John Wiley & Sons.

Boak, E. H. and I. L. Turner (2005). "Shoreline definition and detection: a review." Journal of Coastal Research **21**(4): 688.

Bokuniewicz, H., R. Gordon and K. Kastens (1977). "From and migration of sand waves in a large estuary, Long Island Sound." Marine geology **24**(3): 185-199.

Boothroyd, J. C. and G. M. Ashley (1975). "Processes, bar morphology, and sedimentary structures on braided outwash fans, northeastern Gulf of Alaska."

Bouma, T. J., M. Friedrichs, B. Van Wesenbeeck, S. Temmerman, G. Graf and P. Herman (2009). "Density-dependent linkage of scale-dependent feedbacks: A flume study on the intertidal macrophyte Spartina anglica." Oikos **118**(2): 260-268.

Bowen, A. and D. Lindley (1977). "A wind-tunnel investigation of the wind speed and turbulence characteristics close to the ground over various escarpment shapes." Boundary-Layer Meteorology **12**(3): 259-271.

Bracken, L. J. and J. Wainwright (2006). "Geomorphological equilibrium: myth and metaphor?" Transactions of the Institute of British Geographers **31**(2): 167-178.

Bradley, E. F. (1983). "The influence of thermal stability and angle of incidence on the acceleration of wind up a slope." Journal of Wind Engineering and Industrial Aerodynamics **15**(1-3): 231-242.

Bradley, R. W. and J. G. Venditti (2017). "Reevaluating dune scaling relations." Earth-Science Reviews **165**: 356-376.

Brander, R. W., P. S. Kench and D. Hart (2004). "Spatial and temporal variations in wave characteristics across a reef platform, Warraber Island, Torres Strait, Australia." Marine geology **207**(1-4): 169-184.

Brodie, K. L. and J. E. McNinch (2011). Beach change during a nor'easter: relationships to wave steepness and inner surf zone dissipation. The Proceedings of the Coastal Sediments 2011: In 3 Volumes, World Scientific**:** 1360-1374.

Bruun, P. (1988). "The Bruun rule of erosion by sea-level rise: a discussion on large-scale two-and three-dimensional usages." Journal of coastal research: 627-648.

Bryant, D. B., M. A. Bryant, J. A. Sharp, G. L. Bell and C. Moore (2019). "The response of vegetated dunes to wave attack." Coastal Engineering.

Burkinshaw, J. R., W. K. Illenberger and I. C. Rust (1993). "Wind-speed profiles over a reversing transverse dune." Geological Society, London, Special Publications **72**(1): 25-36.

Buynevich, I. and J. Donnelly (2006). "Geological signatures of barrier breaching and overwash, southern Massachusetts, USA." Journal of coastal research: 112-116.

Cardona, L. and M. García (2008). "Beach-cast seagrass material fertilizes the foredune vegetation of Mediterranean coastal dunes." Acta Oecologica **34**(1): 97-103.

Carey, W. C. and M. D. Keller (1957). "Systematic changes in the beds of alluvial rivers." Journal of the Hydraulics Division **83**(4): 1331-1331-1331-1324.

Carter, R. (1980). "Vegetation stabilisation and slope failure of eroding sand dunes." Biological Conservation **18**(2): 117-122.

Carter, R. (1991). "Near-future sea level impacts on coastal dune landscapes." Landscape Ecology **6**(1-2): 29-39.

Carter, R., P. A. Hesp and K. F. Nordstrom (1990). Erosional landforms in coastal dunes. Coastal dunes: form and process, Wiley London**:** 217-249.

Carter, R. and P. Wilson (1990). "The geomorphological, ecological and pedological development of coastal foredunes at Magilligan Point, Northern Ireland." Coastal dunes. Form and processes. John Wiley & Sons, Chichester: 129-157.

Carter, R. W. G. (1988). Coastal environments: an introduction to the physical, ecological, and cultural systems of coastlines, Elsevier.

Casella, E., A. Collin, D. Harris, S. Ferse, S. Bejarano, V. Parravicini, J. L. Hench and A. Rovere (2017). "Mapping coral reefs using consumer-grade drones and structure from motion photogrammetry techniques." Coral Reefs **36**(1): 269-275.

Castelle, B., S. Bujan, S. Ferreira and G. Dodet (2017). "Foredune morphological changes and beach recovery from the extreme 2013/2014 winter at a high-energy sandy coast." Marine geology **385**: 41-55.

Castelle, B. and G. Coco (2012). "The morphodynamics of rip channels on embayed beaches." Continental Shelf Research **43**: 10-23.

Castelle, B. and G. Coco (2013). "Surf zone flushing on embayed beaches." Geophysical Research Letters **40**(10): 2206-2210.

Castelle, B., B. Guillot, V. Marieu, E. Chaumillon, V. Hanquiez, S. Bujan and C. Poppeschi (2018). "Spatial and temporal patterns of shoreline change of a 280-km high-energy disrupted sandy coast from 1950 to 2014: SW France." Estuarine, Coastal and Shelf Science **200**: 212-223.

Castelle, B., V. Marieu, S. Bujan, K. D. Splinter, A. Robinet, N. Sénéchal and S. Ferreira (2015). "Impact of the winter 2013–2014 series of severe Western Europe storms on a double-barred sandy coast: Beach and dune erosion and megacusp embayments." Geomorphology **238**: 135-148.

Castelle, B., T. Scott, R. Brander and R. McCarroll (2016). "Rip current types, circulation and hazard." Earth-Science Reviews **163**: 1-21.

Caston, G. (1981). "Potential gain and loss of sand by some sand banks in the Southern Bight of the North Sea." Marine geology **41**(3-4): 239-250.

Charbonneau, B. R., L. S. Wootton, J. P. Wnek, J. A. Langley and M. A. Posner (2017). "A species effect on storm erosion: Invasive sedge stabilized dunes more than native grass during Hurricane Sandy." Journal of Applied Ecology **54**(5): 1385-1394.

Christiansen, M. B. and R. Davidson-Arnott (2004). "Rates of landward sand transport over the foredune at Skallingen, Denmark and the role of dune ramps." Geografisk Tidsskrift-Danish Journal of Geography **104**(1): 31-43.

Church, J. A., P. U. Clark, A. Cazenave, J. M. Gregory, S. Jevrejeva, A. Levermann, M. A. Merrifield, G. A. Milne, R. S. Nerem and P. D. Nunn (2013). "Sea-level rise by 2100." Science **342**(6165): 1445-1445.

Clemmensen, L. B., A. Murray, J. Heinemeier and R. de Jong (2009). "The evolution of Holocene coastal dunefields, Jutland, Denmark: A record of climate change over the past 5000 years." Geomorphology **105**(3-4): 303-313.

Coco, G., N. Senechal, A. Rejas, K. R. Bryan, S. Capo, J. Parisot, J. A. Brown and J. H. MacMahan (2014). "Beach response to a sequence of extreme storms." Geomorphology **204**: 493-501.

Coelho, C., R. Silva, F. Veloso-Gomes and F. Taveira-Pinto (2009). "Potential effects of climate change on northwest Portuguese coastal zones." ICES Journal of Marine Science **66**(7): 1497-1507.

Cohn, N., B. M. Hoonhout, E. B. Goldstein, S. De Vries, L. J. Moore, O. Durán Vinent and P. Ruggiero (2019). "Exploring marine and aeolian controls on coastal foredune growth using a coupled numerical model." Journal of Marine Science and Engineering **7**(1): 13.

Coleman, J. M. (1969). "Brahmaputra River: channel processes and sedimentation." Sedimentary Geology **3**(2-3): 129-239.

Coleman, S. and V. Nikora (2011). "Fluvial dunes: initiation, characterization, flow structure." Earth Surface Processes and Landforms **36**(1): 39-57.

Collinson, J. D. (1970). "Bedforms of the Tana river, Norway." Geografiska Annaler: Series A, Physical Geography **52**(1): 31-56.

Cowell, P., P. Roy and R. Jones (1992). "Shoreface translation model: computer simulation of coastal-sand-body response to sea level rise." Mathematics and computers in simulation **33**(5-6): 603-608.

Cowell, P., P. Roy and R. Jones (1995). "Simulation of large-scale coastal change using a morphological behaviour model." Marine geology **126**(1-4): 45-61.

Crowell, M., B. C. Douglas and S. P. Leatherman (1997). "On forecasting future US shoreline positions: a test of algorithms." Journal of Coastal Research: 1245-1255.

Crowley, K. (1983). "Large-scale bed configurations (macroforms), Platte River Basin, Colorado and Nebraska: primary structures and formative processes." Geological Society of America Bulletin **94**(1): 117-133.

da Silva, R. P., L. J. Calliari and H. A. de Morais Tozzi (2003). "The influence of washouts on the erosive susceptibility of the Rio Grande do Sul coast between Cassino and Chuí beaches, Southern Brazil." Journal of coastal research: 332-338.

Dalrymple, R. W., D. A. Mackay, A. A. Ichaso and K. S. Choi (2012). Processes, morphodynamics, and facies of tide-dominated estuaries. Principles of tidal sedimentology, Springer**:** 79-107.

Davidson-Arnott, R. (2010). Introduction to coastal processes and geomorphology, Cambridge University Press.

Davidson-Arnott, R. G. (2005). "Conceptual model of the effects of sea level rise on sandy coasts." Journal of coastal research: 1166-1172.

Davidson-Arnott, R., P. Hesp, J. Ollerhead, I. Walker, B. Bauer, I. Delgado-Fernandez and T. Smyth (2018). "Sediment budget controls on foredune height: Comparing simulation model results with field data." Earth Surface Processes and Landforms **43**(9): 1798-1810.

Davidson-Arnott, R., P. Hesp, J. Ollerhead, I. Walker, B. Bauer, I. Delgado-Fernandez and T. Smyth (2018). "Sediment budget controls on foredune height: Comparing simulation model results with field data." Earth Surface Processes and Landforms.

Davidson, S. G., P. Hesp and G. M. da Silva (2021). "Rapid Shoreline and Dunefield Change, Salmon Hole, South Australia." Science of The Total Environment: 145406.

Davidson, S. G., P. A. Hesp and G. M. da Silva (2020). "Controls on dune scarping." Progress in Physical Geography: Earth and Environment: 0309133320932880.

Davis Jr, R. A. and D. M. FitzGerald (2004). Beaches and coasts, John Wiley & Sons.

De Battisti, D. and J. N. Griffin (2020). "Below-ground biomass of plants, with a key contribution of buried shoots, increases foredune resistance to wave swash." Annals of botany.

De Winter, R., F. Gongriep and B. Ruessink (2015). "Observations and modeling of alongshore variability in dune erosion at Egmond aan Zee, the Netherlands." Coastal Engineering **99**: 167-175.

De Winter, R. and B. Ruessink (2017). "Sensitivity analysis of climate change impacts on dune erosion: case study for the Dutch Holland coast." Climatic Change **141**(4): 685-701.

de Winter, W., J. Donker, G. Sterk, J. Van Beem and G. Ruessink (2020). "Regional versus local wind speed and direction at a narrow beach with a high and steep foredune." PloS one **15**(1): e0226983.

Dean, R. G., R. Chen and A. E. Browder (1997). "Full scale monitoring study of a submerged breakwater, Palm Beach, Florida, USA." Coastal Engineering **29**(3-4): 291-315.

Dillenburg, S. R. and P. A. Hesp (2009). Coastal barriers–an introduction. Geology and geomorphology of holocene coastal barriers of brazil, Springer**:** 1-15.

Dolan, R., M. S. Fenster and S. J. Holme (1991). "Temporal analysis of shoreline recession and accretion." Journal of Coastal Research: 723-744.

Dolan, R. and B. Hayden (1981). "Storms and shoreline configuration." Journal of Sedimentary Research **51**(3): 737-744.

Donnelly, C., N. Kraus and M. Larson (2006). "State of knowledge on measurement and modeling of coastal overwash." Journal of coastal research: 965-991.

Doody, J. P. (2012). Sand dune conservation, management and restoration, Springer Science & Business Media.

Douglas, B. C. and M. Crowell (2000). "Long-term shoreline position prediction and error propagation." Journal of coastal research: 145-152.

Durán, O., E. J. Parteli and H. J. Herrmann (2010). "A continuous model for sand dunes: Review, new developments and application to barchan dunes and barchan dune fields." Earth Surface Processes and Landforms **35**(13): 1591-1600.

Eamer, J. B. and I. J. Walker (2010). "Quantifying sand storage capacity of large woody debris on beaches using LiDAR." Geomorphology **118**(1-2): 33-47.

Edelman, T. (1969). Dune erosion during storm conditions. Coastal Engineering 1968**:** 719-722.

Eliot, I. and D. Clarke (1989). "Temporal and spatial bias in the estimation of shoreline rate-of-change statistics from beach survey information." Coastal Management **17**(2): 129-156.

Emeis, S., H. P. Frank and F. Fiedler (1995). "Modification of air flow over an escarpment—Results from the Hjardemål experiment." Boundary-Layer Meteorology **74**(1): 131-161.

Ernstsen, V. B., R. Noormets, C. Winter, D. Hebbeln, A. Bartholomä, B. W. Flemming and J. Bartholdy (2005). "Development of subaqueous barchanoid-shaped dunes due to lateral grain size variability in a tidal inlet channel of the Danish Wadden Sea." Journal of Geophysical Research: Earth Surface **110**(F4).

Everard, M., L. Jones and B. Watts (2010). "Have we neglected the societal importance of sand dunes? An ecosystem services perspective." Aquatic Conservation: Marine and Freshwater Ecosystems **20**(4): 476-487.

Feagin, R. A., J. Figlus, J. C. Zinnert, J. Sigren, M. L. Martínez, R. Silva, W. K. Smith, D. Cox, D. R. Young and G. Carter (2015). "Going with the flow or against the grain? The promise of vegetation for protecting beaches, dunes, and barrier islands from erosion." Frontiers in Ecology and the Environment **13**(4): 203-210.

Fearnley, S. M., M. D. Miner, M. Kulp, C. Bohling and S. Penland (2009). "Hurricane impact and recovery shoreline change analysis of the Chandeleur Islands, Louisiana, USA: 1855 to 2005." Geo-Marine Letters **29**(6): 455-466.

Ferentinos, G. and M. Collins (1980). "Effects of shoreline irregularities on a rectilinear tidal current and their significance in sedimentation processes." Journal of Sedimentary Research **50**(4): 1081-1094.

Fernández-Montblanc, T., E. Duo and P. Ciavola (2020). "Dune reconstruction and revegetation as a potential measure to decrease coastal erosion and flooding under extreme storm conditions." Ocean & coastal management: 105075.

Figlus, J., N. Kobayashi, C. Gralher and V. Iranzo (2010). "Wave overtopping and overwash of dunes." Journal of Waterway, Port, Coastal, and Ocean Engineering **137**(1): 26-33.

Figueiredo, S. d. and L. Calliari (2006). "Washouts in the central and northern littoral of Rio Grande do Sul state, Brazil: distribution and implications." Journal of Coastal Research, SI **39**: 366-370.

Finnigan, J. (1988). "Air flow over complex terrain." Flow and transport in the natural environment: Advances and applications: 183-229.

Finnigan, J., M. Raupach, E. F. Bradley and G. Aldis (1990). "A wind tunnel study of turbulent flow over a two-dimensional ridge." Boundary-Layer Meteorology **50**(1): 277-317.

Fisher, J. S., S. P. Leatherman and F. C. Perry (1975). Overwash processes on assateague island. Coastal Engineering 1974**:** 1194-1212.

Flemming, B. (1980). "Sand transport and bedform patterns on the continental shelf between Durban and Port Elizabeth (southeast African continental margin)." Sedimentary Geology **26**(1-3): 179-205.

Flemming, B. (2000). The role of grain size, water depth and flow velocity as scaling factors controlling the size of subaqueous dunes. Marine sandwave dynamics, international workshop.

Flemming, B. W. and A. Bartholomä (2012). "Temporal variability, migration rates and preservation potential of subaqueous dune fields generated in the Agulhas Current on the southeast African continental shelf." Sediments, Morphology and Sedimentary Processes on Continental Shelves: Advances in Technologies, Research, and Applications: 229-247.

Fotheringham, D. (2009). "Shoreline Erosion at Port Office Rock Near Beachport, South Australia." Coastal Management Branch, Department for Environment and Heritage South Australia, Technical Report **9**.

Francken, F., S. Wartel, R. Parker and E. Taverniers (2004). "Factors influencing subaqueous dunes in the Scheldt Estuary." Geo-Marine Letters **24**(1): 14-21.

Fraser, G. S., S. W. Bennett, G. A. Olyphant, N. J. Bauch, V. Ferguson, C. A. Gellasch, C. L. Millard, B. Mueller, P. J. O'Malley and J. N. Way (1998). "Windflow circulation patterns in a coastal dune blowout, south coast of Lake Michigan." Journal of coastal research: 451-460.

Fuller, J. A. (2002). "Bank recession and lakebed downcutting; response to changing water levels at Maumee Bay State Park, Ohio." Journal of Great Lakes Research **28**(3): 352-361.

Gallop, S. L., K. R. Bryan, G. Coco and S. Stephens (2011). "Storm-driven changes in rip channel patterns on an embayed beach." Geomorphology **127**(3-4): 179-188.

Gallop, S. L., D. M. Kennedy, C. Loureiro, L. A. Naylor, J. J. Muñoz-Pérez, D. W. Jackson and T. E. Fellowes (2020). "Geologically controlled sandy beaches: Their geomorphology, morphodynamics and classification." Science of The Total Environment: 139123.

Gares, P. A. and K. F. Nordstrom (1995). "A cyclic model of foredune blowout evolution for a leeward coast: Island Beach, New Jersey." Annals of the Association of American Geographers **85**(1): 1-20.

Genz, A. S., C. H. Fletcher, R. A. Dunn, L. N. Frazer and J. J. Rooney (2007). "The predictive accuracy of shoreline change rate methods and alongshore beach variation on Maui, Hawaii." Journal of Coastal Research: 87-105.

Giles, P. and S. McCann (1997). "Foredune development on îles de la Madeleine (Québec), Atlantic Canada." Canadian Journal of Earth Sciences **34**(11): 1467-1476.

Girardi, J. D. and D. M. Davis (2010). "Parabolic dune reactivation and migration at Napeague, NY, USA: Insights from aerial and GPR imagery." Geomorphology **114**(4): 530-541.

Gong, W. and A. Ibbetson (1989). "A wind tunnel study of turbulent flow over model hills." Boundary-Layer Meteorology **49**(1): 113-148.

Goodbred, S. L. and Y. Saito (2012). Tide-dominated deltas. Principles of tidal sedimentology, Springer**:** 129-149.

Gretener, P. E. (1979). "Pore pressure: fundamentals, general ramifications and implications for structural geology (revised edition)."

Grilliot, M., I. Walker and B. Bauer (2019). "The role of large woody debris in beach-dune interaction." Journal of Geophysical Research: Earth Surface.

Grilliot, M. J., I. J. Walker and B. O. Bauer (2018). "Airflow dynamics over a beach and foredune system with large woody debris." Geosciences **8**(5): 147.

Grilliot, M. J., I. J. Walker and B. O. Bauer (2019). "Aeolian sand transport and deposition patterns within a large woody debris matrix fronting a foredune." Geomorphology **338**: 1-15.

Guisado-Pintado, E. and D. W. Jackson (2018). "Multi-scale variability of storm Ophelia 2017: The importance of synchronised environmental variables in coastal impact." Science of The Total Environment **630**: 287-301.

Guisado-Pintado, E. and D. W. Jackson (2019). "Coastal impact from high-energy events and the importance of concurrent forcing parameters: the cases of Storm Ophelia (2017) and Storm Hector (2018) in NW Ireland." Frontiers in Earth Science **7**: 1-18.

Gustavson, T. C. (1978). "Bed forms and stratification types of modern gravel meander lobes, Nueces River, Texas." Sedimentology **25**(3): 401-426.

Hacker, S. D., P. Zarnetske, E. Seabloom, P. Ruggiero, J. Mull, S. Gerrity and C. Jones (2012). "Subtle differences in two non-native congeneric beach grasses significantly affect their colonization, spread, and impact." Oikos **121**(1): 138-148.

Hanley, M., S. Hoggart, D. Simmonds, A. Bichot, M. Colangelo, F. Bozzeda, H. Heurtefeux, B. Ondiviela, R. Ostrowski and M. Recio (2014). "Shifting sands? Coastal protection by sand banks, beaches and dunes." Coastal Engineering **87**: 136-146.

Hansen, E., S. DeVries-Zimmerman, D. van Dijk and B. Yurk (2009). "Patterns of wind flow and aeolian deposition on a parabolic dune on the southeastern shore of Lake Michigan." Geomorphology **105**(1-2): 147-157.

Hanson, B. A. and C. Seeger (2015). "Georeferencing a Raster Dataset."

Harms, J. and R. Fahnestock (1965). "Stratification, bedforms, and flow phenomena (with an example from the Rio Grande): Society of Economic Paleontologists and Mineralogists Special Publication 12."

Harms, J. C., S. JB and W. RG (1982). "Structures and sequences in clastic rocks."

Harris, P., G. Ashley, M. Collins and A. James (1986). "Topographic features of the Bristol Channel sea-bed: a comparison of SEASAT (synthetic aperture radar) and side-scan sonar images." International Journal of Remote Sensing **7**(1): 119-136.

Harris, P. and M. Collins (1984). "Bedform distributions and sediment transport paths in the Bristol Channel and Severn Estuary, UK." Marine geology **62**(1-2): 153-166.

Heathfield, D. K. and I. J. Walker (2011). "Analysis of coastal dune dynamics, shoreline position, and large woody debris at Wickaninnish Bay, Pacific Rim National Park, British Columbia." Canadian Journal of Earth Sciences **48**(7): 1185-1198.

Hemer, M., K. McInnes and R. Ranasinghe (2013). "Projections of climate change-driven variations in the offshore wave climate off south eastern Australia." International Journal of Climatology **33**(7): 1615-1632.

Hersen, P. (2004). "On the crescentic shape of barchan dunes." The European Physical Journal B-Condensed Matter and Complex Systems **37**(4): 507-514.

Hesp, P. (1988). "Morphology, dynamics and internal stratification of some established foredunes in southeast Australia." Sedimentary Geology **55**(1-2): 17-41.

Hesp, P. (1988). "Surfzone, beach, and foredune interactions on the Australian South East Coast." Journal of coastal research: 15-25.

Hesp, P. (2000). "Coastal sand dunes: form and function. Coastal Dune Vegetation Network." Forest Research, Rotorua.

Hesp, P. (2002). "Foredunes and blowouts: initiation, geomorphology and dynamics." Geomorphology **48**(1-3): 245-268.

Hesp, P. (2012). "Surfzone-beach-dune interactions."

Hesp, P., R. Keane, D. Fotheringham and S. Davidson (2018). Current Status and Management Options for Salmon Hole/Post Office Rock Beach Flinders University, Adelaide, SA

Hesp, P. and T. Smyth (2019). "Dunes created by vegetation and topography. ." In: I. Livingstone and A. Warren (Eds.), Aeolian Geomorphology: a New Introduction.

Hesp, P., I. Walker, S. Namikas, R. Davidson-Arnott, B. Bauer and J. Ollerhead (2009). "Storm wind flow over a foredune, Prince Edward Island, Canada." Journal of coastal research: 312-316.

Hesp, P. A. (2013). "Conceptual models of the evolution of transgressive dune field systems." Geomorphology **199**: 138-149.

Hesp, P. A., R. Davidson-Arnott, I. J. Walker and J. Ollerhead (2005). "Flow dynamics over a foredune at Prince Edward Island, Canada." Geomorphology **65**(1-2): 71-84.

Hesp, P. A., Y. Dong, H. Cheng and J. L. Booth (2019). "Wind flow and sedimentation in artificial vegetation: Field and wind tunnel experiments." Geomorphology.

Hesp, P. A. and R. Hyde (1996). "Flow dynamics and geomorphology of a trough blowout." Sedimentology **43**(3): 505-525.

Hesp, P. A. and T. A. Smyth (2016). "Jet flow over foredunes." Earth Surface Processes and Landforms **41**(12): 1727-1735.

Hesp, P. A. and T. A. Smyth (2019). "CFD flow dynamics over model scarps and slopes." Physical Geography: 1-24.

Hesp, P. A., T. A. Smyth, P. Nielsen, I. J. Walker, B. O. Bauer and R. Davidson-Arnott (2015). "Flow deflection over a foredune." Geomorphology **230**: 64-74.

Hesp, P. A. and B. G. Thom (1990). "Geomorphology and evolution of active transgressive dunefields." Coastal dunes: form and process **253**: 88.

Hesp, P. A., I. J. Walker, C. Chapman, R. Davidson-Arnott and B. O. Bauer (2013). "Aeolian dynamics over a coastal foredune, Prince Edward Island, Canada." Earth Surface Processes and Landforms **38**(13): 1566-1575.

Hilton, M. J., S. V. Hatcher, S. J. Wakes and T. M. Konlechner (2016). "Flow deflection and deceleration across a simple foredune." Journal of coastal research(75): 293-297.

Himmelstoss, E. A., R. E. Henderson, M. G. Kratzmann and A. S. Farris (2018). Digital Shoreline Analysis System (DSAS) version 5.0 user guide. Open-File Report. Reston, VA.

Holloway, P. (1996). "A field investigation of water exchange between a small coastal embayment and an adjacent shelf." Coastal and Estuarine Studies: 145-158.

Horta, J., S. Oliveira, D. Moura and Ó. Ferreira (2018). "Nearshore hydrodynamics at pocket beaches with contrasting wave exposure in southern Portugal." Estuarine, Coastal and Shelf Science **204**: 40-55.

Houser, C. (2013). "Alongshore variation in the morphology of coastal dunes: Implications for storm response." Geomorphology **199**: 48-61.

Houser, C., C. Hapke and S. Hamilton (2008). "Controls on coastal dune morphology, shoreline erosion and barrier island response to extreme storms." Geomorphology **100**(3-4): 223-240.

Houser, C. and S. Mathew (2011). "Variability in foredune height depends on the alongshore correspondence of transport potential and sediment supply." Geomorphology **125**(1): 62-72.

Houser, C., P. Wernette, E. Rentschlar, H. Jones, B. Hammond and S. Trimble (2015). "Post-storm beach and dune recovery: Implications for barrier island resilience." Geomorphology **234**: 54-63.

Houser, C., P. Wernette and B. A. Weymer (2018). "Scale-dependent behavior of the foredune: Implications for barrier island response to storms and sea-level rise." Geomorphology **303**: 362-374.

Hsu, S.-A. (1977). Boundary-layer meteorological research in the coastal zone, Louisiana State University.

Innocenti, R. A., R. A. Feagin and T. P. Huff (2018). "The role of Sargassum macroalgal wrack in reducing coastal erosion." Estuarine, Coastal and Shelf Science **214**: 82-88.

IPCC (2014). Climate Change 2014: Synthesis Report. Contribution of Working Groups I, II and III to the Fifth Assessment Report of the Intergovernmental Panel on Climate Change [Core Writing Team, R.K. Pachauri and L.A. Meyer (eds.)]. IPCC, Geneva, Switzerland,**:** 151pp.

Ireland, H. (1959). "Silica in sediments: Soc." Econ. Paleontologists and Mineralogists, Spec. publ(7).

Jackson, D., J. Beyers, K. Lynch, J. Cooper, A. Baas and I. Delgado-Fernandez (2011). "Investigation of three-dimensional wind flow behaviour over coastal dune morphology under offshore winds using computational fluid dynamics (CFD) and ultrasonic anemometry." Earth Surface Processes and Landforms **36**(8): 1113-1124.

Jackson, D. W., A. Cooper, A. Green, M. Beyers, E. Guisado-Pintado, E. Wiles, K. Benallack and M. Balme (2020). "Reversing transverse dunes: Modelling of airflow switching using 3D computational fluid dynamics." Earth and Planetary Science Letters **544**: 116363.

Jackson, D. W., S. Costas and E. Guisado-Pintado (2019). "Large-scale transgressive coastal dune behaviour in Europe during the Little Ice Age." Global and Planetary Change **175**: 82-91.

Jackson, N. L. and K. F. Nordstrom (2018). "Aeolian sediment transport on a recovering storm-eroded foredune with sand fences." Earth Surface Processes and Landforms **43**(6): 1310-1320.

Jackson, P. and J. Hunt (1975). "Turbulent wind flow over a low hill." Quarterly Journal of the Royal Meteorological Society **101**(430): 929-955.

James, N., Y. Bone, M. Joury, I. Malcolm and T. K. Kyser (2018). "Diagenesis and compositional partitioning of quaternary cool-water carbonate aeolianites: southeastern Australia." Journal of Sedimentary Research **88**(4): 431-448.

Jarmalavicius, D., J. Satkunas, G. Zilinskas and D. Pupienis (2012). "The influence of coastal morphology on wind dynamics." Estonian Journal of Earth Sciences **61**(2): 120.

Jensen, N. O. and E. W. Peterson (1978). "On the escarpment wind profile." Quarterly Journal of the Royal Meteorological Society **104**(441): 719-728.

Johns, B., T. Chesher and R. Soulsby (1990). "The modelling of sandwave evolution resulting from suspended and bed load transport of sediment." Journal of Hydraulic Research **28**(3): 355-374.

Jones, N., J. M. Kain and A. Stride (1965). "The movement of sand waves on Warts Bank, Isle of Man." Marine geology **3**(5): 329-336.

Kennedy, D. and C. Woodroffe (2002). "Fringing reef growth and morphology: a review." Earth-Science Reviews **57**(3-4): 255-277.

Kennedy, D. M. (2003). "Surface lagoonal sediments on Lord Howe Island, Tasman Sea." Journal of coastal research: 57-63.

Kennedy, D. M. and J. L. Woods (2012). "The influence of coarse woody debris on gravel beach geomorphology." Geomorphology **159**: 106-115.

Kennedy, J. (1969). "The Formation of Sediment Ripples, Dunes, and Antidunes." Annual Review of Fluid Mechanics **1**(1): 147-168.

Kobayashi, N., C. Gralher and K. Do (2013). "Effects of woody plants on dune erosion and overwash." Journal of Waterway, Port, Coastal, and Ocean Engineering **139**(6): 466-472.

Kocurek, G., M. Townsley, E. Yeh, K. Havholm and M. Sweet (1992). "Dune and dune-field development on Padre Island, Texas, with implications for interdune deposition and water-table-controlled accumulation." Journal of Sedimentary Research **62**(4): 622-635.

Konlechner, T. M., E. E. Buckley, M. J. Hilton and S. J. Wakes (2016). "Downwind dune dynamics following Ammophila arenaria invasion." Journal of coastal research **75**(sp1): 298-302.

Kostaschuk, R., M. Church and J. Luternauer (1989). "Bedforms, bed material, and bedload transport in a salt-wedge estuary: Fraser River, British Columbia." Canadian Journal of Earth Sciences **26**(7): 1440-1452.

Kostaschuk, R. and P. Villard (1996). "Flow and sediment transport over large subaqueous dunes: Fraser River, Canada." Sedimentology **43**(5): 849-863.

Kroy, K., S. Fischer and B. Obermayer (2005). "The shape of barchan dunes." Journal of Physics: Condensed Matter **17**(14): S1229.

Lancaster, N. (1985). "Variations in wind velocity and sand transport on the windward flanks of desert sand dunes." Sedimentology **32**(4): 581-593.

Lancaster, N. (1988). "The development of large aeolian bedforms." Sedimentary Geology **55**(1-2): 69-89.

Lancaster, N. (1995). Geomorphology of desert dunes, Psychology Press.

Lancaster, N., W. Nickling, C. M. Neuman and V. Wyatt (1996). "Sediment flux and airflow on the stoss slope of a barchan dune." Geomorphology **17**(1-3): 55-62.

Langhorne, D. (1982). "A study of the dynamics of a marine sandwave." Sedimentology **29**(4): 571-594.

Lapetina, A. and Y. P. Sheng (2014). "Three-dimensional modeling of storm surge and inundation including the effects of coastal vegetation." Estuaries and coasts **37**(4): 1028-1040.

Largeau, J. and V. Moriniere (2007). "Wall pressure fluctuations and topology in separated flows over a forward-facing step." Experiments in Fluids **42**(1): 21-40.

Le Cozannet, G., C. Oliveros, B. Castelle, M. Garcin, D. Idier, R. Pedreros and J. Rohmer (2016). "Uncertainties in sandy shorelines evolution under the Bruun rule assumption." Frontiers in Marine Science **3**: 49.

Leatherman, S. (1979). "Beach and dune interactions during storm conditions." Quarterly Journal of Engineering Geology and Hydrogeology **12**(4): 281-290.

Leatherman, S. P. and R. E. Zaremba (1987). "Overwash and aeolian processes on a US northeast coast barrier." Sedimentary Geology **52**(3-4): 183-206.

Lee, J. H., A. Sousa, E. Parteli and H. Herrmann (2005). "Modelling formation and evolution of transverse dune fields." International Journal of Modern Physics C **16**(12): 1879-1892.

Long, J. T. and R. P. Sharp (1964). "Barchan-dune movement in imperial valley, California." Geological Society of America Bulletin **75**(2): 149-156.

Lowe, R. J., J. L. Falter, S. G. Monismith and M. J. Atkinson (2009). "Wave-driven circulation of a coastal reef–lagoon system." Journal of Physical Oceanography **39**(4): 873-893.

Lowe, R. J., C. Hart and C. B. Pattiaratchi (2010). "Morphological constraints to wave-driven circulation in coastal reef-lagoon systems: A numerical study." Journal of Geophysical Research: Oceans **115**(C9).

Luijendijk, A., G. Hagenaars, R. Ranasinghe, F. Baart, G. Donchyts and S. Aarninkhof (2018). "The state of the world's beaches." Scientific reports **8**(1): 1-11.

Lynch, K., I. Delgado-Fernandez, D. W. Jackson, J. Cooper, A. C. Baas and J. Beyers (2013). "Alongshore variation of aeolian sediment transport on a beach, under offshore winds." Aeolian Research **8**: 11-18.

Lynch, K., D. W. Jackson and J. A. G. Cooper (2008). "Aeolian fetch distance and secondary airflow effects: the influence of micro-scale variables on meso-scale foredune development." Earth Surface Processes and Landforms: The Journal of the British Geomorphological Research Group **33**(7): 991-1005.

Lynch, K., D. W. Jackson and J. A. G. Cooper (2009). "Foredune accretion under offshore winds." Geomorphology **105**(1-2): 139-146.

Lynch, K., D. W. Jackson and J. A. G. Cooper (2010). "Coastal foredune topography as a control on secondary airflow regimes under offshore winds." Earth Surface Processes and Landforms: The Journal of the British Geomorphological Research Group **35**(3): 344-353.

Marinho, B., C. Coelho, M. Larson and H. Hanson (2018). "Long-term coastal evolution modelling of longshore bars." Coastal Engineering Proceedings(36): 97-97.

Martínez, M., A. Intralawan, G. Vázquez, O. Pérez-Maqueo, P. Sutton and R. Landgrave (2007). "The coasts of our world: Ecological, economic and social importance." Ecological Economics **63**(2-3): 254-272.

Mason, J., B. T. Cardenas, M. D. Day, M. Daniller-Varghese, S. C. Brothers, G. Kocurek and D. Mohrig (2020). "Pattern evolution and interactions in subaqueous dune fields: North Loup River, Nebraska, USA." Journal of Sedimentary Research **90**(12): 1734-1746.

Masselink, G., B. Castelle, T. Scott, G. Dodet, S. Suanez, D. Jackson and F. Floc'h (2016). "Extreme wave activity during 2013/2014 winter and morphological impacts along the Atlantic coast of Europe." Geophysical Research Letters **43**(5): 2135-2143.

Masselink, G., L. Cointre, J. Williams, R. Gehrels and W. Blake (2009). "Tide-driven dune migration and sediment transport on an intertidal shoal in a shallow estuary in Devon, UK." Marine geology **262**(1-4): 82-95.

Masselink, G. and C. Pattiaratchi (2001). "Seasonal changes in beach morphology along the sheltered coastline of Perth, Western Australia." Marine Geology **172**(3-4): 243-263.

Masselink, G. and J. A. Puleo (2006). "Swash-zone morphodynamics." Continental Shelf Research **26**(5): 661-680.

Masselink, G. and A. D. Short (1993). "The effect of tide range on beach morphodynamics and morphology: a conceptual beach model." Journal of coastal research: 785-800.

Masselink, G. and S. van Heteren (2014). "Response of wave-dominated and mixed-energy barriers to storms." Marine geology **352**: 321-347.

Mathew, S., R. G. Davidson-Arnott and J. Ollerhead (2010). "Evolution of a beach–dune system following a catastrophic storm overwash event: Greenwich Dunes, Prince Edward Island, 1936–2005." Canadian Journal of Earth Sciences **47**(3): 273-290.

Matias, A., Ó. Ferreira, A. Vila-Concejo, T. Garcia and J. A. Dias (2008). "Classification of washover dynamics in barrier islands." Geomorphology **97**(3-4): 655-674.

Maximiliano-Cordova, C., K. Salgado, M. L. Martínez, E. Mendoza, R. Silva, R. Guevara and R. A. Feagin (2019). "Does the functional richness of plants reduce wave erosion on embryo coastal dunes?" Estuaries and coasts **42**(7): 1730-1741.

Maximiliano-Cordova, C., K. Salgado, M. L. Martínez, E. Mendoza, R. Silva, R. Guevara and R. A. Feagin (2019). "Does the Functional Richness of Plants Reduce Wave Erosion on Embryo Coastal Dunes?" Estuaries and coasts: 1-12.

McArdle, S. B. and A. McLachlan (1991). "Dynamics of the swash zone and effluent line on sandy beaches." Marine ecology progress series. Oldendorf **76**(1): 91-99.

McCarroll, R. J., R. W. Brander, I. L. Turner, H. E. Power and T. R. Mortlock (2014). "Lagrangian observations of circulation on an embayed beach with headland rip currents." Marine geology **355**: 173-188.

McCarroll, R. J., G. Masselink, N. G. Valiente, T. Scott, E. V. King and D. Conley (2018). "Wave and tidal controls on embayment circulation and headland bypassing for an exposed, macrotidal site." Journal of Marine Science and Engineering **6**(3): 94.

McKee, E. D. (1979). Introduction to a study of global sand seas. A study of global sand seas, Professional Paper. **1052:** 1-19.

McLean, R. and J.-S. Shen (2006). "From foreshore to foredune: foredune development over the last 30 years at Moruya Beach, New South Wales, Australia." Journal of coastal research: 28-36.

Meucci, A., I. R. Young, M. Hemer, E. Kirezci and R. Ranasinghe (2020). "Projected 21st century changes in extreme wind-wave events." Science advances **6**(24): eaaz7295.

Micheli, E. and J. Kirchner (2002). "Effects of wet meadow riparian vegetation on streambank erosion. 2. Measurements of vegetated bank strength and consequences for failure mechanics." Earth Surface Processes and Landforms: The Journal of the British Geomorphological Research Group **27**(7): 687-697.

Mikelsen, H. (1989). "Wind flow and sediment transport over a low coastal dune."

Momiji, H. and A. Warren (2000). "Relations of sand trapping efficiency and migration speed of transverse dunes to wind velocity." Earth Surface Processes and Landforms: The Journal of the British Geomorphological Research Group **25**(10): 1069-1084.

Morton, R. A. (2002). "Factors controlling storm impacts on coastal barriers and beaches: a preliminary basis for near real-time forecasting." Journal of coastal research: 486-501.

Morton, R. A., J. G. Paine and J. C. Gibeaut (1994). "Stages and durations of post-storm beach recovery, southeastern Texas coast, USA." Journal of coastal research: 884-908.

Morton, R. A. and A. H. Sallenger Jr (2003). "Morphological impacts of extreme storms on sandy beaches and barriers." Journal of coastal research: 560-573.

NASA (2021). "Sea Level Projection Tool." Retrieved 6-9-21, 2021, from sealevel.nasa.gov/ipcc-ar6-sea-level-projection-tool.

Nassar, K., W. E. Mahmod, H. Fath, A. Masria, K. Nadaoka and A. Negm (2019). "Shoreline change detection using DSAS technique: Case of North Sinai coast, Egypt." Marine Georesources & Geotechnology **37**(1): 81-95.

Needham, H. F., B. D. Keim and D. Sathiaraj (2015). "A review of tropical cyclone-generated storm surges: Global data sources, observations, and impacts." Reviews of Geophysics **53**(2): 545-591.

Neuman, C. M., N. Lancaster and W. Nickling (1997). "Relations between dune morphology, air flow, and sediment flux on reversing dunes, Silver Peak, Nevada." Sedimentology **44**(6): 1103-1111.

Neuman, C. M., N. Lancaster and W. Nickling (2000). "The effect of unsteady winds on sediment transport on the stoss slope of a transverse dune, Silver Peak, NV, USA." Sedimentology **47**(1): 211-226.

Nicholls, R. J. and A. Cazenave (2010). "Sea-level rise and its impact on coastal zones." Science **328**(5985): 1517-1520.

Nichols, R. L. and A. F. Marston (1939). "Shoreline changes in Rhode Island produced by hurricane of September 21, 1938." Bulletin of the Geological Society of America **50**(9): 1357-1370.

Niedoroda, A. (1966). "Preliminary study of transverse bars on low energy beaches." Coastal Research Notes **2**(3): 3-4.

Nishi, R. and N. C. Kraus (1997). Mechanism and calculation of sand dune erosion by storms. Coastal Engineering 1996**:** 3034-3047.

Nishi, R., M. Sato and H. Wang (1995). Field observation and numerical simulation of beach and dune scarps. Coastal Engineering 1994**:** 2434-2448.

Ochieng, C. A. and P. L. Erftemeijer (1999). "Accumulation of seagrass beach cast along the Kenyan coast: a quantitative assessment." Aquatic botany **65**(1-4): 221-238.

Ollerhead, J., R. Davidson-Arnott, I. J. Walker and S. Mathew (2013). "Annual to decadal morphodynamics of the foredune system at Greenwich Dunes, Prince Edward Island, Canada." Earth Surface Processes and Landforms **38**(3): 284-298.

Orford, J. D. and R. Carter (1984). "Mechanisms to account for the longshore spacing of overwash throats on a coarse clastic barrier in southeast Ireland." Marine geology **56**(1-4): 207-226.

Oyedotun, T. D. J. B. S. f. G., Geomorphological Techniques. ISSN (2014). "Shoreline geometry: DSAS as a tool for historical trend analysis." 2047-0371.

Pachauri, R. K., M. R. Allen, V. R. Barros, J. Broome, W. Cramer, R. Christ, J. A. Church, L. Clarke, Q. Dahe and P. Dasgupta (2014). Climate change 2014: synthesis report. Contribution of Working Groups I, II and III to the fifth assessment report of the Intergovernmental Panel on Climate Change, IPCC.

Parker, W. (1975). Sediment mobility and erosion on a multibarred foreshore (southwest Lancashire, UK), Wiley and Sons: London.

Parsons, D. R., I. J. Walker and G. F. Wiggs (2004). "Numerical modelling of flow structures over idealized transverse aeolian dunes of varying geometry." Geomorphology **59**(1-4): 149-164.

Parteli, E. J., J. S. Andrade Jr and H. J. Herrmann (2011). "Transverse instability of dunes." Physical review letters **107**(18): 188001.

Phillips, B., J. Brown, J.-R. Bidlot and A. Plater (2017). "Role of beach morphology in wave overtopping hazard assessment." Journal of Marine Science and Engineering **5**(1): 1.

Phillips, J. D. (2009). "Changes, perturbations, and responses in geomorphic systems." Progress in physical geography **33**(1): 17-30.

Phillips, J. D. (2011). "Emergence and pseudo-equilibrium in geomorphology." Geomorphology **132**(3-4): 319-326.

Phillips, J. D. (2014). "Thresholds, mode switching, and emergent equilibrium in geomorphic systems." Earth Surface Processes and Landforms **39**(1): 71-79.

Pires, L. B., L. F. de Souza, G. Fisch and R. Gielow (2011). "Numerical study of the atmospheric flow over a coastal cliff." International journal for numerical methods in fluids **67**(5): 599-608.

Pires, L. B. M., G. Fisch, R. Gielow, L. F. Souza, A. C. Avelar, I. Paula and R. Girardi (2015). "A study of the internal boundary layer generated at the Alcantara Space Center." American Journal of Environmental Engineering **5**(1A): 52-64.

Piscioneri, N., T. A. Smyth and P. A. Hesp (2019). "Flow dynamics over a foredune scarp." Earth Surface Processes and Landforms **44**(5): 1064-1076.

Prasetya, G. (2006). Protection from coastal erosion. Proceeding of the regional technical workshop on coastal protection in the aftermath of the Indian Ocean Tsunami, Thailand.

Preoteasa, L. and A. Vespremeanu-Stroe (2017). Foredunes dynamics on the Danube delta coast. Landform Dynamics and Evolution in Romania, Springer**:** 581-606.

Price, W. A. (1997). Bars. Geomorphology. Berlin, Heidelberg, Springer Berlin Heidelberg**:** 55-58.

Pries, A. J., D. L. Miller and L. C. Branch (2008). "Identification of structural and spatial features that influence storm-related dune erosion along a barrier-island ecosystem in the Gulf of Mexico." Journal of coastal research **24**(sp3): 168-175.

Psuty, N. (2008). The coastal foredune: a morphological basis for regional coastal dune development. Coastal Dunes, Springer**:** 11-27.

Psuty, N. P. and T. M. Silveira (2010). "Global climate change: an opportunity for coastal dunes??" Journal of Coastal Conservation **14**(2): 153-160.

Pye, K. and S. Blott (2008). "Decadal-scale variation in dune erosion and accretion rates: an investigation of the significance of changing storm tide frequency and magnitude on the Sefton coast, UK." Geomorphology **102**(3-4): 652-666.

Pye, K. and H. Tsoar (2008). Aeolian sand and sand dunes, Springer Science & Business Media.

Qian, G., Z. Dong, W. Luo and J. Lu (2011). "Mean airflow patterns upwind of topographic obstacles and their implications for the formation of echo dunes: A wind tunnel simulation of the effects of windward slope." Journal of Geophysical Research: Earth Surface **116**(F4).

Qian, G., Z. Dong, W. Luo, Z. Zhang and A. Zhao (2012). "Airflow patterns upwind of obstacles and their significance for echo dune formation: A field measurement of the effects of the windward slope angle." Science China Earth Sciences **55**(4): 545-553.

Quilty, J. and A. Wearne (1975). "Evaluation of a phase of extreme coastline erosion." J. Soil. Conserv. Ser. NSW **31**: 179-192.

Rahmstorf, S. (2007). "A semi-empirical approach to projecting future sea-level rise." Science **315**(5810): 368-370.

Ramos, R., M. Freitas, C. Bristow, C. Andrade, H. Hermozilha, C. Grangeia and M. S. Matias (2011). "Sedimentary architecture of the Santo André transverse dunes (Portugal) interpreted from ground-penetrating radar." Journal of coastal research: 303-307.

Rasmussen, K. (1989). "Some aspects of flow over coastal dunes." Proceedings of the Royal Society of Edinburgh, Section B: Biological Sciences **96**: 129-147.

Raudkivi, A. (1966). "Bed forms in alluvial channels." Journal of Fluid Mechanics **26**(3): 507-514.

Reade, T. M. (1881). "III.—Æolian Sandstone." Geological Magazine **8**(5): 197-198.

Reesink, A., D. Parsons, P. Ashworth, J. Best, R. Hardy, B. Murphy, S. McLelland and C. Unsworth (2018). "The adaptation of dunes to changes in river flow." Earth-Science Reviews **185**: 1065-1087.

Reffet, E., S. Courrech du Pont, P. Hersen and S. Douady (2010). "Formation and stability of transverse and longitudinal sand dunes." Geology **38**(6): 491-494.

Ritchie, W. (1972). "The evolution of coastal sand dunes." Scottish Geographical Magazine **88**(1): 19-35.

Roelvink, D., A. Reniers, A. Van Dongeren, J. V. T. De Vries, R. McCall and J. Lescinski (2009). "Modelling storm impacts on beaches, dunes and barrier islands." Coastal Engineering **56**(11-12): 1133-1152.

Rubin, D. M. and A. M. Rubin (2013). "Origin and lateral migration of linear dunes in the Qaidam Basin of NW China revealed by dune sediments, internal structures, and optically stimulated luminescence ages, with implications for linear dunes on Titan: Discussion." Bulletin **125**(11-12): 1943-1946.

Ruggiero, P., P. Komar, W. McDougal and R. Beach (1997). Extreme water levels, wave runup and coastal erosion. Coastal Engineering 1996**:** 2793-2805.

Ruz, M.-H. and E. J. Anthony (2008). "Sand trapping by brushwood fences on a beach-foredune contact: the primacy of the local sediment budget." Zeitschrift für Geomorphologie, Supplementary Issues **52**(3): 179-194.

Ruz, M.-H. and C. Meur-Ferec (2004). "Influence of high water levels on aeolian sand transport: upper beach/dune evolution on a macrotidal coast, Wissant Bay, northern France." Geomorphology **60**(1-2): 73-87.

Ruz, M. H., A. Héquette and A. Maspataud (2009). "Identifying forcing conditions responsible for foredune erosion on the northern coast of France." Journal of coastal research(56): 356.

Ryan, D. A., B. P. Brooke, H. C. Bostock, L. C. Radke, P. J. Siwabessy, N. Margvelashvili and D. Skene (2007). "Bedload sediment transport dynamics in a macrotidal embayment, and implications for export to the southern Great Barrier Reef shelf." Marine geology **240**(1-4): 197-215.

Sallenger, A. (2000). "Storm impact scale for barrier islands." Journal of coastal research: 890-895.

Sancho, F., T. Abreu, F. D'Alessandro, G. Tomasicchio and P. Silva (2011). "Surf hydrodynamics in front of collapsing coastal dunes." Journal of coastal research: 144-148.

Saunders, K. E. and R. G. Davidson-Arnott (1990). Coastal dune response to natural disturbances. Canadian Symposium on Coastal Sand Dunes.

Saye, S. E. and K. Pye (2007). "Implications of sea level rise for coastal dune habitat conservation in Wales, UK." Journal of Coastal Conservation **11**(1): 31-52.

Schatz, V. and H. J. Herrmann (2006). "Flow separation in the lee side of transverse dunes: a numerical investigation." Geomorphology **81**(1-2): 207-216.

Schmidt, K., J. Roering, J. Stock, W. Dietrich, D. Montgomery and T. Schaub (2001). "The variability of root cohesion as an influence on shallow landslide susceptibility in the Oregon Coast Range." Canadian Geotechnical Journal **38**(5): 995-1024.

Schwarz, C., G. Ruessink, C. Böhm and J. Donker (2019). Wind and sand transport over vegetated coastal foredunes. Geophysical Research Abstracts.

Schwarz, M., F. Preti, F. Giadrossich, P. Lehmann and D. Or (2010). "Quantifying the role of vegetation in slope stability: a case study in Tuscany (Italy)." Ecological Engineering **36**(3): 285-291.

Segura, L., J. Hansen and R. Lowe (2018). "Seasonal Shoreline Variability Induced by Subtidal Water Level Fluctuations at Reef-Fringed Beaches." Journal of Geophysical Research: Earth Surface **123**(3): 433-447.

Sekovski, I., F. Stecchi, F. Mancini and L. Del Rio (2014). "Image classification methods applied to shoreline extraction on very high-resolution multispectral imagery." International Journal of Remote Sensing **35**(10): 3556-3578.

Serafim, M. B. and J. Bonetti (2017). "Vulnerabilidade das Praias do estado de santa catarina a eventos de erosão e inundação costeira: Proposta metodológica baseada em um índice multicritério." Vulnerability of santa catarina beaches to coastal erosion and flooding: A methodological approach based on a multicriterial index **8**(2): 36-54.

Shepard, F. P. (1950). Beach cycles in southern California, CORPS OF ENGINEERS WASHINGTON DC BEACH EROSION BOARD.

Short, A. (1979). "Three dimensional beach-stage model." The Journal of Geology **87**(5): 553-571.

Short, A. (2007). "Australian rip systems–friend or foe?" Journal of coastal research: 7-11.

Short, A. and P. Hesp (1982). "Wave, beach and dune interactions in southeastern Australia." Marine geology **48**(3-4): 259-284.

Short, A. and L. Wright (1983). Physical variability of sandy beaches. Sandy beaches as ecosystems, Springer**:** 133-144.

Short, A. D. (1999). Handbook of beach and shoreface morphodynamics.

Short, A. D. (2006). "Australian beach systems—nature and distribution." Journal of coastal research **22**(1 (221)): 11-27.

Short, A. D. (2010). "Role of geological inheritance in Australian beach morphodynamics." Coastal Engineering **57**(2): 92-97.

Short, A. D. (2019). Australian Coastal Systems. Cham, Switzerland.

Short, A. D. (2019). Australian Coastal Systems: Beaches, Barriers and Sediment Compartments, Springer Nature.

Short, A. D. and P. A. Hesp (1984). Beach and Dune Morphodynamics of the South East Coast of South Australia, University of Sydney, Department of Geography, Coastal Studies Unit.

Silva, R., M. Martínez, I. Odériz, E. Mendoza and R. Feagin (2016). "Response of vegetated dune–beach systems to storm conditions." Coastal Engineering **109**: 53-62.

Simm, J., A. Brampton, N. Beech and J. Brooke (1996). Beach management manual, Construction Industry Research and Information Association.

Smetacek, V. and A. Zingone (2013). "Green and golden seaweed tides on the rise." Nature **504**(7478): 84-88.

Smith, A. B., D. W. Jackson and J. A. G. Cooper (2017). "Three-dimensional airflow and sediment transport patterns over barchan dunes." Geomorphology **278**: 28-42.

Smith, G. L. and G. A. Zarillo (1990). "Calculating long-term shoreline recession rates using aerial photographic and beach profiling techniques." Journal of Coastal Research: 111-120.

Smith, J. D. and S. McLean (1977). Boundary layer adjustments to bottom topography and suspended sediment. Elsevier oceanography series, Elsevier. **19:** 123-151.

Smith, N. D. (1974). "Sedimentology and bar formation in the upper Kicking Horse River, a braided outwash stream." The Journal of Geology **82**(2): 205-223.

Smyth, T. A. and P. A. Hesp (2015). "Aeolian dynamics of beach scraped ridge and dyke structures." Coastal Engineering **99**: 38-45.

Smyth, T. A., D. W. Jackson and J. A. G. Cooper (2012). "High resolution measured and modelled three-dimensional airflow over a coastal bowl blowout." Geomorphology **177**: 62-73.

Smyth, T. A., D. W. Jackson and J. A. G. Cooper (2013). "Three dimensional airflow patterns within a coastal trough–bowl blowout during fresh breeze to hurricane force winds." Aeolian Research **9**: 111-123.

Southard, J. B. (1971). "Representation of bed configurations in depth-velocity-size diagrams." Journal of Sedimentary Research **41**(4): 903-915.

Splinter, K. D., E. T. Kearney and I. L. Turner (2018). "Drivers of alongshore variable dune erosion during a storm event: Observations and modelling." Coastal Engineering **131**: 31-41.

Splinter, K. D. and M. L. Palmsten (2012). "Modeling dune response to an East Coast Low." Marine geology **329**: 46-57.

Stephens, S., R. Bell and K. Black (2001). "Complex circulation in a coastal embayment: Shelf-current, wind and density-driven circulation in Poverty Bay, New Zealand." Journal of coastal research: 45-59.

Stride, A. (1982). Offshore tidal deposits: sand sheet and sand bank facies. Offshore tidal sands, Springer**:** 95-125.

Suanez, S., R. Cancouët, F. Floc'h, E. Blaise, F. Ardhuin, J.-F. Filipot, J.-M. Cariolet and C. Delacourt (2015). "Observations and predictions of wave runup, extreme water levels, and medium-term dune erosion during storm conditions." Journal of Marine Science and Engineering **3**(3): 674-698.

Suter, J. R., D. Nummedal, A. K. Maynard and P. Kemp (1982). A process-response model for hurricane washovers. Coastal Engineering 1982**:** 1459-1478.

Suziedelyte Visockiene, J., D. Brucas and U. Ragauskas (2014). "Comparison of UAV images processing softwares." Journal of Measurements in Engineering **2**(2): 111-121.

Svasek, J. and J. Terwindt (1974). "Measurements of sand transport by wind on a natural beach." Sedimentology **21**(2): 311-322.

Sweet, M. and G. Kocurek (1990). "An empirical model of aeolian dune lee-face airflow." Sedimentology **37**(6): 1023-1038.

Sytnik, O., L. Del Río, N. Greggio and J. Bonetti (2018). "Historical shoreline trend analysis and drivers of coastal change along the Ravenna coast, NE Adriatic." Environmental Earth Sciences **77**(23): 1-20.

Taebi, S., R. J. Lowe, C. B. Pattiaratchi, G. N. Ivey, G. Symonds and R. Brinkman (2011). "Nearshore circulation in a tropical fringing reef system." Journal of Geophysical Research: Oceans **116**(C2).

Tao, J., Z. B. Wang, Z. Zhou, F. Xu, C. Zhang and M. J. Stive (2019). "A morphodynamic modeling study on the formation of the large-scale radial sand ridges in the Southern Yellow Sea." Journal of Geophysical Research: Earth Surface **124**(7): 1742-1761.

Taylor, P. A., P. J. Mason and E. F. Bradley (1987). "Boundary-layer flow over low hills." Boundary-Layer Meteorology **39**(1): 107-132.

Tessier, B. (2012). Stratigraphy of tide-dominated estuaries. Principles of tidal sedimentology, Springer**:** 109-128.

Thieler, E. R., E. A. Himmelstoss, J. L. Zichichi and A. Ergul (2009). The Digital Shoreline Analysis System (DSAS) Version 4.0 - An ArcGIS extension for calculating shoreline change. Open-File Report. Reston.

Thieler, E. R. and R. S. Young (1991). "Quantitative evaluation of coastal geomorphological changes in South Carolina after Hurricane Hugo." Journal of coastal research: 187-200.

Thom, B. and W. Hall (1991). "Behaviour of beach profiles during accretion and erosion dominated periods." Earth Surface Processes and Landforms **16**(2): 113-127.

Thom, B. G., M. Shepherd, C. Ly, P. Roy, G. Bowman and P. Hesp (1992). "Coastal geomorphology and quaternary geology of the Port Stephens-Myall Lakes area."

Thornton, E. B., J. MacMahan and A. Sallenger Jr (2007). "Rip currents, mega-cusps, and eroding dunes." Marine geology **240**(1-4): 151-167.

To, D. V. and P. T. P. Thao (2008). "A shoreline analysis using DSAS in Nam Dinh Coastal Area." International Journal of Geoinformatics **4**(1).

Tsoar, H. (1983). Wind tunnel modeling of echo and climbing dunes. Developments in Sedimentology, Elsevier. **38:** 247-259.

Tsoar, H. (1985). "Profiles analysis of sand dunes and their steady state signification." Geografiska Annaler: Series A, Physical Geography **67**(1-2): 47-59.

Tsoar, H., D. G. Blumberg and Y. Stoler (2004). "Elongation and migration of sand dunes." Geomorphology **57**(3-4): 293-302.

Tsoar, H., B. White and E. Berman (1996). "The effect of slopes on sand transport—Numerical modelling." Landscape and Urban Planning **34**(3-4): 171-181.

Tsoar, H. and D. H. Yaalon (1983). "Deflection of sand movement on a sinuous longitudinal (seif) dune: use of fluorescent dye as tracer." Sedimentary Geology **36**(1): 25-39.

Uruba, V. and M. Knob (2009). "Dynamics of a boundary layer separation." Engineering Mechanics **16**(1): 29-38.

Valiente, N. G., G. Masselink, R. J. McCarroll, T. Scott, D. Conley and E. King (2020). "Nearshore sediment pathways and potential sediment budgets in embayed settings over a multi-annual timescale." Marine geology: 106270.

van Bemmelen, C. (2018). "Beach Scarp Morphodynamics: Formation, Migration, and Destruction."

van de Graaff, J. (1986). "Probabilistic design of dunes; an example from the Netherlands." Coastal Engineering **9**(5): 479-500.

van de Graaff, J. (1994). "Coastal and dune erosion under extreme conditions." Journal of coastal research: 253-262.

Van Dijk, P., S. Arens and J. Van Boxel (1999). "Aeolian processes across transverse dunes. II: Modelling the sediment transport and profile development." Earth Surface Processes and Landforms: The Journal of the British Geomorphological Research Group **24**(4): 319-333.

Van Dijk, T. A. and M. G. Kleinhans (2005). "Processes controlling the dynamics of compound sand waves in the North Sea, Netherlands." Journal of Geophysical Research: Earth Surface **110**(F4).

van Rijn, L. C. (2009). "Prediction of dune erosion due to storms." Coastal Engineering **56**(4): 441-457.

van Scheltinga, R. C. T., G. Coco, M. G. Kleinhans and H. Friedrich (2020). "Observations of dune interactions from DEMs using through-water Structure from Motion." Geomorphology **359**: 107126.

Van Thiel de Vries, J., J. Van de Graaff, B. Raubenheimer, A. Reniers and M. Stive (2007). Modeling inner surf hydrodynamics during storm surges. Coastal Engineering 2006: (In 5 Volumes), World Scientific**:** 896-908.

Vellinga, P. (1982). "Beach and dune erosion during storm surges." Coastal Engineering **6**(4): 361-387.

Vitousek, S., P. L. Barnard and P. Limber (2017). "Can beaches survive climate change?" Journal of Geophysical Research: Earth Surface **122**(4): 1060-1067.

Vousdoukas, M. I., L. Mentaschi, E. Voukouvalas, M. Verlaan, S. Jevrejeva, L. P. Jackson and L. Feyen (2018). "Global probabilistic projections of extreme sea levels show intensification of coastal flood hazard." Nature communications **9**(1): 2360.

Walker, I., R. Davidson-Arnott, P. Hesp, B. Bauer and J. Ollerhead (2009). "Mean flow and turbulence responses in airflow over foredunes: new insights from recent research." Journal of coastal research: 366-370.

Walker, I. J. (1999). "Secondary airflow and sediment transport in the lee of a reversing dune." Earth Surface Processes and Landforms: The Journal of the British Geomorphological Research Group **24**(5): 437-448.

Walker, I. J. (2000). Secondary airflow and sediment transport in the lee of transverse dunes, University of Guelph Guelph.

Walker, I. J., P. A. Hesp, R. G. Davidson-Arnott, B. O. Bauer, S. L. Namikas and J. Ollerhead (2009). "Responses of three-dimensional flow to variations in the angle of incident wind and

profile form of dunes: Greenwich Dunes, Prince Edward Island, Canada." Geomorphology **105**(1-2): 127-138.

Walker, I. J., P. A. Hesp, R. G. Davidson-Arnott and J. Ollerhead (2006). "Topographic steering of alongshore airflow over a vegetated foredune: Greenwich Dunes, Prince Edward Island, Canada." Journal of coastal research: 1278-1291.

Walker, I. J. and W. G. Nickling (2002). "Dynamics of secondary airflow and sediment transport over and in the lee of transverse dunes." Progress in physical geography **26**(1): 47-75.

Walker, I. J. and W. G. Nickling (2003). "Simulation and measurement of surface shear stress over isolated and closely spaced transverse dunes in a wind tunnel." Earth Surface Processes and Landforms: The Journal of the British Geomorphological Research Group **28**(10): 1111-1124.

Walker, I. J. and D. H. Shugar (2013). "Secondary flow deflection in the lee of transverse dunes with implications for dune morphodynamics and migration." Earth Surface Processes and Landforms **38**(14): 1642-1654.

Walmsley, J. L. and A. D. Howard (1985). "Application of a boundary-layer model to flow over an eolian dune." Journal of Geophysical Research: Atmospheres **90**(D6): 10631-10640.

Wang, P. and M. H. Horwitz (2007). "Erosional and depositional characteristics of regional overwash deposits caused by multiple hurricanes." Sedimentology **54**(3): 545-564.

Wang, T. and Z. Yang (2018). "The Nonlinear Response of Storm Surge to Sea-Level Rise: A Modeling Approach." Journal of coastal research.

Watson, A. (1986). "Grain-size variations on a longitudinal dune and a barchan dune." Sedimentary Geology **46**(1-2): 49-66.

Watson, S. J., H. Neil, M. Ribó, G. Lamarche, L. J. Strachan, K. MacKay, S. Wilcox, T. Kane, A. Orpin and S. Nodder (2020). "What we do in the shallows: Natural and anthropogenic seafloor geomorphologies in a drowned river valley, New Zealand." Frontiers in Marine Science.

Weaver, C. M. and G. F. Wiggs (2011). "Field measurements of mean and turbulent airflow over a barchan sand dune." Geomorphology **128**(1-2): 32-41.

Weaver, R. J. and D. N. Slinn (2005). Effect of wave forcing on storm surge. Coastal Engineering 2004: (In 4 Volumes), World Scientific**:** 1532-1538.

Weisse, R. and A. Plüβ (2006). "Storm-related sea level variations along the North Sea coast as simulated by a high-resolution model 1958–2002." Ocean Dynamics **56**(1): 16-25.

Wells, J. T. (1995). Tide-dominated estuaries and tidal rivers. Developments in sedimentology, Elsevier. **53:** 179-205.

Weymer, B. A., C. Houser and J. R. Giardino (2013). "Poststorm Evolution of Beach-Dune Morphology: Padre Island National Seashore, Texas." Journal of coastal research **31**(3): 634-644.

Wiggs, G. F., I. Livingstone and A. Warren (1996). "The role of streamline curvature in sand dune dynamics: evidence from field and wind tunnel measurements." Geomorphology **17**(1-3): 29-46.

Wischmeier, W. H. and D. D. Smith (1978). "Predicting rainfall erosion losses-a guide to conservation planning." Predicting rainfall erosion losses-a guide to conservation planning.

Worden, R. and S. Burley (2003). "Sandstone diagenesis: the evolution of sand to stone."

Worden, R., M. Mayall and I. Evans (2000). "The effect of ductile-lithic sand grains and quartz cement on porosity and permeability in Oligocene and lower Miocene clastics, South China Sea: prediction of reservoir quality." AAPG bulletin **84**(3): 345-359.

Wright, L., J. Chappell, B. Thom, M. Bradshaw and P. Cowell (1979). "Morphodynamics of reflective and dissipative beach and inshore systems: Southeastern Australia." Marine geology **32**(1-2): 105-140.

Wright, L., B. Thom and J. Chappell (1978). Morphodynamic variability of high-energy beaches. Coastal Engineering 1978**:** 1180-1194.

Wright, L., B. Thom and R. Higgins (1980). "Wave influences on river-mouth depositional process: examples from Australia and Papua New Guinea." Estuarine and Coastal Marine Science **11**(3): 263-277.

Wright, L. D., A. D. Short and M. Green (1985). "Short-term changes in the morphodynamic states of beaches and surf zones: an empirical predictive model." Marine geology **62**(3-4): 339-364.

Yaalon, D. (1967). "Factors affecting the lithification of eolianite and interpretation of its environmental significance in the coastal plain of Israel." Journal of Sedimentary Research **37**(4): 1189-1199.

Yalin, M. S. (1964). "Geometrical properties of sand wave." Journal of the Hydraulics Division **90**(5): 105-119.

Yao, Z., T. Wang, Z. Han, W. Zhang and A. Zhao (2007). "Migration of sand dunes on the northern Alxa Plateau, Inner Mongolia, China." Journal of arid environments **70**(1): 80-93.

Yassin, M. and M. Al Harbi (2013). "Numerical simulation on wind flow over step-shaped cliff topography with rough surface."

Young, I. R. and G. J. Holland (1996). "Atlas of the oceans: wind and wave climate." Oceanographic Literature Review **7**(43): 742.

Young, I. R. and A. Ribal (2019). "Multiplatform evaluation of global trends in wind speed and wave height." Science **364**(6440): 548-552.

Zeman, O. and N. O. Jensen (1987). "Modification of turbulence characteristics in flow over hills." Quarterly Journal of the Royal Meteorological Society **113**(475): 55-80.

Zhang, K., B. C. Douglas and S. P. Leatherman (2004). "Global warming and coastal erosion." Climatic Change **64**(1-2): 41.

Zhou, J., Z. Wu, D. Zhao, W. Guan, C. Zhu and B. Flemming (2020). "Giant sand waves on the Taiwan Banks, southern Taiwan Strait: Distribution, morphometric relationships, and hydrologic influence factors in a tide-dominated environment." Marine geology **427**: 106238.